2000

KINETICS AND MECHANISMS OF MACROMOLECULAR DISPOSITION IN THE RAT LUNG

Masahiro Sakagami

SCHOOL OF PHARMACY
VIRGINIA COMMONWEALTH UNIVERSITY

This is to certify that the dissertation prepared by Masahiro Sakagami, M.S., entitled **"Kinetics and mechanisms of macromolecular disposition in the rat lung"** has been approved by his committee as satisfactory completion of the dissertation requirements for the degree of Doctor of Philosophy.

[redacted]

Peter R. Byron, Ph.D., Director of Dissertation

[redacted]

Jurgen Venitz, M.D., Ph.D., School of Pharmacy

[redacted]

Mohamadi A. Sarkar, Ph.D., School of Pharmacy

[redacted]

William H. Soine, Ph.D., School of Pharmacy

[redacted]

Joseph J. Feher, Ph.D., School of Medicine

[redacted]

Peter R Byron, Ph.D., Chairman, School of Pharmacy

[redacted]

Victor A. Yanchick, Ph.D., Dean, School of Pharmacy

[redacted]

Jack L. Haar, Ph.D., Dean, School of Graduate Studies

September 13, 2000

Date

KINETICS AND MECHANISMS OF MACROMOLECULAR DISPOSITION IN THE RAT LUNG

A dissertation submitted in partial fulfillment
of the requirement for the degree of

Doctor of Philosophy

at Virginia Commonwealth University

By

Masahiro Sakagami, M.S.
Waseda University, Japan
1990

Director: Peter R. Byron, Ph.D.
Professor, Chair
Department of Pharmaceutics, School of Pharmacy

Virginia Commonwealth University
Richmond, Virginia
December, 2000

DEDICATIONS

TO MY PRECIOUS PARENTS

ACKNOWLEDGMENT

I would like to sincerely thank Dr. Peter R. Byron, not only for his unsurpassed supervision of this project, but also for his gracious understanding of my career enhancement. He has always been helpful and supportive to me in Richmond with a positive and creative attitude. He will surely be my long-time mentor.

I have been fortunate for having such professional graduate committee members: Dr. Jurgen Venitz, Dr. Mohamadi Sarkar, Dr. Joseph J. Feher and Dr. William H. Soine. They have generously provided their valuable time and knowledge. Without their input, the project would be poorer.

I am also grateful to Dr. Frantisek Rypacek and the Czech Academy of Sciences. He has always provided excellent polymers in a timely manner. Several discussions via e-mail were truly helpful and enjoyable. This project and my living expenses were financially supported by the Medical College of Virginia Foundation and the Czech Academy of Sciences.

To all current and ex-ARGers: Michael, Joanne, Dilraj, Chris, Michelle, Martyn, Rajiv, Jennifer, Rose, Shuguang, Xiaobin, John, Stefano and Joan; to all friends in my graduate study in Pharmaceutics, thanks for their daily support and friendship. It is the most valuable fortune for me to have such excellent and trusted friends here, in the US.

My appreciation is extended to the excellent graduate faculty and administrative assistants in Pharmaceutics for their kind help and support. Especially, to Mr. Clark March who has frequently suffered from all sorts of questions that I asked. He always gave me appropriate advice on any occasions.

I would like also to send my special thanks to Sian and Katie, who gave me heartwarming family-feelings, which I could not feel here, from my own family.

To all of my precious friends, Katsu, Tomoyo, Mariko, Miwa, Chizuru, Kazuya, Osami, Shino and Fumiko; to many MCV-Japanese members, you have always encouraged and entertained me in various ways. I found this to be very valuable and appreciated.

Finally, I would like to sincerely express my gratitude to my loving parents, Dad and Mom, and a sister, Akiko, back in Japan. They have always believed in me and supported me in my goal, which I expressed them five years ago. I could not have achieved this without their love, understanding, encouragement and support.

I arrived at the Richmond International Airport on August 11, 1996. Coincidentally, I finally finish this dissertation on August 10, 2000. This past four years have truly been enjoyable and will surely be unforgettable throughout my whole life.

TABLE OF CONTENTS

APPENDICES

LIST OF TABLES

LIST OF FIGURES

ABBREVIATIONS

<Symbols>

a	exponent of Mark-Houwink equation
A	absorption
A_M	total surface area available for absorption
ADP	adenosine 5'-diphosphate
AGT	artificial glass thorax
ANOVA	analysis of variance
ATP	adenosine 5'-triphosphate
AUC	area under the curve
[B]	cumulative amount of solute absorbed into the blood in vivo
BSA	bovine serum albumin
BW	body weight
C_{mes}	measured concentrations of control samples
$C_{nøm}$	known concentrations of control samples
cAMP	cyclic adenosine 5'-monophosphate
cGMP	cyclic guanosine 5'-monophosphate
95%CI	95 % confidence interval
Conc.	concentration
CV%	coefficient of variation (SD/mean x 100 [%])
D	deposition
D_{ad}	administered dose, calculated by $D_L - (D_{ctg} + D_{cnl})$
D_{cnl}	solute amount remaining in the tracheal cannula after administration.

D_{ctg}	solute amount remaining in the dosing cartridge after administration.
D_L	loading solute dose in the dosing cartridge.
D_M	solute's diffusion coefficient through the pulmonary membranes
DEA	Drug Enforcement Administration
DI	distribution
DMF	dimethylformamide
DMSO	dimethylsulfoxide
DNP	2,4-dinitrophenol
E	elimination
Eqn.	equation
%error	% difference from nominal value
EtOH	ethyl alcohol
F	fluorophore
F	a fraction of administered dose delivered to the pulmonary region
FD-4	FITC-labeled dextran 40
Fig.	Figure
FITC	fluorescein isothiocyanate
F-Na	sodium fluorescein
F-PHEA	fluorophore-labeled PHEA
F-PSI	fluorophore-labeled PSI
g	gravity
$\Delta G_o'$	ATP hydrolysis energy
GI	gastrointestinal
GPC	gel permeation chromatography
h	thickness of the pulmonary membranes
h_i	fraction height of HPGPC elution curve
HE	hydroxyethyl
HEG	monohydroxyethyl glutamine
HPGPC	high performance gel permeation chromatography

HPLC	high performance liquid chromatography
IACUC	Institutional Animal Care and Use Committee
IC_{50}	concentrations at which 50 % of active absorption inhibition was obtained
ICH	International Conference on Harmonization
id	internal diameter
IgG	immunoglobulin G
IMC	Institute of Macromolecular Chemistry
IPRL	isolated perfused rat lung
K	Mark-Houwink constant [mL/g]
$k_{a,P}$	first-order passive absorption rate constant from the pulmonary region
$k_{a,TB}$	first-order passive absorption rate constant from the tracheo-bronchial region
K_D	solute's membrane/donor solution phase partition coefficient
$k_{E,PT}$	first-order mucociliary clearance rate constant from the pulmonary to the tracheo-bronchial region
$K_{m,P}$	"affinity" or dose at which the active absorption rate = $0.5 \cdot V_{max,P}$
l	length
L	left lung lobe
LD_{50}	lethal dose at which 50 % of animals are dead
LOD	limit of detection
LOQ	limit of quantification
M	metabolism
M_B	solvent molecular weight
$[M]_P$	solute amount remaining to be absorbed in the pulmonary region
$[M]_{P+TB}$	solute amount remaining to be absorbed in the total airway region
$[M]_{TB}$	solute amount remaining to be absorbed in the tracheo-bronchial region
MC	mucociliary clearance
MDI	metered dose inhaler

Mean	mean value
min	minute
MON	monensin
Mn	number-averaged molecular weight
MSC	Model Selection Criterion
Mw	weight-averaged molecular weight
MW	molecular weight
MW_i	molecular weight of polymer fraction
MWD	molecular weight distribution
N	number
N	normality (concentration)
N_o	Avogadro's number
N/A	not applicable or not availabe
NIH	National Institute of Health
NOC	nocodazole
od	outer diameter
p	probability
[P]	cumulative solute amount absorbed from the pulmonary region into the recirculating perfusate of the IPRL
P-11, P-12	propellant (chlorofluorocarbons)
PAC	pulmonary artery cannula
PBS	phosphate buffered saline
PC	right postcaval or median lobe
P_d	polydispersity (P_d = Mw/Mn)
PEO	polyethyleneoxide
pH	negative log of hydrogen ion concentration or activity
PHEA	poly-α,β-[N(2-hydroxyethyl)-D,L-aspartamide]
PSI	polysuccinimide
R	rate constant ratio
R	the gas-law constant

R^2	R-squared value
r_A	effective radius of the solute molecule
RI	right inferior or diaphragmatic lobe
RM	right middle lobe
rpm	revolution per minute
RS	right superior or apical lobe
RSD	relative standard deviation
S	slope of the calibration curve
SD	sample standard deviation
SE	sample standard error
sec	second
t	time
T	the absolute temperature
$T_{1/2}$	half-life
$[\%T]_{active,control}$	% of F-PHEA dose transferred to perfusate in 30 minutes by active mechanisms in the absence of inhibitors
$[\%T]_{active,inh}$	% of F-PHEA dose transferred to perfusate in 30 minutes by active mechanisms in the presence of inhibitors
$[\%T]_{obs,inh}$	experimentally-observed result for % of F-PHEA dose transferred to perfusate in 30 minutes in the presence of inhibitors
$[\%T]_{passive}$	theoretically-calculated % of F-PHEA dose transferred to perfusate in 30 minutes by passive mechanisms
TB	trachea and bronchi
Temp.	temperature
™	trade mark
TRH	thyrotropin releasing hormone
TS	tissue sequestration
USP	the United States Pharmacopeia
V	effective fluid volume in the airways (where solutes are dissolved)
V'_A	solute's molar volume at its normal boiling temperature
V_e	elution volume

$V_{max,P}$	maximum rate of active absorption from the pulmonary region
vs.	versus
v/v	volume per voulme
W_I	weight fraction
w/v	weight per volume
ε	absorption coefficient $(mM \cdot cm)^{-1}$
ϕ_B	solvent association factor
$[\eta]$	intrinsic viscosity
η_B	viscosity of the medium in which diffusion occurs
λ_{em}	emission wavelength
λ_{ex}	excitation wavelength
σ	standard deviation of the response intercept of the calibration curve

<Units>

cc	cubic centimeter
^oC	temperature, degree centigrade
Da	Dalton
g	gram
m	meter
L	liter
M	molar concentration

<Multiplicative prefixes>

k	kilo- (10^3)
m	milli- (10^{-3})
c	centi- (10^{-2})
μ	micro- (10^{-6})
n	nano- (10^{-9})
p	pico- (10^{-12})

<Mathematical symbols>

%	percentage
≈	approximately equal to
>	greater than
>>	much greater than
<	smaller than
<<	much smaller than

ABSTRACT

KINETICS AND MECHANISMS OF MACROMOLECULAR DISPOSITION IN THE RAT LUNG

By Masahiro Sakagami, M.S.

A dissertation submitted in partial fulfillment of the requirement for the degree of Doctor of Philosophy at Virginia Commonwealth University

Virginia Commonwealth University, 2000

Director: Peter R. Byron, Ph.D.
Professor
Department of Pharmaceutics, School of Pharmacy

The kinetics and mechanisms of macromolecular absorption from the airways of the rat lung were studied in vivo and in vitro, following identical solute administration methods. The isolated perfused rat lung (IPRL) was used as an in vitro model, and the disposition of 7.4 and 4.3 kDa fluorophore-labeled polyhydroxyethylaspartamide (F-PHEA) and other small and macromolecular reference solutes was investigated across doses and in the presence of a variety of biochemical inhibitors.

Absorption profiles of F-PHEA, and the solute's lung distribution at different times after administration, were statistically identical in vivo and in vitro, showing that the IPRL possessed a viable mucociliary escalator and that macromolecular solute absorption rates from the IPRL were predictive of those in vivo. A kinetic model of the IPRL incorporating mucociliary clearance alongside active and passive absorption was developed and validated. This model was employed successfully to analyze each solute's absorption components from the rat lung following simultaneous, across-dose, nonlinear regression analysis of airway-to-perfusate absorption data. 7.4 and 4.3 kDa F-PHEA absorption from the pulmonary lung compartment occurred actively via the polyaspartamide transporter with values for $V_{max,P}$ and $K_{m,P}$ of 4.37/3.60 μg/min and 56.6/76.8 μg, respectively. In contrast, the magnitude of F-PHEA's passive absorption component, $k_{a,P}$, was inversely related to its molecular weight, consistent with the absorption of a small proportion of each solute dose passing by restricted diffusive transport through tight junctions in the pulmonary epithelium.

The active component of 7.4 kDa F-PHEA absorption, which enhanced airway-to-perfusate transfer at low doses, was significantly inhibited in the IPRL at lowered temperature (25 ^{o}C; 68.4 %) and in the presence of 1.0 mM 2,4-dinitrophenol (53.3 %), 100 μM ouabain (75.8 %), 30.0 μM monensin (66.0 %) and 30.0 μM nocodazole (68.4 %). This suggested that polyaspartamide-transporter was dependent on ATP-derived energy, and probably employed an intracellular vesicular transcytotic mechanism. The airway-to-perfusate transfer of 376 Da fluorescein and 4.4 kDa fluorophore-labeled dextran had no active (dose-dependent) absorption component. However, each of these

solutes showed values for solute's molecular weight-dependent passive absorption and solute-independent mucociliary clearance, when compared to those for F-PHEA.

CHAPTER I

BACKGROUND AND SIGNIFICANCE

Innovations in biotechnology have produced a wide variety of new macromolecular therapeutics and currently, there are at least 30 compounds approved in the US market and over 130 candidates now in human clinical trials (Patton, 1998). Despite this tremendous opportunity, the systemic delivery of these macromolecules, mostly proteins and peptides is still quite limited due to poor absorption through many of the body's epithelia. Oral administration of these large molecules undergoes extensive enzymatic and acid digestion in the gastrointestinal (GI) tract, resulting in negligible absorption of intact molecules through the GI mucosal membrane. The skin offers an even less permeable barrier due to their large molecular size. The nasal route affords only low bioavailability for proteins and peptides (e.g., $\leq$ 3.0 % for insulin) and especially, its high variability is believed to be problematic (Patton, 1998). As a result, the major route of administration for these compounds has been largely limited to parenteral administration via injection.

In contrast, it is now becoming clear that inhalation offers promising prospects for macromolecular delivery (Patton and Platz, 1992; Adjei and Gupta, 1994; Byron and Patton, 1994; Patton, 1998). The lung is known to have an enormous absorptive surface area (102 m^2 in human) covered by an extremely small volume of fluid (10-20 mL in human) and the entire cardiac output rushes through its capillary network which lies ≤ 1 μm beneath the absorptive surface (Patton, 1996; Patton, 1998). Table I.1 shows many of the proteins and peptides, which are currently being developed or studied as inhalation drug candidates. Even following inefficient aerosol administration, the absolute bioavailability of leuprolide acetate (MW = 1.2 kDa), a nonapeptide with potent luteinizing hormone releasing hormone agonist activity, was as high as 18 % in healthy human volunteers (Adjei and Garren, 1990). Insulin (51 amino acid, MW = 5.7 kDa) administration via nebulization has been successfully shown to lower blood glucose in diabetes patients (Laube *et al.*, 1993; Liu *et al.*, 1993). Table I.2 shows animal studies in which macromolecular absorption was studied. Regardless of species, most of the proteins and peptides in Table I.2 were readily absorbed from the lung, demonstrating much higher bioavailability, when compared to other routes of administration.

In order to appreciate the potential for systemic drug delivery of macromolecules via the airways, it is necessary to understand and recognize the nature of the pulmonary barrier. Typical statistics for average human lung are shown in Table I.3, compared to those for Sprague-Dawley rats. Following 17 bifurcations, the surface area of the alveolar region has been shown to be enormous, compared to that of the tracheo-bronchial region

Table I.1. Proteins and peptides that are currently being developed or studied as inhalation drug candidates.

Protein/Peptide	MW [kDa]	Indications (Research phase)	Reference [1]
Leuprolide acetate	1.2	Infertility, endometriosis (Ph.I)[2]	Adjei, 1990
Cyclosporin	1.2	Refractory transplant/organ rejection, asthma	Iacono, 1996
Calcitonin	3.4	Osteoporosis, Pagets disease (Ph.I)	Patton, 1997
Insulin	5.7	Type I/II diabetes (Ph.III)	Laube, 1993
Heparin	15-20	Blood clotting	Patton, 1997
IL-2[*1]	18	Renal cancer	Huland, 1992
hG-CSF[*2]	18.8	Cancer	Fuchs, 1994
IFN-γ [*3]	18-20	Chronic granulomatous diseases	Jaffe, 1991
IFN-β[*4]	19-22	Lung cancer, multiple sclerosis	Halme, 1994
IFN-α[*5]	19-22	Lung cancer, hepatitis	Kinnula, 1989
rhDNAse[*6]	37	Cystic fibrosis (Launched)	Gonda, 1997
α_1-antitrypsin	52	Cystic fibrosis α_1-antitrypsin deficiency	McElvaney, 1991 Hubbard, 1989
IL-R[*7]	90	Asthma (Ph.I/II)	Patton, 1997

[1] Only first auhors and years of publication; details are described in References.
[2] Ph. = Phase.
[*1] Interleukin-2; [*2] human granulocyte colony-stimulating factor; [*3] interferon-γ ; [*4] interferon-β; [*5] interferon-α; [*6] recombinant human deoxyribonuclease and [*7] interleukin receptor.

Table I.2. Bioavailability and T_{max} for proteins and peptides in experimental animals following solution instillation into the lung.

Protein/Peptide	MW [kDa]	Animal	T_{max}[1] [hrs]	BA%[2] [%]	Reference[3]
RGD peptide*1	0.7	rat	0.68	22	Adjei, 1997
GHR peptide*2	0.9	dog	0.17	43	Adjei, 1997
DDAVP*3	1.1	rat	1.3	20-45	Adjei, 1997
Cyclosporin	1.2	dog	1.0	N/A	Adjei, 1997
Leuprolide	1.2	dog	0.37	5-59	Adjei, 1997
Detirelex	1.7	dog	7.6	27	Adjei, 1997
Somatostatin28	3.1	rat	< 1	N/A	Adjei, 1997
VIP*4	3.3	rat	< 1	N/A	Adjei, 1997
Calcitonim	3.4	rat	0.25	17	Adjei, 1997
Glip	3.5	rat	0.17	3.5	Patton, 1998
Glucagon	3.5	rat	< 1	N/A	Adjei, 1997
PTH*5	4.3	rat	0.25	8	Patton, 1998
Insulin	5.8	rat	0.33	14	Okumura, 1992
GM-CSF*6	17.7	rat	0.50	16.9	Patton, 1998
G-CSF*7	18.6	rat	2.5	12	Niven, 1994
IFN-α*8	19.0	rat	4.5	19-56	Adjei, 1997
hGH *9	22.0	rat	6.0	3-36	Colthorpe, 1995
Albumin	68.0	rat	20.0	4.5	Adjei, 1997
IL-1R*10	90.0	rat	12.0	17.7	Patton, 1998
IgG*11	150.0	rat	16.0	1.7	Adjei, 1997

[1] T_{max} is used for an indicator of absorption rapidity, though it is a fucntion of both absorption and elimination; [2] bioavailability relative to subcutaneous injection and [3] only first authors and years of publication; details are described in References.

*1 Arginine-glycine-aspartic acid peptide; *2 glycine-histidine-arginine peptide;
*3 1-deaminocysteine-8-D-arginine vasopressin; *4 vasoactive intestinal peptide; *5 parathyroid hormone;
*6 granulocyte-macrophage colony-stimulating factor; *7 granulocyte colony-stimulating factor;
*8 interferon-α; *9 human growth hormone; *10 interleukin-1 receptor and *11 immunoglobulin G

Table I.3. Statistics of human lung and its cells, compared to Sprague-Dawley rat.

	Human (70 kg)	**SD rat** [1] (0.3 kg)	**Reference** [2]
Airway branching pattern	Relatively symmetrical	Strongly monopoidal	Warheit, 1989
Number of branches	23-26	12-20	Warheit, 1989
Surface area [m^2]			
Alveoli	102	0.4	Stone, 1992;
Tracheo-bronchi	~2.5	~0.01	Mercer, 1994
Cellular thickness [μm]			
Alveoli	0.2	0.1	Murchie, 1993;
Tracheo-bronchi	10-58	13.2	Patton, 1996
Lining fluid volume [mL]			
Alveoli	7-20	0.08*[1]	Anderson, 1992;
Tracheo-bronchi	4-9	N/A*[2]	Patton, 1996
Alveoli			
Lining fluid thickness [μm]	0.07	0.2	Weibel, 1963; Bastacky, 1995
% surface of type I	92.9	96.4	Crapo, 1982;
% surface of type II	7.1	3.6	Warheit, 1989
Estimated pore diameter [nm]			
Alveoli	N/A*[2]	0.4, 50	Chandra, 1992
Tracheo-bronchi	N/A*[2]	14-19	
Mucociliary clearance			
Rate [mm/min]	0.5-21	4.5	Byron, 1986;
half-life [min]	0.7, 4.2	0.6-1.3	Taylor, 1994; Adjei, 1997

[1] Sprague-Dawley; [2] Only first authors and years of publication; details are described in References.
*[1] Calculated from (fluid thickness x surface area); *[2] not available.

(102 m^2 *vs.* ~2.5 m^2; Stone *et al.*, 1992; Mercer *et al.*, 1994; Patton, 1996). Furthermore, the barrier thickness in the alveolar region is known to be ≤ 1.0 μm (often 0.1-0.2 μm), which is much thinner than ≥ 10 μm of that in the tracheo-bronchial airways (Patton, 1996). It is quite reasonable to believe therefore, that the alveolar membranes are favorable for large solute absorption, although clearly deep lung delivery via inhalation is required (Byron and Patton, 1994; Patton, 1996).

Alveolar membranes are composed of alveolar epithelium (adjacent to the airways), basement membrane and capillary endothelium (adjacent to the blood vessels; Corrin, 1987). As the barrier becomes thick, alveolar epithelium and capillary endothelium are separated by an interstitial space (the origin of the lung lymphatics; Corrin, 1987). On the epithelial cell surface, there is a smooth lining fluid layer, topped with a monomolecular layer of surfactant. The overall thickness of this barrier ranges from 0.1 to 1 μm (0.2 μm in average; Table I.3). Between epithelium and endothelium, it has been shown that small solute permeation through capillary endothelium proceeds 10 to 100 times faster than that through alveolar epithelium (Barrowcliffe and Jones, 1987). In mammalian lungs, the equivalent pore radii calculated from physiological studies are 0.6-1.0 nm for the epithelium and over 4.0-5.8 nm for the endothelium, showing the latter to be much more permeable to solutes and proteins (Taylor *et al.*, 1965; Taylor and Gaar, 1970; Gorin and Stewart, 1979; Lanken *et al.*, 1985; Effros *et al.*, 1986; Barrowcliff and Jones, 1987). The interstitial space and the basement membrane is believed to be an insignificant barrier for solute and fluid transport, compared to either the epithelial or endothelial membranes

(Corrin, 1987). It is likely therefore, that alveolar epithelium is the most formidable barrier for solute absorption from this alveolar region. Indeed, a microscopic study demonstrated that horseradish peroxidase (MW = 44 kDa) could hardly penetrate to the interstitium following airway administration, even though it was abundantly observed in the interstitium after intravenous administration (Lee, 1990; McLaughlin *et al.*, 1993).

As opposed to the four major cell types found in the tracheo-bronchial airway epithelium, the alveolar epithelium is composed of only two principal cells. These are known as type I (squamous or membranous pneumocyte) and type II (granular pneumocyte) cells (Corrin, 1987). Type I cells are observed microscopically as flattened cells, covering 93-97 % of alveolar surface (Table I.3), and are known to have few cytoplasmic organelles (Burri, 1983). It appears that these cells are incapable of mitotic division (Corrin, 1987) and their basic physiological function is believed to prevent fluid loss into the airways, yet facilitate rapid gas exchange (Burri, 1983; Corrin, 1987). In contrast, type II cells are observed as cuboidal cells, which function to maintain and repair the type I cell population by proliferation (Williams, 1990). These cells are also responsible for secreting surfactant and regulating fluid balance and interestingly, have much higher metabolic function than type I pneumocytes (Willams, 1990). Type I cells are connected to each other or to type II cells in the epithelial layer by tight junctions, with type II cells generally occupying the "corners" of alveoli (Corrin, 1987; Williams, 1990). There is also a small number of alveolar type III cells distinguished by their brush

border, occasionally seen in rats, but not in the human (Meyrick and Reid, 1968; Burri, 1983). However, their function remains unclear.

Generally, solutes are believed to be absorbed by diffusion and/or partitioning. Typically, in the case of hydrophilic solutes like most proteins and peptides, the tight junctions (*zonula occludens*, ZO; Williams, 1990) are believed to be the primary morphological elements through which solutes can pass by paracellular absorption. Because the lipophilic nature of the cellular membranes is likely to prohibit the passage of hydrophilic macromolecular solutes, this would appear to be one possible route of transfer for these molecules. The tight junctions are now known to be complex structures of multiple proteins, which serve as intricate and dynamic fasteners of cells to each other (Schneeberger and Lynch, 1992). Alveolar epithelial tight junctions have been shown to form a network of 3 to 5 interconnected strands that are similar in appearance in both alveolar type I and type II cells (Schneeberger and Lynch, 1991). As an interconnected series of strands and grooves, it is believed that these can represent relatively impermeable structures in which channel-like discontinuities or "pores" reside. Such "pores" may alternate between open and closed configurations like channels in biomembranes (Claude, 1978; Reuss, 1991), and their tightness may respond to external stimuli (Bhat *et al.*, 1993; Wang *et al.*, 1993). Thus, it is possible that increased permeability through "opened" tight junctions may be one way in which macromolecules could enter the systemic circulation from the airways. These hypothesized aqueous "pores", representing various sizes in the pulmonary membrane, were demonstrated in early studies by Schanker in the rat (Enna and Schanker, 1972; Lanman *et al.*, 1973;

Burton and Schanker, 1974a and 1974b; Burton *et al.*, 1974; Schanker and Burton, 1976; Schanker and Hemberger, 1983; Brown and Schanker, 1983), although actual "pores" have yet to be confirmed by morphological studies.

As well as restricted diffusive transepithelial transport via tight junctions (paracellular absorption), it is now known that the alveolar epithelium, especially type I cells contain numerous cytoplasmic and cell-membrane-associated clathrin-coated and nonclathrin-coated, "caveolae". These represent vesicles that actively transport fluid, solutes and macromolecules including proteins and peptides (Patton, 1996; Campbell *et al.*, 1998). These endocytotic and/or transcytotic vesicles have been observed microscopically with diameters of 50-100 nm within the cytoplasm of both alveolar type I and type II epithelial cells (Williams, 1990; Williams, 1992; Campbell *et al.*, 1998). Although the subject of vesicular trafficking is complex (Williams, 1990; Williams, 1992) and vesicles may be trafficked via multiple routes (Patton and Platz, 1992; Patton, 1996), this simple picture is at least capable of explaining some of the results for unexpectedly high macromolecular bioavailability shown in Table I.2 following solute administration into the airways. It is necessary in fact, to explain the rapid and extensive pulmonary absorption of insulin (5.7 kDa) and growth hormone (22 kDa), compared to the much slower absorption for similarly-sized inulin (5.3 kDa) and dextran (20 kDa), to propose either transcytotic protein absorption via active endocytotic mechanisms or spontaneous increases in the size of "pores" in the tight junctions induced by each solute's presence (Enna and Schanker, 1972; Takada *et al.*, 1978; Ohtani *et al.*, 1991; Colthorpe

et al., 1992; Folkesson *et al.*, 1992). If vesicular transport is the mechanism, which currently seems the most feasible, these vesicles must release their contents into the interstitium by exocytosis. The solutes could then subsequently traverse the capillary endothelial cell either by transcytosis or (more likely) simple diffusion through the more "leaky" intercellular endothelial junctions, and enter the systemic circulation (Williams, 1990; Williams, 1992).

In addition to these absorption processes, solutes deposited in the lung are also known to be subject to one or more of its natural defense mechanisms. The most rapid of these and thus, the most likely process to affect solute absorption, is that of mucociliary clearance (Lansley, 1993; Cammer and Mossberg, 1993; Kim and Folisbee, 1997). The process is known to occur due to ciliated cells in the conducting airways possessing cilia which beat in a coordinated fashion. This occurs within the periciliary fluid beneath a viscoelastic layer lining the respiratory tract (Lansley, 1993; Cammer and Mossberg, 1993; Kim and Folisbee, 1997) and hence, it is primarily believed to exist in tracheo-bronchial airways where ciliated cells are found microscopically. Nevertheless, recent evidence has also suggested the presence of an alveolo-bronchiolar clearance mechanism, in which migrating solutes, lining fluid and/or macrophages are transporterd from the alveoli to mucociliary clearance region, followed by subsequent mucociliary clearance (Green, 1973; Warheit, 1989). These clearance processes are believed to become slower as the respiratory tract is descended (Brain and Blanchard, 1993; Camner and Mossberg, 1993). Such clearance kinetics of small particles over 24 hours can be characterized using

a bi-exponential kinetic model with half-lives of 0.7 and 4.2 hours in the human. The latter half-life probably represents the half-life for alveolo-bronchiolar clearance (Byron, 1986).

Bi-exponential mucociliary clearance kinetics over 24 hours, as seen in the human (Byron, 1986), have yet to be demonstrated in small rodents like rats. While highly variable, apparent linear rates of mucociliary clearance in the tracheo-bronchial region were similar between the human and rat (0.5-21 vs. 4.5 mm/min, respectively; Table I.3); other long-term studies (≥ 24 hours) showed faster mucociliary clearance rates in small rodents (rats, guinea pigs and rabbits) than in large mammals such as dogs and humans (Snipes *et al.*, 1983; Warheit, 1989). Despite the uncertainties associated with the presence of alveolo-bronchiolar clearance and its interspecies differences, Taylor *et al.*, (1994) recently reported a value of 1.3 hours for the mucociliary clearance half-life for tin colloid in rabbits, following the colloids administration as an aerosol into the deep lung. This may represent a mixture between the alveolo-bronchiolar clearance rate and tracheo-bronchial rate in small rodents, since the value was larger than that of 0.6 hours for tracheo-bronchial mucociliary clearance obtained following intratracheal instillation (Taylor *et al.*, 1994). Furthermore, recent in vivo studies in rats and guinea pigs have shown that mucociliary clearance competes significantly with absorption following deep lung administration, especially when absorption is rate-determined (Lansley, 1993; Taylor *et al.*, 1994; Sakagami *et al.*, 1996; Byron *et al.*, 2000). It is likely therefore, that mucociliary clearance and alveolo-bronchiolar clearance transport macromolecular

solutes from their primary absorption depot in the lower airways quite efficiently, thus competing kinetically with absorption processes (Byron *et al.*, 2000).

Solute disposition in the lung following inhalation is a complex function of deposition and mucociliary clearance, active and passive absorption, tissue sequestration and metabolism (Byron, 1986; Byron and Phillips, 1990). Furthermore, different regions of the airways are believed to function differently, at least with respect to absorption and mucociliary clearance, as described above. In fact, the absorption could be active and/or passive from both alveolar and the tracheo-bronchial regions and region-specific, simultaneous mucociliary clearance could function competitively with both of the absorption. Unfortunately, the kinetic and mechanistic characterization of these processes is quite difficult due to a lack of appropriate experimental systems, and this largely remained theoretical (Byron, 1986; Byron and Phillips, 1990).

Whole rat studies in vivo have been combined with intratracheal instillation and used extensively in several laboratories (Enna and Schanker, 1972; Brain *et al.*, 1976; Takada *et al.*, 1978; Pritchard *et al.*, 1985; Folkesson *et al.*, 1996; Leong *et al.*, 1998). These studies have demonstrated some of the solute absorption characteristics from the airways, especially as they were related to solute partitioning, diffusion, size and electric charge (Enna and Schanker, 1972; Brown and Schanker, 1983). Some evidence of saturable active absorption via carrier proteins (Enna and Schanker *et al.*, 1973) has also been documented. Unfortunately, these studies require considerable animal sacrifice to

avoid the huge inter-rat variations in the derived data (Brain *et al.*, 1976; Pitchard *et al.*, 1985; Folkesson *et al.*, 1996; Leong *et al.*, 1998). Furthermore, much of the variation reported in the literature is associated with non-reproducible airway dosing (CV% > 15 %) and solute distribution in the lung and hence, because of the uncertainties related to the technique, inter-study comparisons are difficult. On the other hand, recent biotechnological advances have allowed scientists to utilize cell culture systems to study solute absorption and metabolism (Audus *et al.*, 1990). Specifically, cultured alveolar epithelial cell monolayers have been used increasingly to determine monolayer permeability to solutes (Wang *et al.*, 1993; Morimoto *et al.*, 1993; Kim and Crandall, 1996). These in vitro studies provide clear kinetic information specific to each type of cell monolayer. They can be manipulated easily by lowering temperatures and the use of absorption modulators and/or inhibitors, enabling the identification of possible mechanisms and pathways of absorption (Morimoto *et al.*, 1993; Kim and Crandall, 1996). Currently, alveolar type I cell monolayers can be cultured only from alveolar type II cells, followed by their differentiation (Cheek *et al.*, 1989; Kim and Crandall, 1996). However, there are many uncertainties and variables associated with lung cell isolation and culture, which remain undescribed in the literature [e.g., enzymes being used, contents and concentrations of culture media (Dobbs, 1990)]. Thus, methods rarely produce comparable results between laboratories and unfortunately, values for solute permeability through such monolayers hardly provide useful predictive information relating to solute absorption through the intact lung.

The Aerosol Research Group at Virginia Commonwealth University has employed the isolated perfused rat lung (IPRL) preparation, combined with the highly reproducible, "forced solution instillation" technique for solute administration into the airways for some years (Niven and Byron, 1988; Byron and Niven, 1990; Sun, 1995; Visich, 1996, Kovelesky, 1998). The preparation offers the "reality" of a whole lung organ housed in a well-controlled environment, without the complications of variability induced by the presence of respiration, variable blood flow, solute deposition and the presence of the remainder of the body (Levey, 1966; Mehendale *et al.*, 1981; Roberts, 1984; Niven, 1988). Even though the magnitude of the lung's mucociliary clearance had previously been unknown in this preparation, it appeared that some of its effects could be seen over the period of an absorption study (Byron *et al.*, 1986). Therefore, it was possible that the preparation could be used as an in vitro model providing rates and/or rate constants for solute absorption from the airways and for mucociliary clearance. Then, these values could also be used to interpret an otherwise, exceedingly complex in vivo situation following the assembly of data from a series of well-designed in vivo and in vitro studies. Because the preparation had been used previously, to illustrate the presence of a "difficult to characterize" polyaspartamide airway-to-pefusate transporter (Sun *et al.*, 1999), the IPRL was refined in this thesis, and used to investigate and characterize the mechanisms of absorption of same well-defined model polypeptides.

This dissertation targets the knowledge and model deficiency in the area of macromolecular pulmonary solute absorption and clearance and aims to enhance our

understanding of solute disposition in the lung following inhalation. By developing and validating the IPRL preparation as a model of the in vivo rat lung, it has proven possible to describe pulmonary solute disposition in the IPRL, in such a way that the kinetic behavior of the polyaspartamide transporter (Sun *et al.*, 1999) in vivo can be predicted. Because this transporter operates in the presence of simultaneous mucociliary clearance, it was necessary to first characterize the kinetics of that process, as it related to solute absorption from the airways. As a result, this thesis contains a unique kinetic analysis of lobar to tracheo-bronchial (mucociliary) solute clearance kinetics in the rat. By studying the effects of molecular weight, IPRL perfusion temperature and biochemical process inhibitors upon both poyaspartamide (PHEA) transport and the absorption of model solutes known to be absorbed passively, the magnitude of the PHEA transporter's carrying-power was explored in the rat lung. All of these processes are discussed with respect to their importance in the prediction of the biopharmaceutical properties of molecules delivered by inhalation.

CHAPTER II

HYPOTHESES

Theoretically, macromolecules and other solutes may be absorbed from the airways via vesicular endocytotic or transcytotic transport and/or diffusive transfer through intercellular tight junctions (paracellular pathways). However, precise analysis of absorption data in the lung is complex and may be confounded by the presence of competing mucociliary clearance. In fact, there is a general lack of appropriate models for interpreting the pulmonary disposition of solutes in vivo. Thus, the goal of this research was to determine and model the kinetics of macromolecular solute absorption from the airways of the rat lung in vivo and in vitro. Specifically, the characterization and study of the kinetics of the absorption mechanisms and pathways responsible for model polypeptidic polymers required the development and study of sophisticated disposition models in lung. Then, by studying the pulmonary disposition (in vivo and in vitro) of 4.3 and 7.4 kDa metabolically-stable polyaspartamides (F-PHEA), alongside that of small and large reference solutes, the thesis project was designed to test five major hypotheses. These were:

(a) That the in vitro isolated perfused rat lung (IPRL) possessed a viable mucociliary escalator that was kinetically indistinguishable from that in the whole rat. Thus, that macromolecular mucociliary clearance rates into the tracheo-bronchial regions of the lung would occur both in vivo and in vitro, and that absorption rates from the pulmonary regions of the IPRL should be predictive of those in vivo.

(b) That sophisticated kinetic models can be developed which incorporate mucociliary clearance and simultaneous active and passive solute absorption from the airways of the rat lung. Then, that a study of the pulmonary disposition of actively and passively transferred solutes, in a variety of doses, could be used alongside these models to correctly characterize the capacity and affinity of the airway-to-blood transporter for polyaspartamide (F-PHEA).

(c) That the IPRL preparation could be manipulated by its maintenance at lowered temperature and the presence of metabolic inhibitors. Then, that a similar modeling approach could be employed to determine the degree of inhibition of the polyaspartamide (F-PHEA) transporter.

(d) That the magnitude and nature of polyaspartamide transporter inhibition, afforded by the presence of metabolic and transcytosis inhibitors, should enable some of the transport mechanisms and pathway to be elucidated.

(e) That smaller molecular weight polyasparatamides possess increased passive airway-to-perfusate transport rates, while their active transport remains comparable to that of their large counterparts.

The work described in Chapters 3, 4 and 5 of this thesis were designed to test each of these hypotheses in turn. Chapter 3 is focused on hypothesis (a) and (b), and describes the development and in vivo validation of all the kinetic modeling to be employed throughout the remainder of the thesis. Chapter 3 is limited to work performed at 37 ^{o}C or the normal rat lung. Chapter 4 describes the effects of reduced temperature and biochemical inhibition upon the polyaspartamide transporter. In so doing, it tests hypothesis (c) and (d) above. In Chapter 5, the kinetic models are employed to test hypothesis (e) and to compare the passive and active components of polyaspartamide transport between a 4.3 kDa and a 7.4 kDa F-PHEA.

CHAPTER III

MODELING SOLUTE DISPOSITION IN THE RAT LUNG: EVALUATING REGIONAL ABSORPTION KINETICS IN VIVO AND IN VITRO, IN THE PRESENCE OF CILIARY CLEARANCE

III.a INTRODUCTION

Solute disposition in the lung following inhalation is a complex function of deposition and mucociliary clearance, active and passive absorption, tissue sequestration and metabolism. Because different regions of the airways are believed to function differently with respect to the way they handle solutes, complex kinetic models have been proposed to describe their disposition following inhalation (Fig. III.1; Byron, 1986; Byron and Phillips, 1990; Byron and Patton, 1994). Unfortunately however, such models are often largely theoretical due to a lack of appropriate experimental systems, which enable their study. For example, while conventional "textbook" wisdom states that passive absorption of xenobiotics is more rapid from alveoli than tracheo-bronchial airways (Brown and Schanker, 1983; Schanker *et al.*, 1986; Fig. III.1), proving such an assumption is quite difficult, since mucociliary clearance can complicate the analysis of

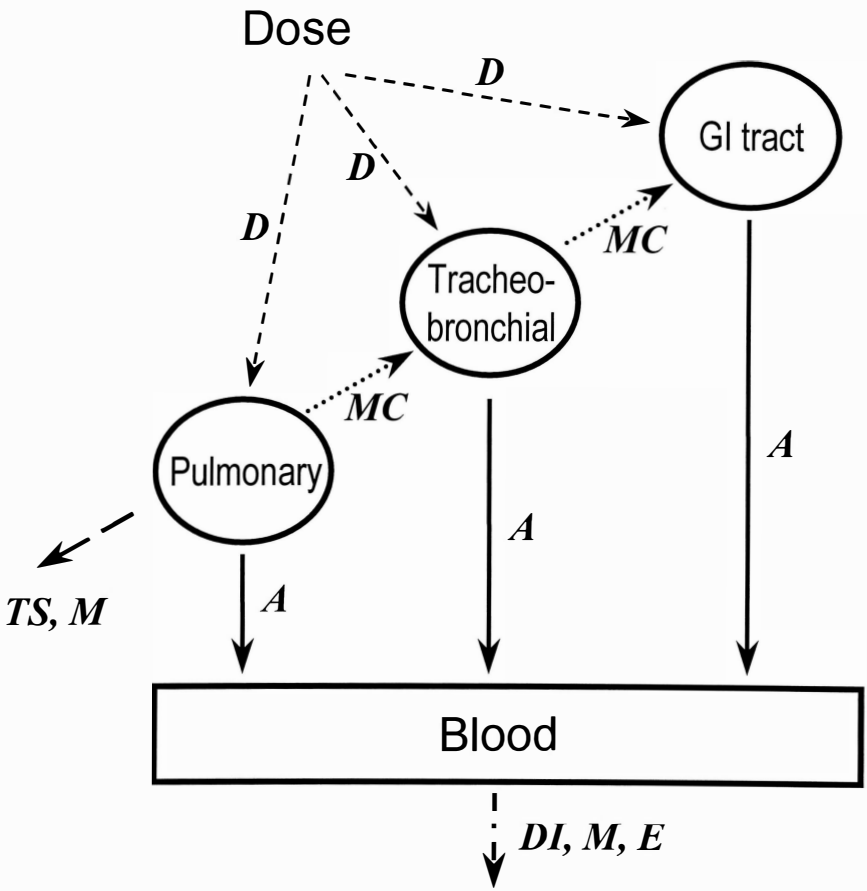

Figure III.1. A "mechanistic" kinetic model for solutes administered by inhalation. Key: *D* - deposition; *A* - absorption; *MC* - mucociliary clearance; *TS* - tissue sequestration; *M* - metabolism; *DI* - distribution; *E* - elimination. The model was originally proposed by Byron (1986) and has been modified and redrawn.

these absorption data (Colthorpe *et al.*, 1992; Byron *et al.*, 2000). Indeed, the eventual proof or disproof of assumptions like this must rely upon *either* the simultaneous kinetic analysis of in vivo data [for blood and several lung compartments in accord with model(s) like that shown in Fig. III.1] *or* an assembly of well-designed in vivo and in vitro studies, in which data and parameters from the in vitro models are well-correlated and can be incorporated in the analysis of the in vivo situation. Thus, such in vitro models are required for providing transport rates and/or rate constants, which can be used to interpret an otherwise, exceedingly complex in vivo situation. The isolated perfused rat lung (IPRL), as used in this thesis will be shown to be ideal for this purpose. The preparation offers the "reality" of a whole lung organ housed in a well-controlled environment, without the complications of variability induced by the presence of respiration, variable blood flow, solute deposition and other biological variations due to the presence of the remainder of the body (Levey, 1966; Mehendale *et al.*, 1981; Roberts, 1984; Niven, 1988).

In this chapter, the IPRL will be shown to possess a viable, reproducible, solute-independent mucociliary clearance that is kinetically indistinguishable, statistically, from that in the whole rat. By careful selection of non-sequestered and non-metabolized solutes [TS = M = 0; Fig. III.1; Appendix V] and their airway administration in vivo and in vitro (IPRL), solute absorption rates from the IPRL will be shown to be predictive of those from the pulmonary lung compartment in vivo. Using improved kinetic analyses based on the model shown in Fig. III.1, the capacity and affinity of a previously reported,

active transport process for macromolecular absorption (Niven *et al.*, 1990; Byron *et al.*, 1991, Byron *et al.*, 1994; Sun, 1995; Sun *et al.*, 1999) will be evaluated and shown to be a property of only the pulmonary region of the rat lung preparation (that region which is perfused by the pulmonary circulation). For these purposes, solute disposition kinetics of model small and macromolecules [376 Da sodium fluorescein (F-Na), 4.4 kDa FITC-labeled dextran 40 (FD-4) and 7.4 kDa fluorophore-labeled polyhydroxy-ethylaspartamide (F-PHEA)] following identical initial regional distribution in the lung were followed with time in the IPRL and compared to those seen in vivo.

III.b MATERIALS AND METHODS

III.b.1 MODEL SOLUTES: F-Na, FD-4 AND F-PHEA

Sodium fluorescein (F-Na; 376 Da) and the macromolecular polysaccharide, FITC-labeled dextran (FD-4; weight- (Mw) and number- (Mn) averaged molecular weights = 4.4 and 3.4 kDa; polydispersity, P_d (Mw/Mn) = 1.3) were purchased from Sigma Chemical Company (St. Louis, MO). These model solutes were used as indicators for passive absorption in the IPRL and/or in vivo (Byron *et al.*, 1986; Matsukawa *et al.*, 1997). Weight-averaged 7.4 kDa fluorophore-labeled poly-α,β-[N(2-hydroxyethyl)-D,L-aspartamide] (F-PHEA) was synthesized, purified and characterized by Dr. Frantisek Rypacek at the Institute of Macromolecular Chemistry, Czech Academy of Sciences,

Prague, Czech Republic (Niven *et al.*, 1990 and Appendix III). This was used as a non-metabolized model macromolecule with a peptidic backbone in the IPRL, which was known to be absorbed by a combination of active and passive mechanisms into perfusate (Niven *et al.*, 1990; Byron *et al.*, 1991, Byron *et al.*, 1994; Sun, 1995; Sun *et al.*, 1999). All these molecules are shown in Fig. III.2. Briefly, F-PHEA was synthesized as follows: polysuccinimide (PSI), prepared by polymerization of D,L-aspartic acid, was reacted with small amounts of 2-aminoethyl-carbonyl-6-aminofluorescein (to give F-PSI with 0.3 mole% of fluorophore with respect to monomer subunits). F-PSI was reacted with excess ethanolamine to give the completely ring-opened product, F-PHEA. Following purification and lyophilization, the polymer was characterized in terms of its molecular weight distribution (MWD) by high performance gel permeation chromatography (HPGPC) or calibrated columns (Appendix III). The single batch of F-PHEA (FR7150) used throughout these experiments had a weight- (Mw) and number- (Mn) averaged molecular weights of 7420 and 6620 Da, respectively, and a polydispersity (P_d=Mw/Mn) of 1.12 (Appendix III). Its fluorophore content was 0.3 mole% with respect to the monomer (Appendix III).

III.b.2 ANIMALS

The research adhered to the NIH Principles of Laboratory Care and was approved by the Institutional Animal Care and Use Committee (IACUC; Project 9710-2468) at

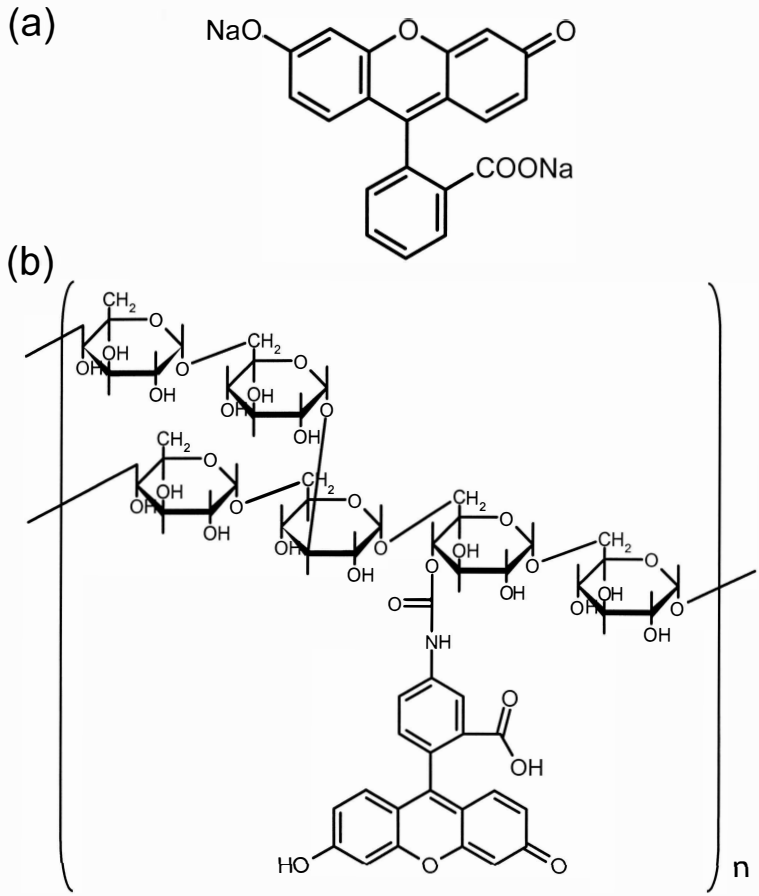

Figure III.2. Chemical structures of model solutes used in the IPRL and the in vivo studies: (a) sodium fluorescein (F-Na); (b) FITC-labeled dextran 4000 (FD-4). Weight- (Mw) and number- (Mn) averaged molecular weights of FD-4 (Lot 106H1180) were 4400 and 3385, respectively, with a polydispersity (Mw/Mn) = 1.3. FITC-substitution sites are randomly associated with any free hydroxyl group (De Belder and Gratath, 1973). In the above diagram, the fluorophore is shown attached at the 4-hydroxyl for illustrative purposes only. The degree of fluorophore substitution was 0.5 mole% fluorophore per glucose unit.

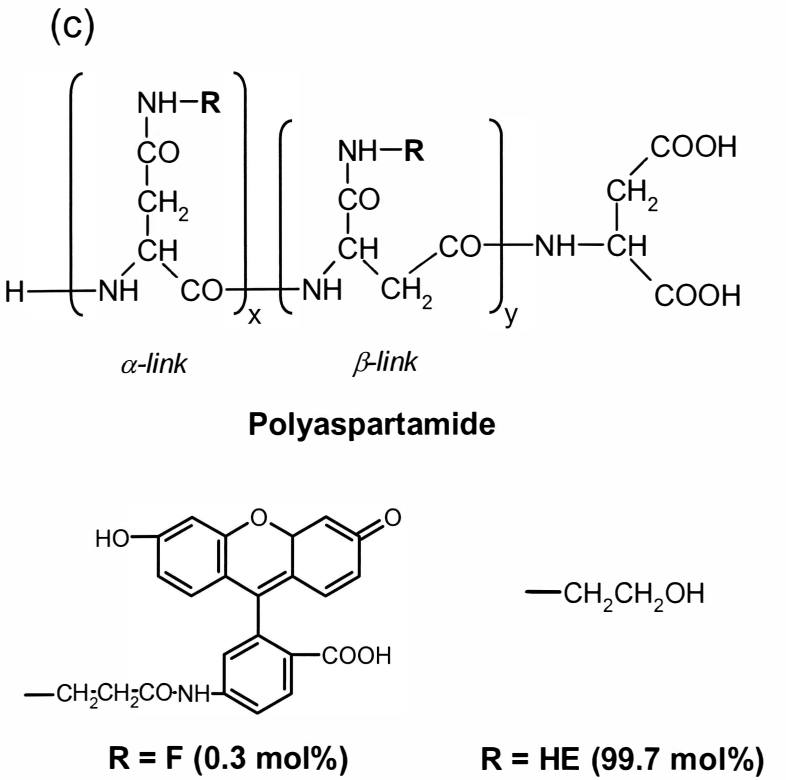

Figure III.2. Chemical structure of model solutes used in the IPRL and the in vivo studies: (c) fluorophore-labeled poly-α,β-[N(2-hydroxyethyl)-D,L-aspartamide] (F-PHEA). Weight- (Mw) and number- (Mn) averaged molecular weights of F-PHEA were 7420 and 6620, respectively, with a polydispersity (Mw/Mn) = 1.12. The polymer was labeled randomly with 0.3 mole% of fluorophore with respect to monomer subunits; the remaining R-groups were hydroxyethyl. The ratio of x:y is believed to be approximately 50 % (Niven and Byron, 1988; Sun, 1995, Sun *et al.*, 1999).

Virginia Commonwealth University. Specific pathogen free (C.V.F.-certified virus free), male Sprague-Dawley rats weighing 310-390 g were purchased from Hilltop Lab Animals Inc. (Scottsdale, PA). Prior to experimentation, the animals had free access to water and food and were housed in rooms controlled between 18-26 ^{o}C and 40-70 % relative humidity. Dark-light cycling occurred every 12 hours and animals were acclimated for $\geq$ 7 days prior to use.

III.b.3 IN VIVO LUNG ABSORPTION FOLLOWING "FORCED SOLUTION INSTILLATION"

A series of in vivo whole animal studies were performed using methods modified from those developed by Enna and Schanker (1972), but employing the reproducible "forced solution instillation" technique for solute administration into the airways described by Byron and Niven (1988). Rats were anesthetized by intraperitoneal injection of pentobarbital (50 mg/kg; Abbott Laboratories, North Chicago, IL). Each rat was placed in the supine position and the trachea cannulated with a stainless cannula (od = 2.2 mm, id = 1.9 mm, length = 32 mm) at its 4th cartilaginous ring and tied in place; 22 mm of the cannula was inserted into the trachea from the 5th tracheal cartilaginous ring. Immediately following natural expiration, a metal dosing cartridge (od = 1.2 mm, id = 1.0 mm, length = 138 mm) containing nominal doses of F-Na (0.02 mg) or F-PHEA (0.2 and 1.0 mg) in 0.1 mL aqueous solution was inserted through the tracheal cannula until its tip

was projected 0.5 mm beyond the cannula terminus, into the trachea. The dosing solution was administered as a coarse spray into the airways by a single actuation of a propellant-only metered dose inhaler (25 μL; Byron and Niven, 1988; Sun, 1995; Sun *et al*., 1999); this inflated the lung with about 5.5 mL of propellant vapor and simultaneously, accomplished "forced solution instillation" (Byron and Niven, 1988; Sun, 1995; Sun *et al*., 1999). The dosing cartridge was removed within 1-2 seconds of actuation allowing the recommencement of normal respiration. Body temperatures and anesthesia were maintained using a heat lamp and repeat pentobarbital injection (25 mg/kg every 60 minutes). The tracheal cannula was left in place throughout each experiment, irrespective of the time allowed for absorption to preclude solute absorption from swallowed materials. At the end of each experiment, the cannula was washed and solute remaining in the cannula was determined by the validated analytical methods described in Section III.b.5 and Appendix IV. At different time intervals following administration (sacrifice times of 0, 5, 10, 20, 30, 60, and 120 minutes for F-Na and 0, 5, 10, 20, 30, 45, 60, 120 and 180 minutes for F-PHEA following administration), solute remaining in each lung region was determined as follows: the thorax was opened and the ribs flapped backward to expose the lungs. The tracheal cannula was attached to a positive pressure ventilator (tidal volume = 4.5 mL and respiration rate = 16 /min; Model 802, New England Medical Instruments Inc., Medway, MA). The pulmonary artery was cannulated through the upper right ventricle and the bottom of the left auricle and both sides of each ventricle were promptly amputated and the blood flushed from the lung by continuous free perfusion of oxygenated Krebs-Henseleit buffer solution containing 4 % (w/v) bovine serum albumin

(pH 7.4) at a flow rate of 15 mL/min for 1-2 minutes (Byron and Niven, 1988; Sun, 1995; Appendix II). The lungs were then removed from the body exactly as if an IPRL preparation was to be performed (Byron and Niven, 1988; Sun, 1995; Appendices I and II) except that the removal was immediately followed by a visual inspection for any signs of pulmonary edema (glossy appearance on lung lobes; Roberts, 1984, Sun, 1995; Sun *et al.*, 1999); lung preparations showing edema were discarded. The complete procedure from the first incision to tissue isolation was accomplished in ≤ 5 minutes. Viable lungs were dissected into tracheo-bronchi and the five lung lobe regions (left lung (L), right postcaval or median lobe (PC), right superior or apical lobe (RS), right middle lobe (RM) and right inferior or diaphragmatic lobe (RI)). At each sacrifice time, four rats with fully viable lungs were studied for each dosing solution. Each lung region was weighed and homogenized (10,000 rpm for 2 minutes; Biohomogenizer, Fisher Scientific, Springfield, NJ) in phosphate buffered saline (PBS; pH 7.4, 0.05 M phosphate in 0.15 M NaCl solution). Homogenates were centrifuged (Fisher Scientific, Springfield, NJ) at 1,500 g for 15 minutes, the supernatants filtered (0.45 μm nylon, 4 mm, Alltech Associates, Deerfield, IL) and the solute remaining uncleared determined by the validated analytical methods described in Section III.b.5 and Appendix IV. The absorption results were expressed as mean % of administered dose remaining to be absorbed in the lung ± sample standard deviation *vs.* time. The individual results from each rat are reported in detail in Appendix VII.

III.b.4 PULMONARY ABSORPTION IN THE IPRL FOLLOWING "FORCED SOLUTION INSTILLATION"

The IPRL preparation and the dosing method ("forced solution instillation") are carefully controlled in these laboratories and have been described in detail previously (Byron and Niven, 1988 and Appendix I). They were used unchanged in this thesis. Briefly, a rat lung was surgically removed and housed in an artificial glass thorax (AGT) maintained at 37 ^{o}C. Krebs-Henseleit solution with 4 % (w/v) bovine serum albumin was used as perfusate (200 mL) and recirculated through the pulmonary circulation via the pulmonary artery at a constant flow rate of 15 mL/min. A metal dosing cartridge containing nominal doses of F-Na (0.01, 0.02 and 0.04 mg), FD-4 (0.1 and 0.2 mg) or F-PHEA (0.1, 0.2, 0.5, 1.0 and 5.0 mg) in 0.1 mL aqueous solution was inserted into the trachea via a tracheal cannula; the tip of the cartridge was allowed to project 0.5 mm beyond the cannula's terminus into the trachea. A metered dose inhaler (containing propellants only) was connected to the dosing cartridge and cannula and actuated once (Byron and Niven, 1988; Sun, 1995; Sun *et al*., 1999). The dosing solution was propelled into the lung as a coarse spray and the lung was inflated simultaneously with 5.5 mL of propellant vapor ("forced solution instillation"). The dosing cartridge was removed and the lung allowed to deflate to a residual volume dictated by the maintenance of 2-5 cm H_2O negative pressure in the artificial glass thorax (AGT; Fig. AI.1 in Appendix I). At 37 ^{o}C, the IPRL viability was maintained for 180 minutes as evidenced by the absences of any sign of edema and/or a discontinuous increase in the amount of solute absorbed into

the perfusate (Roberts, 1984; Sun *et al*., 1999; Appendix I). The perfusate samples were taken from a well-mixed reservoir at different time intervals following administration. Solute concentrations in the perfusate were determined by using validated analytical methods described in Section III.b.5 and Appendix IV. Four fully viable preparations were studied for each dosing solution and the results expressed as mean % of administered dose transferred to perfusate ± sample standard deviation *vs.* time. Individual results from each IPRL are reported in Appendix VII.

In some experiments, the initial and the final regional solute distributions in the IPRL were studied in groups of four IPRL preparations. In these experiments, IPRL perfusion was halted either immediately after administration (for initial distribution) or at the end of the experiment (120 and 180 minutes following administration for F-Na and F-PHEA, respectively). Subsequently, the lung was removed from the artificial glass thorax (AGT) and dissected into tracheo-bronchi and five lung lobe regions, as described above. Following homogenization and clean up, remaining solutes were determined by using validated analytical methods described in Section III.b.5 and Appendix IV. The absorption results from each group (n=4) were expressed as mean % of administered dose ± sample standard deviation. The individual results from each IPRL are reported in Appendix VII.

III.b.5 QUANTITATIVE DETEMINATION OF MODEL SOLUTES IN AQUEOUS, PERFUSATE AND LUNG HOMOGENATE SAMPLES

Highly sensitive and quantitative determination methods for F-Na, FD-4 and F-PHEA in aqueous, perfusate and lung homogenate samples were developed and validated, as described in Appendix IV. Fortunately, there was no evidence of lung tissue binding seen with any of these solutes; homogenate supernatants contained ≥ 98 % of the expected concentrations of fluorophore in all cases (Appendix IV). Solutes in aqueous and perfusate samples were analyzed directly or following appropriate dilution by the methods described below for F-Na, FD-4 and F-PHEA. Those in lung were determined by either fluorimetry or HPGPC after filtration of supernatant samples (0.45 μm nylon, 4 mm, Alltech Associates, Deerfield, IL), derived from centrifugation (Marathon 22K; 1,500 g for 15 minutes; Fisher Scientific, Springfield, NJ) following lung homogenization in 10 mL phosphate buffered saline (PBS; pH 7.4, 0.05 M phosphate in 0.15 M NaCl solution) at room temperature using a Biohomogenizer (10,000 rpm for 2 minutes; Fisher Scientific, Springfield, NJ).

(1) F-Na

F-Na was analyzed by fluorimetry using a luminescence spectrometer (Model LS 50; Perkin Elmer Ltd., Norwalk, CT; λ_{ex} = 490 nm and λ_{em} = 520 nm) with 3 mL (1 cm) quartz cells (Fisher Scientific, Pittsburgh, PA) following appropriate (≥ 10-fold) sample dilution with 0.1 M NaOH. At these wavelengths, it was found that substantial

fluorescence intensity could originate both from the perfusate and the filtered, centrifuged supernatants of lung homogenate. However, this background fluorescence was ≤ 10 % of fluorescence due to F-Na in all cases, and could be successfully minimized by sample dilution. The LOD for F-Na in the worst case scenario (perfusate samples following 11-fold dilution) was 0.55 ng/mL. The calibration curves for fluorescent intensity due to F-Na concentration were found to be linear within a range of 2-50 ng/mL with precision and accuracy, indicated by RSD (relative standard deviation; n = 6) ≤ 3.0 % and %error (DFN; % difference from nominal; n = 6) ≤ 9.1 % in all cases.

(2) FD-4 and F-PHEA

Irrespective of the analytical matrix, FD-4 and F-PHEA were analyzed by high performance gel permeation chromatography (HPGPC) coupled with fluorescence detection (Model RF-535; Shimadzu Corporation, Kyoto, Japan; λ_{ex} = 486 nm and λ_{em} = 516 nm). The HPGPC column was a Separon^{TM} HEMA-Bio 40 column (8 x 250 mm, 10 µm particle size; Tessek Ltd., Prague, Czech Republic) with a guard column, HEMA-Bio 40 (4.6 x 10 mm, 10 µm particle size; Tessek Ltd., Prague, Czech Republic) and mobile phase of phosphate buffered saline solution (PBS; pH 7.4, 0.05 M phosphate in 0.15 M NaCl solution) supplied at 1.0 mL/min. The protein content of the perfusate and/or the filtered supernatants of lung homogenates contained a fluorescent component interfering with the early peak portion of FD-4 and F-PHEA chromatograms following their direct injection into the HPGPC system. Thus, a rigorous curve stripping *procedure was* employed for the area under the curve (AUC) determination of the chromatograms, as

described previously (Byron *et al.*, 1990; Sun, 1995; Appendix IV). Briefly, this involved subtracting blank, matrix-only, chromatograms from each test chromatogram. Corrected values for area under the curve (AUC) for each solute were linearly related to solute concentration over the ranges of 0.08-1.8 μg/mL (FD-4) and 0.3-2.5 μg/mL (F-PHEA). Subsequently, the calibration curves for each solute were found to be insignificantly different across matrixes (ANOVA), indicating the absence of quenching of solute fluorescence due to matrix or tissue binding effects in lung, for both of these solutes (Appendix IV). Sensitivity, precision and accuracy were determined in all cases and indicated for FD-4 and F-PHEA, respectively, by LOD ≤ 0.03 and ≤ 0.11 μg/mL, RSD ≤ 10.7 and ≤ 9.3 % and %error ≤ 8.8 and 8.2 % (n = 6).

III.b.6 A KINETIC MODEL FOR SOLUTE DISPOSITION IN THE AIRWAYS OF THE IPRL AND IN VIVO

A single kinetic model was proposed to describe the disposition of these solutes following their administration into the airways of the intact rat (in vivo) or the IPRL. This model is shown in Fig. III.3. The model assumed two lung regional components, separated based on their perfusion; the pulmonary (lobar) and tracheo-bronchial regions, which are perfused, respectively, by the pulmonary and the bronchial circulations. Tracheal cannulation throughout all of these experiments precluded absorption from the gastrointestinal (GI) tract. Our choice of solutes also precluded interference from

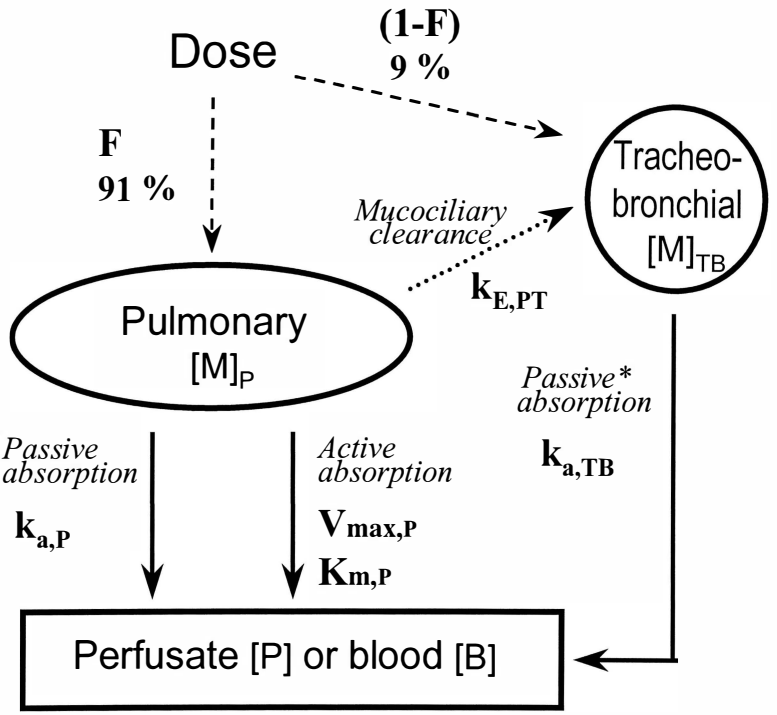

Figure III.3. A new kinetic model for solutes administered into the airways of the rat lung.
* Passive absorption from the tracheo-bronchial region is not present in the IPRL due to the severance of the bronchial circulation during surgery ($k_{a,TB} = 0$ in the IPRL).
Key: F - initial average penetration fraction following administration (0.91); $V_{max,P}$ and $K_{m,P}$ - the maximum rate and "affinity" of Michaelis-Menten-type active absorption, respectively; $k_{a,P}$ and $k_{a,TB}$ - first-order rate constants for passive absorption from the pulmonary and the tracheo-bronchial regions, respectively; $k_{E,PT}$ - first-order rate constant for mucociliary clearance.

metabolism and/or tissue sequestration (Niven, *et al.*, 1990; Byron *et al.*, 1991; Sun, 1995; Appendix V). In the IPRL, unlike the in vivo situation, the tracheo-bronchial perfusion is severed and hence, only pulmonary lobar absorption is possible ($k_{a,TB} = 0$ in Fig. III.3; Mehendale *et al.*, 1981); absorption from both regions is possible in the intact rat. Initially (immediately following administration), solutes were distributed between the two lung regions in a known and reproducible fashion. In practice, this resulted in an initial average penetration fraction, F = 0.91 of each administered dose, reaching the pulmonary region independent of either dose or solute (Section III.b.7). The absorption processes were assumed to be active (Michaelis-Menten-type) and/or passive (first-order kinetics) from the pulmonary region in the IPRL, while absorption from the tracheo-bronchial region in vivo was assumed to be first-order only ($k_{a,TB}$). Mucociliary clearance was assumed to be a viable, equivalent first-order process ($k_{E,PT}$) in both preparations (Byron, 1986).

Thus, in the case of the IPRL, it follows that the rate of change for the amount of solute in perfusate, d[P]/dt due to active, passive or simultaneous active *and* passive absorption, from the pulmonary region can be described, respectively as:

$$(d[P]/dt)_{Active,IPRL} = V_{max,P} \cdot [M]_P / (K_{m,P} + [M]_P) \qquad \text{(Eqn. III.1)}$$

$$(d[P]/dt)_{Passive,IPRL} = k_{a,P} \cdot [M]_P \qquad \text{(Eqn. III.2)}$$

$$(d[P]/dt)_{Active+Passive,IPRL} = V_{max,P} \cdot [M]_P / (K_{m,P} + [M]_P) + k_{a,P} \cdot [M]_P \qquad \text{(Eqn. III.3)}$$

Similarly, the rates of change for the amounts of solute in the pulmonary, tracheo-bronchial and total (pulmonary + tracheo-bronchial) lung compartments are described, respectively as:

$$(d[M]_P/dt)_{IPRL} = - (d[P]/dt) - k_{E,PT}\cdot[M]_P \quad \text{(Eqn. III.4)}$$

$$(d[M]_{TB}/dt)_{IPRL} = k_{E,PT}\cdot[M]_P \quad \text{(Eqn. III.5)}$$

$$(d[M]_{P+TB}/dt)_{IPRL} = - (d[P]/dt) \quad \text{(Eqn. III.6)}$$

where [P] is the cumulative solute amount absorbed from the pulmonary region into the recirculating perfusate of the IPRL, $[M]_P$, $[M]_{TB}$, $[M]_{P+TB}$ are the solute amounts remaining to be absorbed from the pulmonary, tracheo-bronchial and total lung airway regions, respectively; $V_{max,P}$ is the maximum rate of active absorption, $K_{m,P}$ is the "affinity" or dose at which the active absorption rate = $0.5\cdot V_{max,P}$, $k_{a,P}$ is the first-order passive absorption rate constant from the pulmonary region and $k_{E,PT}$ is the first-order mucociliary clearance rate constant from the pulmonary to the tracheo-bronchial region. It should be noted that the rates of change for solute amount in the perfusate of the IPRL, d[P]/dt, is a function of the solute amount remaining to be absorbed from the pulmonary region, $[M]_P$ (Eqns. III.1-3) and thus, a function of the mucociliary clearance rate constant, $k_{E,PT}$.

In vivo, when absorption into blood can also occur via the bronchial circulation, an additional passive absorption rate from the tracheo-bronchial region ($k_{a,TB}\cdot[M]_{TB}$) is

required in the model, even though mucociliary clearance and absorption from the pulmonary region were assumed equivalent to those in the IPRL. As a result, the rates of change for solute amounts in the blood, $d[B]/dt$, and the pulmonary, $d[M]_P/dt$, tracheo-bronchial, $d[M]_{TB}/dt$, and total (pulmonary + tracheo-bronchial; $d[M]_{P+TB}/dt$) lung compartments are described, respectively as:

$$(d[B]/dt)_{in\ vivo} = (d[P]/dt) + k_{a,TB}\cdot[M]_{TB} \qquad \text{(Eqn. III.7)}$$

$$(d[M]_P/dt)_{in\ vivo} = (d[M]_P/dt)_{IPRL} = -(d[P]/dt) - k_{E,PT}\cdot[M]_P \qquad \text{(Eqn. III.8)}$$

$$(d[M]_{TB}/dt)_{in\ vivo} = -(d[M]_{TB}/dt)_{IPRL} - k_{a,TB}\cdot[M]_{TB} \qquad \text{(Eqn. III.9)}$$

$$(d[M]_{P+TB}/dt)_{in\ vivo} = -(d[P]/dt) - k_{a,TB}\cdot[M]_{TB} \qquad \text{(Eqn. III.10)}$$

where $[B]$ is the cumulative amount of solute absorbed into the blood in vivo, $k_{a,TB}$ is the first-order passive absorption rate constant from the tracheo-bronchial region and $d[P]/dt$ is the rates of change for solute amount in the perfusate of the IPRL due to active, passive or simultaneous active *and* passive absorption from the pulmonary region, as described in Eqns. III.1-3. Therefore, the rates of change for cumulative solute amount in the blood circulation in vivo, $d[B]/dt$, remains a function of the mucociliary clearance rate constant, $k_{E,PT}$.

III.b.7 SIMULTANEOUS CURVE FITTING AND PARAMETER ESTIMATION

For each solute, curve fitting and parameter estimation to the model shown in Fig. III.3 was performed by unweighted, nonlinear least-mean-square regression analysis (Scientist™, MicroMath Scientific Software, Salt Lake City, UT) of all data, across doses following its collection from either the IPRL or the in vivo experiments.

(1) Curve fitting in the IPRL

In the IPRL, the unweighted data for mean % of administered dose transferred to perfusate *vs.* time was fitted across doses (e.g., all data points in Fig. III.10), in order to determine the best estimates of the solute-specific rate constants for each process. The fraction of the administered dose delivered to the pulmonary region, F, was fixed throughout this process at its experimentally-determined average value, 0.91 (0.910±0.003; mean±SD; n=12), so that the initial conditions were:

$[M]_{P,\ t=0}$ / [administered dose] = 0.91

$[M]_{TB,\ t=0}$ / [administered dose] = 0.09

$[P]_{t=0}$ / [administered dose] = 0.00

<F-Na and FD-4>

Absorption of F-Na and FD-4 in the IPRL was assumed to be passive and apparent first-order from the pulmonary compartment only. Accordingly, average data for % of

administered dose transferred to perfusate was fitted across doses to the following equations:

$$(d[P]/dt)_{Passive,IPRL} = k_{a,P} \cdot [M]_P \quad \text{(Eqn. III.2)}$$

$$(d[M]_P/dt)_{IPRL} = - (d[P]/dt) - k_{E,PT} \cdot [M]_P \quad \text{(Eqn. III.4)}$$

$$(d[M]_{TB}/dt)_{IPRL} = k_{E,PT} \cdot [M]_P \quad \text{(Eqn. III.5)}$$

with the initial conditions described above.

<F-PHEA>

Absorption of F-PHEA in the IPRL was assumed to be due to the sum of active (dose-dependent) and passive (first-order) processes from the pulmonary compartment. Accordingly, average data for % of administered dose transferred to perfusate was fitted across doses to the following equations:

$$(d[P]/dt)_{Active+Passive,IPRL} = V_{max,P} \cdot [M]_P/(K_{m,P} + [M]_P) + k_{a,P} \cdot [M]_P \quad \text{(Eqn. III.3)}$$

$$(d[M]_P/dt)_{IPRL} = - (d[P]/dt) - k_{E,PT} \cdot [M]_P \quad \text{(Eqn. III.4)}$$

$$(d[M]_{TB}/dt)_{IPRL} = k_{E,PT} \cdot [M]_P \quad \text{(Eqn. III.5)}$$

with identical initial conditions to those described above.

(2) Curve fitting in the intact rat

Absorption of F-Na in the intact rat was assumed to be due to the sum of its passive (first-order) absorption from both the pulmonary and the tracheo-bronchial compartments. Accordingly, average data for % of administered dose remaining to be absorbed was fitted to the following equations:

$$(d[B]/dt)_{in\ vivo} = (d[P]/dt) + k_{a,TB}\cdot[M]_{TB} \qquad \text{(Eqn. III.7)}$$

$$(d[M]_P/dt)_{in\ vivo} = (d[M]_P/dt)_{IPRL} = -(d[P]/dt) - k_{E,PT}\cdot[M]_P \qquad \text{(Eqn. III.8)}$$

$$(d[M]_{TB}/dt)_{in\ vivo} = -(d[M]_{TB}/dt)_{IPRL} - k_{a,TB}\cdot[M]_{TB} \qquad \text{(Eqn. III.9)}$$

$$(d[P]/dt)_{Passive,IPRL} = k_{a,P}\cdot[M]_P \qquad \text{(Eqn. III.2)}$$

with identical initial conditions to those described above.

The model fits were assessed using "goodness-of-fit" parameters, such as the program's calculated Model Selection Criterion (MSC), R-squared (R^2), a review of standard deviation of final parameter estimates and visual inspection of all residuals. Initial estimate assignment for each solute to initiate the fitting and additional methodological details are described in Appendix VI.

III.c RESULTS

III.c.1 INITIAL REGIONAL DISTRIBUTION OF SOLUTES IN LUNG: IN VIVO *VS.* THE IPRL

Because the regional deposition of solutes in the lung is believed to be a determinant of subsequent absorption and mucociliary clearance kinetics (Byron, 1986; Byron and Phillips, 1990; Colthorpe *et al.*, 1992; Byron and Patton, 1994; Hill *et al.*, 1996), it was necessary to ensure that "forced solution instillation", as used in this thesis, provided identical initial solute distribution both in vivo and in vitro. The percentages propelled from the identical dosing cartridges for F-Na (nominal dose = 0.02 mg) and F-PHEA (nominal dose = 1.0 mg), in vivo and in vitro are shown in Table III.1 alongside their coefficients of variation. Mean percentages propelled from the cartridge differed insignificantly across solutes and studies (ANOVA) and thus, dosing was highly reproducible (CV% $\leq$ 5.6 %) and solute/dose-independent. Figures III.4 and III.5 show initial regional distributions for F-Na and F-PHEA, respectively between the in vivo and in vitro studies. Despite preferential solute distributions in the left (L) lung and the right inferior (RI) lobe, it was found that overall regional lobar distribution of solutes was not effectively different across both solutes and studies. These results demonstrated that the "forced solution instillation" technique successfully provided identical initial regional distribution of solutes in the rat lung between in vivo and in vitro.

Table III.1. Percentages propelled from the dosing cartridge and their coefficients of variation (CV%) for F-Na and F-PHEA following "forced solution instillation" in vivo and in vitro (IPRL).

	In vivo		IPRL	
	% propelled from the cartridge[a]	CV%[b]	% propelled from the cartridge[a]	CV%[b]
F-Na[c]	92.28±5.18	5.6	94.73±1.70	1.8
F-PHEA[c]	97.25±1.92	1.8	93.35±3.78	4.1

Data: mean ± standard deviation (n=4)
% propelled from the dosing cartridge were not significantly different across solutes and studies (Two-way ANOVA).

[a] % propelled from the cartridge

$$= \frac{\text{(Loading dose) - (dose remaining in the cartridge)}}{\text{(Loading dose)}} \times 100$$

[b]

$$\text{CV\%} = \frac{\text{(Standard deviation)}}{\text{(Mean)}} \times 100 \quad (n = 4)$$

[c] Nominal doses: F-Na = 0.02 mg; F-PHEA = 1.0 mg

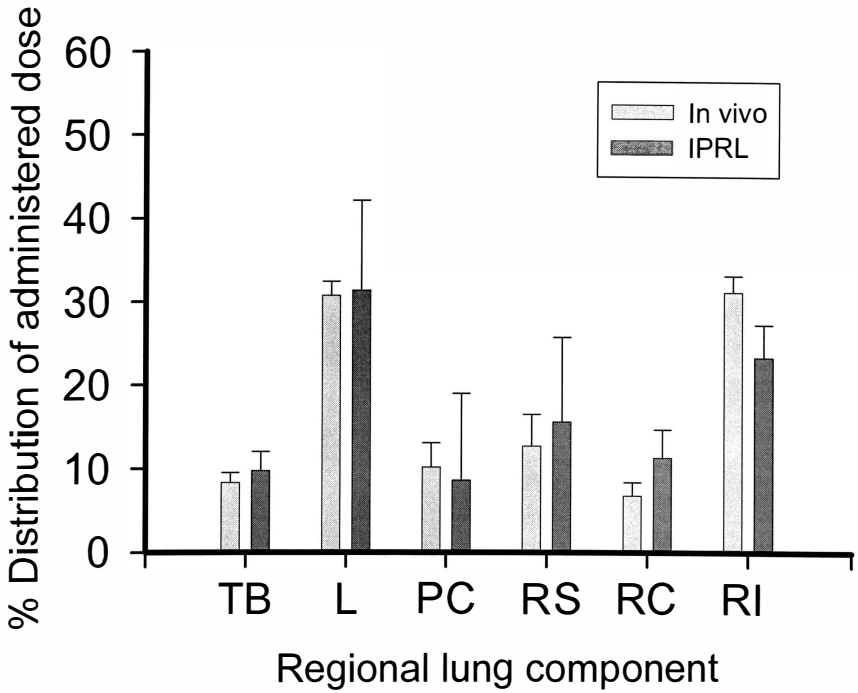

Figure III.4. Initial regional F-Na distribution in the lung following "forced solution instillation" in vivo and in vitro at a nominal dose of 0.02 mg. Error bars are sample standard deviations with n=4.
Overall regional distribution between the in vivo and the IPRL studies was found to be insignificantly different (Two-way ANOVA with an interaction). Keys: *TB* - trachea and major bronchi; *L* through *RI* = lobes e.g., *L* - left lung; *PC* - right postcaval; *RS* - right superior; *RC* - right center; *RI* - right inferior (Byron and Niven, 1988).

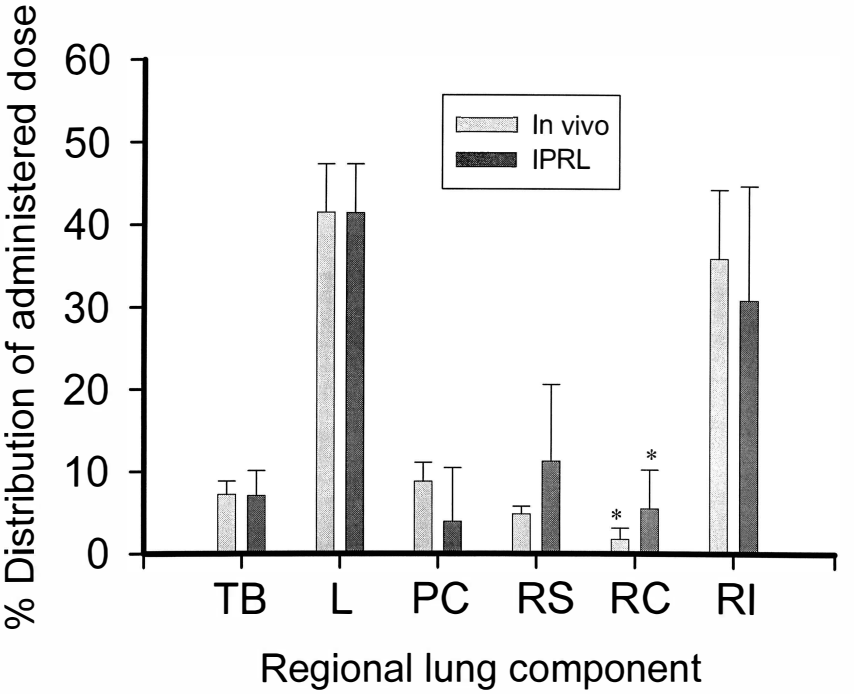

Figure III.5. Initial regional F-PHEA distribution in the lung following "forced solution instillation" in vivo and in vitro at a nominal dose of 1.0 mg. Error bars are sample standard deviations with n=4.
Regional distribution between the in vivo and the IPRL studies was found to be insignificantly different except right center (RC) distribution (Two-way ANOVA with an interaction). * indicates significant difference ($p<0.05$). Keys: *TB* - trachea and major bronchi; *L* through *RI* = lobes e.g., *L* - left lung; *PC* - right postcaval; *RS* - right superior; *RC* - right center; *RI* - right inferior.

III.c.2 ABSORPTION OF SODIUM FLUORESCEIN (F-Na) AND FITC-LABELED DEXTRAN (FD-4)

Average percent remaining (±SD) of the administered dose is shown in Fig. III.6 for F-Na in vivo and in vitro and FD-4 in the IPRL alone. Each data point of the in vivo profiles shows the mean of four separate rat experiments, while each IPRL curve is the mean of several doses (individual doses were repeated four times). Doses are defined in the figure legend. The IPRL profiles were calculated from Eqn. III.11, assuming mass-balance and an absence of tissue sequestration or metabolism (Appendix V):

(% of dose remaining in the lung)

= 100 % - (% of dose transferred to perfusate) (Eqn. III.11)

The solid curves drawn through the IPRL data in Fig. III.6 are the results of simultaneous curve fitting across doses to the model shown in Fig. III.3, assuming that solute transport occurred by passive absorption from the pulmonary region and simultaneous mucociliary clearance. Curves were generated from Eqns. III.2, III.4 and III.5 using "Scientist" along with the best estimates for the model's rate constants shown in Table III.2 for each solute. The solid curve drawn through the in vivo data for F-Na shows the result of linear regression of the log % remaining *vs.* time data. This showed first-order absorption from the lung with an "apparent" rate constant for absorption = 0.043 min^{-1} (half-life = 16.1 minutes). This value represents the rate constant for absorption, as it is determined using the empirical approach of Brown and Schanker (1983) and Schanker *et al.* (1986).

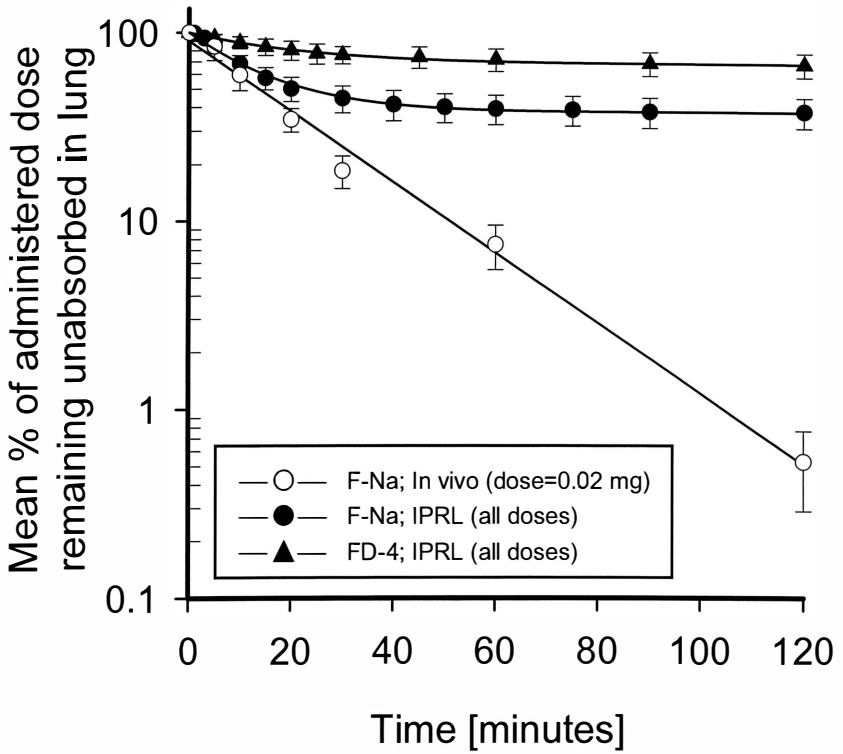

Figure III.6. Mean percentage of administered dose remaining to be absorbed from the rat lung *vs.* time from in vivo and IPRL studies. Error bars are sample standard deviations with n=4.
The IPRL curves are the results of simultaneous across-dose data fitting and the best estimates for each process are shown in Table III.2; the in vivo straight line is a regression of the profiles. All doses (IPRL): *F-Na* - 0.01, 0.02 and 0.04 mg; *FD-4* - 0.1 and 0.2 mg

Notably, while absorption in the intact rat was complete, in the IPRL, only 61.6±6.7 % was absorbed at all sample times ≥ 60 minutes across three doses of F-Na (n=4). This indicated the presence of a substantial unabsorbed portion of the dose (38.4 %; including 9.0 % of the initial tracheo-bronchial deposition) residing in the unperfused (tracheo-bronchial) lung regions at the effective completion of the IPRL absorption process. Absorption of macromolecular FD-4 was found to be slower than F-Na in the IPRL, leaving an unabsorbed residual of about 68.6 %. Thus, for FD-4, 31.4±9.3 % (mean±SD; n=32; at times ≥ 60 minutes) of the administered dose was absorbed, similarly reaching an asymptote at times ≥ 60 minutes following administration.

These asymptotic values for % remaining to be absorbed from the airways of the IPRL were consistent with the presence of a viable mucociliary clearance operating throughout the lifetime of the preparation. Dissection and assay for the % of solute remaining in the tracheo-bronchial and pulmonary lobar regions at fixed times following solute administration are shown for F-Na in Fig. III.7 resulting from both in vivo and in vitro experiments. While F-Na was absorbed from both regions of the lung in vivo (Fig. III.7 (a)), a substantial amount (> 30 %) of F-Na was found in the tracheo-bronchial region of the IPRL following its accumulation there by the mucociliary clearance. Notably, at the time of administration (t = 0), only 9 % of the dose was delivered to the tracheo-bronchial regions (Section III.b.7).

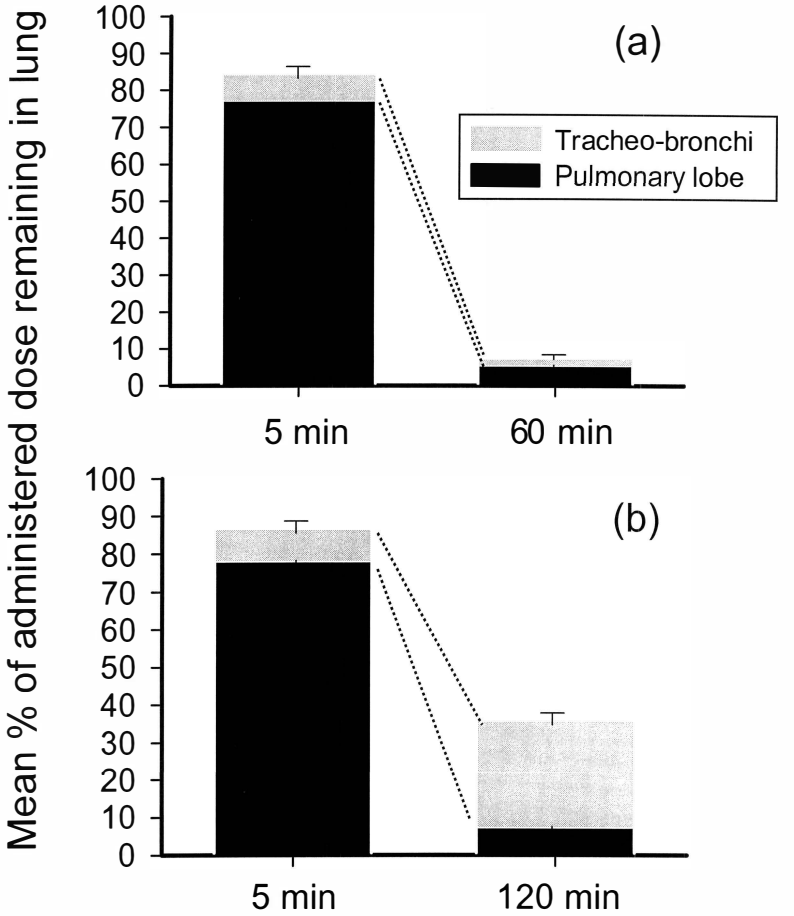

Figure III.7. Mean percentage (±SD; n=4) of administered dose of F-Na remaining to be absorbed from the tracheo-bronchial and the pulmonary lobar regions (a) in vivo and (b) in vitro at 5 and 60 or 120 minutes following administration.

III.c.3 ABSORPTION OF FLUOROPHORE-LABELED POLYHYDROXYETHYLASPARTAMIDE (F-PHEA)

Figure III.8 shows the percent of each administered dose of 7.4 kDa F-PHEA remaining to be absorbed *vs.* time following airway administration in vivo and in vitro at two nominal doses (0.2 and 1.0 mg). IPRL profiles were calculated from Eqn. III.11 by assuming mass-balance. Both pairs of profiles were statistically superimposable at each dose (ANOVA). Furthermore, the profiles were clearly dose-dependent and thus, absorption was non-first-order. At the lower 0.2 mg dose, only 60 % of the administered dose was absorbed, reaching an asymptote at times ≥ 60 minutes, similar to that seen in the case of F-Na in the IPRL (Fig. III.6).

The remaining mean % of administered dose of F-PHEA at 5 and 180 minutes following administration in vivo and in vitro are shown in Fig. III.9. Similar to the behaviors of F-Na in the IPRL, substantial amounts of F-PHEA were transported from the pulmonary into the tracheo-bronchial regions. There was no difference in these effects of the mucociliary clearance in vivo (Fig. III.9 (a)) or in vitro (Fig. III.9 (b); IPRL) at 180 minutes following administration. However, it appeared that a portion of the dose residing anatomically in the pulmonary region of the lung remained unabsorbed in the case of F-PHEA, while none of the dose which was deposited in, or transported to, the tracheo-bronchial region was absorbed in vivo and in vitro.

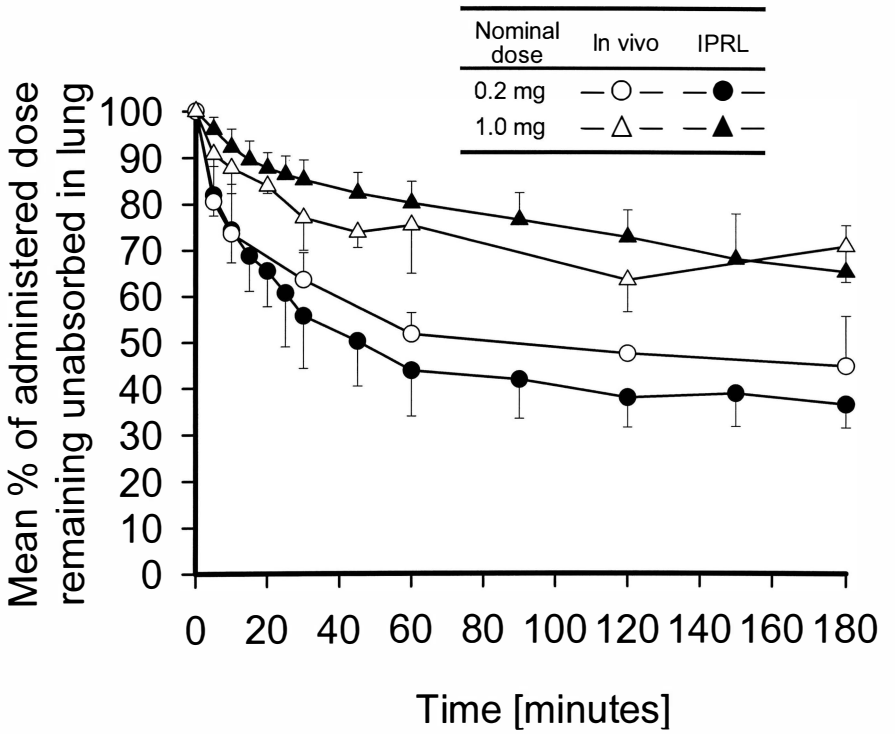

Figure III.8. Mean percentage of administered dose of 7.4 kDa F-PHEA remaining in the lung *vs.* time in vivo and in vitro. Error bars are sample standard deviations with n=4. The curves are the results of linear interpolation. There was no significant difference between in vivo and in vitro data at either of the dose levels tested (ANOVA).

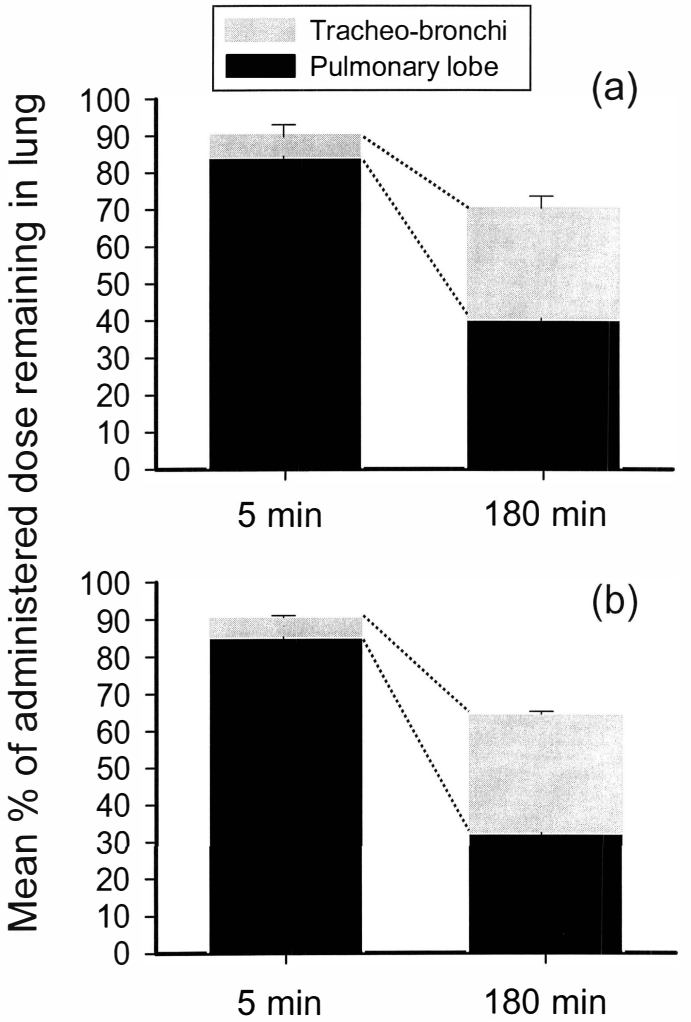

Figure III.9. Mean percentage (±SD; n=4) o f administered dose of F-PHEA remaining to be absorbed from the tracheo-bronchial and the pulmonary lobar regions (a) in vivo and (b) in vitro at 5 and 180 minutes following administration.

III.c.4 KINETIC MODELING OF PULMONARY SOLUTE ABSORPTION IN THE IPRL

Data for % transfer to perfusate *vs.* time from IPRL experiments in which F-Na or FD-4 was administered to the airways could be fitted to the model shown in Fig. III.3 with $k_{a,TB}$, $V_{max,P}$ and $K_{m,P}$ held at zero (= 0). In these cases, % transfer was dose-independent and the across-dose data fits to Eqns. III.2, III.4 and III.5 yielded values for $k_{a,P}$ and $k_{E,PT}$ as shown in Table III.2. However, despite numerous attempts using mean % transfer to perfusate *vs.* time data from individual doses of F-PHEA, it was not possible to obtain unambiguous parameter estimates for $V_{max,P}$, $K_{m,P}$, $k_{a,P}$ and $k_{E,PT}$ unless simultaneous curve fitting was employed across doses. The best estimates for the kinetic parameters describing F-Na, FD-4 and F-PHEA disposition in the IPRL are shown in Table III.2 with curve fits displayed as solid lines in Figs. III.6 and III.10; the latter shows the results of simultaneous across-dose curve fitting of the IPRL data at a series of different nominal doses of F-PHEA (0.1, 0.2, 0.5, 1.0 and 5.0 mg) using Eqns. III.3. III.4 and III.5. The "goodness-of-fit" parameters as provided by "Scientist"-calculated Model Selection Criterion (MSC) were consistently $\geq$ 2.83 with R-squared, $R^2 \geq 0.986$. Individual values for MSC, R^2 and the standard deviations of each kinetic parameter in Fig. III.3 are also shown in Table III.2 following these unweighted nonlinear least-mean-square regression analyses.

Table III.2. Disposition parameters for active and passive absorption and mucociliary clearance for 7.4 kDa F-PHEA, FD-4 and F-Na following their administration into the airways of the isolated perfused rat lung (IPRL) at 37 °C.

Solutes (Mw)	Active absorption			Passive absorption	Mucociliary clearance	MSC; R^2
	$V_{max,P}$ [μg/min]	$K_{m,P}$ [μg]	$V_{max,P}/K_{m,P}$ [min^{-1}]	$k_{a,P}$ [min^{-1}]	$k_{E,PT}$ [min^{-1}]	
F-PHEA (7.4 kDa)	4.37 (0.57)	56.6 (14.7)	0.077	0.001 (0.001)	0.023 (0.001)	3.12; 0.986
FD-4 (4.4 kDa)	N/A	N/A	N/A	0.016 (0.001)	0.029 (0.003)	2.83; 0.990
F-Na (376 Da)	N/A	N/A	N/A	0.048 (0.003)	0.022 (0.002)	3.37; 0.992

Values are the best estimates (SD) following analysis of across-dose data from: *F-PHEA* - nominal doses: 0.1, 0.2, 0.5, 1.0 and 5.0 mg; *FD-4* - nominal doses: 0.1 and 0.2 mg; *F-Na* - nominal doses: 0.01, 0.02 and 0.04 mg.
MSC (Model Selection Criterion) and R^2 (R-squared) were as calculated by "Scientist" (Appendix VI).
N/A indicates "not applicable" (no dose-dependency was observed).
The rate constants for mucociliary clearance, $k_{E,PT}$ were not significantly different across solutes, based on overlapped 95% confidence intervals.

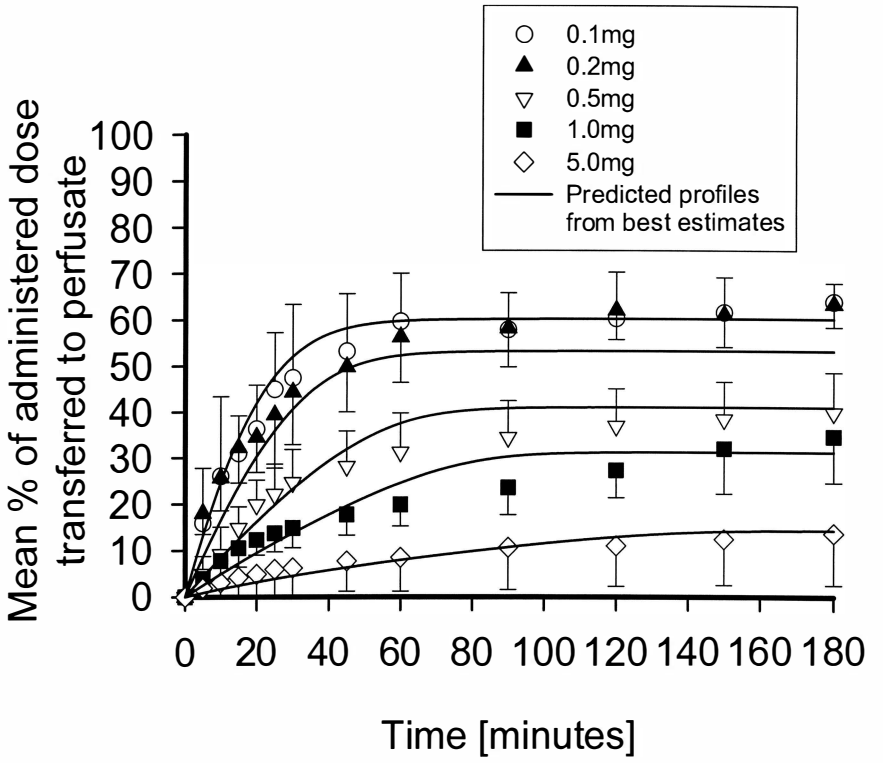

Figure III.10. Mean percentage (±SD; n=4) of administered dose of 7.4 kDa F-PHEA absorbed from the airways of the IPRL into the perfusate *vs.* time at 37°C. The solid curves are the results of simultaneous across-dose curve fitting of all profiles. These were generated using best estimates for each parameter in Fig. III.3, as described in Table III.2.

The rate constants for mucociliary clearance, $k_{E,PT}$ were found to be 0.022±0.002, 0.029±0.003 and 0.023±0.001 min^{-1} for F-Na, FD-4 and F-PHEA, respectively (Table III.2). These were not significantly different across solutes, based on the overlapped 95% confidence intervals (95%CI). Thus, a solute-independent mucociliary clearance with a half-life of 24-32 minutes was shown to exist in the IPRL. The "true" rate constants for passive absorption, $k_{a,P}$ (Fig. III.3) were found to be inversely related to the molecular weights of each of the model solutes, demonstrating the existence of a size-dependent passive absorption mechanism which was probably by simple restricted diffusion (smaller solutes diffuse faster; Martin, 1993; Byron and Patton, 1994). More importantly, even in the case of a small solute, F-Na, the absorption rate constant ($k_{a,P}$ = 0.048±0.003 min^{-1}) was found to be only 2-fold greater than the mucociliary clearance rate constant ($k_{E,PT}$ = 0.022±0.002 min^{-1}). Quite clearly therefore, mucociliary clearance competed with the passive absorption process for most of these solutes after their administration into the airways. Best estimates of $V_{max,P}$ and $K_{m,P}$ enabled calculation of their ratio, $V_{max,P}/K_{m,P}$ = 0.077 min^{-1} as an "intrinsic" rate constant for the active absorption of F-PHEA with comparable units to the first-order constants, $k_{a,P}$ and $k_{E,PT}$. When the value for the ratio, $V_{max,P}/K_{m,P}$ was compared to the rate constant for passive absorption of F-PHEA, $k_{a,P}$ = 0.001 min^{-1}, it was clear that the absorption was dominated by the active process at the lower doses, thus enhancing polymer's absorption rates dramatically. Indeed, the absorption rate seen at nominal 0.2 mg dose of 7.4 kDa F-PHEA was comparable to that for F-Na (376 Da) despite the more than 20-fold difference in the molecular weight.

III.d DISCUSSION

All model solutes used in this thesis were selected so that no degradation, metabolism or significant tissue sequestration (uptake from pulmonary circulation into the lung; Appendix V) was seen. Data in Appendix V shows quite clearly that reverse transfer from perfusate into the lung was negligible for all of these solutes. Thus, absorptive transfer which is shown as a unidirectional process in Fig. III.1 was uncomplicated in these cases by the absence of significant reversible kinetics. Furthermore, tracheal cannulation was maintained during in vivo and in vitro experiments, precluding clearance into extra-lung regions like the gastrointestinal (GI) tract. Both F-Na and FD-4 are known to be absorbed passively from the lung in vivo and in vitro, in the IPRL as well as through in vitro alveolar monolayers (Clark and Byron, 1985; Byron *et al.*, 1986; Matsukawa *et al.*, 1997). Consequently, absorption of these solutes could be studied across doses and expected to show % transfer *vs.* time profiles (Fig. III.6), which were dose-independent. In contrast, it was shown in a series of our previous IPRL studies that F-PHEA absorption was size-selective (≤ 8 kDa) and dose-dependent, but molecular charge-independent (Niven *et al.*, 1990; Byron *et al.*, 1991; *Byron et al.*, 1994; Sun, 1995; Sun *et al.*, 1999). Specifically, 7.4 kDa F-PHEA was believed to be absorbed by both active and passive mechanisms (Sun *et al.*, 1999), although quantifying these processes has proved extremely difficult prior to this investigation (Byron *et al.*, 1994)

The validation of the "forced solution instillation" technique in vivo and in vitro (CV% ≤ 5.6 %) and the proof of its provision of statistically identical initial regional solute distribution in the rat lung (Table III.1; Figs. III.4 and III.5) was crucial in the investigation of the mucociliary clearance and the correction of the kinetic analysis for the effects of this clearance in vivo and in vitro. This highly reproducible dosing technique compares favorably to others in the literature which typically have CV% ≥ 15 % following intratracheal instillation and/or aerosol administration (Brain *et al.*, 1976; Pritchard *et al.*, 1985; Ruzinski *et al.*, 1995; Leong *et al.*, 1998). Preferential solute distribution into the left lung (L) and the right inferior (RI) lobe was similarly observed following intratracheal instillation and aerosol administration in vivo (Brain *et al*, 1976; Pritchard *et al.*, 1985; Ruzinski *et al.*, 1995; Leong *et al.*, 1998) as well as in our previous studies (Byron and Niven, 1988). This seemed inevitable, based on the rat lung's anatomical characteristics, especially when the technique was used during in vivo respiration (Byron and Niven, 1988; Leong *et al.*, 1998).

The IPRL preparation differs from the in vivo rat lung primarily due to its lack of solute absorption from the upper tracheo-bronchial airways; this is due to the severance of the bronchial circulation during surgery (Mehendale *et al.*, 1981). In contrast, mucociliary clearance was shown to be viable in the IPRL for the duration of these experiments and identical to that seen in vivo. As a result, both F-Na (Fig. III.7 (b)) and F-PHEA (Fig. III.9 (b)) were transported into the upper airways quite rapidly and found to accumulate there at 120 and 180 minutes, respectively following administration

predominantly into the alveolar regions of the lung. Interestingly, although the tracheo-bronchial circulation in vivo remained intact and hence, perfused by the bronchial circulation, F-PHEA accumulation in the upper airways was also observed in vivo (Fig. III.9 (a)) and appeared to be consistent with that seen in the IPRL. This showed that F-PHEA absorption from the upper airways was negligible, due probably to the formidable tight junction for passive diffusion and the absence of active transporters for F-PHEA in this region. In contrast, ≥ 99.4 % of administered dose of a small solute, F-Na was absorbed in vivo in an "apparent" first-order fashion over the 120 minutes following solute administration (Fig. III.6). This demonstrated the presence of significant passive absorption from the tracheo-bronchial region for this smaller solute.

The kinetic model shown in Fig. III.3 along with a high precision, cross-dose, cross-solute data set was used successfully to characterize "region-specific" disposition of these model solutes. Mucociliary clearance kinetics were found to be solute-independent and relatively rapid ($k_{E,PT}$ = 0.022-0.029 min^{-1}), such that mucociliary clearance offered significant competition to absorption of most solutes, especially in the IPRL. Clearly, it was necessary to fit the complete kinetic model shown in Fig. III.3 to % solute transfer data, in order to correctly ascribe values to the individual rate processes. The resultant passive absorption rate constants ($k_{a,P}$) were inversely related to solute molecular weight, reasonably demonstrating that this was due to diffusive transport through the pulmonary membranes. Modeling also facilitated the characterization of complex, simultaneous, active and passive absorption of 7.4 kDa F-PHEA alongside its mucociliary clearance

into the tracheo-bronchial airways. As a result, the transporter for 7.4 kDa F-PHEA from the pulmonary airways to blood (Fig. III.8), shown to be present in vivo and in vitro was successfully characterized in the IPRL. A Michaelis-Menten-type active mechanism with maximum rate, $V_{max,P}$ = 4.37±0.57 μg/min and "affinity", $K_{m,P}$ = 56.6±14.7 μg was deduced after taking mucociliary clearance and passive absorption into account (Table III.2). Thus, the IPRL and model shown in Fig. III.3 can best be thought of as a means of analyzing the "region-specific" disposition of solutes in the rat lung.

An attempt to describe such kinetics has been made previously (Byron *et al.*, 1994). In that case, $V_{max,P}$ and $K_{m,P}$ were reported as 3.0±0.3 μg/min and 331±163 μg for 8.4 kDa F-PHEA, respectively. They were estimated from curve fitting of single data points for the individual amounts of F-PHEA absorbed after 30 minutes *vs.* administered dose (Byron *et al.*, 1994). Unfortunately, the transfer data used for that curve fitting showed large variance and the kinetic model assumed negligible passive absorption of F-PHEA, irrespective of dose. More importantly, the curve fitting procedure assumed that the absorption rate was unchanged throughout the first 30 minutes. As a result, the value for $K_{m,P}$ was found to be larger and less precise, compared to that estimated in this thesis ($K_{m,P}$ = 56.6±14.7 μg). In contrast, the kinetic model in this thesis and subsequent curve fitting to this model assumed simultaneous active and passive absorption and it employed the transfer data across time and dose. This included doses well below the value for $K_{m,P}$ (Table III.2). Furthermore, the model (Fig. III.3) enabled the absorption rate to change as a function of time throughout each experiment. Consequently, the values reported for

$V_{max,P}$ = 4.37±0.57 μg/min and $K_{m,P}$ = 56.6±14.7 μg in this thesis are believed to be much more reliable than those described previously (Byron *et al.*, 1994).

Figure III.11 shows the results of IPRL experiments performed with F-Na and FD-4 presented in the form of log-linear (first-order) plots. Mean data from all doses were employed for this purpose. The mean percentage of each administered dose absorbed as time $\rightarrow \infty$ was first determined by averaging all IPRL data in Fig III.6 at time $\geq$ 60 minutes for both solutes. Percentage values for "transferable dose remaining to be absorbed" were then determined from:

$$(\%\text{ of transferable dose remaining to be absorbed}) = \frac{(\%\text{ absorbed})_{time=\infty} - (\%\text{ absorbed})_{time=t}}{(\%\text{ absorbed})_{time=\infty}} \times 100 \qquad \text{(Eqn. III.12)}$$

and plotted on Fig. III.11. These log-linear (first-order) plots and their negative slopes provide values for the apparent absorption rate constants, $k_{a,app}$, for each solute. These were values which would be obtained if the effects of mucociliary clearance was ignored and the data treated in a conventional fashion (Enna and Schanker, 1972; Lanman *et al.*, 1973; Burton and Schanker, 1974a and 1974b; Burton *et al.*, 1974; Schanker and Burton, 1976; Schanker and Hemberger, 1983; Brown and Schanker, 1983). Because of the absence of a bronchial circulation in the IPRL, the absorption kinetics illustrated in Fig. III.11 would be attributed to absorption from the deep lung into the pulmonary circulation (Mehendale *et al.*, 1981; Roberts, 1984). Unfortunately, the negative log-linear slopes,

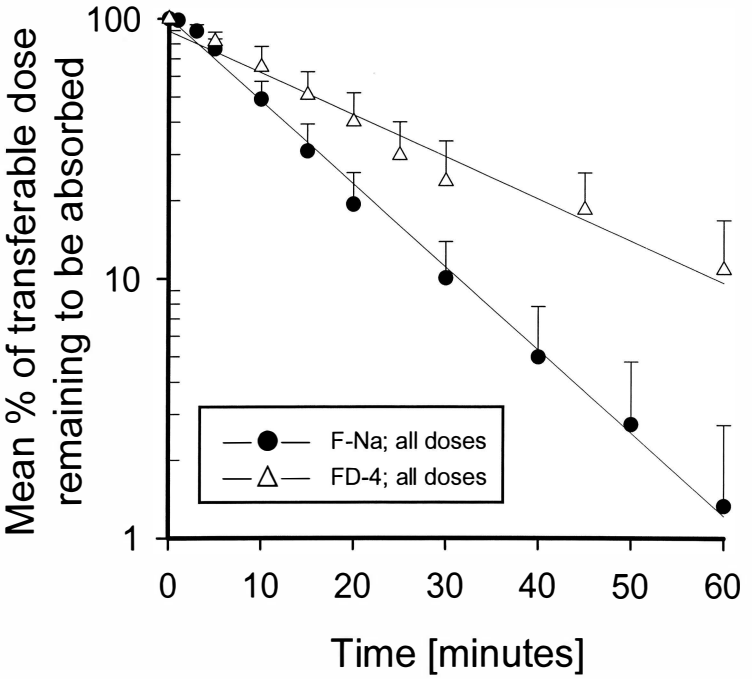

Figure III.11. Mean percentage (±SD) of the transferable dose of F-Na and FD-4 remaining unabsorbed in the airways of the IPRL *vs.* time. Data shown are means from all doses of F-Na (0.01, 0.02 and 0.04 mg; n=12) and FD-4 (0.1 and 0.2 mg; n=8). Solid lines are the results of log-linear regression of each data set. The negative, natural logarithmic slopes provided values for commonly-called, "apparent rate constants for absorption", $k_{a,app}$ = 0.072 and 0.039 min^{-1} for F-Na and FD-4, respectively.

shown in Fig. III.11 grossly overestimate the true values of $k_{a,P}$ for each of these solutes; this because mucociliary clearance was ignored when attributing the figure's slopes entirely to absorption. Table III.3 shows a comparative summary of the rate constants for absorption for F-Na and FD-4. Comparing the values for $k_{a,app}$ with others in Table III.3 shows that the value for the mucociliary clearance constant, $k_{E,PT}$, is a significant component of each apparent rate constant. In practice, $k_{a,app}$ is equaled to the sum of all clearance rate constants existing in the lung (Notari, 1987) and the true values for the fractions of each solute's disappearance which are due to absorption, must take other clearance mechanisms into account. While this point has been noted previously for both in vivo and in vitro studies (Byron, 1986), the magnitude of mucociliary clearance's influence has never been included correctly in a kinetic analysis of solute absorption from the IPRL.

While attempts have been made to correct the values for absorption rate constants obtained in vivo for the effects of mucociliary clearance (Colthorpe *et al.*, 1992; Taylor *et al.*, 1994), these efforts suffer from uncertainties attached to assigning true values for mucociliary clearance rate constants to these phenomena. In practice, the variance of mucociliary clearance kinetics which is known to be associated with different regions of the lung (Byron *et al.*, 2000) mandates the correct assignment of clearance kinetics to each of the organ's absorptive regions. Byron *et al.* (2000), when analyzing in vivo data for beclomethasoone absorption in humans, showed its clear dependence upon regional deposition. Mucociliary clearance, which was known to become faster as the respiratory tract is ascended (Byron, 1986; Brain and Blanchard, 1993; Camner and Mossberg,

Table III.3. Summary of mean rate constants obtained from different kinetic treatments of F-Na and FD-4 IPRL data at 37 °C.

Rate constant		(Mw)	F-Na (376 Da)	FD-4 (4.4 kDa)
$k_{a,P}$ [a]	(min^{-1})		0.048	0.016
$[k_{a,P} + k_{E,PT}]$ [b]	(min^{-1})		0.070	0.045
$k_{a,app}$ [c]	(min^{-1})		0.072	0.039
$k_{a,TB}$ [d]	(min^{-1})		0.042	N/A

[a] Following kinetic analysis in accord with Section III.c.4 (Table III.2).

[b] The sum of $k_{a,P}$ and $k_{E,PT}$ following analysis in accord with Section III.c.4 (Table III.2).

[c] The negative log-linear slope of the linear regression curves shown in Fig. III.11.

[d] Following kinetic analysis using Eqns III.7-10 (and the model in Fig. III.3), fixing $k_{a,P} = 0.048$ min^{-1} and $k_{E,PT} = 0.022$ min^{-1}, obtained from the IPRL.

1993), was shown to have increasing effects upon that drug's apparent absorption rate constant from lung, as its aerosol deposition became more central (Byron *et al*., 2000). Thus, from an in vivo perspective, solutes which are known to be absorbed both from the pulmonary and tracheo-bronchial regions, should be analyzed carefully for the effects of region-dependent absorption kinetics and corresponding mucociliary clearance changes between these regions. In this thesis, only F-Na was studied in vivo and in vitro, as a solute whose absorption was significant from both the upper and lower airways. In the in vivo studies, solute clearance to (and absorption from) the gastrointestinal (GI) tract was precluded by continuous intratracheal intubation.

Based on this rationale, Eqns. III.7-III.10 (and the model in Fig. III.3) were used to fit the in vivo absorption profiles for F-Na (Fig. III.6). By fixing $k_{a,P}$ = 0.048 min^{-1} and $k_{E,PT}$ = 0.022 min^{-1}, their best estimates from the IPRL (Table III.2), it was possible to determine a value for fluorescein's first-order absorption rate constant from the tracheo-bronchial region, $k_{a,TB}$. The in vivo profiles shown in Fig. III.6 were successfully fitted using this approach (MSC = 4.70 and R^2 = 0.997). The best estimate for $k_{a,TB}$ was 0.042±0.011 min^{-1} (half-life = 16.5±5.9 minutes), a value which was insignificantly different from that for pulmonary absorption ($k_{a,P}$ = 0.048±0.003 min^{-1}; based on their overlapped 95 %CI). Thus, fluorescein's passive absorption kinetics appeared to be independent of regional deposition. This observation may or may not be true for other solutes in the lung. However, the result for fluorescein was consistent with those from previous in vivo studies in dogs, where similar F-Na absorption was observed following

the dye's different initial regional lung distribution (Clark and Byron, 1985), although those studies, like the classical absorption works of Schanker's group (Enna and Schanker, 1972; Lanman *et al*., 1973; Burton and Schanker, 1974a and 1974b; Burton *et al*., 1974; Schanker and Burton, 1976; Schanker and Hemberger, 1983; Brown and Schanker, 1983), failed to account correctly for the presence of competing mucociliary clearance from different lung regions.

The multiple absorption profiles for F-PHEA in the IPRL enabled a unique, across-dose data fit to determine values which describe this solute's dose-dependent active absorption kinetics ($V_{max,P}$ and $K_{m,P}$), in the presence of passive absorption and competing mucociliary clearance from the pulmonary lung compartment (Fig. III.3). The "intrinsic rate constant", $V_{max,P}/K_{m,P}$ for macromolecule's active absorption was 0.077 min^{-1}. This value represents a first-order rate constant for F-PHEA absorption which would be observed as dose $\rightarrow$ 0 and demonstrates the importance of F-PHEA-specific carriers/transporters which enhance the absorption of this 7.4 kDa macromolecule ("intrinsic absorption half-life" = 9.0 minutes). Even at doses as high as 1 mg, apparent F-PHEA absorption half-lives (30 minutes) were observed which exceeded all expectations for a molecule of this size. Furthermore, there was no statistical difference between in vivo and in vitro results for this macromolecule (Fig. III.8). This rapid F-PHEA active transport was pulmonary-region-specific and there was no evidence of significant F-PHEA tracheo-bronchial absorption. Thus, F-PHEA absorption characteristics obtained

from the IPRL studies were predictive of the solute's absorption from the "whole-lung", in vivo.

III.e SUMMARY AND CONCLUSION

A comparison of solute disposition profiles following identical initial regional lung distribution by "forced solution instillation" in vivo and in vitro has shown the presence of a reproducible and viable mucociliary clearance process in the IPRL which is predictive of that seen in vivo. Similarly, macromolecular F-PHEA absorption in the IPRL was predictive of that seen in vivo (ANOVA) because transport kinetics and mucociliary clearance of this macromolecule were comparable in the two models. On the other hand, tracheo-bronchial absorption for small solutes like F-Na was significant and hence, F-Na absorption in the IPRL underestimated in vivo absorption. In spite of this fact, simultaneous determinations of small solute (F-Na) absorption in vitro and in vivo, enabled correct kinetic modeling and estimation of the solute's regional absorption rate constants, $k_{a,P}$ and $k_{a,TB}$.

A new "pulmonary-region-specific" kinetic model was developed to characterize solute absorption in the presence of competing mucociliary lung clearance in vitro, in the IPRL, and in vivo. The model successfully determined pulmonary-region-specific descriptors for active (F-PHEA) and passive (F-Na, FD-4 and F-PHEA) absorption. Mucociliary clearance was found to be relatively rapid (half-life values between 24 and

32 minutes), competing with absorption for many solutes administered into the airways. Pulmonary-region-specific rate constants for passive absorption ($k_{a,P}$) were inversely related to molecular weights of solutes, probably corresponding to the restricted diffusive transport theory through pulmonary membranes which is predominant in the literature. The pulmonary-passive absorption rate constant for F-Na (0.048±0.003 min^{-1}) was insignificantly different to its tracheo-bronchial counterpart (0.042±0.011 min^{-1}) obtained in vivo, suggesting deposition-independent absorption for this small solute. Characterization of F-PHEA's active absorption, alongside simultaneous passive absorption and competing mucociliary clearance, revealed its carrier/transporter kinetics from the whole lung organ ($V_{max,P}$ = 4.37±0.57 μg/min and $K_{m,P}$ = 56.6±14.7 μg). The value of F-PHEA's $V_{max,P}/K_{m,P}$ ratio (0.077 min^{-1}) demonstrated that, at lower doses (≤ nominal 0.2 mg dose), this macromolecular model polypeptide was capable of achieving greater or similar absorption rapidity from the lung than 376 Da fluoresein.

CHAPTER IV

PULMONARY ABSORPTION KINETICS OF F-PHEA: EFFECTS OF LOW TEMPERATURES AND METABOLIC INHIBITORS

IV.a INTRODUCTION

A series of our isolated perfused rat lung (IPRL) studies have confirmed the existence of dose-dependent absorption kinetics for a range of co-polymers based on differently substituted polyaspartamides (Niven *et al.*, 1990; Byron *et al.*, 1991; Byron *et al.*, 1994; Sun, 1995; Sun *et al.*, 1999). The tendency of these pulmonary absorption enhancement mechanisms to follow Michaelis-Menten kinetics has suggested the presence of unique airway-to-blood active transporters or carriers for fluorophore-labeled poly-α,β-[N(2-hydroxyethyl)-D,L-aspartamide] (F-PHEA) in the lung's pulmonary airways. These transporters were capable of dramatically enhancing systemic absorption of F-PHEA and its co-polymers following administration into the airways (Niven *et al.*, 1990; Byron *et al.*, 1991; Byron *et al.*, 1994; Sun, 1995; Sun *et al.*, 1999). The absorption was size-selective and dose-dependent (Niven *et al.*, 1990; Sun, 1995; Sun *et al.*, 1999)

as well as being subject to competition from similar-sized, fluorophore-free PHEA (Byron *et al.*, 1994). Specifically, the 7.4 kDa F-PHEA used in this thesis demonstrated simultaneous active and passive absorption and the rate and extent of its airway-to-perfusate transfer appeared to be independent of molecular electronic charge (Sun, 1995; Sun *et al.*, 1999).

The presence of airway-to-blood active transporters/carriers has been documented previously in lung (Gardiner and Schanker, 1970; Enna and Schanker, 1973; Meredith and Boyd, 1995; Hastings *et al.*, 1995; Kim and Crandall, 1996; Folkesson *et al.*, 1996; Shen *et al.*, 1999). Airway-to-blood carriers for fluid, electrolytes, hexoses and amino acids are believed to be important and tightly regulated in order to maintain homeostasis physiologically (Wangensteen and Bartlett, 1984; Kim and Crandall, 1988; Basset *et al.*, 1994; Effros, 1994; Kim and Crandall, 1994;, Matthay *et al.*, 1994). Relatively specific carrier transporters for small anions (Gardiner and Schanker, 1970; Enna and Schanker, 1974; Kim and Crandall, 1994), organic cations (Foth, 1995; Shen *et al.*, 1999) and di- and tri-peptides (Helliwell *et al.*, 1994; Morimoto *et al.*, 1994; Meredith and Boyd, 1995; Yamashita *et al.*, 1997 and 1998) are also present in alveolar and tracheal epithelium. These are known to enhance the active absorption of substrates and enable more rapid passive absorption through tight junctions. Furthermore, it has been shown that extremely large plasma proteins, albumin (68 kDa) and IgG (150 kDa) were actively transcytosed across alveolar epithelium via specific receptors (Albondin and FcRn receptors, respectively; Hasting *et al.*, 1994; Kim *et al.*, 1995; Folkesson *et al.*, 1996). Non-specific

fluid-phase transcytosis has also been shown for horseradish peroxidase (HRP; 44 kDa), but the process was relatively slow (Schneeberger and Karnovsky, 1968; Matsukawa *et al.*, 1996). It seems quite possible therefore, that specific or non-specific airway-to-blood transporters/carriers exist in deep lung, which rapidly transcytose certain macromolecules. Clearly, F-PHEA may be a candidate for such a carrier, while FD-4 was not (Chapter 3). However, whether F-PHEA's dose-dependent absorption is truly due to the presence of an active (energy-dependent) transporter, remains to be substantiated.

Active absorption processes via transporters or carriers are generally believed to rely on the reversible interaction of the substrate with a membrane protein which acts as a carrier (Alberts *et al.*, 1983; Macheras *et al.*, 1995). Following the formation of the substrate-carrier complex, the complex may be internalized into endosomes where cytoplasmic clathrin-coated or nonclathrin-coated vesicles are formed. The vesicles are then believed to be trafficked along microtubules and transcytosed (or absorbed; transporter/receptor-mediated transcytosis). Otherwise, the complex is subjected to changes in conformation in order to discharge the substrate into the cytosol without translocation or transcytosis (carrier-mediated endocytosis). These processes must be directly or indirectly coupled to a source of cellular metabolic energy and most often, this is believed to involve ATP hydrolysis ($ATP \rightarrow ADP + P_i + \Delta G_o'$). Hydrolysis and energy liberation may be effected directly by the transporting carrier proteins or be brought about by the co-transport of Na^+ or H^+ down their electrochemical gradient (Alberts *et al.*, 1983; Andreoli *et al.*, 1986). Several biochemical approaches are now known to be

capable of manipulating these processes and thus, shedding light on the mechanisms and pathways involved with transport. Lowering temperatures in the experimental systems used to study each transporter are believed to non-specifically inhibit ATP hydrolysis rates and thus, decrease utilization of cellular energy required for active absorption (Wangensteen, 1990; Rutschman *et al.*, 1993; Serikov *et al.*, 1993). Several metabolic inhibitors are also useful for specific or non-specific identification of the cellular mechanisms used in transcytosis.

In Chapter 3, the absorption kinetics for 7.4 kDa F-PHEA from the pulmonary airways of the IPRL were precisely characterized at 37 ^{o}C using kinetic modeling. The approach used in that chapter allowed for the presence of competing mucociliary clearance, as shown in Fig. IV.1. In this chapter, airway-to-perfusate transport of 7.4 kDa F-PHEA in the IPRL will be described following its manipulation by several different biochemical approaches. Each of these approaches will be shown to inhibit different aspects of F-PHEA's active absorption, thus enabling us to kinetically analyze the solute's pathways of pulmonary absorption. For these purposes, 7.4 kDa F-PHEA absorption in the IPRL was studied at 25, 30 and 37 ^{o}C, and in the presence and absence of several metabolic inhibitors: 2,4-dinitrophenol (DNP), ouabain (OUA), monensin (MON) and nocodazole (NOC). DNP and OUA purported to specify the importance of ATP-driven intracellular energy (Goodman *et al.*, 1983; Steen *et al.*, 1993; Alberts *et al.*, 1994) for F-PHEA's active absorption, whereas MON and NOC were used as biochemical tools to

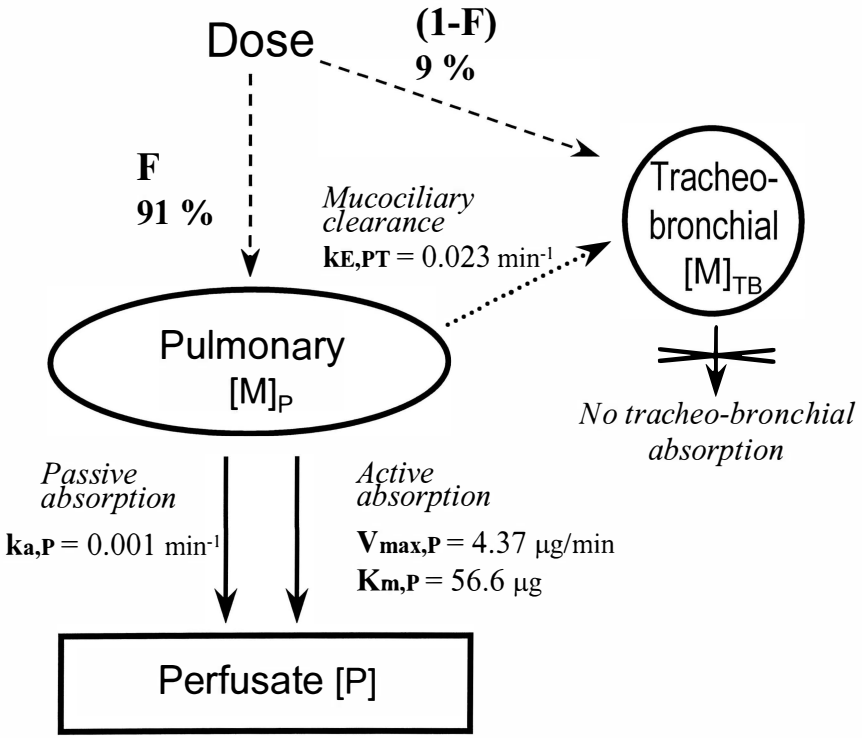

Figure IV.1. Kinetic model and its rate constants for 7.4 kDa F-PHEA disposition in the airways of the isolated perfused rat lung (IPRL) at 37 °C, as described in Chapter 3 Key: F - initial average penetration fraction following administration (0.91); $V_{max,P}$ and $K_{m,P}$ - the maximum rate and "affinity" of Michaelis-Menten-type active absorption, respectively; $k_{a,P}$ - first-order rate constant for passive absorption from the pulmonary region; $k_{E,PT}$ - first-order rate constant for mucociliary clearance.

disrupt endosome and microtubule formation, respectively, during vesicular transcytosis (Mollenhauler *et al.*, 1990; Hastings *et al.*, 1994; Wangensteen *et al.*, 1996).

IV.b MATERIALS AND METHODS

IV.b.1 MODEL SOLUTES: 7.4 kDa F-PHEA AND REFERENCE SOLUTES

Synthesis and preparation of 7.4 kDa fluorophore-labeled poly-α,β-[N(2-hydroxyethyl)-D,L-aspartamide] (F-PHEA; FR7150) has been described in detail previously (Chapter 3 and Appendix III). Its weight- (Mw) and number- (Mn) averaged molecular weights were 7420 and 6620 Da, respectively, with a polydispersity, P_d (Mw/Mn) = 1.12 (Sun, 1995; Appendix III). Its 0.3 mole% fluorophore content (Niven *et al.*, 1990; Appendix III) enabled a high sensitivity assay (Appendix IV). The polymer has shown no degradation, metabolism or lung tissue sequestration in rat lung (Sun, 1995; Appendix V).

Sodium fluorescein (F-Na; Mw =376 Da) and FITC-labeled dextran (FD-4; Mw = 4.4 kDa) were purchased from Sigma Chemical Company (St. Louis, MO). These solutes were used as reference solutes for passive absorption when validating airway-to-perfusate transfer and mucociliary clearance kinetics at 25 ^{o}C and/or in the presence of metabolic inhibitors.

IV.b.2 METABOLIC INHIBITORS: 2,4-DINITROPHENOL, OUABAIN, MONENSIN AND NOCODAZOLE

All metabolic inhibitors, 2,4-dinitrophenol (DNP; lot: 49H5077), ouabain·$8H_2O$ (OUA; lot: 27H0921), monensin (MON; sodium salt; lot: 28H5012) and nocodazole (NOC; lot: 10K4013) were purchased from Sigma Chemical Company (St. Louis, MO) as the purest grades commercially available. These chemical structures are shown in Fig. IV.2. Ethyl alcohol USP (EtOH; AAPER Alcohol and Chemical Company, Shelbyville, KY) and dimethyl sulfoxide (DMSO; HPLC grade ≥ 99.96 % pure; EM Science, Gibbstown, NJ) were used in the vehicles for MON and NOC studies, respectively.

IV.b.3 PULMONARY ABSORPTION IN THE IPRL: EFFECTS OF LOW TEMPERATURES AND METABOLIC INHIBITORS

The IPRL preparation and the dosing method used to deliver solutes into the airways ("forced solution instillation") have been described in detail previously (Byron and Niven, 1988; Chapter 3 and Appendix I). These were used unchanged with the exception of the experimental perturbations described below. The general experimental format which was used for experiments performed in this chapter is shown in Table IV.1. For each experimental condition and/or solution, four fully viable preparations were studied. The absorption results from each group (n=4) were expressed as mean % of

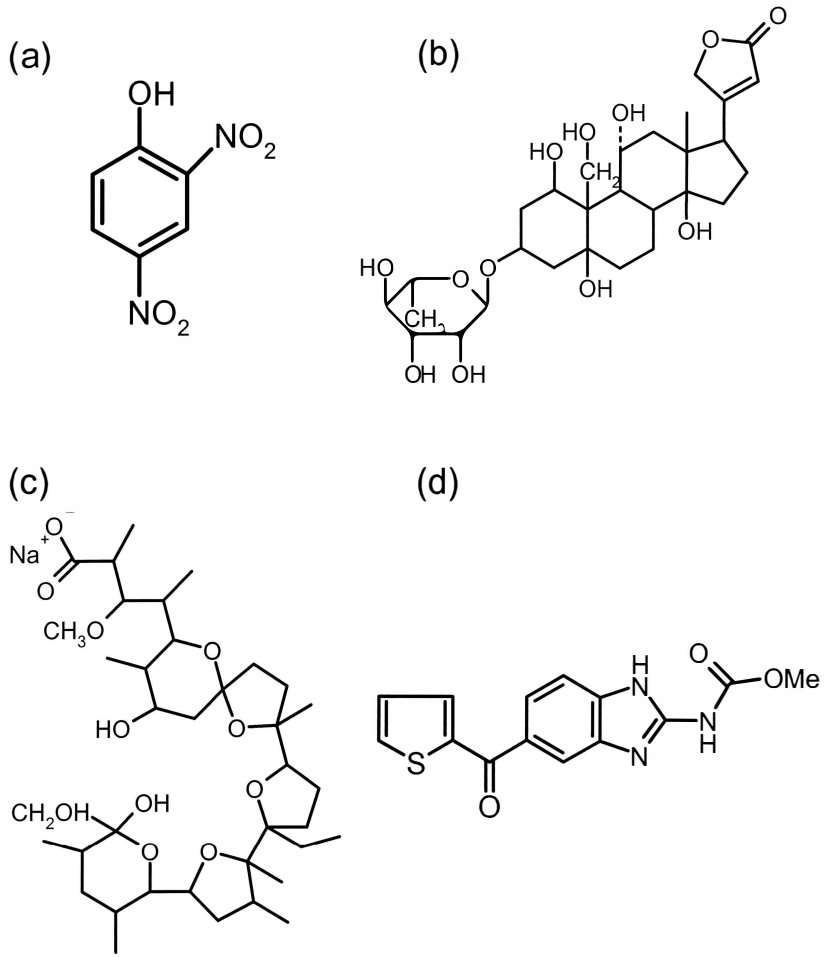

Figure IV.2. Chemical structures of metabolic inhibitors used in the IPRL: (a) 2,4-dinitrophenol (DNP); (b) ouabain (OUA); (c) monensin (MON); (d) nocodazole (NOC).

Table IV.1. Summary of experimental conditions used in this Chapter.

Dosing Solute	Temp.[1] [°C]	Nominal dose [mg]	Vehicle	Metabolic inhibitor			Study period
				Name	Conc.[2]	Inhibitor added	
<Effect of temperature>							
F-PHEA	37	0.1, 0.2, 0.5, 1.0, 5.0	Water	None			180 min.
	30	0.2	Water	None			180 min.
	25	0.2, 0.5, 1.0 5.0	Water	None			180 min.
None	15, 10, 4	N/A[3]	N/A[3]	None			≤ 30 min.
FD-4	37, 25	0.1, 0.2	Water	None			150 min.
F-Na	37, 25	0.01, 0.02, 0.04	Water	None			120 min.
<Effect of inhibitor>							
F-PHEA	37	0.2	Water	DNP[4]	0.05, 0.1, 0.2 0.5, 1.0 mM	To perfusate 15 min. prior to dosing	60 min.
F-Na	37	0.02					
			Water	OUA[5]	5, 10, 100 μM		60 min.
F-PHEA	37	0.2	1.5 % EtOH	MON[6]	5, 10, 30, 100 μM	To airways with solute	120 min.
F-Na	37	0.02					
			1.5 % DMSO	NOC[7]	0.5, 1, 10, 30, 100 μM		120 min.

[1] Temperature; [2] concentration; [3] not applicable; [4] 2,4-dinitrophenol; [5] ouabain; [6] monensin and [7] nocodazole.

administered dose ± sample standard deviation. The individual results from each IPRL are reported in Appendix VII.

For lower temperature studies, perfusate temperatures were adjusted and maintained either at 4, 10, 15, 25 or 30 (±0.5) ^{o}C by modifying the setting of a thermostatically-controlled water circulator (Model 9505, Fisher Scientific, Pittsburgh, PA) used to supply water to the jacketed equipment showing in Fig. AI.1 (B) (Appendix I). Briefly, a rat lung was removed from the body and housed in the jacketed artificial glass thorax (AGT), maintained at those lower temperatures. Its pulmonary circulation was perfused with circulating perfusate solution (Krebs-Heinseleit solution with 4 % bovine serum albumin) from a reservoir whose temperature was similarly controlled by the circulator. Following equilibration for ≥ 5 minutes, F-PHEA (nominal doses of 0.2, 0.5, 1.0 and 5.0 mg) or reference solute (FD-4: 0.1 and 0.2 mg, F-Na: 0.01, 0.02 and 0.04 mg) was administered into the airways as a coarse spray by "forced solution instillation" (Table IV.1). Absorption was followed as a function of time by sampling and analyzing the perfusate, as described in Chapter 3 and Appendix I. Attempts to reduce temperatures below 25 ^{o}C were found to induce rapid edema formation at time ≤ 30 minutes preparation. Thus, the low temperature studies described in this thesis with solutes, only employed perfusate temperatures of 25 and 30 ^{o}C. At these temperatures, IPRL viability for ≥ 180 minutes was attained, as evidenced by the absence of edema and a lack of sharp discontinuities in solute absorption profiles (Figs. IV.6 and IV.7; Appendix I)

The experimental protocols for studying effects of metabolic inhibitors on F-PHEA and F-Na absorption were optimized and/or selected based on the results of preliminary studies and literature information (Basset and Fisher, 1976; Goodman *et al.*, 1983; Basset *et al.*, 1987; Effros *et al.*, 1988; Hastings *et al.*, 1994; Wangensteen *et al.*, 1996). Briefly, all these experiments were performed at 37 ^{o}C. After the cannulated IPRL was placed in the artificial glass thorax (AGT) and perfusate recirculation commenced (Appendix I), 50 mL of the perfusate was removed from the 100 mL reservoir and replaced by 50 mL of fresh perfusate containing various concentrations of DNP or OUA; the inhibitors were directly dissolved in this 50 mL of fresh perfusate. The amounts of each were calculated to result in final concentrations in the circulating perfusate of 0.05, 0.1, 0.2, 0.5 and 1.0 mM for DNP and 5, 50 and 100 μM for OUA following the replacement. At 15 minutes following perfusion with each of these inhibitors, F-PHEA (nominal dose = 0.2 mg) or F-Na (nominal dose = 0.02 mg) was administered into the airways by "forced solution instillation" and its absorption followed with time, as described in Chapter 3 and Appendix I. "Control" absorption profiles, determined in the absence of the inhibitors, were obtained according to an identical protocol (F-PHEA was administered at 15 minutes following perfusion in the absence of inhibitors). IPRL viability was reduced in the presence of DNP and/or OUA to times ≤ 60 minutes. For this reason, absorption profiles were discontinued at times > 60 minutes, when edema onset began. The inhibitors, monensin (MON) and nocodazole (NOC) were co-administered independently with F-PHEA or F-Na. Fluorophore absorption was then followed with time, as described in Chapter 3 and Appendix I. MON and NOC were prepared as stock solutions of 10^{-2} M

in EtOH and DMSO, respectively, and stored at ≤ - 20 °C. Prior to experimentation in the IPRL, dosing solutions (0.1 mL) were prepared from aqueous F-PHEA or F-Na solutions (so that nominal 0.2 and 0.02 mg doses, respectively, were present following admixture with each inhibitor). Various concentrations of MON in EtOH or NOC in DMSO were employed although the final concentrations of these non-aqueous solvents in each dosing vehicle (EtOH and DMSO) were held ≤ 1.5 % (v/v) throughout. The final concentrations of inhibitors in each dosing solution were adjusted to achieve 5, 10, 30 and 100 μM for MON and 0.5, 1, 10, 30 and 100 μM for NOC (Table IV.1). "Control" absorption profiles for F-PHEA were determined in the absence of inhibitors following solute administration in vehicles containing 1.5 % (v/v) EtOH or DMSO. IPRL viability, evidenced by the absence of pulmonary edema was maintained for ≥ 120 minutes in the presence of MON and NOC. Thus, absorption profiles in the presence of these inhibitors were terminated 120 minutes after solute administration.

IV.b.4 KINETIC MODELING, FITTING AND PARAMETER ESTIMATION

The kinetic model for F-PHEA absorption in the IPRL is summarized in Fig. IV.1 along with the solute's disposition rate constants at 37 °C, as described in Chapter 3. This model and the method used for data analysis in Chapter 3 was also employed for analyzing absorption at lower temperatures (Sections III.b.6 and III.b.7 in Chapter 3).

Thus, average data for % of administered dose transferred to perfusate (Fig. IV.6) was fitted across doses to the following equations (Eqns. III.3-5 from Chapter 3):

$$(d[P]/dt)_{Active+Passive,IPRL} = V_{max,P}\cdot[M]_P/(K_{m,P} + [M]_P) + k_{a,P}\cdot[M]_P \quad \text{(Eqn. III.3)}$$

$$(d[M]_P/dt)_{IPRL} = - (d[P]/dt) - k_{E,PT}\cdot[M]_P \quad \text{(Eqn. III.4)}$$

$$(d[M]_{TB}/dt)_{IPRL} = k_{E,PT}\cdot[M]_P \quad \text{(Eqn. III.5)}$$

where [P] is the cumulative solute amount absorbed from the pulmonary region into the recirculating perfusate of the IPRL, $[M]_P$ and $[M]_{TB}$ are the solute amounts remaining to be absorbed from the pulmonary and the tracheo-bronchial regions, respectively; $V_{max,P}$ is the maximum rate of active absorption, $K_{m,P}$ is the "affinity" or dose at which the active absorption rate = $0.5\cdot V_{max,P}$, $k_{a,P}$ is the first-order passive absorption rate constant from the pulmonary region and $k_{E,PT}$ is the first-order mucociliary clearance rate constant from the pulmonary to the tracheo-bronchial region. The curve fitting and parameter estimation was performed by unweighted, nonlinear least-mean-square regression analysis (Scientist™, MicroMath Scientific Software, Salt Lake City, UT). The fraction of the administered dose delivered to the pulmonary region, F, was fixed throughout fitting at its experimentally-determined average value at 25 °C, 0.91 (0.912±0.013; mean±SD; n=4), so that initial conditions were:

$[M]_{P,\ t=0}$ / [administered dose] = 0.91

$[M]_{TB,\ t=0}$ / [administered dose] = 0.09

$[P]_{t=0}$ / [administered dose] = 0.00

The model fits were validated using "goodness-of-fit" parameters such as the program's calculated Model Selection Criterion (MSC), R-squared (R^2), a review of standard deviation of final parameter estimates and visual inspection of the residuals. Additional methodological details are described in Appendix VI.

IV.b.5 DATA ANALYSIS FOR ACTIVE ABSORPTION INHIBITION IN THE PRESENCE OF METABOLIC INHIBITORS

The rate constants for active and passive absorption of F-PHEA at 37 °C, determined in Chapter 3 (Fig. IV.1), enabled estimation of the contribution of each of these (in the first 30 minutes following administration) to the total absorption rates for this polymer, as a function of administered dose. These are shown in Fig. IV.3 as theoretical curves and actual data points; absorption rates determined between time = 0 and time = 30 minutes. Despite the saturation seen at ≥ 1.0 mg doses, the theoretical active absorption was found to contribute > 50 % of the total process up to and including nominal 5.0 mg dose. At the lower 0.2 mg dose, 97.7 % of this theoretical total absorption rate resulted from active absorption, whereas only 2.3 % was derived from the passive absorption component. The percentage reduction of F-PHEA's active transport seen with inhibitors at 37 °C, was determined (over the first 30 minutes of its absorption) by (a) ensuring that neither $k_{E,PT}$ values (mucociliary clearance) nor $k_{a,P}$ values (passive absorption) for the (passively-absorbed) solute, F-Na, were significantly affected by a

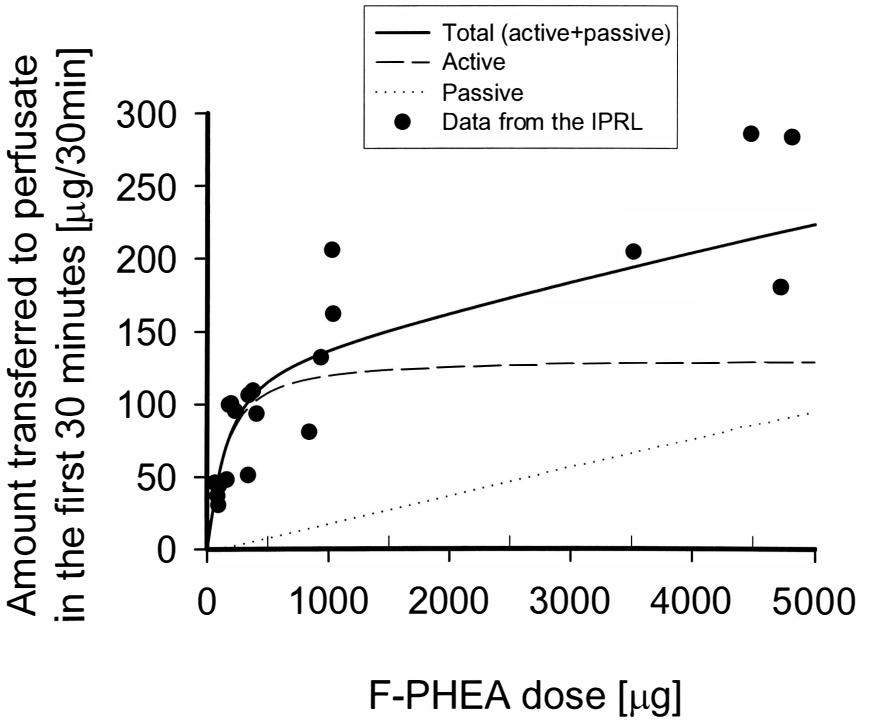

Figure IV.3. F-PHEA amount transferred to perfusate in the first 30 minutes after administration *vs.* initial F-PHEA dose in the airways, at 37 °C. The solid curve was generated using the best estimates for each process in Fig. IV.1, based on Eqn. III.3 in Chapter 3. The dashed and dotted curves, respectively were the model-simulated results for active and passive absorption, based on the rate constants in Fig. IV.1. Data points were the results of each IPRL experiment.

particular inhibitor and (b) comparing the experimental value for absorption of F-PHEA in the presence of the inhibitors, to that obtained in its absence. In each case, a solute-dose-dependent theoretical correction was applied to remove the contribution of passive absorption from these considerations [even though this contribution accounted for only 2.3 % of total absorption rates at a nominal 0.2 mg dose of 7.4 kDa F-PHEA]. Thus, the % of each F-PHEA administered dose transferred after 30 minutes by *active* mechanisms in the presence of inhibitors, $[\%T]_{active,inh}$, was calculated by:

$$[\%T]_{active,inh} = [\%T]_{obs,inh} - [\%T]_{passive} \qquad \text{(Eqn. IV.1)}$$

where $[\%T]_{obs,inh}$ was the experimentally-observed result for % of administered dose transferred to perfusate in 30 minutes in the presence of inhibitor and $[\%T]_{passive}$ was determined from the dotted curve in Fig. IV.3. As a result, the percent of control by each of the inhibitors was calculated from:

$$(\%\ \text{of control}) = \frac{[\%T]_{active,inh}}{[\%T]_{active,control}} \times 100 \qquad \text{(Eqn. IV.2)}$$

where $[\%T]_{active,control}$ was the % of administered dose transferred to perfusate in 30 minutes in the absence of inhibitors. Concentrations, at which 50 % of active absorption inhibition was obtained, or apparent IC_{50} values for inhibition, were estimated, when possible, by extrapolation of data for inhibition (based on Eqn. IV.2) *vs.* logarithmic inhibitor concentrations.

IV.c RESULTS

IV.c.1 PULMONARY ABSORPTION IN THE IPRL AT LOW TEMPERATURE

At temperatures < 25 °C, rapid edema formation was seen as a glossy sheen on the pulmonary lobes beginning within 30 minutes (Appendix I). In contrast, at 25 and 30 °C, edema was absent and the preparation successfully maintained viability for 180 minutes, as evidenced by the lack of sharp discontinuities in solute absorption profiles (Figs. IV.6 and IV.7; Sun, 1995; Appendix I).

Figure IV. 4 shows the percent of each administered dose of 7.4 kDa F-PHEA (nominal 0.2 mg dose) transferred to perfusate in the IPRL *vs.* time at 37, 30 and 25 °C. The rate and extent of absorption were dramatically reduced with lowering perfusion temperatures. This absorption suppression due to reduced temperature was moderated with increasing doses of F-PHEA and, at a nominal 5.0 mg dose, the profiles at 25 °C were insignificantly different from those at 37 °C (Fig. IV.5; ANOVA). This indicated that lowering temperature preferentially suppressed F-PHEA's active absorption component, which was predominant at the lower doses; the passive absorption component was largely unaffected by this maneuver (Table IV.2). Despite this absorption suppression, the absorption profiles at 25 °C were still slightly dose-dependent, as shown in Fig. IV.6. The solid curves through the data in Fig. IV.6 are the results of simultaneous

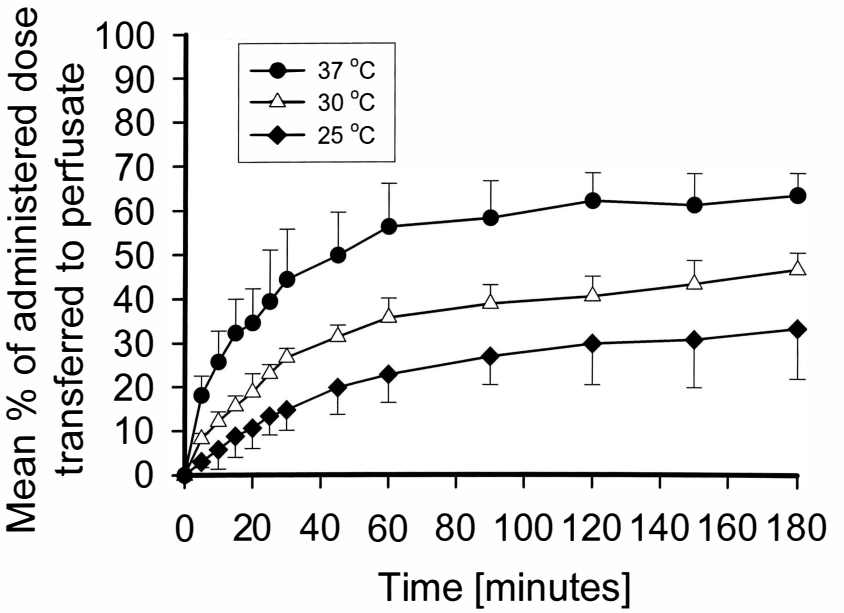

Figure IV.4. Mean percentage of administered dose of 7.4 kDa F-PHEA (nominal dose = 0.2 mg) absorbed from the airways of the IPRL into the perfusate *vs.* time at 37, 30 and 25 °C. Error bars are sample standard deviations with n=4. The solid curves are the results of linear interpolation.

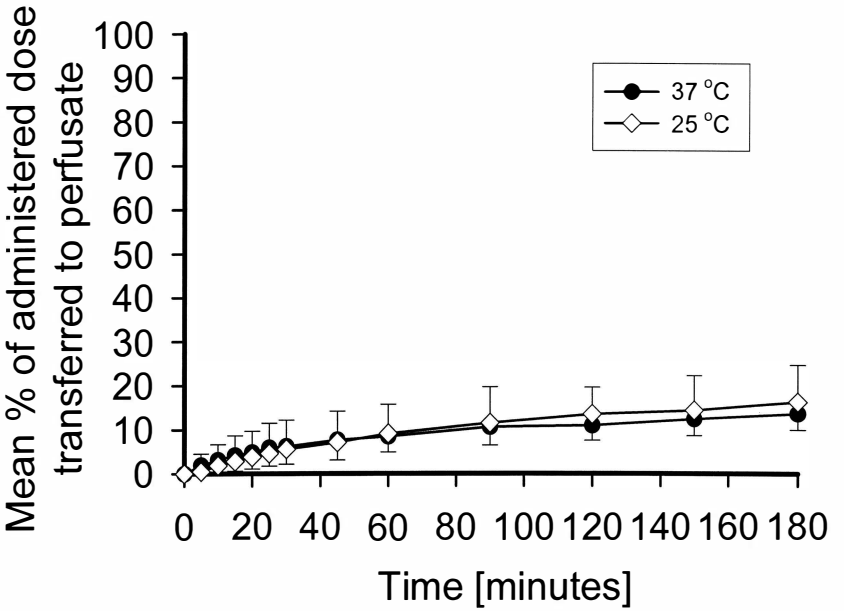

Figure IV.5. Mean percentage of administered dose of 7.4 kDa F-PHEA (nominal dose = 5.0 mg) absorbed from the airways of the IPRL into the perfusate *vs.* time at 37 and 25 °C. Error bars are sample standard deviations with n=4. The solid curves are the results of linear interpolation.

Table IV.2. Disposition parameters for active and passive absorption and mucociliary clearance for 7.4 kDa F-PHEA following its administration into the airways of the isolated perfused rat lung (IPRL) at 37 and 25 °C.

Temp.	Active absorption			Passive absorption	Mucociliary clearance	MSC; R^2
	$V_{max,P}$ [μg/min]	$K_{m,P}$ [μg]	$V_{max,P}/K_{m,P}$ [min^{-1}]	$k_{a,P}$ [min^{-1}]	$k_{E,PT}$ [min^{-1}]	
37 °C	4.37* (0.57)	56.6 (14.7)	0.077	0.001 (0.001)	0.023** (0.001)	3.12; 0.986
25 °C	0.67* (0.10)	30.3 (16.4)	0.022	0.002 (0.001)	0.016** (0.001)	3.74; 0.991

Values are the best estimates (SD) following analysis of across-dose data for F-PHEA. Nominal doses: 0.1, 0.2, 0.5, 1.0 and 5.0 mg at 37 °C; 0.2, 0.5, 1.0 and 5.0 mg at 25 °C. MSC (Model Selection Criterion) and R^2 (R-squared) were as calculated by "Scientist" (Appendix VI).

* and ** indicate significant difference ($p<0.05$) between values of $V_{max,P}$ and $k_{E,PT}$, respectively, based on overlapped 95% confidence intervals.

The values for $K_{m,P}$ and $k_{a,P}$ were insignificantly different between 37 and 25 °C, based on the same approach.

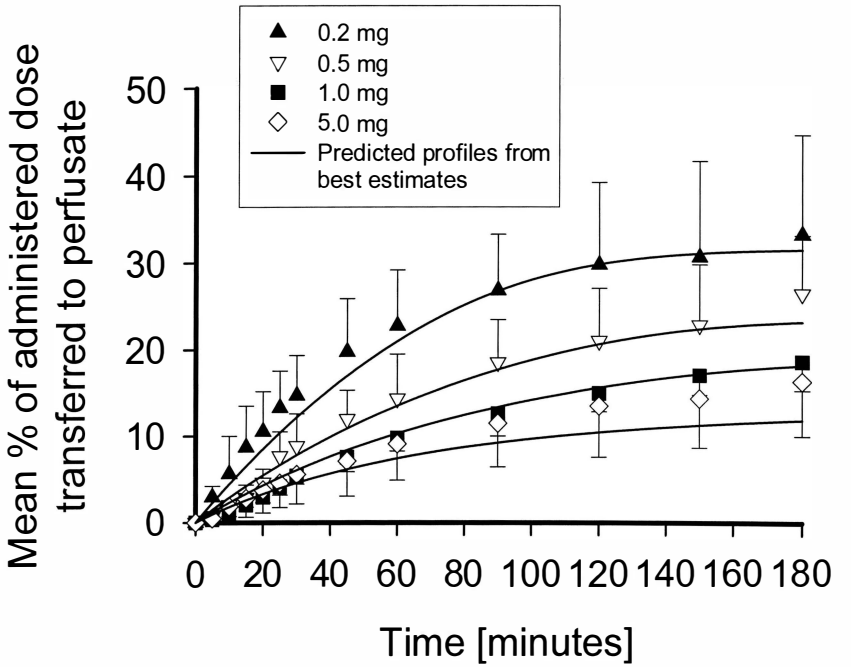

Figure IV.6. Mean percentage (±SD; n=4) of administered dose of 7.4 kDa F-PHEA absorbed from the airways of the IPRL into the perfusate *vs.* time at 25 °C. The solid curves are the results of simultaneous across-dose curve fitting of all profiles. These were generated using the best estimates determined for each parameter at 25 °C, as described in Table IV.2 ($V_{max,P}$, $K_{m,P}$, $k_{a,P}$ and $k_{E,PT}$ = 0.67 [μg/min], 30.3 [μg], 0.002 [min^{-1}] and 0.016 [min^{-1}], respectively).

curve fitting across doses of the 25 °C data (nominal doses of 0.2, 0.5, 1.0 and 5.0 mg) to the model shown in Fig. IV.1. The best parameter estimates from which these curves were generated are shown in Table IV.2 along with those at 37 °C (Chapter 3). The "goodness-of-fit" parameters provided by "Scientist"-calculated Model Selection Criterion (MSC) and R-squared (R^2) were 3.74 and 0.991, respectively, for the 25 °C data, and the parameters were successfully estimated with relatively small standard deviations (Table IV.2). An "intrinsic rate constant" for active absorption, calculated by $V_{max,P}/K_{m,P}$ was found to be much smaller (0.022 min^{-1}) than that determined at 37 °C (0.077 min^{-1}). This active absorption suppression was apparently dominated by the significant decrease in the value of $V_{max,P}$ (maximum rate; 4.37±0.57 → 0.67±0.10 µg/min; $p < 0.05$, based on non-overlapped 95% confidence intervals (95%CI)). The "affinity" of the transporter, $K_{m,P}$, remained effectively constant (56.6±14.7 *vs.* 30.3±16.4 µg, based on overlapped 95%CI). It appeared therefore, that the lower 25 °C perfusion temperature slowed the active absorption process for F-PHEA without modifying the value of dose, at which 50 % saturation was achieved. Nevertheless, the contribution of active absorption to F-PHEA's airway-to-perfusate transfer was still significant at 25 °C (Fig. IV.6).

Average percent transfer (±SD) of administered dose *vs.* time for F-Na and FD-4 at 25 °C is shown in Fig. IV.7. As seen at 37 °C (Fig. III.6 in Chapter 3), these profiles were found to be dose-independent. Data could be fitted to the model shown in Fig. IV.1 in which only passive absorption from the pulmonary region, $k_{a,P}$, and simultaneous

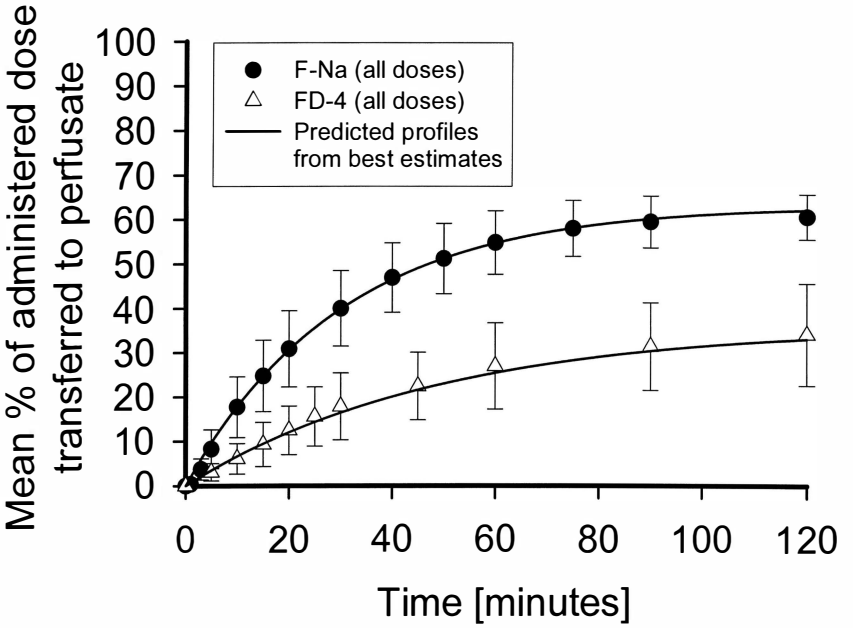

Figure IV.7. Mean percentage of administered dose of F-Na and FD-4 absorbed from the airways of the IPRL into the perfusate *vs.* time at 25 °C. Error bars are sample standard deviations with n=4.
The solid curves are the results of simultaneous across-dose curve fitting and the best estimates for each process are shown in Table IV.2. All doses: *F-Na* - 0.01, 0.02 and 0.04 mg; *FD-4* - 0.1 and 0.2 mg.

mucociliary clearance, $k_{E,PT}$, occurred ($V_{max,P}$ and $K_{m,P} = 0$). The across-dose 25 °C data fits to Eqns. III.2, III.4 and III.5 (Chapter 3) successfully yielded values for $k_{a,P}$ and $k_{E,PT}$, as shown in Table IV.3 along with the values for F-PHEA. The rate constants for passive absorption, $k_{a,P}$, at 25 °C were found to be smaller, compared to those at 37 °C (Table III.2 in Chapter 3), due probably to the solute's lower diffusivity and/or partitioning to the membrane at lower temperatures (Notari, 1987; Martin, 1993). Thus, while it should be noted that there was no significant difference between the values for $k_{a,P}$ for F-PHEA at 37 and 25 °C (0.001±0.001 *vs.* 0.002±0.001 min^{-1}, respectively; based on overlapped 95%CI), these values were less precisely estimated than those for F-Na and FD-4. This was due to the difficulty involved in multiple parameter estimation for solutes like F-PHEA which also possess a much longer passive absorption half-life ($0.693/k_{a,P}$; ≥ 6 hours); one, in fact, which is far larger than the 180 minute IPRL viability during which absorption data could be obtained. For similar reasons, the rate constants for mucociliary clearance, $k_{E,PT}$, were found to be solute-independent, but also smaller at 25 °C, compared to those at 37 °C. This decrease of mucociliary clearance rates with lowering temperature has been consistently observed in other studies (Mercke *et al.*, 1974; Sanderson and Dirksen, 1985) and is most likely to be related to cAMP- and ATP- dependent regulation mechanisms for this process (Lansley, 1993; Camner and Mossberg, 1993).

Table IV.3. Disposition parameters for active and passive absorption and mucociliary clearance for 7.4 kDa F-PHEA, FD-4 and F-Na following their administration into the airways of the isolated perfused rat lung (IPRL) at 25 °C.

Solutes (Mw)	Active absorption			Passive absorption	Mucociliary clearance	MSC; R^2
	$V_{max,P}$ [μg/min]	$K_{m,P}$ [μg]	$V_{max,P}/K_{m,P}$ [min^{-1}]	$k_{a,P}$ [min^{-1}]	$k_{E,PT}$ [min^{-1}]	
F-PHEA (7.4 kDa)	0.67 (0.10)	30.3 (16.4)	0.022	0.002* (0.001)	0.016 (0.001)	3.74; 0.991
FD-4 (4.4 kDa)	N/A	N/A	N/A	0.008* (0.001)	0.012 (0.002)	2.87; 0.985
F-Na (376 Da)	N/A	N/A	N/A	0.023* (0.001)	0.010 (0.002)	3.12; 0.987

Values are the best estimates (SD) following analysis of across-dose data from:
F-PHEA - nominal doses 0.2, 0.5, 1.0 and 5.0 mg; *FD-4* - nominal doses 0.1 and 0.2 mg; *F-Na* - nominal doses 0.01, 0.02 and 0.04 mg.
MSC (Model Selection Criterion) and R^2 (R-squared) were as calculated by "Scientist" (Appendix VI).
N/A indicates "not applicable".
* indicates significant difference ($p<0.05$) between values of $k_{a,P}$, based on overlapped 95% confidence intervals.
The values for $k_{E,PT}$ were insignificantly different across solutes, based on the same approach.

Values of $k_{a,P}$ and $k_{E,PT}$ for FD-4 and F-Na at 37 °C were as follows (Table III.2, Chapter 3):
FD-4 - $k_{a,P}$ = 0.016 (0.001) min^{-1} and $k_{E,PT}$ = 0.029 (0.003) min^{-1};
F-Na - $k_{a,P}$ = 0.048 (0.003) min^{-1} and $k_{E,PT}$ = 0.022 (0.002) min^{-1}.

IV.c.2 PULMONARY ABSORPTION AT 37 °C IN THE PRESENCE OF METABOLIC INHIBITORS

IPRL viability could be maintained for only 60 minutes in the presence of the highest concentrations of DNP and OUA in perfusate and for 120 minutes in the presence of the highest concentrations of MON and NOC in the airways. The lungs displayed edema formation as the appearance of a glossy sheen on the pulmonary lobes thereafter. No data is included in this thesis from such edematous preparations.

(1) Passive absorption and mucociliary clearance kinetics in the presence of inhibitors

The average percent transfer (±SD) of a passively-absorbed small solute, F-Na (nominal dose = 0.02 mg), from airway-to-perfusate is shown in Fig. IV.8 in the absence and the presence of various metabolic inhibitors. The highest concentrations of the metabolic inhibitors used in this thesis (1 mM DNP or 100 μM OUA in perfusate or 100 μM MON or NOC in the airways) showed no significant changes in F-Na absorption profiles throughout the available, viable lifetime of the preparation, when compared to those in the absence of inhibitors (ANOVA). Because F-Na's transfer kinetics were shown previously (Chapter 3) to be passive, and clearly dependent upon mucociliary clearance, this demonstrated that passive absorption and mucociliary clearance kinetics were unaffected by the presence of these inhibitors at the concentrations employed in this thesis.

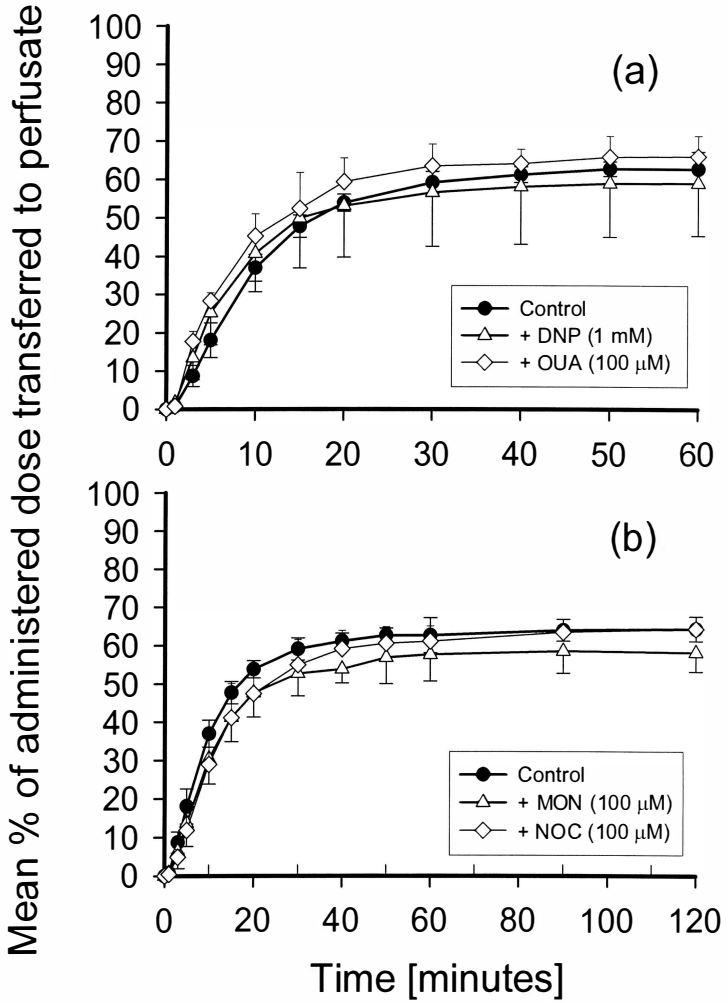

Figure IV.8. Mean percentage (±SD; n=4) of administered dose of F-Na (nominal dose = 0.02 mg) absorbed from the airways of the IPRL into the perfusate *vs.* time. Data shown is in the absence (control) and the presence of (a) 1 mM 2,4-dinitrophenol (DNP) and 100 μM ouabain (OUA) and (b) 100 μM monensin (MON) and 100 μM nocodazole (NOC) at 37 °C. The solid curves are the results of linear interpolation. DNP and OUA were placed in the perfusate at 15 minutes prior to F-PHEA administration and MON and NOC were co-administered into the airways with F-PHEA. Profiles in the presence of the metabolic inhibitors were insignificantly different from the controls (ANOVA).

(2) Pulmonary absorption of 7.4 kDa F-PHEA in the presence of 2,4-dinitrophenol (DNP)

2,4-Dinitrophenol (DNP) was used to inhibit intracellular mitochondrial ATP synthesis (Goodman *et al.*, 1983; Steen *et al.*, 1993; Muranushi, *et al.*, 1994; Alberts *et al.*, 1994) which was presumed to be necessary to provide energy for F-PHEA's active absorption from the airways. The experimental protocol was optimized based on preliminary studies in which different DNP perfusion periods were employed prior to F-PHEA administration into the airways. When 1.0 mM DNP was recirculated for either 5, 15 or 30 minutes prior to F-PHEA administration, the mean values for % of each administered dose of F-PHEA (nominal dose = 0.2 mg) transferred to perfusate in 30 minutes were found to be 24.5±2.4, 16.2±5.3 and 13.4±2.5 % (mean±SD; n=4), respectively. Because the latter two were insignificantly different (*t*-test), a 15 minute pre-perfusion time period was employed in the protocol to maximize the inhibition of F-PHEA absorption without unnecessarily shortening the viable lifetime of the IPRL.

Figure IV.9 shows the percent transfer of F-PHEA (nominal dose = 0.2 mg) from airways to perfusate *vs.* time in the absence (control) and the presence of 0.05, 0.1, 0.2, 0.5 and 1.0 mM DNP in perfusate. Clearly, F-PHEA absorption was suppressed by DNP in a concentration-dependent fashion, demonstrating the likelihood that ATP-driven intracellular energy was necessary for this F-PHEA active absorption from the airways to occur. Based on the assumption that the first 30 minute's data was most reliable, DNP-concentration-dependent inhibition of F-PHEA's *active* absorption was calculated using

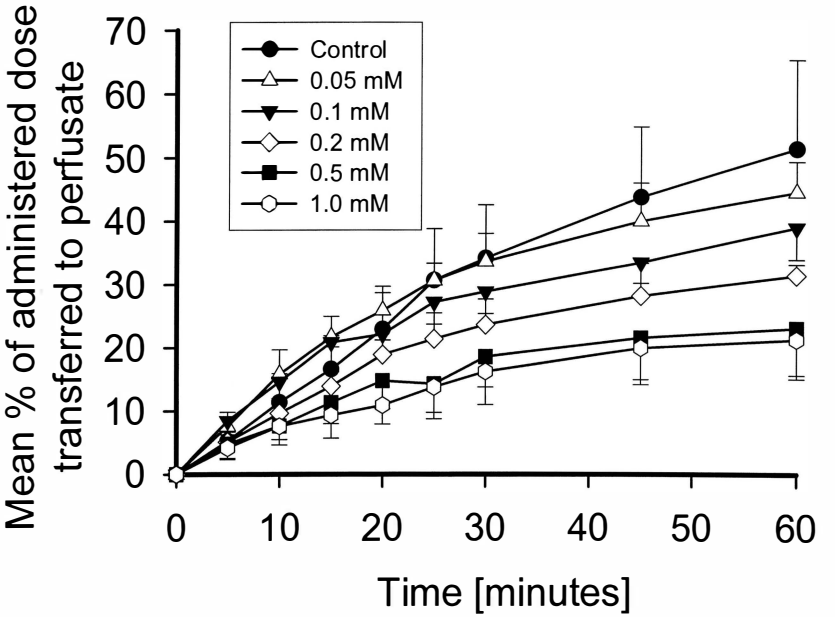

Figure IV.9. Mean percentage of administered dose of 7.4 kDa F-PHEA (nominal dose = 0.2 mg) absorbed from the airways of the IPRL into the perfusate *vs.* time in the presence of various concentrations of 2,4-dinitrophenol (DNP) at 37 °C. DNP was placed into the perfusate at 15 minutes prior to F-PHEA administration. Error bars are sample standard deviations with n=4. The solid curves are the results of linear interpolation.

Eqns. IV.1-2. This is shown in Fig. IV.10. Despite its evident concentration-dependence, the maximum extent of F-PHEA's active absorption inhibition by DNP was found to be only 53.3±7.9 % (mean±SE; n=4) and thus, DNP's IC_{50} value was estimated to be between 0.5 and 1.0 mM in perfusate.

(3) Pulmonary absorption of 7.4 kDa F-PHEA in the presence of ouabain (OUA)

Ouabain (OUA) is a well-known Na^+/K^+-ATPase inhibitor (Basset *et al.*, 1987; Saumon and Martet, 1993; Alberts *et al.*, 1994; Rose and Valdes 1994; Michaut *et al.*, 1996). In this thesis, it was used to relate its inhibition effects of indirect intracellular ATP hydrolysis with F-PHEA's active absorption, since active transport must consume ATP-derived hydrolysis energy either directly or indirectly (Rose and Valdes 1994; Michaut *et al.*, 1996). Similar to the studies using DNP, the experimental protocol was optimized based on preliminary studies in which OUA perfusion periods prior to F-PHEA administration were varied. In the presence of 100 μM OUA circulating for 1, 15 or 30 minutes prior to F-PHEA administration, the % transfer of F-PHEA (nominal dose = 0.2 mg) into perfusate over a 30 minute period was found to be 26.0±2.9, 8.8±3.4 or 11.4±3.7 % (mean±SD; n=3-4), respectively. Because the latter two values differed insignificantly (*t*-test), a 15 minute pre-perfusion time period was again employed to maximize transport inhibition without unnecessarily shortening the IPRL's viable lifetime.

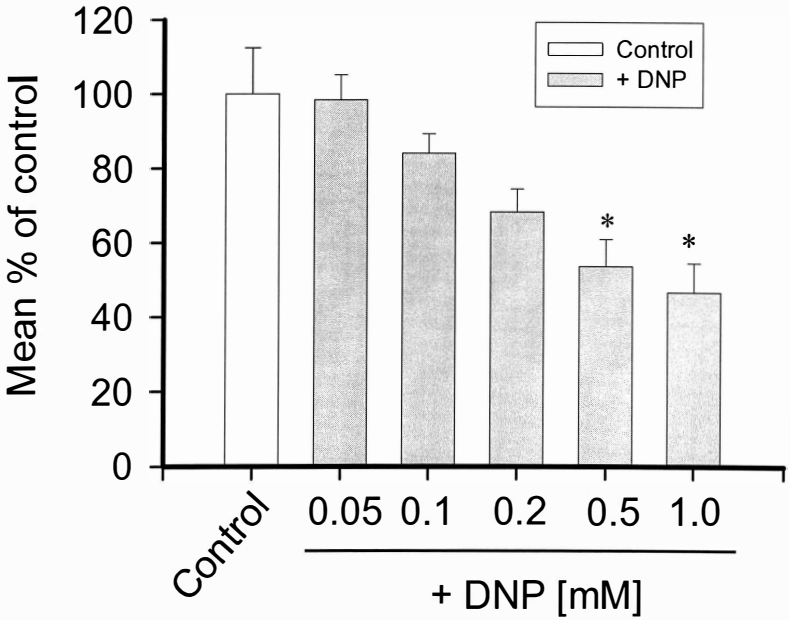

Figure IV.10. Mean percentage of control value for F-PHEA active transfer in the first 30 minutes following administration at 37 °C. The effect of the presence of various concentrations of 2,4-dinitrophenol (DNP) in the perfusate is illustrated (control = 0 mM DNP). Error bars are sample standard errors (SE) with n = 4. DNP was placed in the perfusate at 15 minutes prior to F-PHEA administration.
* indicates significant difference, compared to the control (Dunnett method following multiple ANOVA; $p<0.05$).

The average percent transfer (±SD; n=4) of F-PHEA at a nominal 0.2 mg dose is shown *vs.* time in the absence (control) and the presence of 5, 50 and 100 μM OUA in Fig. IV.11. F-PHEA absorption was inhibited by OUA in a concentration-dependent fashion, suggesting the likelihood that F-PHEA's active absorption required OUA-inhibitable ATP hydrolysis energy in the cells. Figure IV.12 shows the effects of OUA on F-PHEA *active* absorption over the first 30 minutes, calculated using Eqns. IV.1-2. The maximum absorption inhibition due to OUA was found to be 75.9±5.1 % (mean±SE; n=4) with an apparent its IC_{50} value of 30-50 μM in perfusate.

(4) Pulmonary absorption of 7.4 kDa F-PHEA in the presence of monensin (MON) and nocodazole (NOC)

Monensin (MON) is a Na^+/H^+ ionophore used to prevent acidification of intracellular endosomal vesicles (Mollenhauer *et al.*, 1990; Dinter and Berger, 1998), while nocodazole (NOC) is known to depolymerize microtubules in an energy-dependent process (Turner and Tartakoff, 1989; Dinter and Berger, 1998). Both inhibitors were used to inhibit endocytotic (transcytotic) transport processes (Mollenhauer *et al.*, 1990; Dinter and Berger, 1998; Hastings *et al.*, 1994; Deffebach *et al.*, 1996; Wangensteen *et al.*, 1996; Dinter and Berger, 1998) and their inhibition evidence suggested an involvement of intracellular vesicular transport for F-PHEA between the airways and the perfusate. The experimental protocols for these inhibitors were selected from literature in which co-administration of both MON (30-35 μM) and NOC (30-35 μM) had been used to inhibit

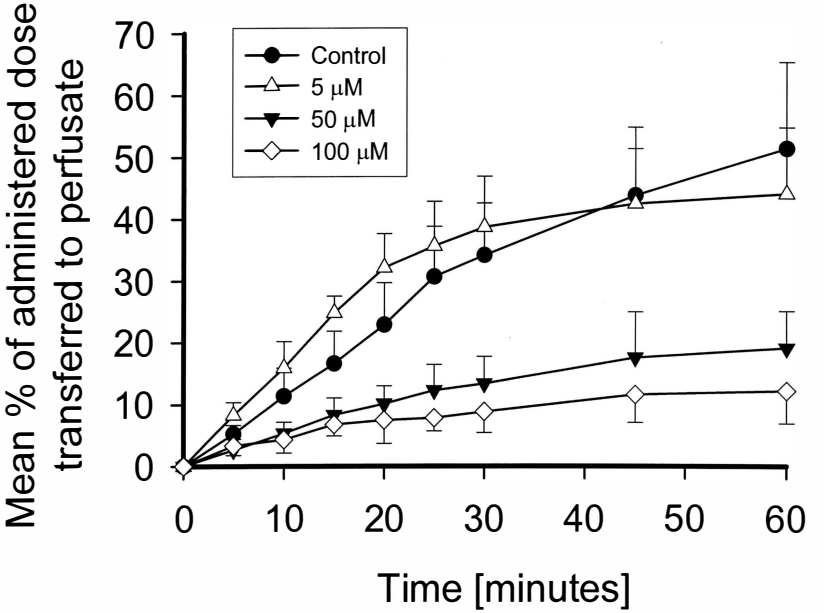

Figure IV.11. Mean percentage of administered dose of 7.4 kDa F-PHEA (nominal dose = 0.2 mg) absorbed from the airways of the IPRL into the perfusate *vs.* time in the presence of various concentrations of ouabain (OUA) at 37 °C. OUA was placed into the perfusate 15 minutes prior to F-PHEA administration into the airways. Error bars are sample standard deviations with n=4. The solid curves are the results of linear interpolation.

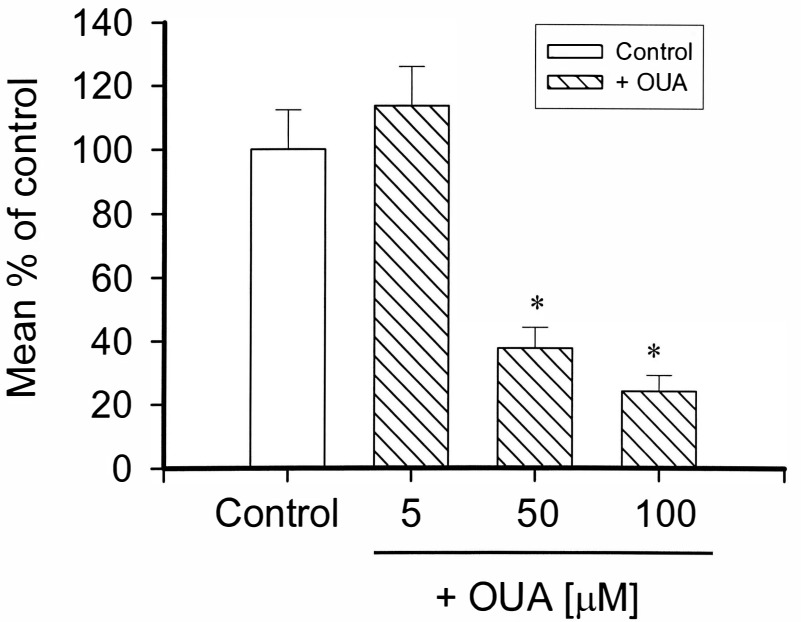

Figure IV.12. Mean percentage of control value for F-PHEA active transport in the first 30 minutes following administration.The effect of the presence of various concentrations of ouabain (OUA) in the perfusate is illustrated (control = 0 μM OUA). Error bars are sample standard errors (SE) with n = 4. OUA was placed in the perfusate at 15 minutes prior to F-PHEA administration.
* indicates significant difference, compared to the control (Dunnett method following multiple ANOVA; $p<0.05$).

receptor-mediated transcytotic absorption of albumin and its riboflavin-conjugates from the airways of the IPRL (Hastings *et al.*, 1994; Wangensteen *et al.*, 1996).

The average percent (±SD; n=4) transfer to perfusate of F-PHEA at nominal 0.2 mg doses is shown *vs.* time in the absence (control) and the presence of MON (5, 10, 30 and 100 μM) and NOC (0.5, 1, 10, 30 and 100 μM) in Figs. IV.13 and IV.14, respectively. F-PHEA *active* absorption was inhibited in a concentration-dependent fashion by both inhibitors, as shown in Fig. IV.15. Apparent IC_{50} values = 10-30 μM for MON and 1-5 μM for NOC were calculated. Based on these results, it appeared that F-PHEA absorption may involve endosomal and microtubular vesicular transport during active transcytosis.

IV.d DISCUSSION

While biochemical approaches like lowered temperature studies and the use of metabolic inhibitors are generally used, these require a thorough validation in each experimental system to ensure that all possible effects of experimental perturbation are considered. To characterize the mechanisms responsible for active absorption of 7.4 kDa F-PHEA from the airways of the IPRL, the viability (absence of pulmonary edema) under all conditions and/or a lack of changes in other kinetic components (e.g., passive absorption and mucociliary clearance) were demonstrated for all metabolic inhibitor

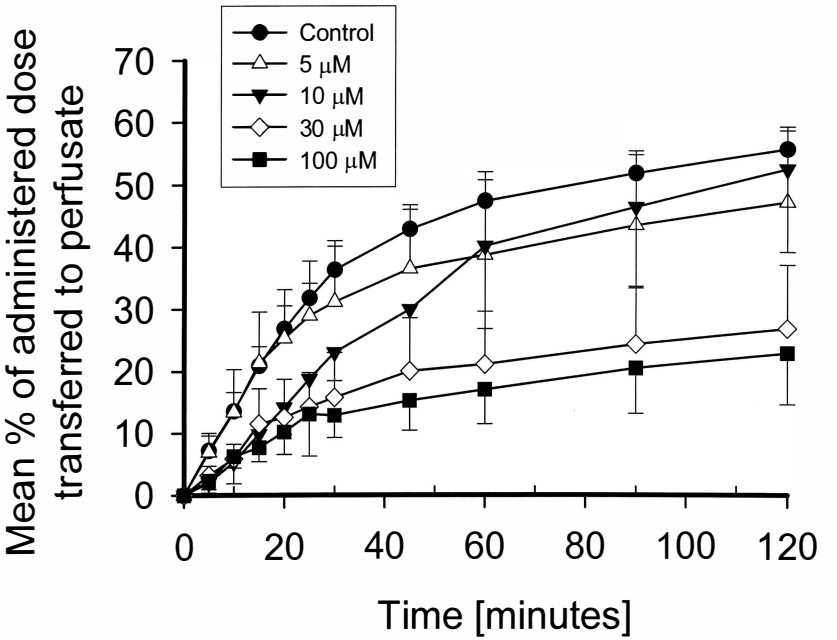

Figure IV.13. Mean percentage of administered dose of 7.4 kDa F-PHEA (nominal dose = 0.2 mg) absorbed from the airways of the IPRL into the perfusate *vs.* time in the presence of various concentrations of monensin (MON) at 37 °C. MON was co-administered into the airways with F-PHEA. Error bars are sample standard deviations with n=4. The solid curves are the results of linear interpolation.

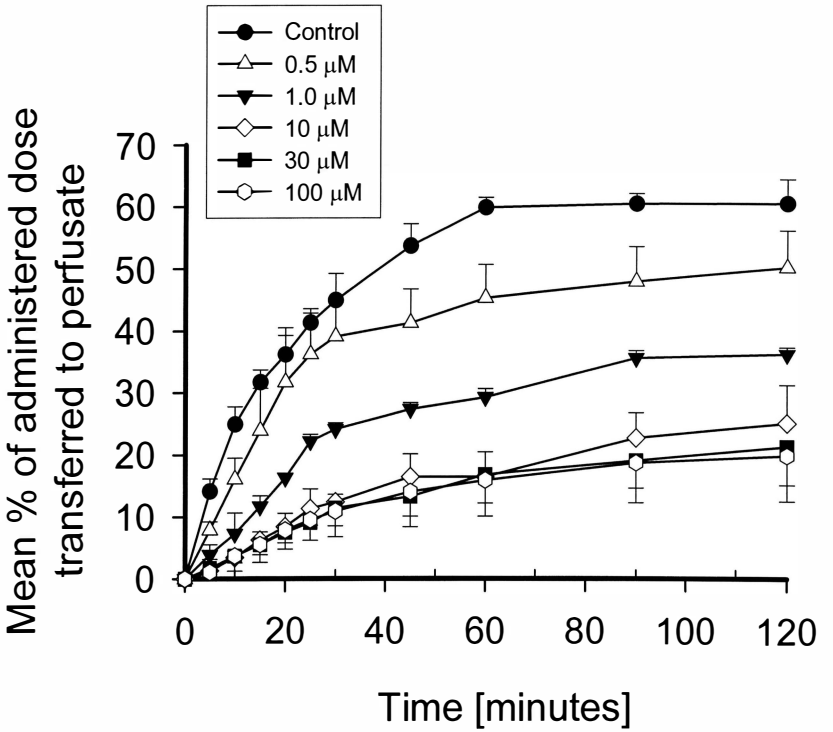

Figure IV.14. Mean percentage of administered dose of 7.4 kDa F-PHEA (nominal dose = 0.2 mg) absorbed from the airways of the IPRL into the perfusate *vs.* time in the presence of various concentrations of nocodazole (NOC) at 37 °C. NOC was co-administered into the airways with F-PHEA. Error bars are sample standard deviations with n=4. The solid curves are the results of linear interpolation.

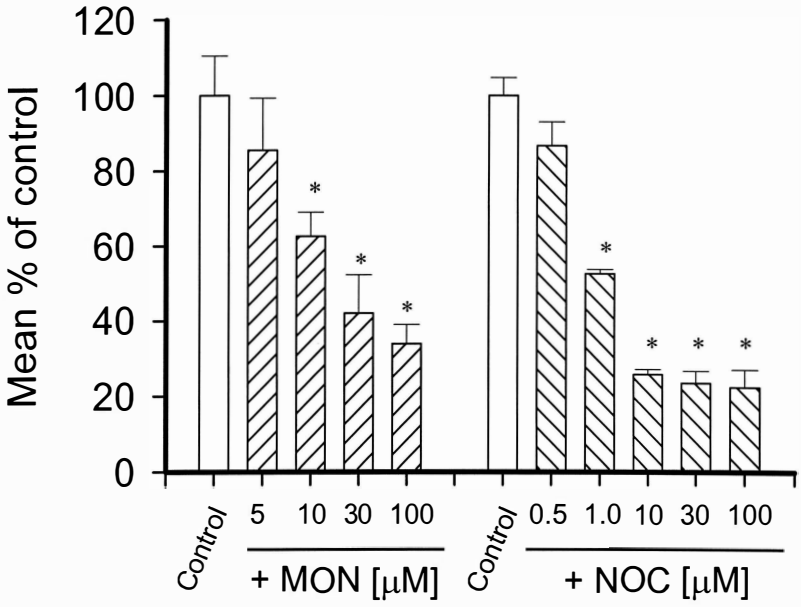

Figure IV.15. Mean percentage of control value for F-PHEA active transport in the first 30 minutes following administration. The effect of the presence of various concentrations of monensin (MON) and nocodazole (NOC) in the airways is illustrated (controls involved sham experiments performed in the absence of inhibitors). Error bars are sample standard errors (SE) with n = 4. MON and NOC were co-administered into the airways with F-PHEA.
* indicates significant difference, compared to each control (Dunnett method following multiple ANOVA; $p<0.05$).

studies. Effects of altered vehicle composition and pre-incubation periods were also studied in control experiments.

In early studies, we found that a lower 4 °C perfusion induced pulmonary edema formation quite rapidly (≤ 12 minutes; Sun, 1995) and this was also found to be true at intermediate temperatures which were significantly < 25 °C (Section IV.c.1). In fact, not only edema, but also discontinuities in the absorption profiles for F-PHEA were observed at 15 °C, as shown in Fig. AI.7 (b) (Appendix I). These effects precluded the use of such low temperature conditions in this thesis. Table IV.4 is a summary of the isolated perfused lung (IPL) studies in the literature, in which low temperature perfusion has been used. Most IPL study periods have been limited to ≤ 30 minutes at 4-10 °C and thus, it is likely that pulmonary edema occurred rapidly in all rat studies. The use of autologous blood or plasma as the perfusate in larger animal studies may well reduce this problem (Table IV.4). In contrast, in this thesis, extremely low temperatures were found to be unacceptable, while 25 °C perfusion was tolerable and successful in maintaining IPRL viability for ≥ 180 minutes; this, with no display of pulmonary edema and no discontinuities in absorption profiles (Figs. IV.6 and IV.7). Because all metabolic inhibitors used in this thesis (2,4-dinitrophenol (DNP), ouabain (OUA), monensin (MON) and nocodazole (NOC)) also induced edema formation concentration-dependently (those with highest concentrations being the greatest offenders), IPRL studies were limited to only 60 minutes in the presence of DNP and OUA and 120 minutes for MON and NOC at their highest concentrations. It is likely that the occurrence

Table IV.4. Summary of the isolated perfused lung (IPL) studies performed at lower temperatures (from the literature).

IPL	Temp.	Perfusate	Study period	Substrate	Reference[1]
<Studies for pulmonary disposition>					
Rat	4 °C	Buffer	30 min	Imipramine	Junod, 1972
		Buffer	< 10 min	Propranolol	Dollery, 1976
		Buffer	30 min	Choline	Johnson, 1979
		Buffer	30 min	Phenylamine	Ben-Harari, 1980
		Buffer	7 min	Albumin-gold	Villaschi, 1986
		Buffer	< 15 min	Propanediamine	Slosman, 1987
		Buffer	< 15 min	Guanidine	Slosman, 1988
	8 °C	Buffer	1 min	Antipyrine	Cua, 1990
Guinea pig	5 °C	Buffer	30 min	PGE_2 *1	Pitt, 1985
Rabbit	5 °C	Buffer	1 min	Antipyrine	Effros, 1985
	10 °C	Buffer	< 20 min	BPAAP*2	Ashton, 1985
Rabbit	12 °C	Blood	4.5 hr	BSA*3	Hostetler, 1981
Dog	15 °C	Plasma	< 1 min	^3H_2O	Chinard, 1986
Goat	7, 18, 30 °C	Blood	4 hr	Albumin	Serikov, 1993
<Studies for pulmonary edema>					
Rabbit	28 °C	Buffer	< 2 hr		Nicolaysen, 1971
		Plasma	< 6 hr		
Dog	25 °C	Blood	2 hr		Veith, 1971

[1] Only first authors and years of publication; details are described in References.
*1 Prostagrandin E_2, *2 benzoyl-phenylalanyl-alanyl-proline and *3 bovine serum albumin

of pulmonary edema was related to the inhibition of Na^+-dependent active fluid resorption from the airways at reduced temperatures and/or the presence of metabolic inhibitors (Hostetter *et al.*, 1981; Serikov *et al.*, 1993; Basset *et al.*, 1994; Cott, 1994; Effros, 1994; Hastings *et al.*, 1994; Wangensteen *et al.*, 1996). Rates of fluid resorption have been studied in several IPL preparations and found to be 27-34 pL/cm^2/s at 37 ^{o}C (Basset *et al.*, 1987a and b; Effros *et al.*, 1989; Berg *et al.*, 1989), which can account for 0.5-0.6 mL/hr from the rat lung (assuming its alveolar surface area = 0.5 m^2; Weibel, 1985). This rapid fluid absorption capability is tightly regulated by apical Na^+ channel (ENaC) and basolateral Na^+/K^+-ATPase on alveolar type II epithelial cell membranes and hence, both processes are Na^+-dependent and energy consuming (Basset *et al.*, 1994; Cott, 1994; Effros, 1994). Unfortunately, these active transport processes are also subject to inhibition or modulation by lowered temperature and the same metabolic inhibitors used in this thesis, due to their function-specific inhibition mechanisms. In fact, alveolar fluid absorption was slowed (but not abolished) at 4 ^{o}C and also by the presence of 1mM DNP in rat alveolar type II epithelial cell systems (Goodman *et al.*, 1983) and 100-500 μM ouabain in the IPRL (Basset *et al.*, 1987; Saumon and Martet, 1993; Saldias *et al.*, 1998a and b).

Passive absorption and mucociliary clearance kinetics for the small model solute, F-Na were unaffected by the presence of the metabolic inhibitors (DNP: 1 mM; OUA: 100 μM; MON: 100 μM; NOC: 100 μM) used in this thesis, as shown in Fig. IV.8. Similarly, it was demonstrated in other IPRL studies, that the absorption of small hydrophilic

solutes, mannitol (182 Da) and sucrose (342 Da) were unaffected by the presence of OUA in perfusate (200-500 μM; Sauman and Martet, 1993; Salidias *et al.*, 1998a and b) and MON and NOC administration to the airways (35 μM; Wangensteen *et al.*, 1996), respectively. These results were used to argue that passive absorption and mucociliary clearance kinetics for macromolecular F-PHEA should also be unchanged in their presence, thus enabling a kinetic analysis of F-PHEA's active absorption inhibition due to manipulation of the readily available cellular energy supplies.

In order to maximize the inhibitory effects of metabolic inhibitors on F-PHEA absorption, it was found that 15 minute pre-perfusion in the presence of the inhibitor, prior to solute administration, was required in the case of DNP and OUA. Similarly, and for dissolution purposes, 1.5 % (v/v) EtOH and DMSO solutions were used as administration vehicles for MON and NOC, respectively. Even though these perturbations produced modest changes in the percent of F-PHEA transfer over 30 minutes at a nominal 0.2 mg dose, the overall % transfer in each control group differed insignificantly from the values obtained following aqueous F-PHEA solution administration immediately after perfusion was commenced (0 minute interval; Dunnett method following multiple ANOVA; $p > 0.05$). This is illustrated in Fig. IV.16. In the perfusate-recirculated IPRL, ATP levels and cellular energy charge are maintained for ≥ 100 minutes at 37 ^{o}C according to the literature (Basset *et al.*, 1987; Baker *et al.*, 1999). Furthermore, 1.5 % (v/v) of EtOH and DMSO used as airway administration vehicles were shown to have no effects on protein absorption from the airways (Hastings *et al.*,

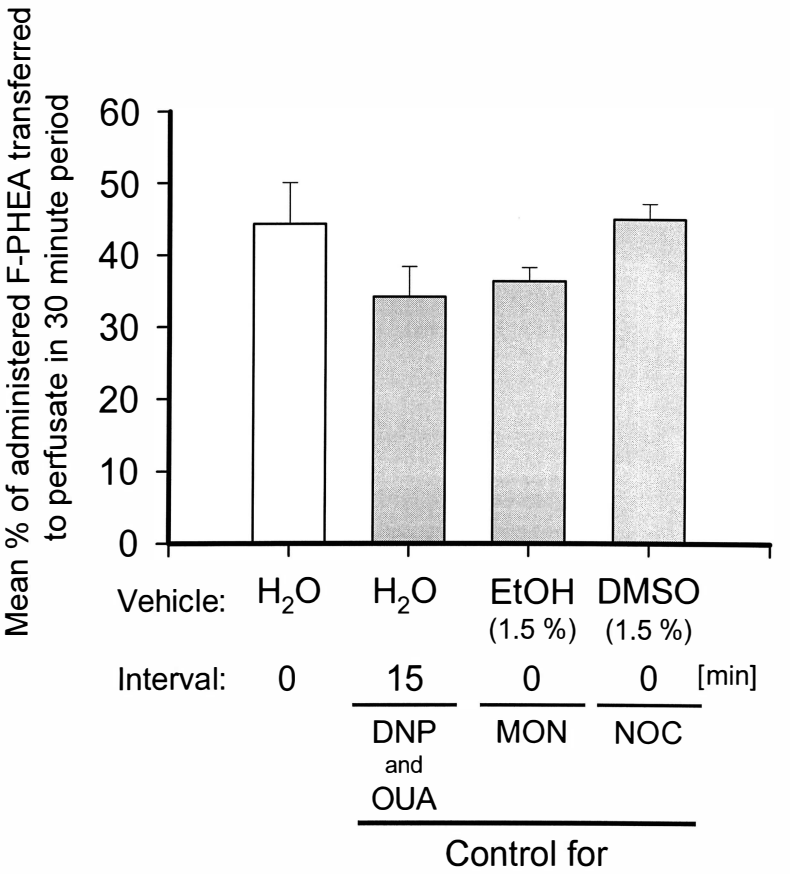

Figure IV.16. Effect of perfusion intervals (prior to administration) and composition of administration vehicles on the mean percentage of the administered dose of 7.4 kDa F-PHEA (nominal dose = 0.2 mg) absorbed from the airways over a 30 minute time period at 37 °C. Each experimental condition was employed as a control group for studying F-PHEA absorption in the presence of metabolic inhibitors. Error bars are sample standard errors (SE) with n = 4. No significant differences were observed in the amounts transferred between control groups, when compared to aqueous F-PHEA administration immediately after perfusion commenced (Dunnett method following multiple ANOVA).

1994; Wangensteen *et al.*, 1996). It is likely therefore, that the active absorption kinetics reported for F-PHEA in Chapter 3 in this thesis were unaffected by the presence of either 15 minute pre-perfusion prior to dosing or the use of EtOH and DMSO in the dosing vehicle. Consequently, inhibitory effects on F-PHEA active absorption should be comparable across inhibitors and be primarily due to the action(s) of the inhibitors themselves.

PULMONARY ABSORPTION KINETICS FOR 7.4 kDa F-PHEA AT LOW TEMPERATURE

Active absorption is generally known to be temperature-sensitive in mammalian cells (Willingham and Pastan, 1985). Its activity is maximal at physiological temperatures (37 ^{o}C), decreased between 15 and 30 ^{o}C and abolished at 4 ^{o}C (Williams *et al.*, 1979; Wangensteen, 1990; Rutschman *et al.*, 1993). These effects are mostly caused by non-specific reduction of ATP utilization and oxidative phosphorylation in combined cell systems at lower temperatures (Williams *et al.*, 1979; Goodman *et al.*, 1983). Thus, reduced temperature, especially the extreme of 4 ^{o}C, has been extensively used to inhibit active absorption processes in solute disposition studies (Borchardt *et al.*, 1996). Unfortunately, in the IPRL preparation used in this thesis, the minimum temperature was limited to 25 ^{o}C due to the rapid induction of pulmonary edema at lower temperatures. As

a result, F-PHEA absorption at 25 °C was suppressed, but still evidently dose-dependent (Fig. IV.6).

Generally, inhibition kinetics and mechanisms are best examined graphically using the double reciprocal plot established by Lineweaver and Burk (Sperelakis, 1995). Such an approach can be criticized because of the need for data transformation prior to curve fitting. Moreover, the approach was not applicable here due to the additional presence of simultaneous passive absorption and competing mucociliary clearance. Thus, the best estimates for each process at 25 °C were obtained by simultaneous across-dose curve fitting (MSC =3.74; R^2 = 0.991) to the kinetic model shown in Fig. IV.1, by nonlinear least-mean-square regression analysis. The results are shown in Tables IV.2 and IV.3. The active absorption component for F-PHEA at 25 °C was dramatically suppressed with respect to its maximal rate, $V_{max,P}$, while the affinity term, $K_{m,P}$, remained largely unaffected. Although similar effects were observed at 15 °C for the saturable uptake of propranolol in isolated and minced rat lung tissues (Iwamoto *et al.*, 1989), this type of inhibition mechanism has been rarely shown at lowered temperatures. The result was consistent with the inhibition of oxidative phosphorylation, similarly to that induced by DNP, but through a different mechanism (Goodman *et al.*, 1983). DNP has often been reported to induce a type of active transport systems (Slater, 1963; Rounds and McMurtry, 1981) where the maximal rate was reduced but "affinity (K_m)" remained unchanged. It may be therefore, that F-PHEA's active absorption was similarly, yet "non-

competitively" inhibited at 25 °C, due simply to the depletion of available energy for its transporter.

The rate constants for passive absorption of F-Na and FD-4, $k_{a,P}$ were found to be about 50 % lower at 25 °C than those at 37 °C (Table IV.3). Based upon passive diffusion theory via partitioning through pulmonary cell membranes (Byron and Patton, 1994), the rate constant, $k_{a,P}$ is described as:

$$k_{a,P} = D_M \cdot A_M \cdot K_D / (h \cdot V) \qquad \text{(Eqn. IV.3)}$$

The parameters D_M, A_M, K_D, h and V are, respectively, the solute's diffusion coefficient through the pulmonary membranes, the total membrane surface area available for absorption, the solute's membrane/donor solution phase partition coefficient, the thickness of the membranes and the effective fluid volume in the airways (in which the solute is dissolved). Provided that A_M, h and V remain unchanged between 37 and 25 °C, the ratio of the rate constants, $R_{(25oC/37oC)}$ should be described by:

$$R_{(25oC/37oC)} = \frac{k_{a,P\,(25oC)}}{k_{a,P\,(37oC)}} = \frac{D_{M\,(25oC)} \cdot K_{D\,(25oC)}}{D_{M\,(37oC)} \cdot K_{D\,(37oC)}} \qquad \text{(Eqn. IV.4)}$$

If the diffusion coefficient, D_M is assumed to be proportional to the absolute temperature, T, based on either Stokes-Einstein (Eqn. IV.5) or Wilke-Chang correlation (Eqn. IV.6) equations:

$$D_M = R \cdot T/(6 \cdot \Pi \cdot \eta_B \cdot N_o \cdot r_A) \qquad \text{(Eqn. IV.5)}$$

$$D_M = 7.4 \times 10^{-10} (\phi_B \cdot M_B)^{1/2} \cdot T/(\eta_B \cdot V'_A{}^{0.6}) \qquad \text{(Eqn. IV.6)}$$

where R is the gas-law constant, T is the absolute temperature, η_B is the viscosity of the medium in which diffusion occurs, N_o is Avogadro's number, r_A is the effective radius of the solute molecule, ϕ_B is the solvent's association factor, M_B is the solvent molecular weight and V'_A is the solute's molar volume at its normal boiling temperature, the rate constant ratio, $R_{(25oC/37oC)}$ (Eqn. IV.4) can be rewritten as:

$$R_{(25oC/37oC)} = \frac{k_{a,P\,(25oC)}}{k_{a,P\,(37oC)}} = 0.96 \cdot \frac{K_{D\,(25oC)}}{K_{D\,(37oC)}} \qquad \text{(Eqn. IV.7)}$$

On such assumption, the value, 0.96 is obtained from the absolute temperature ratio of 25 and 37 ^oC.

The partition coefficients, K_D for F-Na at 37 and 25 ^oC between octanol and phosphate buffered saline (PBS; pH 7.4) were found to be 0.79±0.05 and 0.35±0.05 (mean±SD; n = 3; Sakagami *et al.*, 1997), enabling a calculation of $R_{(25oC/37oC)}$ = 0.43 using Eqn. IV.7. This value was surprisingly consistent with R = 0.48, the experimentally-determined ratio of $k_{a,P}$ at 25 and 37 ^oC (0.023 and 0.048 min^{-1}, respectively) obtained from across-dose curve fitting. The experimental value of R for FD-4, hydrophilic macromolecule absorbed solely by passive mechanisms was 0.5 (0.008

and 0.016 min^{-1} at 25 and 37 °C, respectively). The value was again, surprisingly consistent with theory outlined above, although FD-4 was predominantly absorbed through tight junctions between epithelial cells and it was likely that its absorption was diffusion-determined. This remains to be substantiated in future studies.

Mucociliary clearance rate constants, $k_{E,PT}$ were found to be solute-independent, but significantly slowed at 25 °C, compared to those at 37 °C (Table IV.3). While clearance has been shown to be a complex function of ciliary beat frequency and mucus and periciliary fluid secretions, the rate of mucociliary clearance is known to be regulated by several intracellular ciliomodulators, such as ATP, Ca^{2+}, cAMP, cGMP and protein kinase C (Wanner, 1991; Camner and Mossberg, 1993). Moreover, the process is known to be cellular energy-dependent and recent evidence has suggested that the process could be largely activated by cAMP- and/or ATP- dependent phosphorylation (Lansley, 1993; Camner and Mossberg, 1993). Therefore, it was quite reasonable that at 25 °C, the process was slowed due to an inhibition of cellular energy utilization.

PULMONARY ABSORPTION OF 7.4 kDa F-PHEA IN THE PRESENCE OF METABOLIC INHIBITORS

Active absorption by transporters or carriers must be directly or indirectly coupled to a source of cellular metabolic energy. In most cases, the energy is generated by ATP

hydrolysis (Alberts *et al.*, 1983; Andreoli *et al.*, 1986). A substrate, ATP is primarily synthesized by oxidative phosphorylation catalyzed by ATP synthase in mitochondria, as well as by glycolysis in the cytosol; the former is known to be a predominant mechanism for producing intracellular ATP (Liberman and Sleight, 1995). Subsequent ATP hydrolysis (to ADP, inorganic phosphate and $\Delta G_o'$) is catalyzed by several types of ATPase, such as phosphoenzyme ATPase and mitochondrial ATPase. Among them, Na^+/K^+-ATPase, one of phosphoenzyme ATPase, is known to be responsible for the catalytic hydrolysis of ATP, while simultaneously driving active transport of Na^+ and K^+ ions against their electrochemical gradient across cell membranes (Alberts *et al.*, 1994; Sperelakis, 1995).

2,4-Dinitrophenol (DNP; Fig. IV.2 (a)) is a lipid-soluble weak acid (pKa = 4.1), pharmacologically a proton ionophore. In mammalian cells, the compound removes the proton gradient across mitochondrial membrane without changing electron transport or proton pumping in the organelle. This is known as an uncoupling effect (Alberts *et al.*, 1994) and provides an additional pathway to the use of ATP synthase to enable inward-flow of protons across the mitochondrial membrane ("short-circuiting"; Rognstad and Katz, 1974; Hanstein, 1976; Alberts *et al.*, 1983). Thus, DNP dissipates the proton-motive force in mitochondria and abolishes the organelle's ATP synthesis by oxidative phosphorylation. Because of this action, the compound has been extensively used in several in vitro and in vivo systems, as summarized in Table IV.5, as an ATP-depleting agent and/or ATP-synthesis inhibitor, to study the requirement for cellular energy in

Table IV.5. Summary of absorption inhibition studies using 2,4-dinitrophenol (DNP; from the literature).

Cells/Organs	Substrate	Application	Concentration	% Inhibition	Reference[1]
Rat lung: Slice	DSCG[*3]	Co-incubation	10 mM	14.1 %	Gardiner, 1976
Minced	Propranolol	15min pre-incubation	0.05 mM	50.5 %	Iwamoto, 1989
Type II	Na^+	Co-incubation	1 mM	75.4 %	Goodman, 1983
Pneumocytes	Paraquat	Co-incubation	1 mM	63.0 %	Saito, 1986
Bullfrog lung	H_2O	Co-incubation	1 mM	67.0 %	Schaeffer, 1984
Rabbit alveolar Mϕ[*1]	Propranolol	Co-incubation	0.5-1 mM	52.3 %	Vestal, 1980
Caco-2	Ceftibuten	3hr pre-incubation	0.5 mM	93.4 %	Muranushi, 1994
	AT_2-antagonist[*4]	2hr pre-incubation	1 mM	79.3 %	Soldner, 2000
Hamster intestinal cell culture	Linolenic acid	10min pre-incubation	0.25 mM	79.4 %	Gore, 1993
Rat hepatocyte	Cholic acid	Co-incubation	1 mM	30.0 %	Ohkuma, 1983
	Vecronium	Co-incubation	1 mM	51.5 %	Mol, 1988
	Pravastatin	Co-incubation	1 mM	30.1 %	Komai, 1992
	TBuMA[*5]	3min pre-incubation	0.01 mM	50.0 %	Steen, 1993
IPRK[*2]	Digoxin	Pre-incubation	1 mM	37.5 %	Hori, 1993

[1] Only first authors and years of publication; details are described in References.
[*1] Macrophage; [*2] isolated perfused rat kidney; [*3] disodium cromoglycate; [*4] angiotensin II antagonist (losartan) and [*5] *n*-butylmethylammonium

active transport processes (Table IV.5). It should also be noted that, unlike other "uncouplers" (deoxycholate, oligomycin and unsaturated fatty acids), DNP inhibits mitochondrial ATP synthesis without disrupting the mitochondrial structures at relatively low concentrations (0.5-2.0 mM; Slater, 1963). Furthermore, it has been shown that the compound inhibits all possible pathways of oxidative ATP production in the respiratory chain, whereas other chemical inhibitors, such as rotenone, antimysin A, cyanide and sodium azide, inhibit only parts of the process as well as acting as cell toxins due to their inhibitory effects on oxygen uptake (Sharon and McMurtry, 1981).

A concentration-dependent inhibition of F-PHEA's active absorption was observed in the presence of DNP (Fig.IV.10), demonstrating the necessity of intracellular ATP-derived energy in the active absorption process. However, in the IPRL, it has been shown that depletion of mitochondrial ATP synthesis by DNP (0.8 mM) can be quite readily compensated by the use of glycolytic pathway driven by enhanced glucose uptake (Bassett and Fisher, 1976), causing cellular ATP levels to decrease only by about 63 % following 60 minutes perfusion in the IPRL (Bassett *et al.*, 1989). Consistent with this observation, the maximum magnitude of inhibition for F-PHEA absorption was found to be only 53.3±7.9 % (mean±SE; n=4) at 1.0 mM DNP in perfusate (Fig. IV.10). This was quite different from in vitro cell culture systems like alveolar type II cells or hepatocytes which showed ≥ 75 % inhibition of active processes as a result of ≥ 80 % decrease in cellular ATP in the presence of DNP (Goodman *et al.*, 1983; Muranushi *et al.*, 1994;

Soldner *et al.*, 2000). Nevertheless, comparable concentrations of DNP produced inhibition of the F-PHEA transporter in our preparation (IC_{50} = 0.5-1.0 mM).

Ouabain (OUA; strophantin G; Fig. IV.2 (b)) is a plant-derived cardiotonic steroid or cardiac glycoside and chemically, water-soluble (1.1 mg/mL) and extremely hydrophilic (K_D = 0.01 between octanol and PBS (pH 7.4)). In contrast to DNP's synthetic inhibition of cellular ATP, OUA is known to specifically inhibit a phosphoenzyme, Na^+/K^+-ATPase (Mercer, 1993; Alberts *et al.*, 1994). As a result, the compound inhibits both Na^+ (outward) and K^+ (inward) transport across cell membranes and their concomitant ATP hydrolysis that may generate metabolic energy for active transport either directly (ATP-driven or primary active mechanism) or indirectly (ion-driven or secondary active mechanism; Alberts *et al.*, 1994; Rose and Valdes, 1994). Unfortunately, the inhibition mechanisms for direct, ATP-driven active transport by this Na^+/K^+-ATPase are not fully understood, while it is speculated that such active transport somehow utilizes ATP hydrolysis energy directly generated from Na^+/K^+-ATPase (Miller, 1973; Byrne *et al.*, 1991). Meanwhile, it can be also speculated that inhibition of Na^+ and K^+ transport by OUA may alter the membrane potentials across the cells and thus, active transport may be inhibited (Alberts *et al.*, 1994). In contrast, the inhibition of indirect, ion-driven active transport is more likely to be associated with intracellular Na^+ regulated by Na^+/K^+-ATPase (Byrne *et al.*, 1991). Such Na^+-dependent carriers are co- or counter- transport systems, coupled with downhill movement of Na^+ into the cells. OUA inhibits Na^+/K^+-ATPase, causing an increase of intracellular Na^+ concentration. As a

result, co- or counter- transport systems are no longer driven forward due to the OUA-induced lack of a downhill Na^+ gradient across the membranes. Finally, as a secondary response of an increase of intracellular Na^+ concentrations through Na^+/K^+-ATPase inhibition, OUA must increase intracellular Ca^{2+} concentrations, driving Na^+/Ca^{2+}-counter-transport systems (Alberts *et al.*, 1994).

The Na^+/K^+-ATPase is predominantly located on the basolateral (blood/perfusate) side of the pulmonary membranes and OUA binds to the outer site of this transmembrane protein, competing with K^+ (Alberts *et al.*, 1994). Inhibition of this Na^+/K^+-ATPase is reportedly obtained when 10-500 µM ouabain is applied to the basolateral side (rather than the apical side) in most experimental systems (Alberts *et al.*, 1994; Cott, 1994). Table IV.6 summarizes such organ or cell studies in which OUA has been used. In most cases, OUA has been used to elucidate Na^+-dependent, indirect (ion-driven) active transport mechanisms.

F-PHEA active absorption was found to be significantly inhibited by 62.3 and 75.9 %, respectively, at 50 and 100 µM OUA in perfusate (Dunnet method following multiple ANOVA; $p < 0.05$; Fig. IV.12). This proposed the involvement of OUA-inhibitable ATP hydrolysis, specific membrane potentials or Na^+ and/or Ca^{2+} downhill movement into the cells being associated with the active absorption process for F-PHEA. However, it has been shown previously that F-PHEA absorption from the airways was not affected in the presence of Na^+ following iso-osmotic NaCl solution administration (to the apical side of the pulmonary epithelium; Sun, 1995). This suggested therefore, that Na^+ ion-driven

Table IV.6. Summary of absorption inhibition studies using ouabain (OUA; from the literature).

Cells/Organs	Substrate	Application	Concentration	% Inhibition	Reference[1]
IPRL[*1]	Na^+	20 min pre-perfusion	0.025-0.05 mM	19.2 %	Goodman, 1987
	Na^+	10 min pre-perfusion	0.1 mM	58.4 %	Basset, 1987
	Na^+	10 min pre-perfusion	0.2 mM	34.3 %	Sauman, 1993
	Na^+	10 min pre-perfusion	0.5 mM	61.3 %	Barnard, 1997
	Na^+	0 min pre-prefusion	0.5 mM	50.0 %	Saldias, 1998
Rat Type II	Na^+	1hr co-incubation	0.1 mM	43.0 %	Filippatos, 1997
Rat hepatocyte	Cholic acid	Co-incubation	1 mM	39.0 %	Ohkuma, 1983
	Vecronium	Co-incubation	1 mM	56.3 %	Mol, 1988
Rabbit alveolar Mϕ[*2]	Propranolol	Co-incubation	0.5-1 mM	18.3 %	Vestal, 1980
Bovine BCEC[*3]	β-alanine	Co-incubation	0.5 mM	56.7 %	Komura, 1996

[1] Only first authors and years of publication; details are described in References.
[*1] Isolated perfused rat lung; [*2] macrophage and [*3] bovine brain capillary endothelial cells .

secondary active transport mechanisms were less likely. This required additional firmer evidences for conclusions and detailed mechanisms of the inhibition remained to be substantiated in the future.

PULMONARY ABSORPTION OF 7.4 kDa F-PHEA IN THE PRESENCE OF INHIBITORS OF VESICULAR TRAFFICKING

As opposed to carrier-mediated endocytotic absorption, active absorption by transporters (transcytosis) undergoes intracellular trafficking and vesicular sorting (Alberts *et al.*, 1994). Generally, endosomal pathways in which cytoplasmic clathrin-coated and/or nonclathrin-coated (caveolae) vesicles are formed, are followed by vesicle travel along microtubules to the other side of the membranes (partially by lysosomal degradation; Alberts *et al.*, 1994). Endogenously in the lung, extremely large plasma proteins, albumin (68 kDa) and IgG (150 kDa) have been shown to be transcytosed quite rapidly by specific transporter-mediated mechanisms across extremely thin ($\leq$ 1 μm) alveolar membranes (Hastings *et al.*, 1994; Kim *et al.*, 1995; Folkesson *et al.*, 1996). These processes differ with respect to their endosomal and macrotubular cytoplasmic pathways from the relatively slow adsorptive fluid-phase transcytosis seen with horseradish peroxidase (HRP; 44 kDa) and ferritin (500 kDa; Patton, 1996).

Monensin (MON; Fig. IV.2 (c)) is a carboxylic and/or Na^+ ionophore which exerts stochiometric Na^+/H^+ exchange following its relatively rapid incorporation *into biological*

membranes (due to its hydrophobicity; Dinter and Berger, 1998). Chemically, its open chain structure is capable of ion complexation through a cyclic form stabilized by hydrogen bonding between carboxyl and hydroxyl groups and a metal ion, especially Na^+, can be incorporated to form an ionophore-ion complex through MON's ligand site (Mollenhauer *et al.*, 1990). This complex can traverse biological membranes quite readily and exchange H^+ and Na^+ across those membranes by reversible association. As a result, the compound is known as a classical secretion or exocytosis inhibitor whose action leads to the formation of swollen vesicles near Golgi region at a minimum concentration of 10^{-7} M in mammalian cells (Tartakoff and Vasalli, 1977; Mollenhauer *et al.*, 1990). However, its precise mode of action is unclear; it appears likely that MON somehow affects cytoplasmic acidification mechanisms ("Golgi-perturbing agent"; Dinter and Berger, 1998). The induction of swollen vesicles caused by inhibition of acidification in intracellular organelles, especially in endosomal contents, and their subsequent delivery to lysosomes, has initiated extensive research to study intracellular trafficking during endocytosis and transcytosis, as summarized in Table IV.7. MON has been used as an "endosomotropic agent" providing evidence for intracellular endosomal vesicular transport during transporter/receptor-mediated and fluid-phase endocytosis of several small and macromolecules (Potau *et al.*, 1984; Whittaker *et al.*, 1986; Wilcox *et al.*, 1989; Stenseth *et al.*, 1989; Hastings *et al.*, 1994; Wangensteen *et al.*, 1996).

F-PHEA's active absorption was inhibited by 57.9 and 66.1 %, respectively, when 30 and 100 μM MON were employed in co-administration experiments (Dunnet methods

Table IV.7. Summary of trancytosis and endocytosis studies using monensin (MON; from the literature).

Cells/Organs	Substrate	Application	Concentration	% Inhibition	Reference[1]
<Transcytosis>					
Rat Type II	FITC-Alb[*4]	1hr pre-incubation	30 μM	52.0 %	Hastings, 1994
Rabbit in vivo	HSA[*5]	Co-administration	30 μM	No uptake	
IPRL[*1]	Riboflavin-BSA[*6]	Co-administration	35 μM	64.3 %	Wangensteen, 1996
	BSA	Co-administration	35 μM	24.0 %	
GP[*2] trachea	TR-BSA	Co-incubation	1-10 μM	95.0 %	Deffebach, 1996
primary culture	OA[*7]	Co-incubation	1 μM	94.6 %	
<Endocytosis>					
Rat embryo fibroblast	HRP[*8]	Co-incubation	1 μM (IC_{50}=0.3 μM)	75.0 %	Wilcox, 1982
hepatocyte	Asialo-gP[*9]	Co-incubation	25 μM	75.0 %	Berg, 1983
Mϕ[*3]	Mannose-gP[*9]	Co-incubation	10 μM	74.5 %	Wileman, 1984
Mouse Mϕ[*3]	IgG-coated particles	Co-incubation	10 μM	97.1 %	Hedin, 1985
	Ferritin	Co-incubation	3 μM	17.5 %	Stenseth, 1989
	HRP[*8]	Co-incubation	1-10 μM	70.0 %	
Hamster kidney BHK-21	SF-virus[*10]	Co-incubation	10 μM	97.0 %	Marsh, 1982

[1] Only first authors and years of publication; details are described in References.

[*1] Isolated perfused rat lung; [*2] guinea pig; [*3] macrophage; [*4] albumin; [*5] human serum albumin; [*6] bovine serum albumin; [*7] ovalbumin; [*8] horseradish peroxidase; [*9] glycoprotein and [*10] Semliki Forest virus.

following multiple ANOVA; $p < 0.05$; Fig. IV.15). This suggested that F-PHEA's active absorption involved endosomal vesicular transport. In the IPRL, Wangensteen *et al.* (1996) found similar effects and values for % inhibition of receptor-mediated transcytosis of riboflavin-albumin conjugate from airways following 35 μM MOC co-administration (Table IV.7). Furthermore, effective inhibitory concentrations seen in other endocytosis and transcytosis studies (Table IV.7) were almost consistent with the IC_{50} values obtained from Fig. IV.15 (10-30 μM). Thus, it appeared that F-PHEA's active absorption was via specific transporter-mediated transcytosis which involved endosomal vesicular transport.

Nocodazole (NOC) has been proven to depolymerize microtubules in energy-dependent processes (Turner and Tartakoff, 1989), thus leading to a breakdown in Golgi apparatus structure. The compound has been extensively used for studying Golgi function as a "Golgi-perturbing agent" (Eiler *et al.*, 1989; Alberts *et al.*, 1994; Dinter and Berger, 1998) as well as interupter of microtubule-mediated transport in the cell's endosomal network (e.g., early endosomes through late endosomes), which sorts endosomes and defines their disposition (Alberts *et al.*, 1994; Hastings *et al.*, 1994; Deffebach *et al.*, 1996). Overall, and in this thesis, NOC has been used as a "microtubule-disrupting agent" to elucidate several transporter-mediated transcytotic processes, as shown in Table IV.8.

NOC inhibited F-PHEA's active absorption by 75 % following ≥ 10 μM NON co-administration into the airways (Fig. IV.15). Its IC_{50} value (1-5 μM) was reasonably consistent with other studies in Table IV.8 and therefore, it is suggested that F-PHEA's

Table IV.8. Summary of trancytosis studies using nocodazole (NOC; from the literature).

Cells/Organs	Substrate	Application	Concentration	% Inhibition	Reference[1]
Rat Type II	FITC-Alb [*4]	1hr pre-incubation	30 μM	20.0 %	Hastings, 1994
Rabbit in vivo	HSA[*5]	Co-administration	30 μM	No uptake	
IPRL[*1]	Riboflavin-BSA[*6]	Co-administration	35 μM	62.3 %	Wangensteen, 1996
GP[*2] trachea	TR-BSA	Co-incubation	10-75 μM	73.8 %	Deffebach, 1996
primary culture	OA[*7]	Co-incubation	50 μM	51.1 %	
Caco-2	Aminopeptidase *N*	3hr pre-incubation	30 μM	24.1 %	Eilers, 1989
			30 μM	50.0 %	Matter, 1990
	Botulinum neurotoxin	Co-incubation	10 μM	42.0 %	Maksymowych, 1998
MDCK[*3]	IgG-pIgGR[*8]	2hr pre-incubation	33 μM	60.8 %	Breitfeld, 1990
	85 kDa gP[*9]	Co-incubation	33 μM	19.6 %	Brandli, 1990

[1] Only first authors and years of publication; details are described in References.
[*1] Isolated perfused rat lung; [*2] guinea pig; [*3] Madin-Darby canine kidney cells; [*4] albumin; [*5] human serum albumin; [*6] bovine serum albumin; [*7] ovalbumin; [*8] immunoglobulin G-poly IgG receptor complex and [*9] glycoprotein.

active absorption involved microtubule-mediated transport during the polymer's endosomal vesicular transcytosis.

As summarized in Fig. IV.17, F-PHEA's active transport from airways to perfusate in the IPRL was significantly inhibited at low temperature (25 ^{o}C) and by the presence of several metabolic inhibitors at quite reasonable effective concentrations, when compared to the literature. The inhibition evidence at 25 ^{o}C and 1.0 mM DNP indicated the requirement for ATP-driven intracellular energy, while MON (30 μM) and NOC (30 μM) inhibition suggested that endosomal formation and microtubular transcytosis were required for F-PHEA's active absorption from the airways. Indirect ion (Na^{+}- and/or Ca^{2+}- driven secondary active mechanism remained a possible explanation of the inhibition seen in the presence of OUA (100 μM), although it was unlikely with respect to Na^{+}, based upon the appearance that process was Na^{+}-independent, when the apical side of the membrane was exposed to NaCl in the dosing vehicle (Sun, 1995). However, this mechanism was not truly elucidated and required additional substantiation in the future. Thus, a possible mechanistic scheme for F-PHEA's active absorption, which was consistent with the absorption inhibition evidence shown in Fig. IV.17, is described in Fig. IV.18.

In summary, F-PHEA was actively absorbed from the airways of the rat lung by an ATP-driven energy-dependent, intracellular vesicular transcytotic mechanism, probably via a specific transporter process. While the presence of such transporters on alveolar

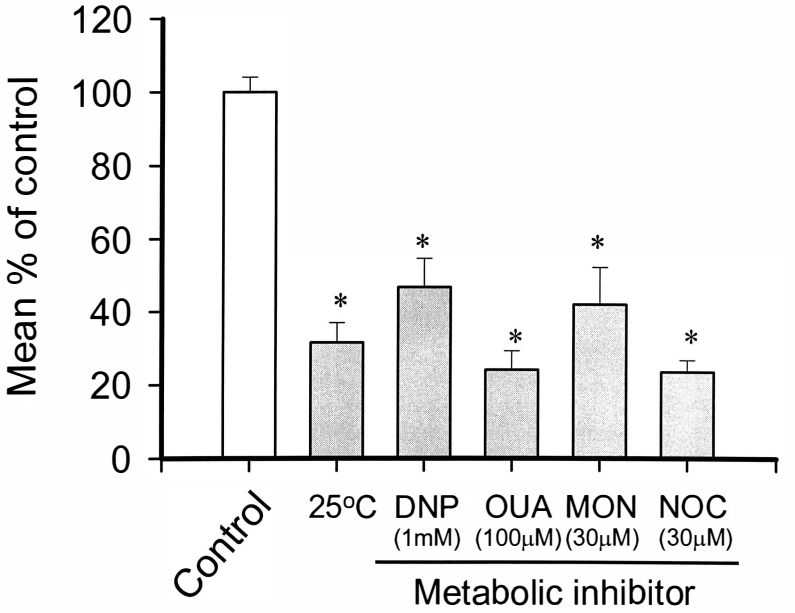

Figure IV.17. Mean percentage of actively-absorbed F-PHEA transferred to perfusate over the 30 minute period following solute administration. Graph shows the absence (control) and the presence of various metabolic inhibitors. Error bars are sample standard errors (SE) with n = 4.
Key: *DNP* - 2,4-dinitrophenol; *OUA* - ouabain; *MON* - monensin; *NOC* - nocodazole.
* indicates significant difference, compared to the control (*t*-test; $p<0.05$).

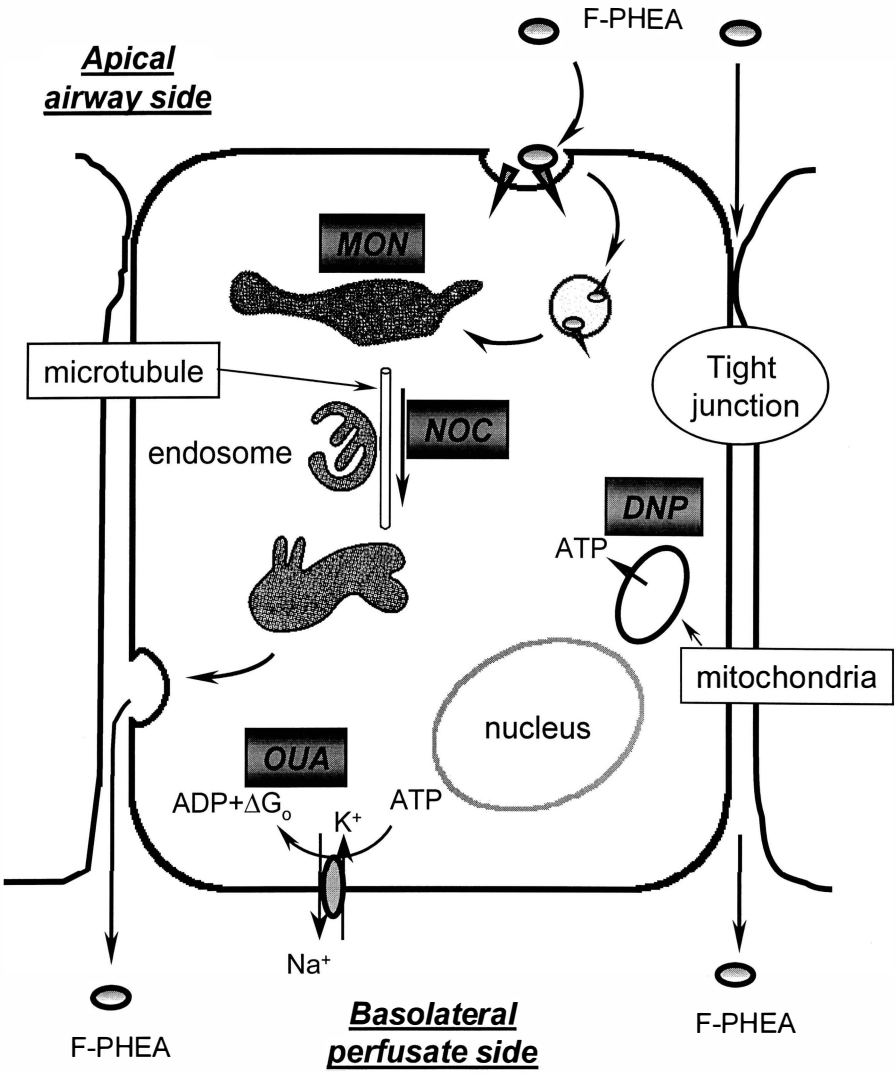

Figure IV.18. Proposed mechanisms for active and passive absorption of F-PHEA and their sites of inhibition from the airways of the IPRL.
Key: *DNP* - 2,4-dinitrophenol; *OUA* - ouabain; *MON* - monensin; *NOC* - nocodazole. OUA inhibited F-PHEA's active absorption, but without a direct link to its Na^+/K^+-ATPase inhibitory effects, which required further substantiation.

membranes has yet to be identified and intracellular trafficking through alveolar epithelial transcytosis is controversial (transcytotic vesicles are often larger than the thickness of alveolar epithelial cells; Patton, 1996), the fact that lysosomes are absent from much of the cytoplasm and abundant vesicles (caveolae) are found in alveolar epithelial cell membranes (Patton, 1996; Campbell *et al.*, 1998) implies that significant transcytotic activity is possible in the pulmonary regions of the lung. It is probable that these mechanisms are involved with the rapid transcytosis of F-PHEA from the airways and that other macromolecular transporters remain to be elucidated in the future.

CHAPTER V

PULMONARY ABSORPTION KINETICS OF F-PHEA: EFFECTS OF MOLECULAR SIZE

V.a INTRODUCTION

In previous chapters, the kinetics and mechanisms describing 7.4 kDa F-PHEA disposition in the airways of the IPRL were characterized precisely, in the presence of competing mucociliary clearance. As a result, simultaneous active and passive absorption kinetics were differentiated and analyzed independently by across-dose curve fitting at 37 and 25 ^{o}C. In this chapter, similar kinetic analysis was extended to describe the disposition of a differently-sized, 4.3 kDa F-PHEA in the IPRL. By comparing the rates of active and passive absorption between the two polymers (7.4 *vs.* 4.3 kDa), the molecular size-selectivity of each process could be studied. For these purposes, 4.3 kDa F-PHEA absorption was studied in the IPRL at 37 and 25 ^{o}C and its absorption kinetics from the pulmonary airways compared to those of its larger counterpart, 7.4 kDa F-PHEA.

V.b MATERIALS AND METHODS

V.b.1 7.4 kDa AND 4.3 kDa F-PHEA

Two, differently-sized, fluorophore-labeled poly-α,β-[N(2-hydroxyethyl)-D,L-aspartamides] (FR7150 and FR7002-5; F-PHEA) were used as model macromolecules. Synthesis and preparation of these polymers has been described in detail previously (Chapter 3 and Appendix III). Their normalized weight-based molecular weight distributions (MWD) were determined by Dr. Rypacek in Prague from their elution profiles following high performance gel permeation chromatography (HPGPC) on calibrated columns. Detection employed UV absorbance at 220 nm (Appendix III). Weight- (M_w) and number- (M_n) averaged molecular weights of each polymer were calculated, based on these profiles. These are shown in Table V.1 along with the polydispersity values ($P_d = M_w/M_n$; Appendix III) and their complete MWD (Fig. V.1). The polymers were defined as 7.4 and 4.3 kDa F-PHEA in this chapter, based upon their weight-averaged molecular weights (M_w), even though there was a degree of overlap in each case (Fig. V.1). Similar to 7.4 kDa F-PHEA, 4.3 kDa F-PHEA was found to carry 0.3 mol% fluorophore with respect to monomer, enabling a similar high sensitivity assay by HPGPC (HEMA-Bio 40 column) to be employed with fluorescence detection (λ_{ex} = 486 nm and λ_{em} = 516 nm; Appendix IV). Once again, a rigorous curve stripping procedure was employed to determine the area under the curve of F-PHEA's

Table V.1. Fluorophore content and molecular weight distributions of 7.4 and 4.3 kDa F-PHEA polymers.

F-PHEA	R[a] [mol%]		M_w[c] [Da]	M_n[c] [Da]	P_d[d]
	F[b]	HE[b]			
FR7150	0.3	99.7	7420	6620	1.12
FR7002-5	0.3	99.7	4308	2245	1.92

[a] A substituent group, R in F-PHEA structure shown below.

[b] F and HE are fluorophore and hydroxyethyl substituents, respectively.

[c] M_w and M_n are HPGPC-determined weight- and number- averaged molecular weights, respectively.

[d] $P_d = M_w / M_n$; polydispersity.

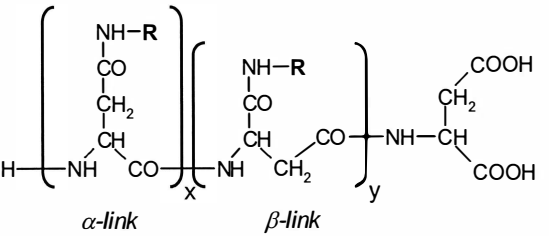

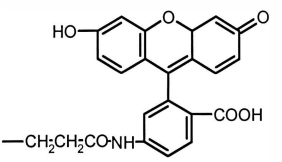

R = F

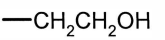

R = HE

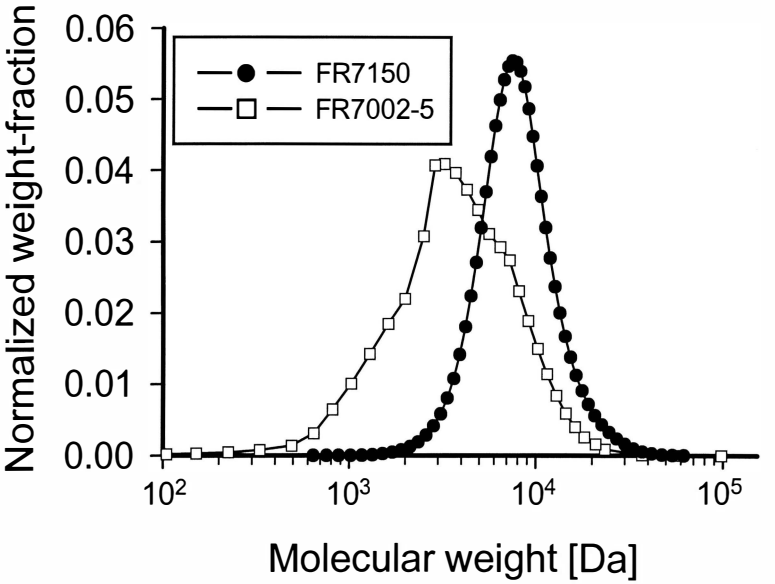

Figure V.1. Normalized weight-based molecular weight distributions of two, differently-sized F-PHEAs, FR7150 and FR7002-5. The chromatograms were monitored by UV absorbance at 220 nm. The column was calibrated with PHEA standards, polyethyleneoxide (PEO), hydroxyethyl glutamine (HEG) and water. Weight- (M_w) and number- (M_n) averaged molecular weights were calculated to be 7420 and 6620 Da for FR7150 and 4308 and 2245 Da for FR7002-5, respectively. Data was supplied by Dr. Rypacek.

chromatograms in both perfusate and filtered supernatant of lung homogenate (Appendix IV; Sun, 1995).

V.b.2 PULMONARY ABSORPTION IN THE IPRL

The IPRL preparation and the dosing method used to deliver F-PHEA into the airways have been described in detail previously (Byron and Niven, 1988; Chapters 3 and 4; Appendix I). These were used unchanged and F-PHEA absorption was studied at both 37 and 25 ^{o}C. Briefly, a rat lung was removed from the body and housed in the jacketed artificial glass thorax (AGT), maintained at either 37 or 25 ^{o}C by water supplied from a thermostatically-controlled water circulator (Model 9505, Fisher Scientific, Pittsburgh, PA). Its pulmonary circulation was perfused with circulating perfusate solution (Krebs-Heinseleit solution with 4 % bovine serum albumin) from a reservoir whose temperature was also controlled by the circulator. 4.3 kDa F-PHEA (nominal doses of 0.1, 0.2 and 1.0 mg) was administered into the airways as a coarse spray by "forced solution instillation" and its absorption was followed as a function of time by sampling and analyzing the perfusate, as described in Chapters 3 and 4 (37 and 25 ^{o}C). Four fully viable preparations were studied for each dosing solution and temperature partnership. The absorption results were expressed as mean % of administered dose transferred to perfusate ± sample standard deviation *vs.* time. The individual results from each IPRL preparation are reported in Appendix VII.

V.b.3 KINETIC MODELING, FITTING AND PARAMETER ESTIMATION

The kinetic model shown in Fig. IV.1 (Chapter 4) and the method used for analyzing F-PHEA absorption data at both 37 and 25 ^{o}C have been described in detail previously and were used unchanged (Chapters 3 and 4). Briefly, average data for % of administered dose transferred to perfusate (Figs. V.2 and V.3) was fitted across doses to Eqns. III.3-5 (from Chapter 3) and the model shown as Fig. IV.1. These equations are restated below:

$$(d[P]/dt)_{Active+Passive,IPRL} = V_{max,P}\cdot[M]_P/(K_{m,P} + [M]_P) + k_{a,P}\cdot[M]_P \qquad \text{(Eqn. III.3)}$$

$$(d[M]_P/dt)_{IPRL} = - (d[P]/dt) - k_{E,PT}\cdot[M]_P \qquad \text{(Eqn. III.4)}$$

$$(d[M]_{TB}/dt)_{IPRL} = k_{E,PT}\cdot[M]_P \qquad \text{(Eqn. III.5)}$$

where [P] is the cumulative solute amount absorbed from the pulmonary region into the recirculating perfusate of the IPRL, $[M]_P$ and $[M]_{TB}$ are the solute amounts remaining to be absorbed from the pulmonary and the tracheo-bronchial regions, respectively; $V_{max,P}$ is the maximum rate of active absorption, $K_{m,P}$ is the "affinity" or dose at which the active absorption rate = $0.5\cdot V_{max,P}$, $k_{a,P}$ is the first-order passive absorption rate constant from the pulmonary region and $k_{E,PT}$ is the first-order mucociliary clearance rate constant from the pulmonary to the tracheo-bronchial region. Unweighted, nonlinear least-mean-square regression analysis was employed for curve fitting and subsequent rate constant determination using Scientist^{TM} (MicroMath Scientific Software, Salt Lake City, UT)

where $V_{max,P}$, $K_{m,P}$, $k_{a,P}$ and $k_{E,PT}$ were allowed to float. The fraction of the administered dose delivered to the pulmonary region, F, was fixed throughout at its experimentally-determined average value, 0.91 (0.913±0.037; mean±SD; n=4), so that initial conditions were:

$[M]_{P, t=0}$ / [administered dose] = 0.91

$[M]_{TB, t=0}$ / [administered dose] = 0.09

$[P]_{t=0}$ / [administered dose] = 0.00

The model fits were assessed using "goodness-of-fit" parameters (Model Selection Criterion (MSC), R-squared (R^2), a review of the standard deviations of final parameter estimates and visual inspection of the residuals), as described in Chapter 3. Additional methodological details are described in Appendix VI.

V.c RESULTS AND DISCUSSION

The analytical sensitivity, precision and accuracy of determination for 4.3 kDa F-PHEA in all matrixes were characterized by an LOD ≤ 0.02 µg/mL, RSD ≤ 8.5 % and %error ≤ 6.2 % (n=6) over the concentration ranges of 0.06-1.0 µg/mL (Appendix IV). Similar to 7.4 kDa F-PHEA, there was no evidence of degradation, metabolism or lung tissue sequestration in rat lung observed with 4.3 kDa F-PHEA (Appendix V), although

the HPGPC technique employed for quantification and MWD assessment of the polyaspartamide was unable to accurately assess changes in the MWD of the smaller (4.3 kDa) polymer used in this thesis.

Average percent transfer (±SD) of 4.3 kDa F-PHEA *vs.* time at 37 and 25 ^{o}C are shown in Figs. V.2 and V.3 across doses. The solid curves drawn through the data points are the results of simultaneous curve fitting across doses to the model shown in Fig. IV.1 (Chapter 4). Curves were generated by "Scientist" using the program's best estimates for the model's rate constants as reported in Table V.2. The rate constants for each process were successfully estimated at both temperatures. Model Selection Criteria (MSC) values $\geq$ 3.7 and R-squared, $R^2 \geq 0.996$ were achieved, although parameter estimates were somewhat less precise when compared to those for 7.4 kDa F-PHEA. Unfortunately, several attempts to decrease the variance of 4.3 kDa F-PHEA's parameter estimates by fixing $k_{E,PT}$, the first-order rate constant for mucociliary clearance, at "across-solute weighted mean values" specific to 37 or 25 ^{o}C (while allowing other kinetic parameters in the model to float) were unsuccessful.

The absorption profiles of 4.3 kDa F-PHEA at 37 ^{o}C were found to be dose-dependent (Fig. V.2) and the magnitude of this dependence was suppressed dramatically at 25 ^{o}C (Fig. V.3). This indicated the presence of a saturable active absorption mechanism which contributed significantly to enhance the polymer's absorption from the airways, as seen in the case of 7.4 kDa F-PHEA (Fig. IV.3, Chapter 4). The absorption

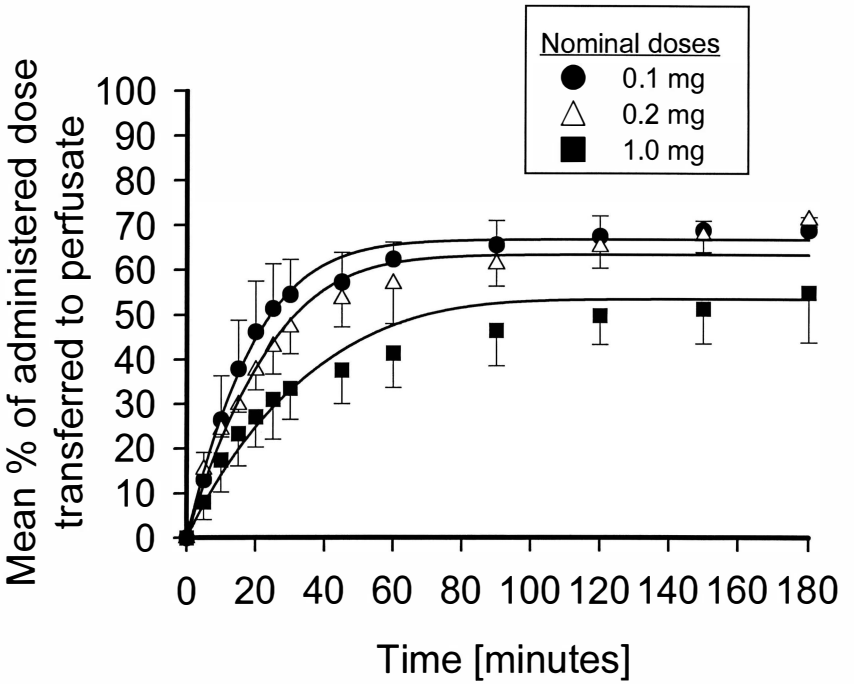

Figure V.2. Mean percentage (±SD; n=4) of administered dose of 4.3 kDa F-PHEA absorbed from the airways of the IPRL into the perfusate *vs.* time at 37 °C. The solid curves are the results of simultaneous across-dose curve fitting of all profiles. These were generated using the best estimates determined for each parameter at 37 °C, as described in Table V.2 ($V_{max,P}$, $K_{m,P}$, $k_{a,P}$ and $k_{E,PT}$ = 3.60 [μg/min], 76.8 [μg], 0.014 [min^{-1}] and 0.016 [min^{-1}], respectively).

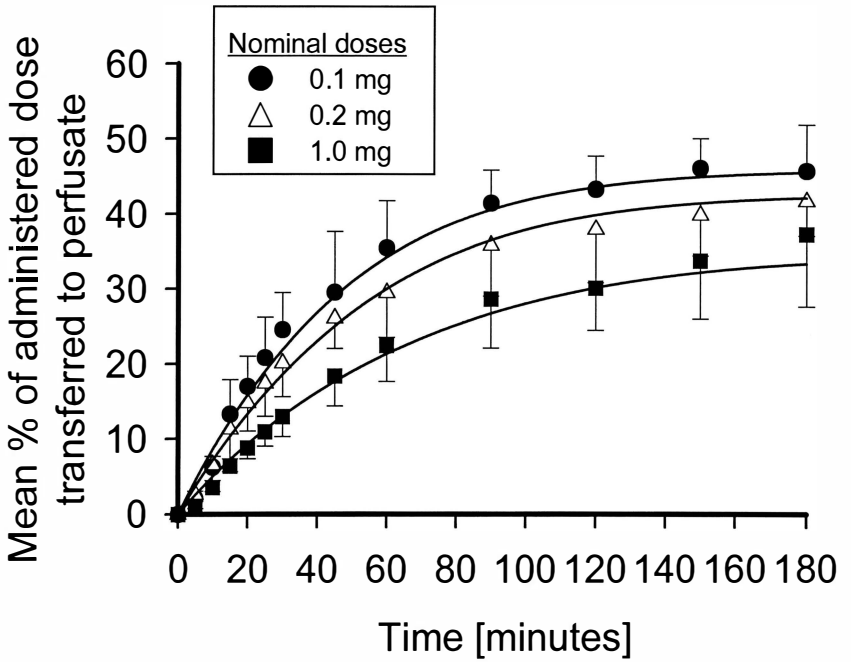

Figure V.3. Mean percentage (±SD; n=4) of administered dose of 4.3 kDa F-PHEA absorbed from the airways of the IPRL into the perfusate *vs.* time at 25 °C. The solid curves are the results of simultaneous across-dose curve fitting of all profiles. These were generated using the best estimates determined for each parameter at 25 °C, as described in Table V.2 ($V_{max,P}$, $K_{m,P}$, $k_{a,P}$ and $k_{E,PT}$ = 0.92 [μg/min], 84.7 [μg], 0.005 [min^{-1}] and 0.012 [min^{-1}], respectively).

Table V.2. Disposition parameters for 4.3 kDa F-PHEA following its administration into the airways of the isolated perfused rat lung (IPRL) at 37 and 25 °C.

Temp.	Active absorption			Passive absorption	Mucociliary clearance	MSC; R^2
	$V_{max,P}$ [μg/min]	$K_{m,P}$ [μg]	$V_{max,P}/K_{m,P}$ [min^{-1}]	$k_{a,P}$ [min^{-1}]	$k_{E,PT}$ [min^{-1}]	
37 °C	3.60* (1.53)	76.8 (46.4)	0.047	0.014** (0.003)	0.016*** (0.001)	3.70; 0.996
25 °C	0.92* (0.31)	84.7 (39.3)	0.011	0.005** (0.001)	0.012*** (0.001)	4.68; 0.998

Values are the best estimates (SD) following analysis of across-dose data for 4.3 kDa F-PHEA. Nominal doses: 0.1, 0.2 and 1.0 mg at 37 and 25 °C.
MSC (Model Selection Criterion) and R^2 (R-squared) were as calculated by "Scientist" (Appendix VI).
*, ** and *** indicate significant difference ($p<0.05$) between values of $V_{max,P}$, $k_{a,p}$ and $k_{E,PT}$ at 37 and 25 °C, respectively, based on non-overlapped 95% confidence intervals.
The values for $K_{m,P}$ were insignificantly different between the 37 and 25 °C conditions, based on the same approach.

profiles are compared between 4.3 and 7.4 kDa F-PHEA at a nominal 0.1 mg dose in Fig. V.4, alongside that of the model polysaccharide, FD-4 (weight-averaged molecular weight (M_w) = 4.4 kDa) in the same dose. Clearly, because of the contribution of the active transport at this small dose, 4.3 kDa F-PHEA showed much faster absorption than FD-4 despite the similarity in their molecular sizes. Interestingly, at a nominal 0.1 mg dose, where active absorption is presumably dominant, the absorption of the 4.3 kDa F-PHEA was found to be no different, statistically, to that of 7.4 kDa F-PHEA (ANOVA); both showed 10-15 minute apparent absorption half-lives. In contrast, at a higher nominal dose of 1.0 mg, the smaller 4.3 kDa F-PHEA showed significantly faster absorption than its larger counterpart, as shown in Fig. V.5 (ANOVA; $p < 0.05$). These results suggested the likelihood that passive absorption contributed significantly to the airway-to-perfusate transfer of 4.3 kDa F-PHEA, whereas the active absorption of the polymer was effectively unchanged for this altered molecular weight distribution (MWD).

The best parameter estimates for each disposition constant in the kinetic model (Fig. IV.1; Chapter 4) are shown in Table V.2 for 4.3 kDa F-PHEA. At 37 ^{o}C, an "intrinsic rate constant" for active absorption, calculated by $V_{max,P}/K_{m,P}$ was found to be 0.047 min^{-1}, whereas a rate constant for passive absorption, $k_{a,P}$ was 0.014 min^{-1}, again demonstrating a significant contribution due to active absorption at low doses of this small-sized F-PHEA. This component was dramatically suppressed at 25 ^{o}C ($V_{max,P}/K_{m,P}$ = 0.011 min^{-1}) in a parallel fashion to the solute's passive absorption. The suppression of the transporter was apparently dominated by a significant decrease in the values for

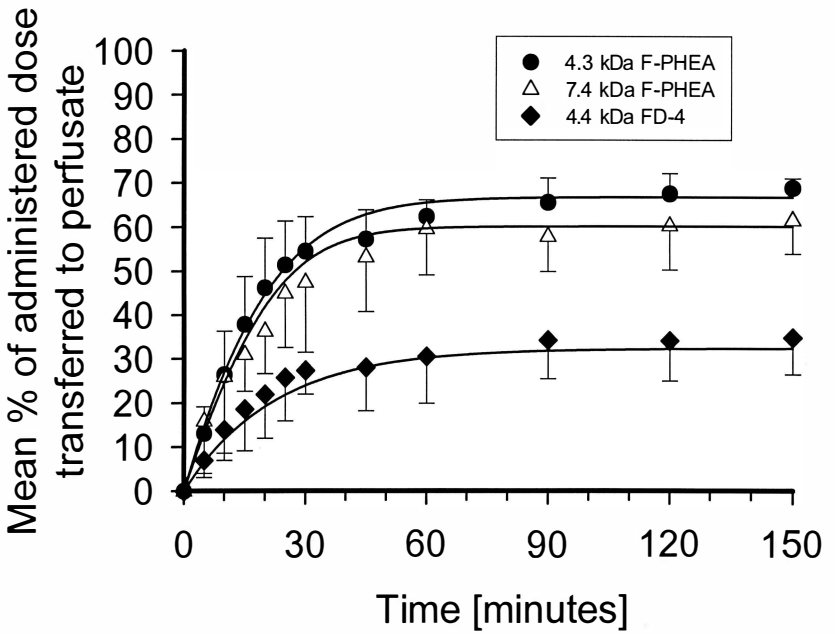

Figure V.4. Mean percentage (±SD; n=4) of administered dose of 4.3 and 7.4 kDa F-PHEA and FD-4 absorbed from the airways of the IPRL at 37 °C (nominal dose = 0.1 mg). The solid curves were generated using best estimates of parameters for each solute at 37 °C according to the model shown in Fig. IV.1 and as described in Tables III.2 (Chapter 3) and V.2 (Chapter 5). Thus, values for $V_{max,P}$, $K_{m,P}$, $k_{a,P}$ and $k_{E,PT}$ were 3.60 [μg/min], 76.8 [μg], 0.014 [min^{-1}] and 0.016 [min^{-1}] and 4.37 [μg/min], 56.6 [μg], 0.001 [min^{-1}] and 0.023 [min^{-1}], respectively (4.3 and 7.4 kDa F-PHEA), while those for $k_{a,P}$ and $k_{E,PT}$ were 0.016 [min^{-1}] and 0.029 [min^{-1}]

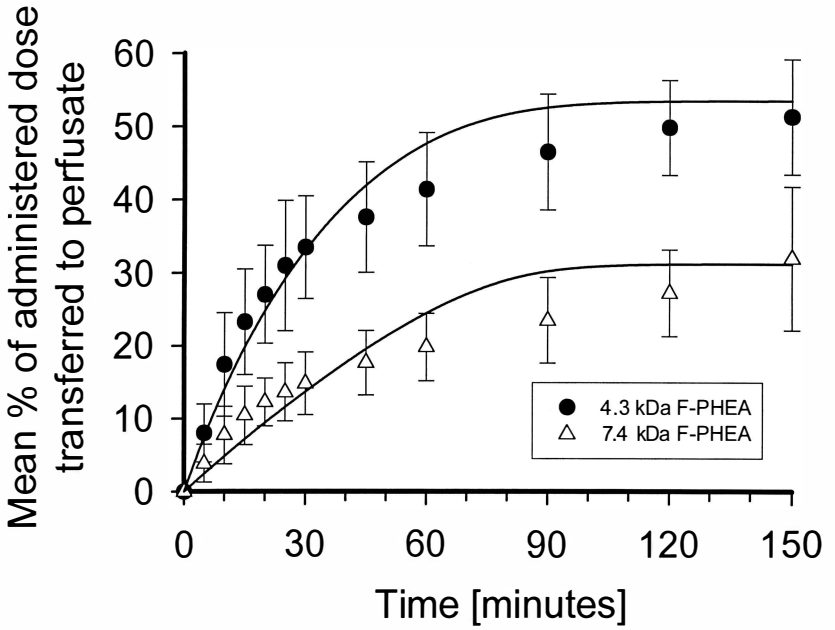

Figure V.5. Mean percentage (±SD; n=4) of administered dose of 4.3 and 7.4 kDa F-PHEA absorbed from the airways of the IPRL at 37 °C (nominal dose = 1.0 mg) . The solid curves are the results of the simultaneous across-dose curve fitting for each MWD. These were generated using best estimates determined for each polymer at 37 °C, as described in Tables III.2 (Chapter 3) and V.2 (Chapter 5).

$V_{max,P}$ (maximum rate; 3.60±1.53 → 0.92±0.31 μg/min; $p < 0.05$), while the "affinity" term, $K_{m,P}$, was unchanged by temperature (76.8±46.4 *vs.* 84.7±38.3 μg). The behavior of 4.3 kDa F-PHEA's kinetic descriptors were similar to those seen with 7.4 kDa F-PHEA (Table IV.2; Chapter 4).

Structural-specificity and/or size-selectivity for transepithelial transporters or carriers have been documented previously in lung (Helliwell *et al.*, 1994; Knickelbein *et al.*, 1997; Yamashita *et al.*, 1998) as well as the other organs (Lepage and Gros, 1993; Gan *et al.*, 1997; Ogihara *et al.*, 1999). These were mostly limited to small solute transport systems such as amino acids, monocarboxylic acids and di- or tri- peptides (Knickelbein *et al.*, 1997; Yamashita *et al.*, 1998; Ogihara *et al.*, 1999). In general, these transporters or carriers were shown to be highly specific to particular chemical structures up to certain molecular sizes. For example, dipeptide transporters for carnosine (β-Ala-L-His) on rabbit tracheal epithelial cells were shown to be only specific to L-configured dipeptides, but not to either amino acids (β-alanine and *L*-histidine) or D-configured dipeptides (β-Ala-*D*-His) or tri-peptides (TRH; Yamashita *et al.*, 1998). Meanwhile, a multi drug resistance protein, P-glycoprotein (Pgp) is known to transport structurally- and/or pharmacologically- unrelated compounds out of the cell quite efficiently (Lepage and Gros, 1993; Seelig, 1998a and 1998b). Its broad spectrum of the substrate specificity was shown to cover anthracyclines (doxorubicin, daunorubicin), alkaloids (reserpine, vinblastine), steroid hormones (aldosterone, hydrocortisone), anesthetics (dibucaine), dye molecules (rhodamine 123) and specific peptides (valinomycin, cyclosporin A), and their

molecular sizes were ranged from 183 Da (phenoxazine) to 1647 Da (α-factor pheromone; Seelig, 1998a and 1998b). In this case, it was speculated that two electron donor groups with a spatial separation of either 2.5±0.3 or 4.6±0.6 Å were necessary as the substrate specificity, rather than particular chemical structures (Lepage and Gros, 1993; Seeling, 1998a and 1998b). It seems quite possible therefore, that F-PHEA transporters, specifically recognizing either chemical structures, molecular moieties or spaces with favorable size limitation exist in lung, which function to transcytose macromolecules quite rapidly from the airways.

Disposition parameters for 4.3 and 7.4 kDa F-PHEA, FD-4 and F-Na are compared in Tables V.3 and V.4 at 37 and 25 °C, respectively. Despite the reduced precision of parameter estimation in the case of 4.3 kDa F-PHEA, there was no significant difference in the polymer's active absorption kinetics; $V_{max,P}$ and $K_{m,P}$ were unchanged (based on the overlapped 95%CI). While F-PHEA's two molecular weight distributions (MWD) overlapped (Fig. V.1), the passive absorption rate constant, $k_{a,P}$ for 4.3 kDa F-PHEA at 37 °C was significantly greater than that for 7.4 kDa F-PHEA (0.014±0.003 vs. 0001±0.001 min^{-1}; mean±SD; $p < 0.05$). Furthermore, values of $k_{a,P}$ for 4.3 kDa F-PHEA were consistent with those for similar-sized 4.4 kDa FD-4 at each temperature.

In contrast to active absorption, passive absorption is generally believed to be regulated by diffusion and partitioning (Notari, 1987; Byron and Phillps, 1990; Byron and Patton, 1994). Specifically for highly hydrophilic solutes like F-PHEA, such absorption should be predominantly controlled by diffusion through membranes where

Table V.3. Disposition parameters for active/passive absorption and mucociliary clearance for 7.4 and 4.3 kDa F-PHEA, FD-4 and F-Na following their administration into the airways of the isolated perfused rat lung (IPRL) at 37 °C.

Solutes (Mw)	Active absorption			Passive absorption	Mucociliary clearance	MSC; R^2
	$V_{max,P}$ [μg/min]	$K_{m,P}$ [μg]	$V_{max,P}/K_{m,P}$ [min^{-1}]	$k_{a,P}$ [min^{-1}]	$k_{E,PT}$ [min^{-1}]	
F-PHEA (7.4 kDa)	4.37 (0.57)	56.6 (14.7)	0.077	0.001 (0.001)	0.023 (0.001)	3.12; 0.986
F-PHEA (4.3 kDa)	3.60 (1.53)	76.8 (46.4)	0.047	0.014 (0.003)	0.016 (0.001)	3.70; 0.996
FD-4 (4.4 kDa)	N/A	N/A	N/A	0.016 (0.001)	0.029 (0.003)	2.83; 0.990
F-Na (376 Da)	N/A	N/A	N/A	0.048 (0.003)	0.022 (0.002)	3.37; 0.992

Values are the best estimates (SD) following analysis of across-dose data from: *7.4 kDa F-PHEA* - nominal doses: 0.1, 0.2, 0.5, 1.0 and 5.0 mg; *4.3 kDa F-PHEA* - nominal doses: 0.1, 0.2 and 1.0 mg; *FD-4* - nominal doses: 0.1 and 0.2 mg; *F-Na* - nominal doses: 0.01, 0.02 and 0.04 mg.
MSC (Model Selection Criterion) and R^2 (R-squared) were as calculated by "Scientist" (Appendix VI).
N/A indicates "not applicable" (no dose-dependency was observed).
There were no significant difference between solutes for values of $V_{max,P}$, $K_{m,P}$ and $k_{E,PT}$ (based on overlapped 95% confidence intervals).

Table V.4. Disposition parameters for active/passive absorption and mucociliary clearance for 7.4 and 4.3 kDa F-PHEA, FD-4 and F-Na following their administration into the airways of the isolated perfused rat lung (IPRL) at 25 °C.

Solutes (Mw)	Active absorption			Passive absorption	Mucociliary clearance	MSC; R^2
	$V_{max,P}$ [μg/min]	$K_{m,P}$ [μg]	$V_{max,P}/K_{m,P}$ [min^{-1}]	$k_{a,P}$ [min^{-1}]	$k_{E,PT}$ [min^{-1}]	
F-PHEA (7.4 kDa)	0.67 (0.10)	30.3 (16.4)	0.022	0.002 (0.001)	0.016 (0.001)	3.74; 0.991
F-PHEA (4.3 kDa)	0.92 (0.31)	84.7 (39.3)	0.011	0.005 (0.001)	0.012 (0.001)	4.68; 0.998
FD-4 (4.4 kDa)	N/A	N/A	N/A	0.008 (0.001)	0.012 (0.002)	2.87; 0.985
F-Na (376 Da)	N/A	N/A	N/A	0.023 (0.001)	0.010 (0.002)	3.12; 0.987

Values are the best estimates (SD) following analysis of across-dose data from: *7.4 kDa F-PHEA* - nominal doses: 0.2, 0.5, 1.0 and 5.0 mg; *4.3 kDa F-PHEA* - nominal doses: 0.1, 0.2 and 1.0 mg; *FD-4* - nominal doses: 0.1 and 0.2 mg; *F-Na* - nominal doses: 0.01, 0.02 and 0.04 mg.
MSC (Model Selection Criterion) and R^2 (R-squared) were as calculated by "Scientist" (Appendix VI).
N/A indicates "not applicable" (no dose-dependency was observed).
There were no significant difference between solutes for values of $V_{max,P}$, $K_{m,P}$ and $k_{E,PT}$ (based on overlapped 95% confidence intervals).

restricted "pore-sizes" exist ("restricted diffusion theory"), for example via tight junctions and due to negligible partitioning (Hastings *et al.*, 1992; Folkesson *et al.*, 1996; Kim and Crandall, 1996). In such a situation, molecular weight and solvated molecular volumes become critical determinants of passive absorption rates where either Stokes-Einstein or Wilke-Chang correlation equations may be of some predictive value (Kydonieus, 1991; Byron and Patton, 1994). In the case of rat alveolar epithelial cell membranes, it is believed that equivalent pore diameters for restricted diffusion are in the range of 0.4-50 nm (Chandra *et al.*, 1992). Such a wide range excludes very little and certainly includes hydrodynamic diameters determined from GPC elution profiles of 3.7 nm for 7.4 kDa F-PHEA (Sun, 1995). Therefore, as molecular size is decreased, passive absorption is more likely to be pronounced in alveolar and tracheal epithelial monolayer systems (Mathias *et al.*, 1996; Matsukawa *et al.*, 1997; Dodoo *et al.*, 2000) as well as in vivo (Effros and Mason; 1983).

These results for $k_{a,P}$ are thus consistent with the existence of molecular size-selectivity and simple restricted diffusion occurring through pulmonary membranes, as seen in other studies (smaller solutes diffuse faster; Effros and Mason, 1983; Hastings *et al.*, 1992; Byron and Patton, 1994; Folkesson *et al.*, 1996; Kim and Crandall, 1996). The rate constants for mucociliary clearance, $k_{E,PT}$, were found to differ insignificantly across solutes at each fixed temperature (based on the overlapped 95%CI), adding further weight to the validity of the model developed in this thesis for IPRL solute disposition.

V.d SUMMARY AND CONCLUSION

Kinetic modeling and across-dose curve fitting enabled the characterization of both the active and passive absorption kinetics of 4.3 kDa F-PHEA from the pulmonary airways of the IPRL, in the presence of competing mucociliary clearance. Mucociliary clearance was temperature-dependent, but solute-independent. The values of this smaller F-PHEA's disposition parameters were consistent with the size-selective passive absorption of F-PHEA through tight junctions as expected. Passive absorption rate constants, $k_{a,P}$, were found to be an inverse function of molecular size and those for 4.3 kDa F-PHEA were similar to those for 4.4 kDa FD-4 (0.014 *vs.* 0.016 min^{-1}, respectively; Table V.3). Thus, despite the presence of polydisperse MWD for F-PHEA polymers, 4.3 kDa F-PHEA showed a higher $k_{a,P}$ value than its larger counterpart (0.014 *vs.* 0.001 min^{-1}, respectively; Table V.3). It is likely therefore, that solutes ≥ 4 kDa are not readily absorbed by passive absorption and that their (larger molecular weight) absorption half-lives were ≥ 45 minutes (Fig. V.1). In contrast, it appeared that the active absorption kinetics ($V_{max,P}$ and $K_{m,P}$) for 7.4 and 4.3 kDa F-PHEA were identical. This evidence suggested that the F-PHEA transporter specifically transported overlapped portions ≥ 4 kDa of the MWD of both polymers (Fig. V.1). Consequently, the absorption of 4.3 kDa F-PHEA from the pulmonary airways was found to be more rapid than that of its 7.4 kDa counterpart (Figs. V.2, V.4 and V.5). However, this was achieved due to an increase in restricted passive diffusion of small oligomers in the distribution, while the transporter

kinetics unchanged. Thus, F-PHEA active transport was PHEA structure-specific with its molecular size-selectivity ≥ 4 kDa.

CHAPTER VI

SUMMARY AND GENERAL CONCLUSIONS

The kinetics of macromolecular solute absorption from the airways were studied and modeled successfully in vivo and in vitro, in the presence of competing mucociliary clearance. The kinetics of the mucociliary escalator appeared to be largely solute-independent and unaffected by lung isolation over the 180 minute duration of isolated perfused rat lung (IPRL) experiments. Specifically, the mechanisms and pathways involved with pulmonary-region-specific, active and passive absorption of model polypeptidic polymers, fluorophore-labeled polyhydroxyethylaspartamide (F-PHEA), were kinetically characterized using a new disposition model in the rat lung (Fig. III.3, Chapter 3). The primary macromolecules used in this thesis were weight-averaged (M_w), 7.4 and 4.3 kDa F-PHEA. These polyaspartamides were bicompatibile, non-immunogenic (Neri *et al.*, 1973) and were shown to be chemically and metabolically stable (Appendix V). The stable fluorophore, attached to each polymer, was used as an analytical marker and this enabled a highly sensitive high performance gel permeation chromatography (HPGPC) assay to be employed in a variety of analytical matrixes (Appendix IV). Furthermore, metabolically-stable (Appendix IV), sodium fluorescein (F-

Na) and FITC-labeled dextran (M_w = 4.4 kDa) were also used in the absorption studies as small and macromolecular reference solutes, especially to validate the kinetics of the IPRL model with respect to its descriptors of passive, molecular weight-dependent absorption and mucociliary clearance.

The IPRL used in this thesis enabled studies to be performed in a whole lung organ, housed in a physiologic orientation in a well-controlled environment. The preparation retained the structural and functional integrity of the whole organ and thus, enabled direct prediction of in vivo absorption results for F-PHEA. In all experiments of in vivo and in vitro, solutes were administered into the airways as a coarse spray of aqueous dosing solution by "forced solution instillation". Solute absorption (or disappearance from the airways) was followed as a function of time throughout the lifetime of the preparation. Statistically identical initial regional lung distribution was achieved using "forced solution instillation" both in vivo and in vitro ($p > 0.05$; Figs. III.4 and III.5, Chapter 3). Thus, a comparison of solute distribution over time, in vivo and in vitro, enabled the IPRL's mucociliary clearance process to be studied and shown to be predictive of that seen in the intact animal. Similarly, F-PHEA absorption in the IPRL was found to be predictive of that seen in vivo (Fig. III.8, Chapter 3), due to the preparation's comparable absorption kinetics and mucociliary clearance. Thus, it was not likely that F-PHEA was absorbed significantly from the tracheo-bronchial regions, either by passive or active mechanisms (Fig. III.9, Chapter 3). On the other hand, the absorption of a small (376 Da) model solute, F-Na was quite different in vivo and in vitro (Fig. III.6, Chapter 3), due to

the presence of its significant tracheo-bronchial absorption in vivo (Fig. III.7, Chapter 3). While F-Na absorption in vitro, underestimated in vivo absorption (Fig. III.6, Chapter 3), its study in the IPRL and correct kinetic modeling enabled successful estimation of its regional rate constants for passive absorption ($k_{a,TB}$ = 0.042±0.011 min^{-1} and $k_{a,P}$ = 0.048±0.003 min^{-1}; Table III.3, Chapter 3). Therefore, for the first time, F-Na's pulmonary disposition was correctly described in this thesis in the presence of the mucociliary clearance and its absorption was shown to be independent of its regional deposition in the lung.

A new kinetic model incorporating active and passive absorption alongside simultaneous mucociliary clearance was developed to characterize solute absorption from the rat lung in vivo and in vitro. This model was used throughout the thesis. Across-dose fitting of solute absorption data enabled the detailed analysis of dose-dependent, Michaelis-Menten-type active absorption of F-PHEA alongside its simultaneous passive absorption and mucociliary clearance components. Hence, the capacity and affinity of F-PHEA's airway-to-blood transporter were precisely characterized. Because the IPRL preparation could also be maintained at lowered temperature (25 ^{o}C) and in the presence of metabolic inhibitors, the effects of these perturbations on F-PHEA absorption were also studied. The preparation was shown to be viable in all such cases (Appendix I and Chapter 4).

Kinetic modeling and across-dose fitting of each solute's airway-to-perfusate transport data enabled a series of conclusions to be drawn:

(1) At 37 ^{o}C, mucociliary clearance ($k_{E,PT}$) was found to be solute-independent and relatively rapid (half-lives ranged between 24 and 32 minutes). Thus, mucociliary clearance competed significantly with the solute absorption in most cases (Table V.3, Chapter 5). The process was slowed by between 45 and 70 % at 25 ^{o}C (Table V.4, Chapter 5), and this was apparently related to its energy-dependent regulation (ATP or cAMP; Lansley, 1993; Camner and Mossberg, 1993).

(2) Pulmonary-region-specific rate constants for passive absorption ($k_{a,P}$) were inversely related to solute molecular weight at both 37 and 25 ^{o}C (Tables V.3 and V.4, Chapter 5, respectively). This observation was consistent with passive solute absorption occurring via tight junctions in pulmonary epithelium. The lowered ($\leq$ 50 %) rate constants for passive absorption, $k_{a,P}$ at 25 ^{o}C may have been due to a combination of lowered solute diffusivity and/or partitioning to the membranes at lower temperatures (Notari, 1987; Martin, 1993) alongside the possibility that tight junctions may have been perturbed by the temperature transition.

(3) Pulmonary-region-specific descriptors for the active absorption of 7.4 kDa F-PHEA were found to be $V_{max,P}$ = 4.37±0.57 μg/min and $K_{m,P}$ = 56.6±14.7 μg at 37 ^{o}C. The "intrinsic rate constant" for its active absorption, $V_{max,P}/K_{m,P}$, was much greater (0.077

min^{-1}) than its passive absorption counterpart ($k_{a,P}$ = 0.002±0.001 min^{-1}; Table III.2, Chapter 3). This clearly demonstrated that the polymer was predominantly absorbed by an active mechanism throughout experimental dosing ranges ≤ 5.0 mg (Fig. IV.3, Chapter 4). As expected, F-PHEA absorption was dramatically suppressed at 25 °C (Fig. IV.4, Chapter 4). Kinetic modeling and associated curve fitting at 25 °C showed that absorption suppression was dominated by a significant decrease in the value of $V_{max,P}$ (maximum rate; 4.37±0.57 → 0.67±0.10 μg/min; $p < 0.05$; Table IV.2, Chapter 4), while the "affinity" remained effectively constant ($K_{m,P}$ = 56.6±14.7 μg (37 °C) and 30.3±16.4 μg (25 °C); Table IV.2, Chapter 4). Thus, the "intrinsic rate constant" for active absorption, $V_{max,P}/ K_{m,P}$, was decreased by 71.4 % (from 0.077 to 0.022 min^{-1}; Table IV.2, Chapter 4) by reducing the temperature to 25 °C, while passive absorption was largely unchanged (Table IV.2, Chapter 4).

(4) 4.3 kDa F-PHEA's active absorption descriptors ($V_{max,P}$ and $K_{m,P}$) were statistically identical to those of its larger counterpart (Table V.3, Chapter 5). Despite the presence of polydispersity in these F-PHEA polymers, the passive absorption rate constant, $k_{a,P}$, for 4.3 kDa F-PHEA was much greater than that for the 7.4 kDa polymer (0.014±0.003 and 0.001±0.001 min^{-1} for 4.3 and 7.4 kDa F-PHEA, respectively; Table V.3, Chapter 5). As expected, the value of $k_{a,P}$ was most similar to that for 4.4 kDa FD-4 (0.014±0.003 and 0.016±0.001 min^{-1} for 4.3 kDa F-PHEA and 4.4 kDa FD-4, respectively; Table V.3, Chapter 5). It is likely therefore, that solutes ≥ 4 kDa in molecular weight are not readily absorbed from the lung by passive

absorption. Overall, the absorption of 4.3 kDa F-PHEA from the pulmonary airways was found to be more rapid than that of the 7.4 kDa polymer (Figs. V.2, V.4 and V.5, Chapter 5), but this was only achieved by an increase in passive absorption of smaller molecules, while the transporter's kinetics were unchanged. Active absorption of the macromolecular polysaccharide, FD-4 did not occur. This molecule showed only dose-independent passive absorption from the airways (Fig. V.4, Chapter 5).

The fact that F-PHEA's active absorption was temperature-sensitive, suggested the existence of a cellular energy requirement for its active absorption. Thus, experimental protocols showing maximum inhibition of F-PHEA absorption without unnecessarily shortening the viable lifetime of the IPRL were optimized for the metabolic inhibitors, 2,4-dinitrophenol (DNP), ouabain (OUA), monensin (MON) and nocodazole (NOC). As a result, 15 minute pre-perfusion periods were employed prior to solute administration in DNP and OUA protocols, while co-administration of solute and inhibitor was used with MON and NOC. In each of these protocols, the airway-to-perfusate absorption profile of a passively-absorbed small solute, F-Na, showed no significant changes in the presence of each inhibitor (1 mM DNP or 100 μM OUA in perfusate or 100 μM MON or NOC in the airways; Fig. IV.8, Chapter 4), demonstrating that passive absorption and mucociliary clearance kinetics (which modified absorption from the pulmonary compartment) were unaffected by these inhibitors. Furthermore, % absorption of 7.4 kDa F-PHEA in the first 30 minutes following administration was unaffected by the presence of a 15 minute pre-

perfusion interval (for DNP or OUA studies) or the use of EtOH and DMSO in the dosing vehicles (for MON and NOC studies; Fig. IV.16, Chapter 4). Therefore, inhibitory effects of these chemical agents on F-PHEA's active absorption were thought to be indicative of their effects on the transporter itself. F-PHEA active absorption was inhibited by DNP, OUA, MON and NOC in a concentration-dependent fashion (Fig. IV.10, III.12 and III.15, Chapter 4). Their effective concentrations (IC_{50} values = 0.5-1.0 mM, 30-50 μM, 10-30 μM and 1-5 μM for DNP, OUA, MON and NOC, respectively) were consistent with literature reports (Tables IV.5-IV.8, Chapter 4). Inhibition by 1 mM DNP indicated a requirement for ATP-derived intracellular energy, while MON (30 μM) and NOC (30 μM) inhibition suggested that endosomal formation and microtubular transcytosis were required for F-PHEA's active absorption (transcytosis) from airways to interstituim and perfusate. Indirect, ion (Na^+ and/or Ca^{2+}) -driven secondary active absorption mechanism remained a possible explanation of the inhibition seen by the use of OUA (100 μM). However, this was unlikely with respect to Na^+, based on our previous findings of apical-Na^+-independent absorption of this polymer (Sun, 1995). Unfortunately, additional substantiation is required for its mechanistic conclusions. Consequently, it was demonstrated that 7.4 kDa F-PHEA was absorbed from the airways of the rat lung by an ATP-driven energy-dependent, intracellular vesicular transcytotic mechanism, probably via a specific transporter, as illustrated schematically in Fig. IV.18 (Chapter 4).

At lower doses (≤ nominal 0.2 mg dose), 7.4 kDa F-PHEA polymer was capable of achieving greater or similar absorption rates from the airways to that of 376 Da sodium

fluoresein (F-Na), despite the more than 20-fold difference in their molecular weights. This was due to the presence of an ATP-driven energy-dependent, intracellular vesicular transcytosis, which accelerates the airway-to-perfusate transfer of this polymer and its co-polymers (Sun *et al.*, 1999). Based on kinetic analysis, the F-PHEA transporter was found to function across molecular weights between 4.3 and 7.4 kDa and to enhance absorption from the airways of the rat lung significantly. The use and discovery of transporters like this, in the pulmonary lung compartment, may enable systemic delivery of certain macromolecules via inhalation to replace their otherwise painful parenteral administration.

APPENDICES

APPENDIX I

THE ISOLATED PERFUSED RAT LUNG PREPARATION OPERATING PROCEDURE

AI.a INTRODUCTION

The isolated perfused rat lung (IPRL) preparation has been widely used in several laboratories as an experimental model for studying pulmonary physiology, pharmacology, metabolism and disposition of various endogenous and exogenous substances (Levey, 1966; Young, 1976; Mehendale *et al.*, 1981; Roberts, 1984; Niven 1988; Uhlig and Wollin, 1994; Baker *et al.*, 1999). The preparation retains the structural and functional integrity of the organ and closely maintains physiological conditions for a maximum 3 hours without introducing whole body complications. Over the last 20 years, our group has developed this preparation for studying the pulmonary absorption of small and macromolecular solutes from the airways after their presentation in solutions or as aerosols. The preparation employs horizontal IPRL suspension (Roberts, 1984; Niven, 1988; Sun, 1995), as opposed to vertical suspension from the trachea, to avoid tracheal stretching as in most other IPRL systems (Young, 1976; Mehendale *et al.*, 1981; Baker *et*

al., 1999). As a result, the preparation avoids rapid edema formation, which often occurred in the vertical IPRL systems without any challenges to the circulatory performance (Roberts, 1984; Niven, 1988; Sun, 1995). Furthermore, the horizontal IPRL suspension allows solute administration into the peripheral airways either by forced solution instillation or as aerosols.

The preparation, despite the presence of minor preparative differences among laboratories, is capable of maintaining its viability for ≥ 180 minutes at 37 ^{o}C with respect to morphological, histological, functional and biochemical parameters (Veith *et al.*, 1967; Niemeier and Bingham 1972; Mehendale *et al.*, 1981; Baker *et al.*, 1999). On the other hand, its viability under low temperature perfusion seems controversial, since most IPRL studies in the literature were performed in less than 30 minutes, unless autologous blood or plasma perfusion was employed (Table IV.4 in Chapter 4). In fact, earlier studies in our laboratory confirmed that 4 ^{o}C perfusion enabled only 12 minutes viability before the preparation became edematous (Sun, 1995).

The research described in this thesis primarily employed the IPRL preparation to study pulmonary disposition and mechanisms of macromolecular solute absorption from the airways. All IPRL preparations were carefully controlled in our laboratory, noting that reproducible results from viable IPRL preparations can be only obtained by highly trained and competent researchers. Most operational details in this thesis adhere to the methods developed by previous workers (Roberts, 1984; Niven, 1988; Sun, 1995; Visich,

1996). In this appendix, the details are documented as "in-house experimental method" to ensure successful and comparable studies. Method details focus especially on the preparation and assessment of viability at lower temperatures and in the presence of metabolic inhibitors. Future workers are encouraged to refer to the "step-by-step standard operating procedures" described by previous researchers (Niven, 1988; Sun, 1995; Visich, 1996).

AI.b MATERIALS AND METHODS

AI.b.1 PERFUSATE

Perfusate was substituted for circulating blood to maintain the viability of the isolated organ. Krebs-Henseleit solution (KHS; Krebs and Henseleit, 1932) with 4 % (w/v) bovine serum albumin (BSA) was the circulating perfusate through pulmonary vasculature of the IPRL. One liter of perfusate contained, in order of addition: (1) 2.00 g D-glucose, (2) 0.35 g KCl, (3) 0.29 g $MgSO_4 \cdot 7H_2O$, (4) 2.10 g $NaHCO_3$, (5) 0.37 g $CaCl_2 \cdot 2H_2O$, (6) 6.92 g NaCl, (7) 0.16 g KH_2PO4 and (8) 40.0 g BSA, in deionized water; this order of addition was critical to avoid precipitate formation. Perfusate was stored in a refrigerator ($\leq 4\ ^oC$) and used within 48 hours of preparation. The perfusate was filtered through a filter paper (Grade 802; size 32.0 cm; 100 folded circles, particle

size retention = 15 μm; Reeve Angel 802; Whatman Inc., Clifton, NJ) and its pH was adjusted to 7.40±0.05 prior to each experiment. Glucose and salts were purchased from Fisher Scientific (Raleigh, NC) and BSA (powder, fraction V) was from Sigma Chemical Company (St. Louis, MO).

AI.b.2 IPRL APPARATUS COMPONENTS

The IPRL apparatus was composed of the following components: (1) artificial glass thorax; (2) perfusate conductor; (3) perfusate pumps; (4) perfusate reservoir; (5) perfusate flow lines and (6) thermostatically-controlled water circulator. A whole apparatus set-up is shown in Fig. AI.1 and each component is described below:

(1) Artificial Glass Thorax (Fig. AI.1, d and Fig. AI.2)

The artificial glass thorax (AGT, Research Glass, Richmond, VA) was used to house the isolated rat lung. The AGT was water-jacketed to maintain constant temperature and its internal volume was 1000 mL. A removable plexi-glass lid covered the AGT and was securely held in place using Cello-Grease (Fisher Scientific, Raleigh, NC) for an airtight fit. The pulmonary artery cannula (PAC) was connected to a perfusate flow line inlet through the lid by a tube fitting (Swagelok™ tube fitting; Crawford Fitting Co., Solon, OH). A pressure gauge (Magnahelic Gauge; Dwyer Inst. Inc., Mich. City, IN) was also connected through another tube fitting on the lid, attached with a 50 mL syringe,

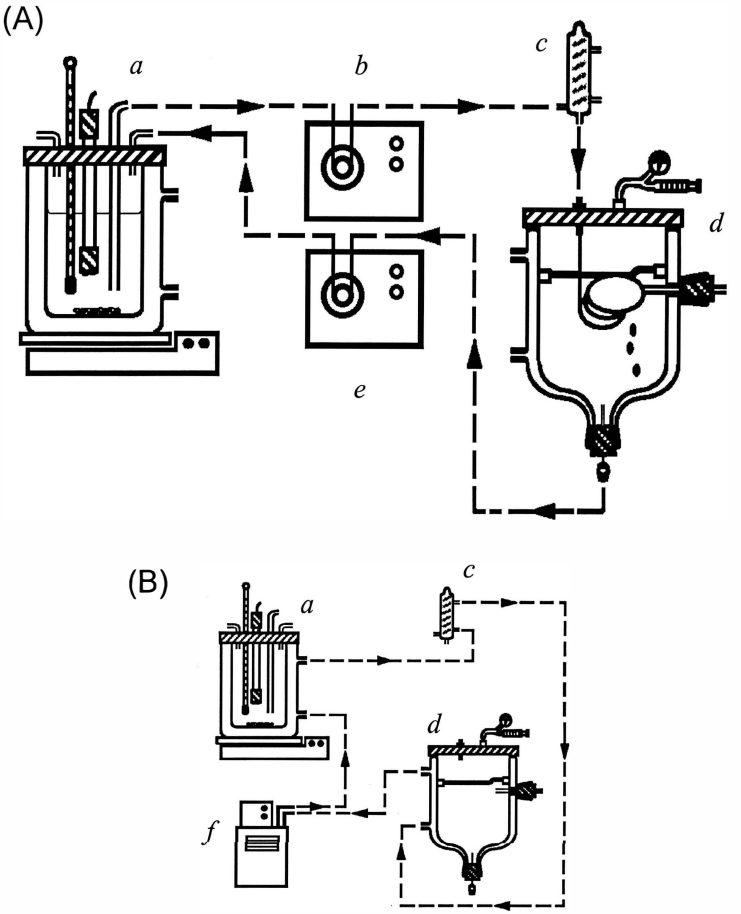

Figure AI.1. A scheme of the isolated perfused rat lung (IPRL) preparation (A) and circulating water flow chart (B). Dashed lines represent flow connections and arrows indicate flow direction. An isolated lung was housed in the artificial glass thorax (AGT; *d*) after pulmonary artery cannulation.
Key: *a* - perfusate reservoir; *b* - "supply" pump; *c* - perfusate conductor; *d* - artificial glass thorax (AGT); *e* - "return"pump; *f* - thermostatically-controlled water circulator. (adapted from Sun, 1995)

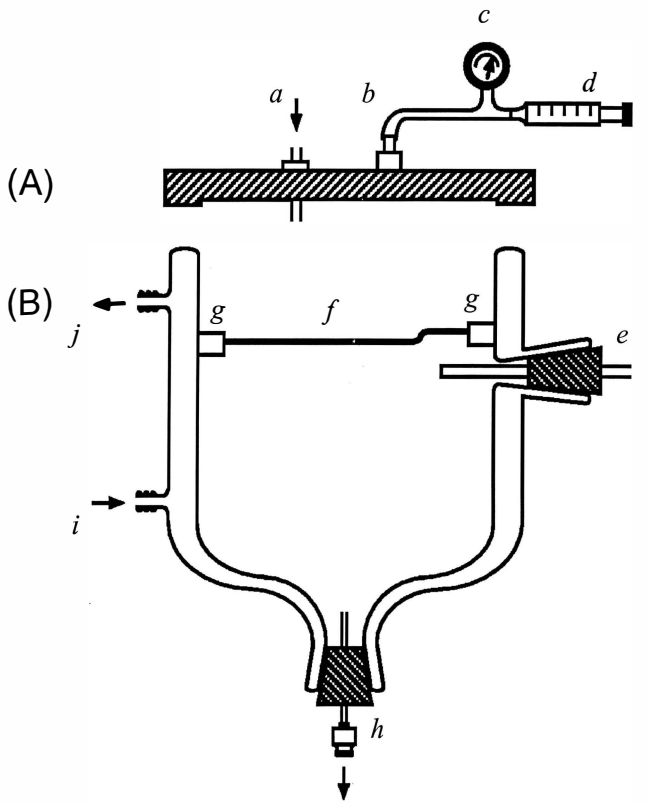

Figure AI.2. A removal plexi-glass lid (A) and artificial glass thorax (AGT; B). Key: *a* - perfusate line orifice; *b* - pressure gauge orifice; *c* - pressure gauge; *d* - 50 mL syringe; *e* - tracheal exit cannula; *f* - esophagus support rod; *g* - glass supporters for esophagus support rod; *h* - perfusate exit; *i* - water jacket inlet; *j* - water jacket outlet. (adapted from Sun, 1995)

so that a slightly negative pressure (2-5 cmH_2O) would be maintained in the AGT throughout experiments (to ensure partial lung inflation). A stainless-steel tubing (od = 2.5 mm, id = 2.0 mm and l = 75 mm), attached to the AGT using size #4 rubber stopper, was exteriorized as a tracheal cannula and to enable solute administration into the airways. The isolated rat lung was suspended horizontally in the AGT by a stainless-steel rod through the esophagus of the rat. The bottom of the AGT was curved to collect the perfusate and subsequently, perfusate was pumped back to the perfusate reservoir (recirculation); stainless-steel tubing (od = 3.0 mm, id = 2.0 mm and l = 50 mm) was attached to the AGT via a size #2 rubber stopper at the bottom of the AGT.

(2) Perfusate Conductor (Fig. AI.1, c and Fig. AI.3)

A glass perfusate conductor was connected to the perfusate flow line tubing and placed between the perfusate reservoir and the AGT. The conductor serves as an air-bubble trap (to collect bubbles in the prefusate) and a thermo-conductor to ensure constant perfusate temperature.

(3) Perfusate Pumps (Fig. AI.1, b and e)

Two MasterFlex™ peristaltic pumps (Model 7520-25; standard pump head, Model 7014-21; MasterFlex size #14 silicone tubing; Cole-Parmer Instrument Co., Vernon Hills, IL) were used as "supply" pump and "return" pump for recirculation through the IPRL. Their flow rates were adjusted to 15 mL/min throughout the experiments.

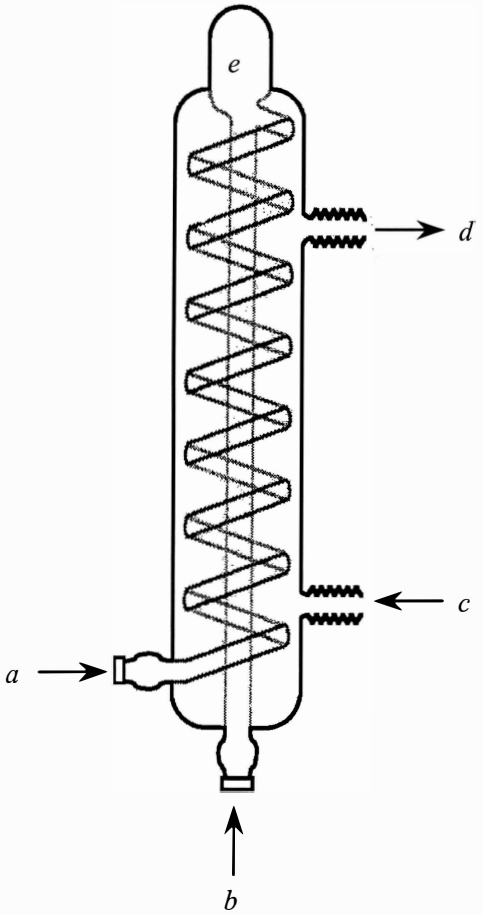

Figure AI.3. Perfusate conductor.
Key: *a* - perfusate inlet; *b* - perfusate outlet; *c* - water jacket inlet; *d* - water jacket outlet; *e* - bubble trap. (adapted from Sun, 1995)

(4) Perfusate Reservoir (Fig. AI.1, a and Fig. AI.4)

The perfusate reservoir was a water-jacketed glass container (double-fused beakers; Research Glass, Richmond, VA) and its internal volume was either 600 or 300 mL. The reservoir was topped with a plexi-glass lid possessing six ports for; (1) perfusate inlet tubing (to "supply" pump), (2) perfusate outlet tubing (from "return" pump), (3) pH electrode (Cat. # 476530; pH meter 220; Corning, Corning, NY), (4) thermometer (Fisher Scientific, Raleigh, NC), (5) carbogen gas (95% O_2 and 5 % CO_2; Airco Co., Richmond, VA) and (6) perfusate samples. Carbogen gas was delivered at about 2 L/min onto the perfusate surface in the reservoir throughout experiments. This rate was known to maintain O_2 saturation from previous work (Byron *et al.*, 1986). The perfusate (adjusted to pH 7.40±0.05) was well-stirred with a teflon fluorocarbon resin-coated magnetic stir bar (l = 3.5 cm; Fisher Scientific, Raleigh, NC) and a stirring plate (Model PC-353; Corning, Corning, NY).

(5) Perfusate Flow Lines (Fig. AI.1)

MasterFlex™ size #14 silicone tubing (od = 5.3 mm, id = 1.6 mm, Cole-Parmer Instrument Co., Vernon Hills, IL) was used to connect the perfusate flow lines between the IPRL components. The flow line started from the perfusate reservoir, through the "supply" pump, the perfusate conductor and the PAC, and from the bottom of the AGT, through the "return" pump to the reservoir. The PAC was a Silastic™ silicone tubing (od = 3.2 mm, id = 2.1 mm; Dow Corning, Midland, MI) with hard tubing (od = 2.0 mm, id = 1.6 mm and l = 10.0 mm; Clay Adams, Parsippany, NJ) inserted at the end of the PAC;

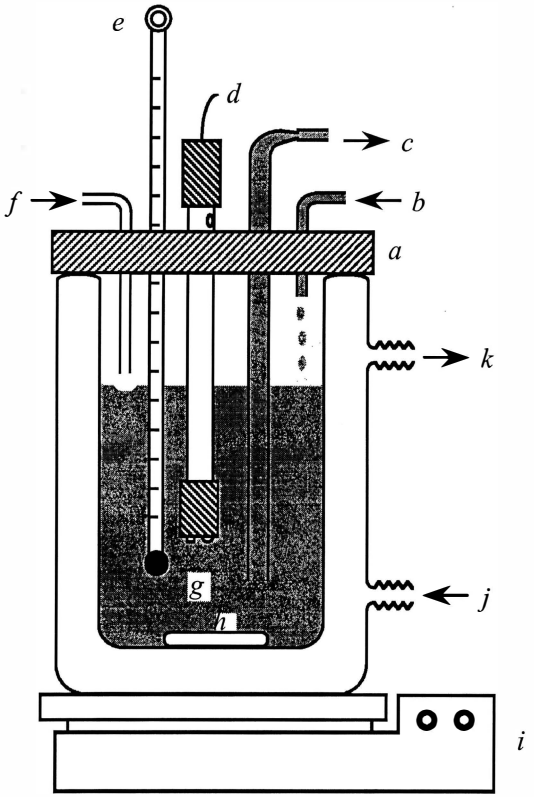

Figure AI.4. Perfusate reservoir.
Key: *a* - reservoir lid; *b* - perfusate inlet (from "return" pump); *c* - perfusate outlet (to "supply" pump); *d* - pH probe; *e* - thermometer; *f* - carbogen inlet; *g* - perfusate; *h* - magnetic stir bar (l = 3.5 cm); *i* - stirring plate (Model PC-353, Corning, NY); *j* - water jacket inlet; *k* - water jacket outlet. (adapted from Sun, 1995)

the hard tubing was inserted to prevent flow line occlusion, when a ligature was tied around the cannulated vessel. The total volume of the flow lines (including internal volume of perfusate conductor) was 22.2 mL.

(6) Thermostatically-controlled Water Circulator (Fig. AI.1)

A constant temperature circulator (Model 9505, Fisher Scientific, Pittsburgh, PA) was used to maintain the perfusate temperature by delivering 37, 30 or 25 ^{o}C water to the water-jacketed flow lines of the perfusate reservoir, the perfusate conductor and the AGT.

AI.b.3 ANIMAL HUSBANDRY AND ANESTHESIA

The research adhered to the NIH Principles of Laboratory Care and was approved by the Institutional Animal Care and Use Committee (IACUC; Project 9710-2468) at Virginia Commonwealth University (VCU). The animals were housed and cared for by the Division of Animal Resources (VCU), based on the NIH Principles, and were handled according to the "Occupational Health Program for Animal Handlers" (OHPAH1, 1996, VCU).

Specific pathogen free (C.V.F.-certified virus free), male Sprague-Dawley rats weighing 310-390 g were purchased from Hilltop Lab Animals Inc. (Scottsdale, PA). The animals were singly housed in polycarbonate cages (18 x 10 x 7 in inch) and the perforated ceilings of each cage covered with non-woven, spun nylon microisolator fabric

to prevent cross contamination. The animals had free access to water and food (RMH 3000 Rodent Chow pellets; Agway, Inc., Ithaca, NY) and were housed in rooms controlled between 18-26 ^{o}C at 40-70 % relative humidity. Dark/light cycling occurred every 12 hours and animals were acclimated for $\geq$ 7 days prior to use.

A rat was weighed and anesthetized intraperitoneally with pentobarbital (50 mg/kg; pentobarbital sodium injection, 50 mg/mL, Abbott Laboratories, Chicago, IL). The rat was gently held in the upright position and its abdomen exposed. Pentobarbital was injected using a Tuberculin syringe (1 cc; Becton Dickinson & Company, Franklin Lakes, NJ). The degree and adequacy of anesthesia was visually determined by the absence of pedal reflex (withdrawal of the extended hind limb) and corneal reflex (eye-blink following a gentle touch to the corneal surface). The use of pentobarbital was rigorously recorded on the "Controlled Substances Record" supervised by the Aerosol Research Group, VCU (Drug Enforcement Administration (DEA) Registration, AM4414962).

AI.b.4 SURGICAL PROCEDURE FOR ISOLATING THE LUNG

Surgical procedures for the isolated perfused rat lung (IPRL) contain numerous steps and a successful operation largely depends on the operator's skills, experience and understanding. A "step-by-step standard operating procedure" was well-documented by previous researchers (Niven, 1988; Sun, 1995; Visich, 1996) and is not duplicated here. Rather, an "in-house experimental method" was documented to ensure successful and

comparable operations with those of previous researchers (Niven, 1988; Sun, 1995; Visich, 1996).

In this thesis, the perfusion temperatures were varied yet held constant at 37, 30 and 25 ^{o}C to kinetically characterize active/passive absorption of solutes from the airways. Furthermore, despite edema formation which was found to occur rapidly, perfusion temperatures were further lowered to < 25 ^{o}C to find the minimum temperature at which 180 minute lung viability could be maintained. In these cases, the perfusion temperatures were simply adjusted and maintained by the thermostatically-controlled water circulator throughout the experiment.

(1) Pre-surgical Preparation

The surgical procedures for successful IPRL preparation required prompt and smooth operation following pre-surgical preparation. All surgical materials and instruments were clean and in place, as described in the "standard operating procedure" (Sun, 1995; Visich, 1996). The glassware and the perfusate flow lines were washed, rinsed and dried-up following each experiment. Periodically, the system was disassembled for thorough cleaning under sonication to remove precipitated protein residues. The perfusate pumps, pH meter and rodent ventilator were calibrated prior to each experiment.

(2) Tracheal Cannulation: Tracheotomy

Following anesthesia, a rat was placed in a supine position and its neck and chest area was dampened with detergent solution applied on a tissue. A 3 cm longitudinal incision was made at the neck skin around 5 cm below the mouth. The neck muscle and the tracheal muscle sheath were vertically cut and separated to expose the trachea and esophagus hidden underneath. At 5^{th} tracheal cartilaginous ring, a piece of thread was tied loosely around the trachea (through an eyelet created through connecting tissues between trachea and esophagus). Then, the trachea was laterally incised between the 4^{th} and 5^{th} cartilaginous rings and the stainless-steel tracheal cannula (od = 2.2 mm, id = 1.9 mm, l = 32 mm) was inserted through the incision. The thread was tightly tied to retain the cannula in place; 22 mm of the cannula was inserted into the trachea from the 5^{th} tracheal cartilaginous ring.

(3) Opening Thoracic Cavity

The abdomen was first opened transversely below the xiphoid cartilage. A small incision was made through the abdominal diaphragm from the ventral side of the thoracic cavity, the rib cage on both sides of the sternum was cut through and the whole thoracic cavity opened. The rib cages were flapped backward in the cranial direction and held in place with a pair of haemostatic forceps to expose the lungs and heart.

(4) Pulmonary Artery Cannulation (PAC)

Heparin (0.1 mL; heparin sodium injection, USP; 1000 U/mL, Pharmacia & Upjohn Company, Kalamazoo, MI) was slowly injected intravenously into the upper right ventricle and subsequently, the thymus (white tissue covering anterior-ventral part of heart) was removed. At about 30 seconds following heparin injection as anticoagulant, the PAC tip (looped back into the perfusate reservoir at this time) was withdrawn from the reservoir and placed near the lung. A 6 mm long incision, perpendicular to pulmonary artery, was made in the upper right ventricle for the PAC and the bottom of the left auricle and both sides of each ventricle amputated to allow the blood to be flushed from the pulmonary circulation. The PAC was immediately inserted into the pulmonary artery through the incision and kept in place temporarily with a pair of artery clips. In a period of 5-7 time positive pressure ventilation via the tracheal cannula (tidal volume = 4.5 mL and respiration rate = 16 /min; Model 802, New England Medical Instruments Inc., Medway, MA), with perfusate flowing at 15 mL/min, the blood was completely removed from the lung. A ligature was inserted to tie the pulmonary artery cannula in place throughout the remainder of the experiment.

(5) Lung and Heart Isolation

The flapped rib cages were removed and the trachea, lung and heart were completely exposed. The trachea and esophagus were held together with the tracheal cannula and subsequently, the lung and heart with the PAC were isolated from the body. Unnecessary tissues (connecting tissues, diaphragm and blood vessels) were carefully

removed and finally, the lung was isolated with both tracheal and pulmonary artery cannulations. The stainless-steel support rod (Fig. AI.1) was slipped through the esophagus and the outer surface of the lung was rinsed by pre-warmed perfusate. The whole procedure from tracheal cannulation to lung removal took no longer than 10 minutes.

(6) Perfusion of the Lung

The isolated rat lung was transferred to the AGT and suspended horizontally by the support rod; the PAC line was allowed to coil inside the AGT without twisting or touching the lung. The tracheal cannula was tightly connected to the exteriorized tracheal cannula port (a stainless-steel tubing attached to the AGT). The plexi-glass lid was placed on the top of the AGT, creating an air-tight condition. Any perfusate lost through the pulmonary circulation was collected and pumped back by the "return" pump to the reservoir (the "return" tubing was previously returned to a waste beaker at this time). A negative pressure (2-5 cm H_2O) inside the AGT was created and maintained by adjusting the syringe, attached to the pressure gauge. Following 3-7 minutes, the "return" tubing was put back into the perfusate reservoir for recirculation. After the re-circulation commenced, the perfusate surface was adjusted to a pre-determined mark (either 200 or 100 mL was employed). Consequently, total volumes of the perfusate were 222.2 or 122.2 mL, respectively (total volume of the flow lines = 22.2 mL). The AGT pressure, perfusate pH, temperature and carbogen gas flow were all checked and adjusted

appropriately to maintain constancy throughout experiments. The perfusate pH values were maintained at 7.40±0.05.

The protocols to study solute absorption in the presence of 2,4-dinitrophenol (DNP) and ouabain (OUA) required 15 minutes perfusion prior to solute administration, as described in Section IV.c.2 (Chapter 4). In these experiments, after the recirculation was commenced, 50 mL of the perfusate was removed from the perfusate reservoir and replaced with 50 mL of fresh perfusate containing various concentrations of DNP and OUA. Subsequently, at time = 15 minutes, solute was administered, as described below.

AI.b.5 SOLUTE DOSING (Fig. AI.5)

The dosing method, "forced solution instillation" was developed by previous researchers (Niven, 1988; Sun, 1995; Visich, 1996) and used unchanged in this thesis. A silicone tubing (od = 2.0 mm, id = 1.0 mm, l = 230 mm, marked for 0.1 mL solution), attached to a Tuberculin syringe (1 cc; Becton Dickinson & Company, Franklin Lakes, NJ) was used as a dosing adapter. A 0.1 mL aliquot of solute dosing solution was exactly measured by the dosing adapter tubing and loaded into a stainless-steel tubing (od = 1.2 mm, id = 1.0 mm, l = 138 mm) used as a dosing cartridge. The cartridge containing solute solution was slipped through the tracheal cannula port exteriorized outside the AGT, until its tip projected 0.5 mm beyond the cannula terminus, into the trachea. A metered dose inhaler (MDI, containing fluorocarbon propellants alone, 40 % P-11 and 60 % P-12

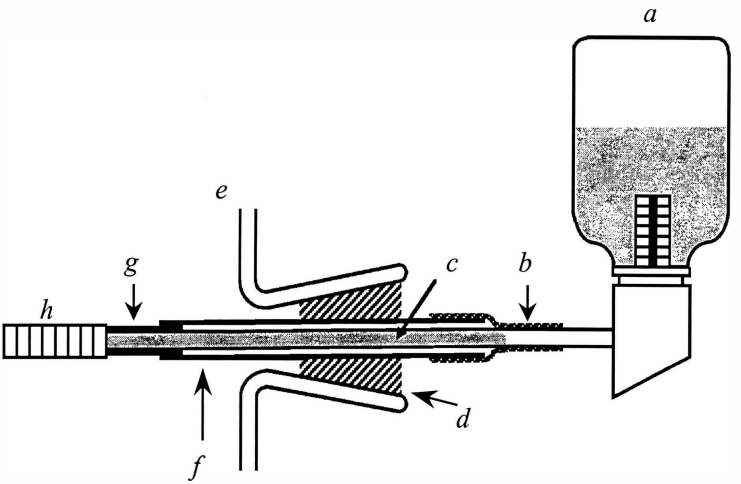

Figure AI.5. Solute dosing method; "forced solution instillation".
Aqueous dosing solution in the dosing cartridge was propelled into the lung as a coarse spray with simultaneous inflation by MDI actuation.
Key: *a* - MDI (propellant only); *b* - a teflon tubing; *c* - dosing cartridge containing 0.1 mL dosing solution; *d* - rubber stopper; *e* - artificial glass thorax (AGT); *f* - exit tracheal cannula; *g* - tracheal cannula; *h* - rat trachea. (adapted from Sun, 1995)

(w/w), 50.5 psig at 25 °C, 25 μL per actuation) was connected to the other side of the cartridge and actuated once. The dosing solution was propelled into the lung as a coarse spray and the lung was inflated simultaneously with 5.5 mL of propellant vapor. Immediately, the dosing cartridge and MDI were removed from the tracheal cannula port and the lung allowed to deflate to a residual volume dictated by the maintenance of the 2-5 cm H_2O negative pressure inside the AGT.

After administration, administered solute doses were determined by subtracting the amount of solute recovered from all non-biological components from the known amounts of solute loaded into the dosing cartridge. A 0.1 mL aliquot of each solute solution was independently, but similarly measured using the dosing adapter and placed into known volumes of deionized water ("loaded" solute in the cartridge). The dosing cartridge and the tracheal cannula (with the tracheal cannula port) were rinsed with 50 mL deionized water immediately following administration and at the end of the experiments, respectively ("recovered" solute from non-biological dosing components). Both "loaded" and "recovered" solutes were determined using validated analytical methods described in Appendix IV and were then used to determine each administered dose.

AI.b.6 PERFUSATE SAMPLING

0.5 or 1.0 mL of perfusate was withdrawn from the perfusate reservoir prior to dosing (time = 0 [minute]) and at various time intervals (depending on solutes) following

solute administration by "forced solution instillation". Fresh perfusate was not replaced to compensate for sampling losses; rather, these sampling losses were assessed and corrected during data handling to determine each amount of solute in perfusate *vs.* time profiles.

AI.b.7 REGIONAL SOLUTE DISTRIBUTION IN LUNG

In some experiments, the initial and final regional solute distribution was determined. On these occasions, IPRL perfusion was halted immediately following solute administration (initial distribution) or at the end of the experiment (final distribution). Subsequently, the lung was removed from the AGT and dissected into tracheo-bronchi and five lung lobe regions (Fig. AI.6; left lung lobe (L), right postcaval or median lobe (PC), right superior or apical lobe (RS), right middle lobe (RM) and right inferior or diaphragmatic lobe (RI)). Each component was stored in 20 mL glass vials (Fisher Scientific, Ralcigh, NC) at $\leq$ - 20 ^{o}C prior to analysis. Following homogenization and clean up, remaining solutes were determined by using validated analytical methods described in Appendix IV.

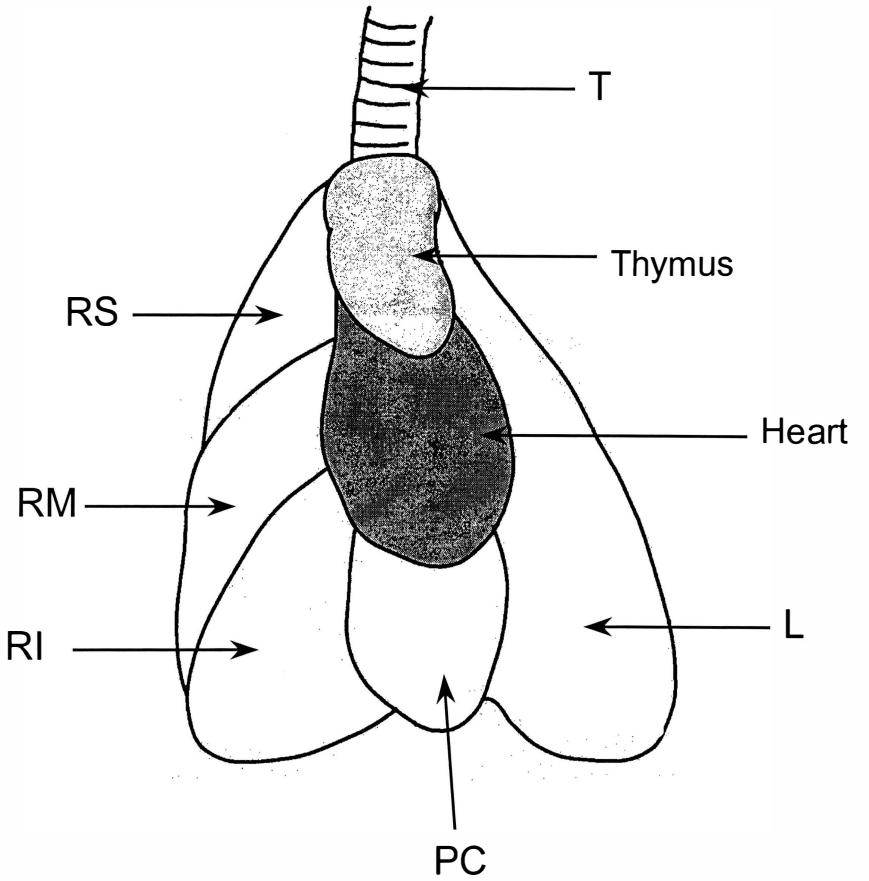

Figure AI.6. Schematic representation of rat trachea and lung lobes.
Key: *T* - trachea; *L* - left long lobe; *PC* - right postcaval or median lobe; *RS* - right superior or apical lobe; *RM* - right middle lobe; *RI* - right inferior or diaphragmatic lobe. (adapted from Sun, 1995)

AI.c RESULTS AND DISCUSSION

ASSESSMENT OF IPRL VIABILITY

Several criteria and/or indicators to assess the IPRL viability quantitatively and qualitatively have been proposed in the literature (Basset and Fisher, 1976; Wiersma and Roth, 1980; Fisher *et al.*, 1980; Mehendale *et al.*, 1981; Roberts, 1984; Basset *et al.*, 1987a; Niven, 1988; Baker *et al.*, 1999). These were visual inspection for signs of pulmonary edema (Roberts, 1984; Byron *et al.*, 1986; Niven, 1988; Byron and Niven, 1990), wet/dry lung weight ratios (≤ 6.2 as viable lungs; Basset and Fisher, 1976; Fisher *et al.*, 1980; Uhlig and Wollin, 1994), potassium efflux (Ward and Buttery, 1979), filtration coefficient measurement (Uhlig and Wollin, 1994), biochemical parameter changes (ATP content, reduced glutathione and glutathione reductase; Fisher *et al.*, 1980; Baker *et al.*, 1999) and histopathologic examination (Mehendale *et al.*, 1981; Okumura *et al.*, 1978; Ward and Buttery, 1979). In this thesis, similar to the methods used by our previous researchers (Roberts, 1984; Niven, 1988; Sun, 1995; Visich, 1996), signs of pulmonary edema were carefully monitored by visual inspection. Any sign of pulmonary edema was cause for the IPRL preparation to be designated "non-viable". Results from "non-viable" preparations were rejected and are not reported in this thesis. This method was used owing to its sensitivity as a means of identification and detection of physiological abnormalities in the IPRL.

At 37 ^{o}C, the IPRL was known to maintain viability for 180 minutes. This was evidenced by the absence of any signs of pulmonary edema. Similarly, 180 minutes viability could be maintained at 30 and 25 ^{o}C. However, at 4-15 ^{o}C, pulmonary edema occurred within 30 minutes following preparation, regardless of solute administration. This resulted in lung swelling, followed by fluid flooding from the tracheal cannula. When edema occurred, the (blood-free) lungs changed in outside color and texture from smooth white to a gray and/or patchy appearance, which was identified during experiments. In contrast, other indicators like wet/dry lung weight ratios could be obtained only after experiments terminated. Wet-dry weight ratios were shown to be insensitive measures of non-viability, especially in its early phases (Roberts, 1984); accordingly these ratios were not determined in this thesis.

A discontinuity in solute transfer profiles (airway-to-perfusate permeability changes) was also useful for identifying viability changes of direct importance to these studies (Sun, 1995). Figure AI.7 (A) shows F-PHEA transfer profiles in the presence of pulmonary edema created by intentional scratching of the left lung lobe during preparation (lung surface must not be touched during isolation; Roberts, 1984). At 10 min, immediately after pulmonary edema was visually observed in the left lung lobe, the solute transfer profiles showed a sudden discontinuity. Even in this case, it is unlikely that a wet/dry lung weight ratio was markedly elevated, since the other four lung lobes appeared to be completely viable. In fact, this IPRL showed a fluid flooding from the tracheal cannula at time = 45 minutes (35 minutes after the lung appearance was

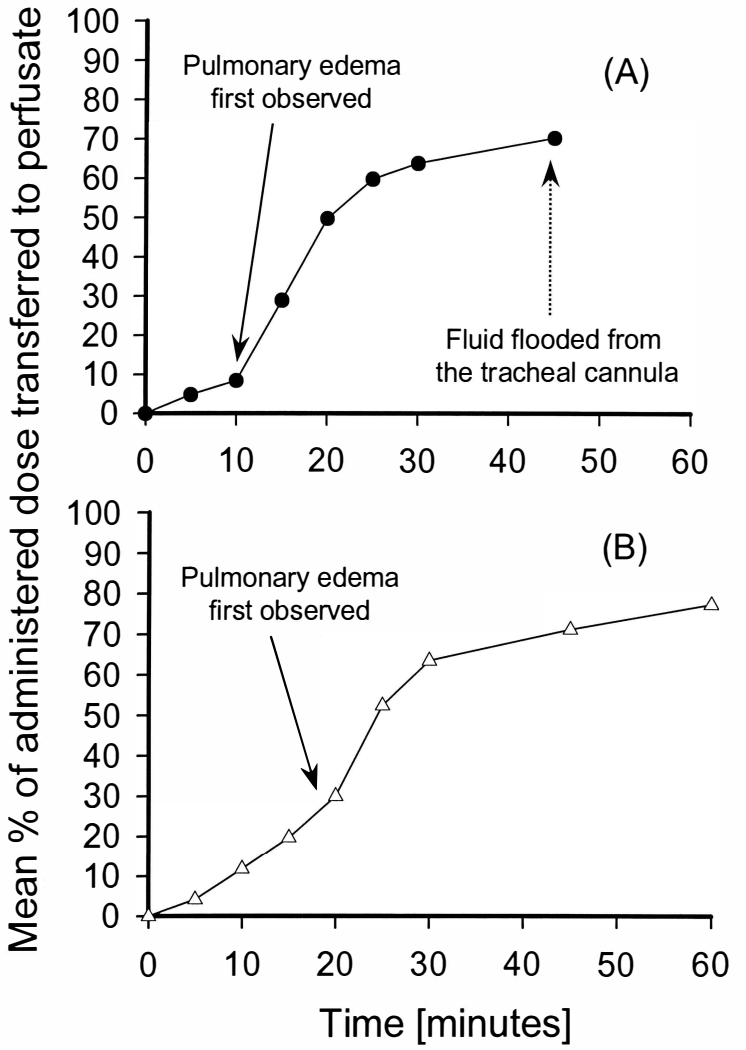

Figure AI.7. Percentage of administered dose of 7.4 kDa F-PHEA absorbed from the airways of the IPRL into the perfusate *vs.* time (A) after pulmonary edema was created by intentional scratching of the left lung lobe during preparation and (B) by holding the IPRL at 15 °C.

edematous). Similar discontinuous solute airway-to-perfusate transfer was also observed at 15 °C, as shown in Figure AI.7 (B). In this case, pulmonary edema was gradually formed, but a fluid flooding from the tracheal cannula was not observed even at 60 minutes. There was no such discontinuity in the solute transfer profiles seen at 30 and 25 °C, as shown in Figs. IV.4, IV.6 and IV.7 (Chapter 4) nor was there any appearance of edema. For these reasons, it was possible to ensure 180 minutes viability at 25, 30 and 37 °C.

In Chapter IV, to kinetically characterize the mechanisms responsible for the active absorption of F-PHEA from the airways, the IPRL studies were performed in the presence of various metabolic inhibitors, 2,4-dinitrophenol (DNP), ouabain (OUA), monensin (MON) and nocodazole (NOC). The experimental protocols using these inhibitors were optimized based upon preliminary studies and/or conditions selected from literature information (Basset and Fisher, 1976; Goodman *et al.*, 1983; Basset *et al.*, 1987; Effros *et al.*, 1988; Hastings *et al.*, 1994; Wangensteen *et al.*, 1996). As a result, prior to solute administration, 15 minutes pre-dosing perfusion intervals were required in the case of DNP and OUA, while 1.5 % (v/v) EtOH and DMSO solutions were used as administration vehicles for MON and NOC, respectively. Because of these protocol and dosing solution changes, IPRL preparation began to show pulmonary edema formation (glossy appearance) at 60 minutes in the presence of DNP (1 mM) and OUA (100 μM) in perfusate and at 120 minutes in the presence of MON (100 μM) and NOC (100 μM) in the airways. Accordingly, data is only reported from these experiments for times at which

edema was absent. Clearly, some changes in IPRL viability are unavoidable, due probably to the simultaneous inhibition of fluid absorption from the airways by some of these inhibitors (Hostetter *et al.*, 1981; Serikov *et al.*, 1993; Basset *et al.*, 1994; Cott, 1994; Effros, 1994; Hastings *et al.*, 1994; Wangensteen *et al.*, 1996).

AI.d SUMMARY AND CONCLUSION

An isolated perfused rat lung (IRPL) preparation was validated and employed to study the pulmonary absorption kinetics of small and macromolecular solutes from the airways. The apparatus components and surgical steps were carefully controlled by adhering to the "standard operating procedure" described by our previous researchers (Niven, 1988; Sun 1995; Visich, 1996). Methods followed in this thesis to ensure successful and comparable IPRL studies were only changed as necessary to enable the required experimental perturbations. The viability/non-viability of the IPRL was assessed based upon its appearance (sign of pulmonary edema by visual inspection) and the resultant solute transfer profiles (discontinuity of the profiles), as described in previous studies (Niven, 1988; Sun 1995; Visich, 1996). Consequently, $\geq$ 25 ^{o}C perfusion was found to maintain the viability for 180 minutes, whereas $<$ 25 ^{o}C perfusion rapidly induced edema formation, precluding the use of such conditions for absorption studies. Similarly, the IPRL viability could be maintained for 60 or 120 minutes in the presence of metabolic inhibitors, DNP and OUA or MON and NOC, respectively.

APPENDIX II

THE OPERATING PROCEDURE FOR IN VIVO WHOLE RAT STUDIES

AII.a INTRODUCTION

In vivo whole animal (rat) studies for solute absorption from the lung were originally developed by Enna and Schanker (1972), employing an intratracheal solution instillation technique for solute administration into the airways. Profiles for solute remaining unabsorbed from the airways and the lungs *vs.* time were used to provide data on solute disposition in vivo, in the presence of anesthesia. Unfortunately, and while the technique is widely used, it has been shown that considerable animal sacrifice is required to obtain such absorption profiles and to avoid huge inter-rat variations in derived data (Brain *et al.*, 1976; Pitchard *et al.*, 1985; Folkesson *et al.*, 1996; Leong *et al.*, 1998). Much of the variation reported in the literature is associated with non-reproducible dosing and it is because of the uncertainties associated with the technique that inter-study comparisons are difficult with the exception of a small series performed by Schanker's group (Enna and Schanker, 1972; Lanman *et al.*, 1973; Burton and Schanker, *1974*a and

1974b; Burton *et al.*, 1974; Schanker and Burton, 1976; Schanker and Hemberger, 1983; Brown and Schanker, 1983).

The in vivo whole rat studies described in this thesis were used to perform an in vivo - in vitro correlation and to compare results directly with those obtained in the in vitro isolated perfused rat lung (IPRL) preparation. Because the regional deposition of solutes in the lung is believed to be a determinant of subsequent absorption and mucociliary clearance kinetics (Byron, 1986; Byron and Phillips, 1990; Colthorpe *et al.*, 1992; Byron and Patton, 1994; Hill *et al.*, 1996), it was necessary to employ an identical and reproducible forced solution instillation for solute administration into the airways, exactly as used in the IPRL. This device-oriented technique has been shown to maximize dosing consistency and hence, minimize the variability "between-rats" and "between- and within- operators" (Byron and Niven, 1988; Sun, 1995), enabling the initial solute distribution both in vivo and in vitro (IPRL) to be comparable. Importantly, reproducible results can only be obtained, when the procedure adheres to the standard operating procedure described in this appendix. It is especially important to ensure that the anesthetic regime used in vivo and in vitro is identical for the results to remain comparable. Future workers are encouraged to refer to the original methods developed by Enna and Schanker (1972) for animal surgery and Byron and Niven (1988) for solute dosing and blood removal from pulmonary circulation prior to lung removal from the animal.

AII.b MATERIALS AND METHODS

AII.b.1 PERFUSATE AND THE IPRL APPARATUS

Krebs-Henseleit solution with 4% (w/v) bovine serum albumin (BSA) was prepared, as described in Appendix AI.b.1 and used as perfusate for clearing the blood from the pulmonary circulation at the time of animal sacrifice following solute administration. Perfusate was stored in a refrigerator ($\leq 4\ ^{o}C$) and used within 48 hours of preparation following filtration through a filter paper (Grade 802; size 32.0 cm; 100 folded circles, particle size retention = 15 μm; Reeve Angel 802; Whatman Inc., Clifton, NJ). The perfusate reservoir, conductor, "supply" pump and flow lines used in the IPRL (Appendix AI.b.2) were utilized to pump the perfusate into the pulmonary circulation via the pulmonary artery cannula. The whole set-up was maintained at 37 ^{o}C using a thermostatically-controlled water circulator (Model 9505, Fisher Scientific, Pittsburgh, PA).

AII.b.2 ANIMAL HUSBANDRY

The research adhered to the NIH Principles of Laboratory Care and was approved by the Institutional Animal Care and Use Committee (IACUC; Project 9710-2468) at

Virginia Commonwealth University (VCU). The animals were housed and cared for by the Division of Animal Resources (VCU) and handled according to the "Occupational Health Program for Animal Handlers" (OHPAH1, 1996, VCU).

Specific pathogen free (C.V.F.-certified virus free), male Sprague-Dawley rats (310-390 g; Hilltop Lab Animals Inc., Scottdale, PA) were used throughout. The animals were housed singly in rooms controlled between 18-26 ^{o}C and 40-70 % relative humidity and allowed free access to water and food (RMH 3000 Rodent Chow pellets; Agway, Inc., Ithaca, NY). Dark/light cycling occurred every 12 hours and animals were acclimated for $\geq$ 7 days prior to use.

AII.b.3 PROCEDURE FOR IN VIVO WHOLE RAT STUDIES

Surgical procedures for in vivo whole rat studies were originally developed by Enna and Schanker (1972) and modified by our laboratory. The reproducible "forced solution instillation" technique (identical to that used in the IPRL) was employed for solute administration into the airways. At different sacrifice times following administration, the blood was removed from the pulmonary circulation, the lung removed from the body and remaining solutes in the lung determined from each of these excised lungs by use of the validated analytical methods described in Appendix IV. The procedure described below in detail is subdivided as follows: (1) tracheal cannulation (tracheotomy), (2) solute

dosing ("forced solution instillation"), (3) pulmonary blood removal and (4) lung and heart isolation.

These surgical procedures required prompt and smooth operation following pre-surgical animal preparation. All surgical materials and instruments were clean and in place, as described in Appendix AI.b.4.

(1) Tracheal Cannulation: Tracheotomy

The procedure was identical to that described for the IPRL (Appendix AI.b.4). Briefly, a rat was weighed and anesthetized by intraperitoneal injection of pentobarbital (50 mg/kg; pentobarbital sodium injection, 50 mg/mL, Abbott Laboratories, North Chicago, IL). [In the event that dosing and sacrifice were to be separated for ≥ 60 minutes, further anesthetic was administered at 60 minute intervals in doses of 25 mg/kg intraperitoneally.] Each rat was placed in the supine position and a longitudinal incision was made at the neck skin. Subsequently, the neck muscle and the tracheal muscle sheath were vertically separated to expose the trachea and esophagus hidden beneath. The stainless-steel tracheal cannula (od = 2.2 mm, id = 1.9 mm, l = 32 mm) was inserted through the incision made at the 4^{th} tracheal cartilaginous ring. This was then tied tightly and secured in place using cotton thread; 22 mm of the cannula was inserted into the trachea from the 5^{th} tracheal cartilaginous ring. The tracheal cannula was left in place throughout each experiment, irrespective of the time allowed for absorption to preclude solute absorption from swallowed materials. The cannula was washed and the washings

also analyzed at the end of each experiment using the validated analytical methods described in Appendix IV.

(2) Solute Dosing

Forced aqueous solution instillation (Appendix AI.b.5) was used to provide identical initial solute distribution in vivo and in vitro. The technique was unchanged when performing the in vivo experiments except that care was employed to phase administration along with the rat inspiration. A silicone tubing (od = 2.0 mm, id = 1.0 mm, l = 230 mm, marked for 0.1 mL solution) and a stainless-steel tubing (od = 1.2 mm, id = 1.0 mm, l = 138 mm) were used as a dosing adapter and a dosing cartridge, respectively. A 0.1 mL aliquot of F-PHEA or F-Na solution was precisely measured by the dosing adapter and loaded into the dosing cartridge (Appendix AI.b.5). Immediately following natural expiration, the metal dosing cartridge was inserted through the tracheal cannula until its tip projected 0.5 mm beyond the cannula terminus, into the rat's trachea. A propellant-only metered dose inhaler (MDI, 40 % P-11 and 60 % P-12 (w/w), 50.5 psig at 25 ^{o}C, 25 μL per actuation) connected to the other side of the cartridge was actuated once. Thus, the dosing solution was expelled as a coarse spray into the airways; this inflated the lung with about 5.5 mL of propellant vapor and simultaneously, accomplished "forced solution instillation" (time = 0 [minute]). The dosing cartridge was removed within 1-2 seconds of actuation allowing the recommencement of normal respiration; in the event that natural respiration was not rapidly (≤ 1 minute) recommenced, the rat was sacrificed as before, but the lung was discarded prior to data

collection. The administered solute doses were determined, as described in Appendix AI.b.5. Body temperatures were maintained using a heat lamp. Adequacy of anesthesia was assessed by the absence of pedal and/or corneal reflexes and maintained by repeat pentobarbital intraperitoneal injection (25 mg/kg every 60 minutes).

(3) Pulmonary Blood Removal

At 3 minutes prior to each designated sacrifice time, while the rats continued to respire under anesthesia through the endotracheal tube, the abdomen was opened transversely and the rib cage was severed, on both sides of the sternum (from the abdominal diaphragm). The ribs were flapped backward to expose the lung and heart. Heparin (0.1 mL; heparin sodium injection, USP; 1000 U/mL, Pharmacia & Upjohn Company, Kalamazoo, MI) was slowly injected (over a period of 10 seconds) into the upper right ventricle and the tip of the pulmonary artery cannula (PAC; which was supplied with flowing perfusate from the reservoir) was inserted through an incision made in the upper right ventricle. The bottom of the left auricle and both sides of each ventricle were promptly amputated and the blood flushed from the lung by continuous free perfusion of oxygenated perfusate through the PAC at a flow rate of 15 mL/min. Blood removal was completed with the lung respirated using positive pressure ventilation (tidal volume = 4.5 mL, respiration rate = 16 /min; Model 802, New England Medical Instruments Inc., Medway, MA) for 1-2 minutes by attaching a small animal ventilator to the tracheal cannula. Complete blood removal took $\leq$ 3 minutes. Sacrifice times were

adjusted accordingly, by noting the actual time between dosing the airways and complete lung isolation.

(4) Lung and Heart Isolation

The blood-free lung and heart were promptly removed from the body exactly as if an IPRL preparation was to be performed (Byron and Niven, 1988; Sun, 1995; Appendix I) except that the removal was immediately followed by visual inspection for any signs of pulmonary edema (glossy appearance on lung lobes; Roberts, 1984; Sun, 1995; Sun *et al.*, 1999); lung preparations showing edema were discarded. The PAC, heart and unnecessary tissues (connecting tissues, diaphragm and blood vessels) were carefully removed and the lung was isolated. The complete procedure from first incision to tissue isolation was accomplished in ≤ 5 minutes. Viable lungs were dissected into tracheo-bronchi and the five lung lobe regions (Fig. AI.6; left lung (L), right postcaval or median lobe (PC), right superior or apical lobe (RS), right middle lobe (RM) and right inferior or diaphragmatic lobe (RI)). Each component was stored in 20 mL glass vials (Fisher Scientific, Raleigh, NC) at - 20 ^{o}C prior to analysis. Each lung region was weighed and solutes remaining to be absorbed from each lung region were determined by the methods described in Appendix IV following homogenization and centrifugation. At each sacrifice time, four fully viable lungs were studied for each dosing solution.

AII.b.4 ASSESMENT OF VIABLE CONDITION

Long-term anesthesia (maximum 3 hours) maintained by repeat pentobarbital injection, with or without forced lung inflation by MDI actuation during solute dosing, were occasionally found to induce "abnormal respiration" (e.g., bronchospasm). Animals showing such problems were sacrificed as before, but discarded prior to data collection. The incidence of such effects was about 3.0 %. Lungs showing signs of pulmonary edema had a much lower incidence (≤ 1.0 %) and were also excluded from sets subjected to chemical and data analysis.

APPENDIX III

SYNTHESIS AND CHARACTERIZATION OF FLUOROPHORE-LABELED POLY-α,β-[N(2-HYDROXYETHYL)-D,L-ASPARTAMIDE] (F-PHEA)

Two, weight-averaged 7.4 and 4.3 kDa fluorophore-labeled poly-α,β-[N(2-hydroxyethyl)-D,L-aspartamide] (F-PHEA; Fig. AIII.1) were synthesized, purified and characterized by Dr. Frantisek Rypacek at the Institute of Macromolecular Chemistry (IMC), Prague, Czech Republic. Their molecular weight distribution (MWD) and content of fluorophore label were determined following reconstitution of lyophilized polymers by Dr. Rypacek in Prague prior to shipping. A single batch (FR7150 and FR7002-5 for 7.4 and 4.3 kDa F-PHEA, respectively) of each was used throughout this thesis.

The model macromolecule, poly-α,β-[N(2-hydroxyethyl)-D,L-aspartamide] (PHEA) used in this thesis was originally designed and synthesized for use as a plasma expander (Neri *et al.*, 1973; Antoni *et al.*, 1974) and/or drug carrier (Drobnik *et al.*, 1979a; Giammona *et al.*, 1994). Chemically, the polymer is highly water-soluble (aqueous solubility ≥ 50 mg/mL) and hydrophilic (partition coefficient between octanol

and phosphate buffer (pH7.4), $K_D < 0.001$ at 37 °C) due to its hydrogen bonding capacity (Neri *et al.*, 1974). It is believed to be biocompatibile and non-toxic and in fact, in vivo rabbit studies showed no critical immunogenicity and antigenicity following intravenous administration ($LD_{50} > 300$ mg/kg; Neri *et al.*, 1973). Importantly, the polymer appears to have high resistance to enzymatic proteolysis due to random distribution of α- and β-peptidic linkages and synthesis from a racemic mixture of D- and L- configured aspartic acid residues (Drobnik *et al.*, 1979a and b; Rypacek *et al.*, 1980; Byron *et al.*, 1991). As a result, no degradation, metabolism or significant tissue sequestration was seen for this polymer in the rat lung, as shown in Appendix V.

The synthesis of F-PHEA used in this thesis is fully described elsewhere (Rypacek *et al.*, 1979; Rypacek *et al.*, 1980; Niven, *et al.*, 1990; Sun, 1995) and is shown schematically in Fig. AIII.1. Briefly, polysuccinimide (PSI) was prepared and fractionated by a fractional precipitation method (Vlasak *et al.*, 1979) and reacted with 2-aminoethyl-carbonyl-6-aminofluorescein (F; Rypacek *et al.*, 1980). Typically, 3 g of PSI was reacted with 162 mg F for 4 days at 60 °C in 30 mL dimethylformamide (DMF) containing 0.4 mmol triethylamine. This fluorophore-labeled PSI (F-PSI) was then precipitated with methanol (for removal of unreacted F) and the product was dried under vacuum (80 °C, 48 hours). The product was re-dissolved in DMF and subsequently, the solution was cooled at 0 °C, followed by an addition of excess ethanolamine (2 mol equivalents with respect to succinimide units) to give the completely ring-opened product, F-PHEA. The mixture was stirred for 24 hours at ambient temperature,

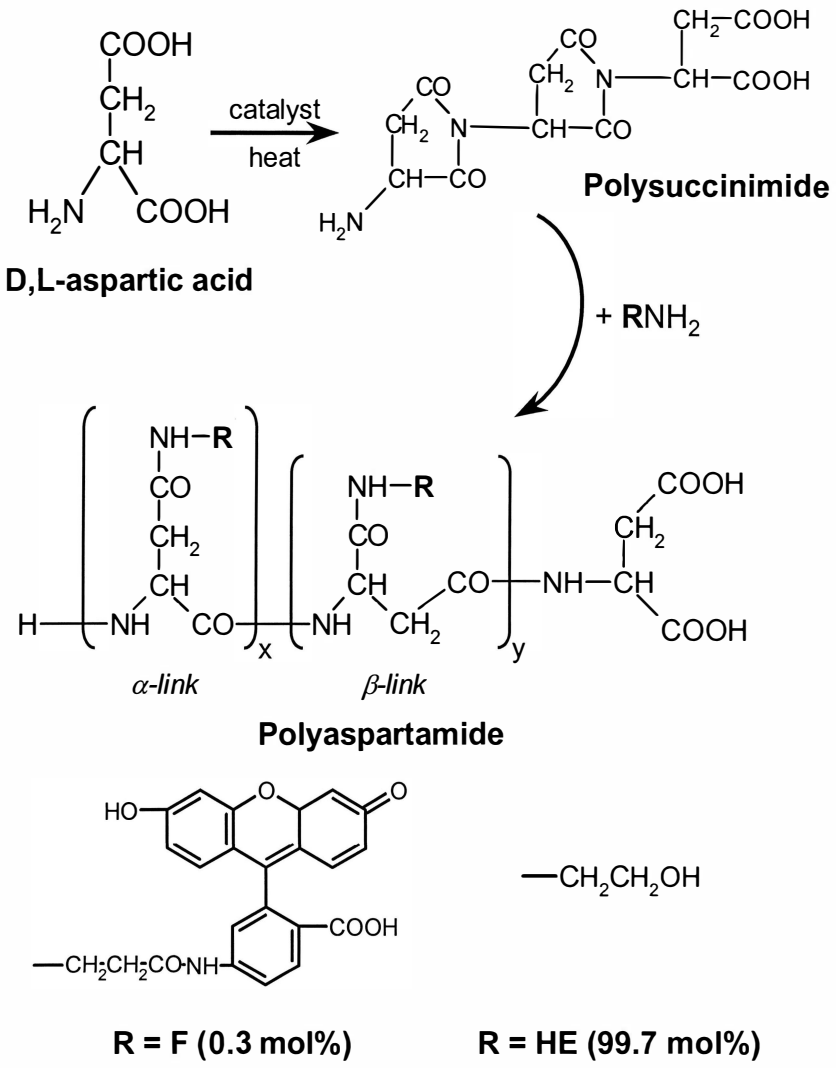

Figure AIII.1. Synthetic route of 7.4 and 4.3 kDa F-PHEA from D,L-aspartic acid via polysuccinimide (PSI). 0.3 % R groups in F-PHEA were substituted by F (fluorophore) and the remainder of the R groups were HE (hydroxyethyl).

neutralized with acetic acid, dialyzed exhaustively against distilled water and finally, concentrated under vacuum. F-PHEA was purified by preparative gel permeation chromatography (GPC) on a Sephadex G-25 Fine column (50 x 400 mm, Pharmacia, Uppsala, Sweden) using water as the mobile phase to remove small molecular weight materials. The final F-PHEA was isolated from collected fractions, followed by freeze-drying. Samples with a narrow molecular weight distribution (MWD) were prepared by dissolving F-PHEA in pH 7.8 phosphate buffered saline (PBS; 0.05 M phosphate containing 0.15 M NaCl) followed by GPC on Sephacryl S-200 (40 x 700 mm column; Pharmacia) using the same buffer as the mobile phase. Individual fractions from the broad polymer peak were concentrated to ≤ 20 mL and desalted by GPC on Sephadex 25-F (50 x 400 mm column; Pharmacia) in water. A typical yield from 3 g of PSI was about 3.1 g F-PHEA (Sun, 1995). Following freeze-drying, lyophilized polymers were stored in the dark over silica gel prior to use (Niven *et al.*, 1990). Target weight-averaged molecular weights were achieved by the use of controlled reaction temperatures during acid catalyzed thermal polycondensation and final fractional precipitation of PSI from DMF/water solution (Niven *et al.*, 1990; Sun, 1995). For example, for synthesis of weight-averaged 7.4 kDa F-PHEA, the reaction temperature for polycondensation was maintained between 145 and 155 °C in order to obtain PSI with molecular weight ≈ 10^4.

The molecular weight distributions (MWD) of F-PHEA were determined by quantitative, high performance gel permeation chromatography (HPGPC) on a HEMA-Bio 40 high-pressure column (8 x 250 mm, 10 μm particle size; Tessek Ltd., Prague,

Czech Republic) with guard column (3 x 30 mm). All HPGPC measurements were performed in a mobile phase of 0.05 M phosphate buffer (pH 7.4) containing 0.15 M NaCl, supplied at 1.0 mL/min. Typical chromatograms for 4.3 kDa F-PHEA (FR7002-5) determined by UV absorbance at 220 nm in Prague and by fluorescence (excitation and emission wavelengths = 486 and 516 nm, respectively) in Richmond are shown in Fig. AIII.2. Both chromatograms were totally superimposable (ANOVA) with respect to elution profiles, successfully demonstrating that the columns were universally calibrated between the two institutions.

The calibration curve for this HPGPC column system is shown in Fig. AIII.3. In this calibration, the elution curve was monitored by Waters Model 484 UV-VIS absorbance detector at 220 nm with Waters Baseline-810 Datastation. The column was calibrated with three samples of PHEA with known molecular weight distributions (MWD), monodispersed polyethyleneoxide (PEO), hydroxyethyl glutamine (HEG) and water. The calibration was plotted in terms of log ($[\eta]\cdot MW$) *vs.* elution volume ($[\eta]$: viscosity; Fig. AIII.3). Subsequently, the molecular weight was derived from this plot using coefficients of the Mark-Houwink equation ($[\eta] = K\cdot MW^a$; Yau *et al.*, 1979) for PHEA ($K = 2.32 \times 10^{-3}$ mL/g, $a = 0.87$) and PEO ($K = 5.05 \times 10^{-2}$ mL/g, $a = 0.67$).

The molecular weight distributions of the prepared F-PHEA were determined from the calibration curve (assuming that GPC chromatogram height, h_i, was proportional to mass of polymer with MW_i) and the chromatograms of each sample by the curve summation method of Yau *et al.* (1979). The normalized molecular weight distributions of two, differently-sized F-PHEA (FR7150 and FR7002-5), determined by Dr. Rypacek

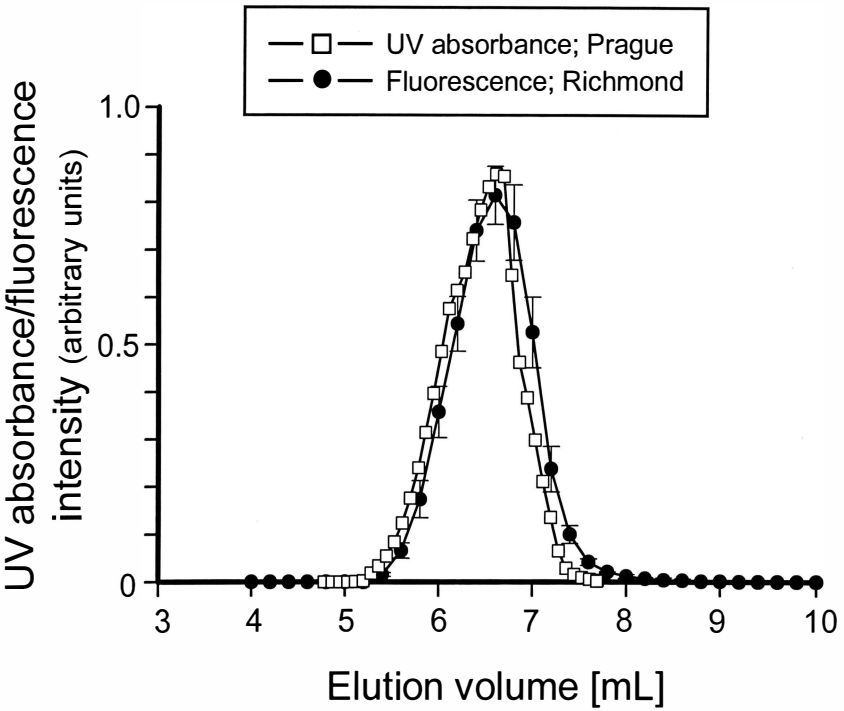

Figure AIII.2. Typical gel permeation chromatograms for 4.3 kDa F-PHEA (FR7002-5) determined by UV absorbance at 220 nm in Prague and fluorescence (excitation and emission wavelengths = 486 and 516 nm, respectively) in Richmond. Data was normalized so that mean values for Y_{max} between UV and fluorescence measurements were equal. High performance GPC (HPGPC) was performed in 0.05 M phosphate buffer (pH 7.4) containing 0.15 M NaCl, supplied at 1.0 mL/min. UV data was supplied by Dr. Rypacek (n=1) and fluorescence data was mean±sample standard deviations (n=5).
Both profiles were statistically superimposable (ANOVA).

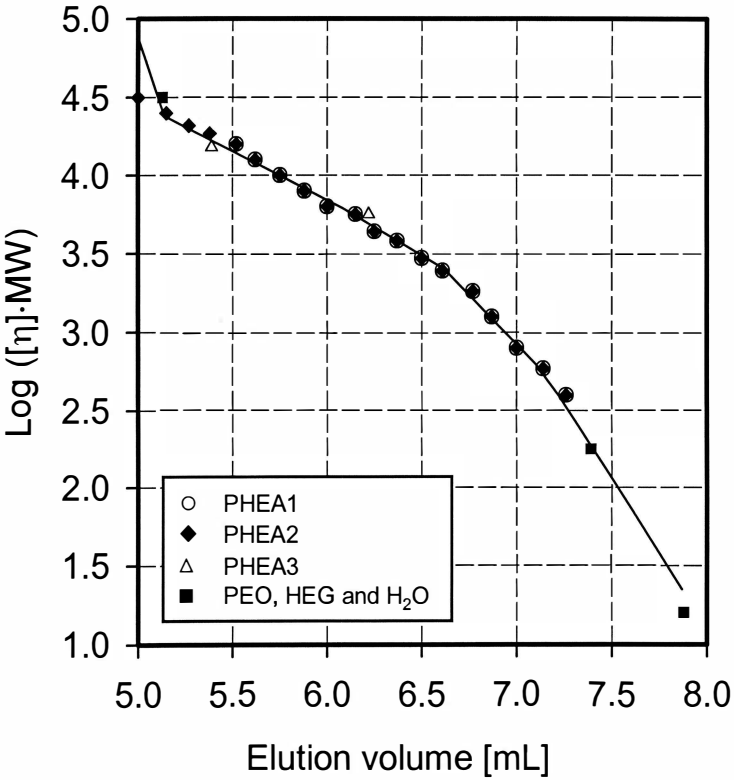

Figure AIII.3. Calibration curve for HEMA-Bio40 gel permeation column. The molecular weight was derived using coefficients of the Mark-Houwink equation (Yau *et al.*, 1979). Three PHEA standards (PHEA1, 2 and 3), monodispersed polyethyleneoxide (PEO), monohydroxyethyl glutamine (HEG) and water were used for constructing the calibration curve. Data was supplied by Dr. Rypacek in Prague.

in Prague are shown in Figs. AIII.4 and AIII.5, respectively. Weight- (M_w) and number- (M_n) averaged molecular weights and polydispersity (P_d) were calculated from the following equations and are shown in Table AIII.1:

$$Mw = (\Sigma(W_i \cdot MW_i)) / \Sigma W_i \qquad \text{(Eqn. AIII.1)}$$

$$Mn = \Sigma W_i / \Sigma (W_i/MW_i) \qquad \text{(Eqn. AIII.2)}$$

$$P_d = M_w / M_n \qquad \text{(Eqn. AIII.3)}$$

where W_i is the fraction of the i th molecular weight fraction by weight, MW_i (Yau *et al.*, 1979). As a result, weight-averaged molecular weights (M_w) of these two, differently-sized F-PHEA (FR7150 and FR7002-5) were found to be 7420 and 4308 Da, respectively, as shown in Table AIII.1. Hence, the polymers were named as 7.4 and 4.3 kDa F-PHEA, respectively throughout this thesis.

The content of fluorophore label in the polymers was determined from the absorption spectrum of their solutions in 0.1 N NaOH using $\varepsilon = 88$ $[mM \cdot cm]^{-1}$ as the absorption coefficient of N-aspartylamidoethyl-carbonyl-6-fluorescein at 492 nm (pH = 9.0; Neri *et al.*, 1973), assuming that its absorptivity was unchanged, when bound to PHEA. The fluorophore labels were randomly uniform across polymers (Rypacek, 1990-1999; personal communications) and found to be 0.3 mole% in both batches of F-PHEA with respect to the monomer subunits.

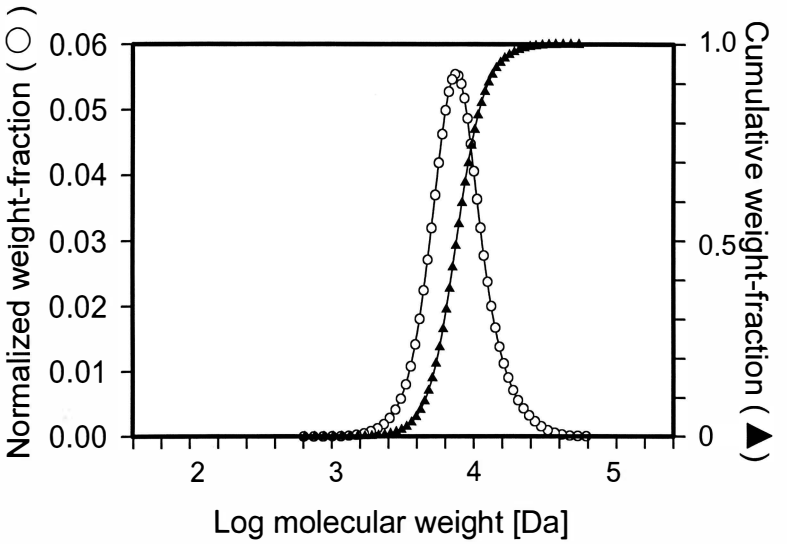

Figure AIII.4. Normalized weight-based molecular weight distribution of 7.4 kDa F-PHEA (FR7150). Weight- (M_w) and number- (M_n) averaged molecular weights were calculated to be 7420 and 6620 Da, respectively. Data was supplied by Dr. Rypacek in Prague.

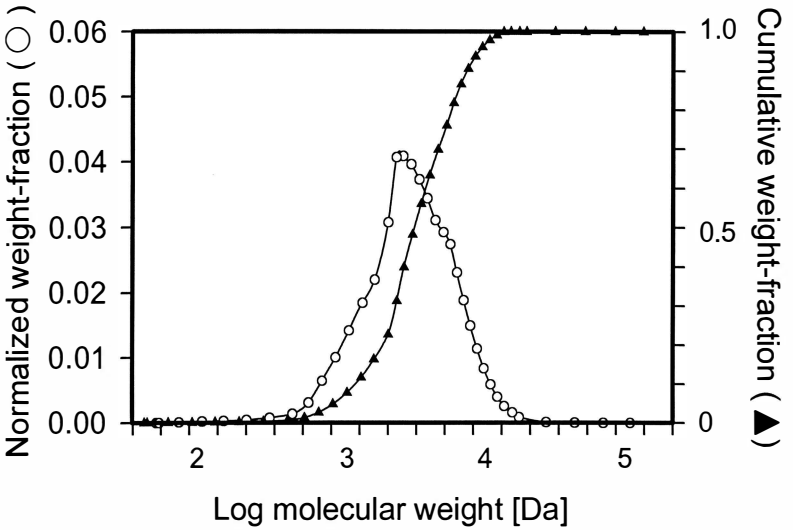

Figure AIII.5. Normalized weight-based molecular weight distribution of 4.3 kDa F-PHEA (FR7002-5). Weight- (M_w) and number- (M_n) averaged molecular weights were calculated to be 4308 and 2245 Da, respectively. Data was supplied by Dr. Rypacek in Prague.

Table AIII.1. Fluorophore content and molecular weight characterization for F-PHEA.

F-PHEA	R[a] [mol%]		M_w[c] [Da]	M_n[c] [Da]	P_d[d]
	F[b]	HE[b]			
FR7150	0.3	99.7	7420	6620	1.12
FR7002-5	0.3	99.7	4308	2245	1.92

[a] A substituent group, R in F-PHEA structure shown below. Mol% is with respect to monomer subunits.

[b] F and HE are fluorophore and hydroxyethyl substituents, respectively.

[c] M_w and M_n are HPGPC-determined weight- and number- averaged molecular weights, respectively, based upon column calibration using PHEA standards.

[d] $P_d = M_w / M_n$; polydispersity.

APPENDIX IV

QUANTITATIVE DETERMINATION OF MODEL SOLUTES IN AQUEOUS, PERFUSATE AND LUNG HOMOGENATE SAMPLES

AIV.a INTRODUCTION

Highly sensitive and quantitative methods were necessary to precisely characterize solute disposition in the airways following administration in small doses. These analytical methods were rigorously validated for each solute through the use of appropriate validation protocols (Linder and Wainer, 1996). In this thesis, weight-averaged 7.4 and 4.3 kDa fluorophore-labeled poly-α,β-[N(2-hydroxyethyl)-D,L-aspartamide] (F-PHEA), fluorescein isothiocyanate (FITC)- labeled dextran 40 (FD-4) and sodium fluorescein were used as model macromolecular and small solutes by virtue of their stable fluorescence labels for sensitive detection. Each of these solutes had the same (constant) fluorophore/chromophore and could thus be detected in a similar fashion. F-PHEA and FD-4 were analyzed by high performance gel permeation chromatography (HPGPC), coupled with fluorescence detection, whereas F-Na was determined by fluorimetry. Each

solute was analyzed in aqueous, perfusate and lung homogenate samples for determination of the dose, absorption and regional lung distribution in both in vitro isolated perfused rat lung (IPRL) and in vivo whole rat studies. A common complication introduced by the use of these matrixes was found to be the low level fluorescence contribution of proteins present in each matrix. There was also a need to prove that under typical assay conditions, analyte loss due to binding to matrix component was not an issue. Therefore, in this appendix, all quantitative analytical methods are described for each solute in each matrix sample after validation according to the recent ICH guidelines (ICH4, 1996). These methods were used to ensure analytical validity throughout the experiments described in this thesis.

AIV.b DEFINITIONS AND CALCULATIONS

(1) Specificity or Selectivity

Specificity or selectivity was defined as the measure of the analytical method's ability to specifically isolate the solutes of interest from other possible matrix constituents, which may interfere with the quantification. During analyses in this thesis, perfusate and lung homogenate were used as matrixes. These interference could be detected from proteins in the matrixes, which caused overlapped elution profiles in HPGPC for F-PHEA and FD-4 (as shown in Fig. AIV.1), and additional fluorescence intensity during fluorimetry for F-Na. However, it appeared that no critical effects, such

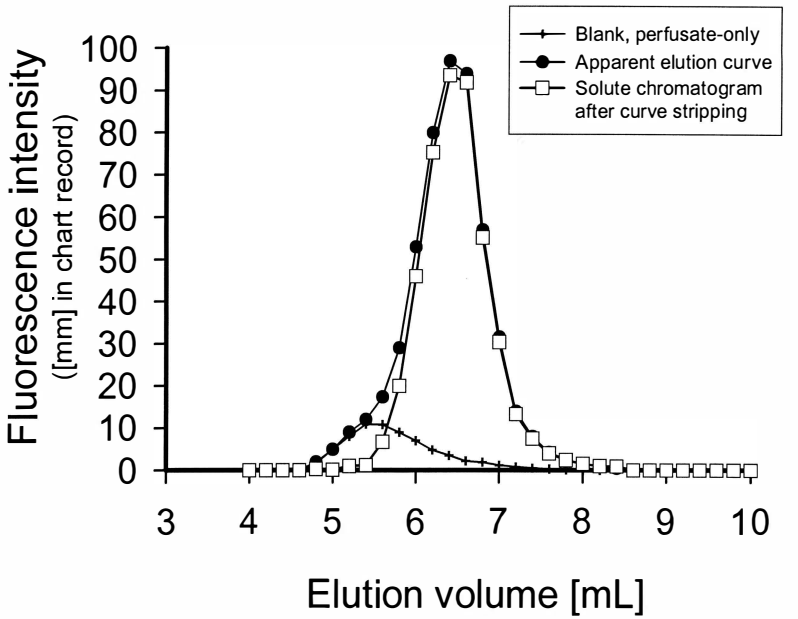

Figure AIV.1. A typical high performance gel permeation chromatogram for 7.4 kDa F-PHEA (FR7150) in IPRL perfusate, blank perfusate and the solute, F-PHEA, which was constructed by curve stripping.

as binding and/or quenching were observed (e.g., homogenate samples contained ≥ 98.0 % of the expected concentrations of fluorophore in all cases) and these were found to be present as simple additional fluorescence in all of those samples. As a result, quantitative determination could be achieved by rigorously stripping interference profiles in HPGPC for F-PHEA and FD-4 and by constructing calibration curves for fluorescence of F-Na following adequate dilution of the matrixes in 0.1 N aqueous NaOH.

(2) Linearity of Calibration

Linearity was evaluated across the range of concentrations to be used for actual analytical determinations. Linearity of calibration curves was assessed using appropriate statistical methods. In this thesis, regression analysis (regression equation and correlation coefficient) was performed from various solute concentrations ($n \geq 6$) and documented alongside each actual calibration curve.

(3) Detection and Quantification Limits: LOD and LOQ

LOD and LOQ are defined as the smallest concentrations of the solutes of interest that can be detected and quantified in the samples, respectively, with a given level of confidence. Currently, ICH is promoting the use of the standard deviation of the response intercept of calibration curves (response *vs.* concentration) using linear least-square-regression for the determination (ICH Q2B, 1996; Paino and Moore, 1999). LOD and LOQ values were calculated from this standard deviation and the slope of calibration

curve and hence, for 95 and 99 % of confidence, these were given by the following equations:

$$LOD = 3.3 \cdot \sigma / S \qquad \text{(Eqn. AIV.1)}$$

$$LOQ = 10 \cdot \sigma / S \qquad \text{(Eqn. AIV.2)}$$

where σ and S are the standard deviation of the response intercept and the slope, respectively, both of which are calculated from the calibration curves. Values for LOD and LOQ were calculated for all of the assays used in this thesis in each of the matrixes.

(4) Precision or Repeatability

Precision or repeatability was defined as relative standard deviation (RSD) from six identical determinations using control samples (samples with known concentration) and calculated from the following equation:

$$RSD = \frac{SD}{Mean} \times 100 \qquad \text{(Eqn. AIV.3)}$$

where Mean and SD, respectively, were sample mean and standard deviation of six determinations for each control sample. In this thesis, three different concentration samples (high, middle and low) covering the extremes and center of the analytical range to be determined were used as control samples for which RSD values were calculated.

(5) Accuracy

Accuracy was similarly defined as % error (%error = DFN; % difference from nominal concentration) for six determinations using control samples with known concentrations. Values for %error were calculated from the following equation:

$$\%error = \frac{C_{mes} - C_{nom}}{C_{nom}} \times 100 \qquad \text{(Eqn. AIV.4)}$$

where C_{nom} and C_{mes}, respectively are known and measured concentrations of control samples. In this thesis, three different concentration samples (high, middle and low) covering the extremes and center of the analytical range to be determined were used as control samples for which %error values were calculated.

AIV.c ANALYTICAL VALIDATION FOR QUANTITATIVE DETERMINATION

AIV.c.1 PREPARATION OF VALIDATION SAMPLES

Perfusate was prepared as described in Appendix AI.b.1, whereas lung homogenates were derived from homogenization of tissue samples in 10 mL phosphate buffered saline (PBS; pH 7.4, 0.05 M phosphate in 0.15 M NaCl) at room temperature

using a BioHomogenizer (10,000 rpm for 2 minutes; Fisher Scientific, Springfield, NJ). Validation samples (for calibration curve and precision/accuracy) were prepared by spiking different, but known amounts of each model solute into either aqueous buffer, perfusate or lung homogenate. Aqueous and perfusate samples were analyzed directly or following appropriate dilution by the methods described below. Those in lung homogenates were determined after filtration of supernatant samples (0.45 μm, nylon, 4mm, Alltech Associates, Deerfield, IL) derived from centrifugation (Marathon 22K; 1,500 g for 15 minutes, Fisher Scientific, Springfield, NJ) of the lung homogenate. All spiking volumes were minimized, compared to matrix volumes (less than 10 % volume additions were used) and theoretical concentrations were mathematically calculated, based on spiking method employed.

AIV.c.2 QUANTIFICATION OF 7.4 AND 4.3 kDa F-PHEA AND FD-4

High performance gel permeation chromatography (HPGPC), coupled with fluorescence detection was used for quantitative determination of 7.4 and 4.3 kDa F-PHEA and FD-4 regardless of the sample matrix. The HPGPC column was a Separon™ HEMA-Bio 40 high-pressure column (8 x 250 mm, 10 μm particle size; Tessek Ltd., Prague, Czech Republic) with a guard column (HEMA-Bio 40; 4.6 x 10 mm, 10 μm particle size; Tessek Ltd., Prague, Czech Republic). The mobile phase was phosphate buffered saline solution (PBS; pH 7.4, 0.05 M phosphate in 0.15 M NaCl solution),

supplied at 1.0 mL/min by a HPLC pump (Model LC-7A Bio Liquid Chromatograph; Shimadzu Corporation, Kyoto, Japan). Samples (100 μL) were introduced onto the column by Rheodyne injection valve (100 μL; Model 7125; Cotati, CA). Fluorescence intensity was detected using 486 and 516 nm excitation (λ_{ex}) and emission (λ_{em}) wavelengths, respectively (Model RF-535 Fluorescence HPLC Monitor; Shimadzu Corporation, Kyoto, Japan). Output was recorded with a calibrated chart recorder (1 cm/min; Fisher Recordall, Series 5000; Fisher Scientific, Springfield, NJ). All chemicals were purchased from Fisher Scientific (Raleigh, NC) and the freshly-prepared mobile phase was vacuum-filtered through a 0.45 μm filter (plain; nylon; 47 mm; Alltech, Deerfield, IL) prior to each analysis.

The HPGPC chromatograms for polydispersed F-PHEA and FD-4 were digitized manually by measuring their heights (h_i) at every 0.2 mL of elution volume (V_e) between 4.0 and 12.0 mL and reconstructed on a spreadsheet, as shown in Table AIV.1. The area under the curves (AUC_i) in each elution volume ($V_{e,i}$) interval due to the solute were calculated by the trapezoidal rule and summed to determine the cumulative AUC values (ΣAUC) as fluorescence-elution peak areas due to solute in the samples. The protein content of the perfusate (4 % BSA) and the filtered supernatant of lung homogenate contained a fluorescent component interfering with the early portion of F-PHEA and FD-4 chromatograms following their direct injection into the HPGPC system, as shown in Fig. AIV.1; the chromatograms were typified by 7.4 kDa F-PHEA. Thus, a rigorous curve stripping procedure was employed for the AUC determination of the chromatograms, as described previously (Table AIV.1 and Fig. AIV.1; Byron *et al.*,

Table AIV.1. Data sheet example of F-PHEA quantification in a perfusate sample by use of a rigorous curve stripping procedure [7.4 kDa F-PHEA nominal dose: 5.0 mg; sampling time: 20 minutes].

V_e [mL]	$h_{i,B1}$ [mm]	$h_{i,B2}$ [mm]	$h_{i,Bmean}$ [mm]	h_i [mm]	h_i' [mm]	AUC_i [mm x mL]	ΣAUC [mm x mL]
4.0	0.0	0.0	0.0	0.0	0.0	0.00	90.35
4.2	0.0	0.0	0.0	0.0	0.0	0.00	90.35
4.4	0.0	0.0	0.0	0.0	0.0	0.00	90.35
4.6	0.0	0.0	0.0	0.0	0.0	0.00	90.35
4.8	1.0	2.2	1.6	1.9	0.3	0.04	90.35
5.0	4.7	5.0	4.9	4.9	0.1	0.05	90.31
5.2	7.9	8.1	8.0	9.0	1.0	0.11	90.26
5.4	10.8	10.9	10.9	12.0	1.2	0.22	90.15
5.6	11.0	10.5	10.8	17.4	6.7	0.78	89.93
5.8	9.2	8.8	9.0	29.0	20.0	2.67	89.15
6.0	7.1	6.9	7.0	53.0	46.0	6.60	86.48
6.2	5.0	4.5	4.8	80.0	75.3	12.13	79.88
6.4	3.9	3.0	3.5	97.0	93.6	16.88	67.75
6.6	2.3	2.0	2.2	94.0	91.9	18.54	50.87
6.8	1.8	1.9	1.9	57.0	55.2	14.70	32.33
7.0	1.4	1.0	1.2	31.6	30.4	8.56	17.63
7.2	1.0	0.5	0.8	14.0	13.3	4.37	9.07
7.4	0.7	0.3	0.5	8.0	7.5	2.08	4.70
7.6	0.5	0.0	0.3	4.2	4.0	1.15	2.62
7.8	0.2	0.0	0.1	2.5	2.4	0.64	1.47
8.0	0.0	0.0	0.0	1.5	1.5	0.39	0.83
8.2	0.0	0.0	0.0	1.0	1.0	0.25	0.44
8.4	0.0	0.0	0.0	0.5	0.9	0.19	0.19
8.6	0.0	0.0	0.0	0.0	0.0	0.00	0.00
8.8	0.0	0.0	0.0	0.0	0.0	0.00	0.00
9.0	0.0	0.0	0.0	0.0	0.0	0.00	0.00
9.2	0.0	0.0	0.0	0.0	0.0	0.00	0.00
9.4	0.0	0.0	0.0	0.0	0.0	0.00	0.00
9.6	0.0	0.0	0.0	0.0	0.0	0.00	0.00
9.8	0.0	0.0	0.0	0.0	0.0	0.00	0.00
10.0	0.0	0.0	0.0	0.0	0.0	0.00	0.00
10.2	0.0	0.0	0.0	0.0	0.0	0.00	0.00
10.4	0.0	0.0	0.0	0.0	0.0	0.00	0.00
10.6	0.0	0.0	0.0	0.0	0.0	0.00	0.00
10.8	0.0	0.0	0.0	0.0	0.0	0.00	0.00
11.0	0.0	0.0	0.0	0.0	0.0	0.00	0.00
11.2	0.0	0.0	0.0	0.0	0.0	0.00	0.00
11.4	0.0	0.0	0.0	0.0	0.0	0.00	0.00
11.6	0.0	0.0	0.0	0.0	0.0	0.00	0.00
11.8	0.0	0.0	0.0	0.0	0.0	0.00	0.00
12.0	0.0	0.0	0.0	0.0	0.0	0.00	0.00

$h_{i,B1}$ and $h_{i,B2}$ are the chromatogram heights of two-sets of blank, solute-free (perfusate-only) samples and $h_{i,Bmean}$ is the average value at each elution volume (this data provided the baseline chromatogram). h_i and h_i' represent the apparent and the corrected heights, respectively, of the F-PHEA elution chromatogram; the latter is calculated from $h_i - h_{i,Bmean}$.

1990; Sun, 1995). This involved two-sets of blank, matrix-only chromatograms and a determination of their average heights ($h_{i,Bmean}$). Values for the matrix were subtracted from the apparent heights (h_i) of solute-containing chromatograms of either perfusate or filtered supernatant samples. Thus, the corrected heights (h_i'), determined after baseline subtraction, enabled a calculation of the total area under the chromatogram due to the solute (ΣAUC), which was related directly to the solute concentration in those samples (Table IV.1).

Analytical validation for 7.4 and 4.3 kDa F-PHEA and FD-4 in each sample (aqueous, perfusate and lung homogenate samples) are summarized in Tables AIV.2, AIV.3 and AIV.4, respectively and their calibration curves are shown in Fig. AIV.2. Corrected (stripped) HPGPC chromatograms obtained from solute-spiked perfusate and filtered supernatant of lung homogenate were found to be insignificantly different from original chromatograms following solute injection in aqueous buffer. This was true with respect to both molecular weight distribution (MWD), as evidenced by elution curve shape and values for resultant ΣAUC, as shown in Fig. AIV. 3 (ANOVA); the chromatograms were typified by 7.4 kDa F-PHEA. This result was clear evidence that protein binding and quenching of these macromolecules due to the presence of the matrix components was negligible at the concentrations being studied (Byron *et al.*, 1990). Consequently, analyses were effectively unchanged across matrixes and remained highly sensitive with unchanged response factors (LOD ≤ 0.1 μg/mL). These fluorescence-HPGPC methods were successfully validated for both F-PHEA and FD-4 with values for

Table AIV.2. A summary of the analytical validation performed for 7.4 kDa F-PHEA (FR7150) determinations in aqueous, perfusate and lung homogenate samples

	Aqueous buffer[1]			**IPRL perfusate**[2]			**Lung homogenate**[3]		
Calibration range[4] [μg/mL]	0.09-2.5			0.33-2.5			0.15-2.5		
Regression[5]	Y = 90.42 X + 1.13			Y = 93.46 X + 2.15			Y = 90.49 X + 2.31		
R[6]	0.9997			0.9967			0.9997		
LOD[7] [μg/mL]	0.03			0.11			0.05		
LOQ[8] [μg/mL]	0.09			0.33			0.15		
Nominal conc. [μg/mL]	0.1	1.0	2.0	0.4	1.3	1.8	0.2	0.9	2.1
Precision[9] [%] (RSD)	9.3	2.3	2.5	4.2	4.4	2.4	8.7	3.9	1.5
Accuracy[10] [%] (%error)	1.6	2.9	1.3	7.7	1.5	0.8	8.2	2.2	0.2

[1] Phosphate buffered saline (PBS; pH 7.4, 0.05 M phosphate in 0.15 M NaCl); [2] Krebs-Henseleit buffer solution containing 4 % (w/v) bovine serum albumin; [3] lung tissue homogenized in 10 mL PBS; [4] concentration range in which linearity was proven; [5] regression equation between total area under the curve (ΣAUC) of the corrected (stripped) chromatogram (Y: [mm·mL]) and F-PHEA concentration (X: [μg/mL]) from $n \geq 6$; [6] correlation coefficient of the regression equation; [7] detection limit determined by Eqn. AIV.1; [8] quantification limit determined by Eqn. AIV.2; [9] RSD determined by Eqn. AIV.3 (n=6) and [10] % error (difference from nominal) determined by Eqn. AIV.4 (n=6).

Table AIV.3. A summary of the analytical validation performed for 4.3 kDa F-PHEA (FR7002-5) determinations in aqueous, perfusate and lung homogenate samples

	Aqueous buffer[1]			IPRL perfusate[2]			Lung homogenate[3]		
Calibration range[4] [μg/mL]	0.02-1.0			0.06-1.0			0.06-1.0		
Regression[5]	Y = 180.27 X + 0.51			Y = 182.72 X + 0.70			Y = 179.94 X + 1.40		
R[6]	0.9999			0.9994			0.9990		
LOD[7] [μg/mL]	0.006			0.019			0.019		
LOQ[8] [μg/mL]	0.024			0.062			0.063		
Nominal conc. [μg/mL]	0.1	0.4	0.8	0.1	0.4	0.8	0.1	0.4	0.8
Precision[9] [%] (RSD)	8.5	2.1	1.2	7.9	1.4	1.2	5.4	1.1	1.5
Accuracy[10] [%] (%error)	3.5	2.1	1.5	6.2	3.5	1.5	3.9	2.2	1.3

[1] Phosphate buffered saline (PBS; pH 7.4, 0.05 M phosphate in 0.15 M NaCl); [2] Krebs-Henseleit buffer solution containing 4 % (w/v) bovine serum albumin; [3] lung tissue homogenized in 10 mL PBS; [4] concentration range in which linearity was proven; [5] regression equation between total area under the curve (ΣAUC) of the corrected (stripped) chromatogram (Y: [mm·mL]) and F-PHEA concentration (X: [μg/mL]) from $n \geq 6$; [6] correlation coefficient of the regression equation; [7] detection limit determined by Eqn. AIV.1; [8] quantification limit determinedby Eqn. AIV.2; [9] RSD determined by Eqn. AIV.3 (n=6) and [10] % error (difference from nominal) determined by Eqn. AIV.4 (n=6).

Table AIV.4. A summary of the analytical validation performed for 4.4 kDa FITC-dextran 40 (FD-4) determinations in aqueous, perfusate and lung homogenate samples

	Aqueous buffer[1]			IPRL perfusate[2]			Lung homogenate[3]		
Calibration range[4] [μg/mL]	0.08-1.8			0.04-1.7			0.07-1.6		
Regression[5]	Y = 161.43 X - 1.21			Y = 162.53 X + 1.49			Y = 161.06 X + 2.46		
R[6]	0.9996			0.9998			0.9997		
LOD[7] [μg/mL]	0.027			0.014			0.022		
LOQ[8] [μg/mL]	0.080			0.041			0.066		
Nominal conc. [μg/mL]	0.1	0.6	1.1	0.3	0.7	1.3	0.3	0.7	1.4
Precision[9] [%] (RSD)	10.7	1.5	1.1	5.3	4.1	6.1	9.4	3.9	2.9
Accuracy[10] [%] (%error)	8.8	0.8	1.0	4.9	2.1	0.4	5.2	1.8	1.5

[1] Phosphate buffered saline (PBS; pH 7.4, 0.05 M phosphate in 0.15 M NaCl); [2] Krebs-Henseleit buffer solution containing 4 % (w/v) bovine serum albumin; [3] lung tissue homogenized in 10 mL PBS; [4] concentration range in which linearity was proven; [5] regression equation between total area under the curve (ΣAUC) of the corrected (stripped) chromatogram (Y: [mm·mL]) and FD-4 concentration (X: [μg/mL]) from $n \geq 6$; [6] correlation coefficient of the regression equation; [7] detection limit determined by Eqn. AIV.1; [8] quantification limit determined by Eqn. AIV.2; [9] RSD determined by Eqn. AIV.3 (n=6) and [10] % error (difference from nominal) determined by Eqn. AIV.4 (n=6).

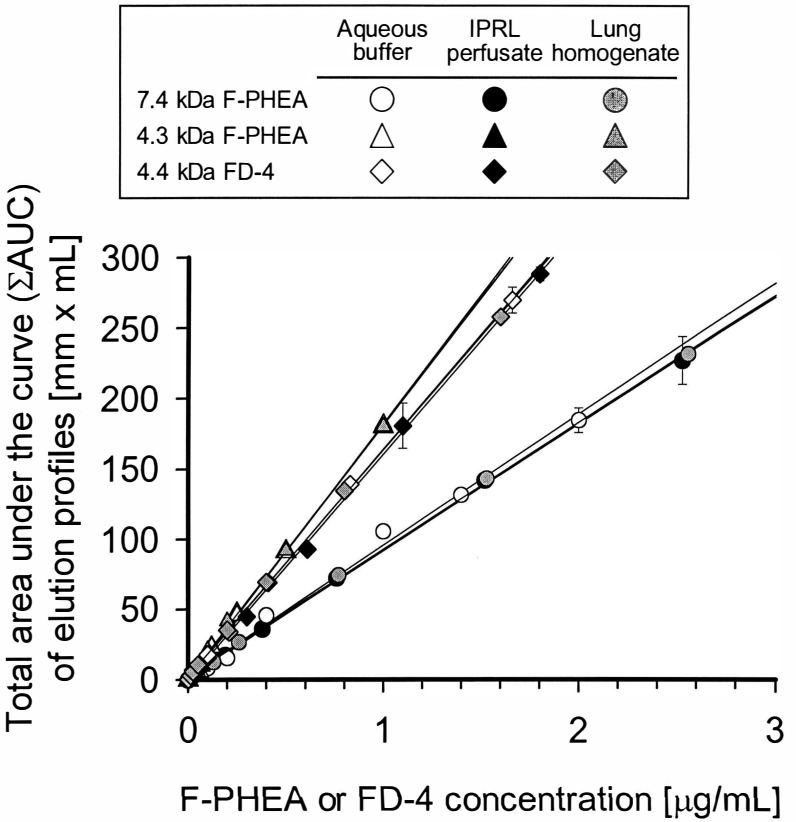

Figure AIV.2. Calibration curves for 7.4 and 4.3 Da F-PHEA and FD-4 in aqueous, perfusate and lung homogenate samples. These were detected by fluorescence (excitation and emission wavelengths = 486 and 516 nm, respectively) following HPGPC. HPGPC was performed in 0.05 M phosphate buffer (pH 7.4) containing 0.15 M NaCl, supplied at 1.0 mL/min. Most error bars for sample standard deviations (n=4) are smaller than symbol sizes. Solid lines are the results of linear regression of each data set.

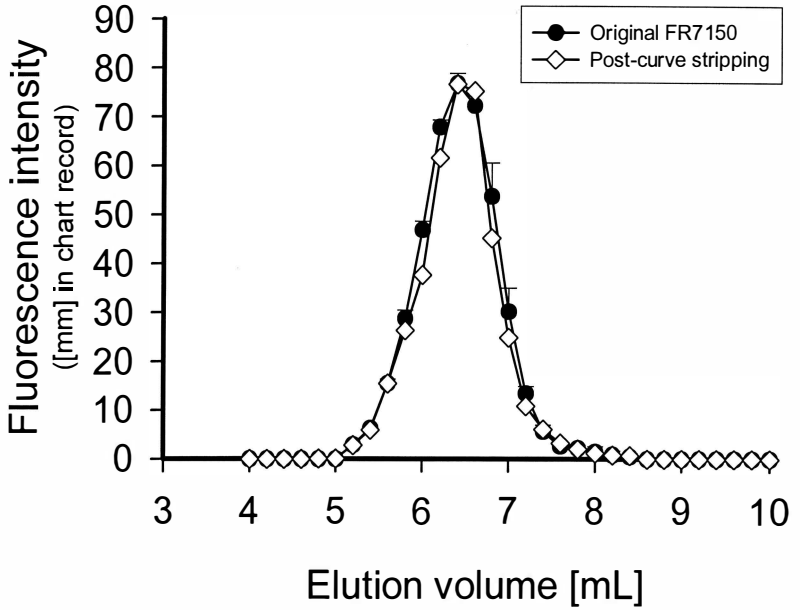

Figure AIV.3. A high performance gel permeation chromatogram for 7.4 kDa F-PHEA (FR7150) constructed from elution profiles of F-PHEA/perfusate samples by curve stripping (as shown in Fig. AIV.1), compared to the original polymer's chromatogram after solution preparation in buffer. The original chromatogram is shown as mean ± sample standard deviation (n=5).
The profiles differed insignificantly (ANOVA).

precision (RSD ≤ 10.7 %) and accuracy (%error ≤ 8.8 %), which enabled their use in Chapters 3-5 of this thesis.

AIV.c.3 QUANTIFICATION OF SODIUM FLUORESCEIN (F-Na)

F-Na was analyzed by fluorimetry using a luminescence spectrometer (Model LS 50; slit = 10 nm, integration = 1.0 second; Perkin Elmer Ltd., Norwalk, CT) at 490 and 520 nm of excitation (λ_{ex}) and emission (λ_{em}) wavelengths, respectively. All concentrations for F-Na in this thesis were corrected for water content and are expressed in terms of the mass of the anhydrous material (Byron *et al.*, 1986). At these wavelengths, it was found that substantial fluorescence intensity could originate both from the perfusate and the filtered supernatant of lung homogenate. However, these were found to be simple background fluorescence in all cases without showing evidence of analyte binding, quenching or metabolism. Thus, it was possible to minimize the effect by a ≥ 10-fold sample dilution in 0.1 N NaOH. In most cases, 0.3 mL of perfusate or filtered supernatant of lung homogenate was diluted with 3.0 mL of 0.1 N NaOH (11-fold dilution). Fluorescence intensity was measured in a quartz cell (3mL, 1 cm, Fisher Scientific, Pittsburgh, PA).

Analytical validation across matrixes for F-Na in aqueous, perfusate and lung homogenate samples is summarized in Table AIV.5 and calibration curves from three

Table AIV.5. A summary of the analytical validation performed for sodium fluorescein (F-Na) determinations in aqueous, perfusate and lung homogenate samples

	Aqueous buffer[1]			IPRL perfusate[2]			Lung homogenate[3]		
Calibration range[4] [ng/mL]	1.6-50.0			1.7-50.0			1.5-50.0		
Regression[5]	Y = 16.51 X + 1.85			Y = 16.68 X + 6.57			Y = 16.56 X + 16.63		
R[6]	0.9995			0.9995			0.9998		
LOD[7] [ng/mL]	0.53			0.55			0.48		
LOQ[8] [ng/mL]	1.62			1.65			1.46		
Nominal conc. [ng/mL]	0.9	5.5	28.0	1.0	5.0	20.0	0.6	5.9	22.7
Precision[9] [%] (RSD)	1.4	0.1	0.2	0.8	0.2	0.1	3.0	1.0	0.1
Accuracy[10] [%] (%error)	0.2	1.5	2.0	9.1	1.0	0.2	2.2	0.1	0.8

[1] Phosphate buffered saline (PBS; pH 7.4, 0.05 M phosphate in 0.15 M NaCl); [2] Krebs-Henseleit buffer solution containing 4 % (w/v) bovine serum albumin; [3] lung tissue homogenized in 10 mL PBS; [4] concentration range in which linearity was proven; [5] regression equation between fluorescence intensity (Y: [-]) and F-Na concentration (X: [ng/mL]) from $n \geq 6$; [6] correlation coefficient of the regression equation; [7] detection limit determined by Eqn. AIV.1; [8] quantification limit determined by Eqn. AIV.2; [9] RSD determined by Eqn. AIV.3 (n=6) and [10] % error (difference from nominal) determined by Eqn. AIV.4 (n=6).

matrix samples are shown in Fig. AIV.4. Negligible fluorescence intensities (4.6±0.2 and 13.3±0.1 from the perfusate and the filtered supernatant of lung homogenate samples, respectively; mean±SD, n=4) were present as background fluorescence following 11-fold dilution and hence, the LOD for the worst scenario was found to be 0.55 ng/mL. The analyses were not different across sample matrixes (Table AIV.5). Consequently, this highly sensitive fluorimetric method was successfully validated for F-Na with precision (RSD ≤ 3.0 %) and accuracy (%error ≤ 9.1 %), sufficient for use in this thesis.

AIV.c.4 SAMPLE ANALYSIS FROM THE IPRL AND IN VIVO

All samples were analyzed by adhering to the validated methods and the sample preparation described above. In no cases were results quoted for solute concentrations where assayed concentration was less than LOQ. More than two spiked standard samples were analyzed along with a blank, matrix-only sample for each analytical series collected. These were used to construct calibration curves for the analytical series in question. The consistency of the ΣAUC values or the values for fluorescence intensity of the standards were checked in each analysis alongside the calibration curves and standards were found to be reproducible throughout the experiments performed in this thesis (responses differed by < 5 % from expected values in all cases).

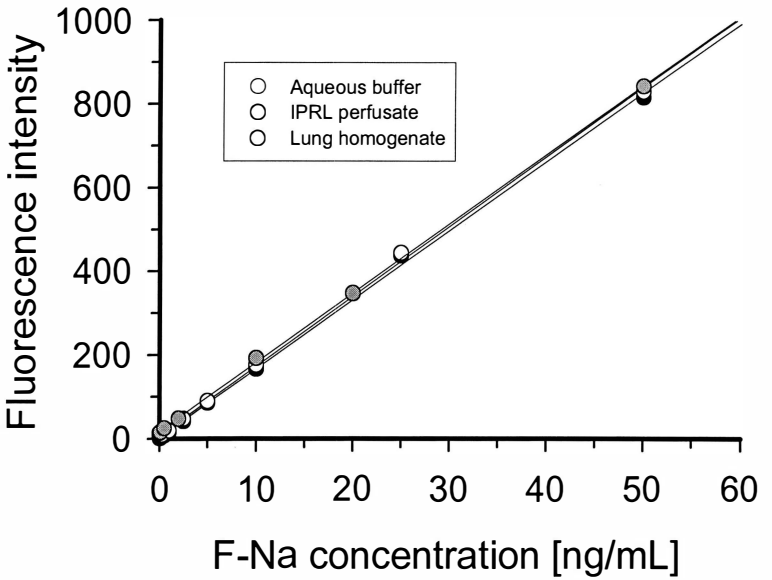

Figure AIV.4. Calibration curves for F-Na in aqueous, perfusate and lung homogenate samples. The latter two samples were diluted ≥ 11-fold with 0.1 N NaOH. These were detected by fluorimetry (excitation and emission wavelengths = 490 and 520 nm, respectively). All error bars for sample standard deviations (n=4) are smaller than symbol sizes. Solid lines are the results of linear regression of each data set.

APPENDIX V

METABOLISM AND TISSUE BINDING OF MODEL SOLUTES IN THE RAT LUNG

AV.a INTRODUCTION

Although the use of the isolated perfused rat lung (IPRL) preparation precludes "systemic" clearance, solute disposition in the lung may still be complicated by "local" clearance, such as lung metabolism and tissue/protein binding (Byron, 1986; Byron and Phillips, 1990). These effects were precluded in the case of the model solutes, fluorophore-labeled poly-α,β-[N(2-hydroxyethyl)-D,L-aspartamide] (F-PHEA), FITC-dextran 40 (FD-4) and sodium fluorescein (F-Na). These were first selected to reduce the likelihood of their showing metabolism and binding by the rat lung, based both on previous studies (Neri, *et al.*, 1973; Niven, 1988; Sun, 1995) and literature reports (Takada *et al.*, 1978; Ohtani *et al.*, 1991; Matsukawa *et al.*, 1997). Indeed, the metabolism in and binding to the IPRL system was shown to be negligible, as described in this appendix.

AV.b SOLUTE METABOLISM BY THE RAT LUNG: IN VITRO STUDIES USING LUNG HOMOGENATE

Blood-free lungs were obtained, according to the operating procedure of the IPRL (Appendix I). The lung was homogenized in 60 mL phosphate buffered saline (PBS; 0.05 M phosphate and 0.15 M NaCl; pH 7.4) using a BioHomogenizer (10,000 rpm for 2 minutes; Fisher Scientific, Springfield, NJ) at room temperature. The homogenate suspension (50 mL) was placed in a 200 mL water-jacketed glass beaker (Research Glass, Richmond, VA), maintained at 37 ^{o}C and stirred on a stirring plate (Model PC-353; Corning, Corning, NY) with a teflon fluorocarbon resin-coated magnetic stir bar (l = 3.5 cm; Fisher Scientific, Raleigh, NC) throughout experiments. After ≥ 5 minutes, a PBS solution (25 μL) containing either 7.4 or 4.3 kDa F-PHEA (0.02 mg) or FD-4 (0.02 mg) or F-Na (0.005 mg) was added to the suspension and incubation commenced at 37 ^{o}C (time = 0 [minute]). At different time intervals over a 120-180 minutes incubation period, samples (0.5 mL) were withdrawn from the homogenate suspension and centrifuged at room temperature for 15 minutes (1725 rpm; Savent® Speed Vac, SC110, Forma Scientific, Inc., Marietta, OH). Subsequently, the supernatant was filtered through an 0.45 μm syringe filter (4 mm, cellulose acetate, Alltech Associates, Deerfield, IL) and analyzed by the validated methods described in Appendix IV.

Average solute concentrations (± SD; n = 4) in the incubation homogenate for 7.4 and 4.3 kDa F-PHEA, FD-4 and F-Na *vs.* time are shown in Fig. AV.1. Each measured

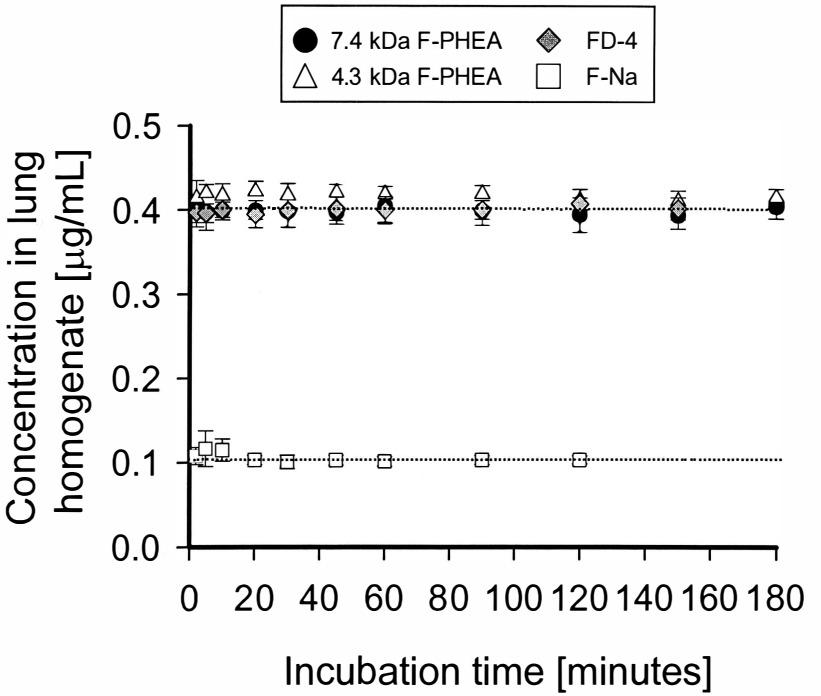

Figure AV.1. Average concentrations (± SD; n=4) of 7.4 and 4.3 kDa F-PHEA, FD-4 and F-Na in lung homogenate *vs.* time. Each solute was incubated in the lung homogenate at 37 °C. Dashed lines were theoretical concentrations; 0.4 µg/mL for F-PHEA and FD-4 and 0.1 µg/mL for F-Na.

solute concentration was incubation time-independent and consistent with the theoretical value ± 3 % (0.4 μg/mL for F-PHEA and FD-4; 0.1 μg/mL for F-Na) throughout the 120-180 minutes incubation at 37 °C. The molecular weight distributions (MWD) for 7.4 and 4.3 kDa F-PHEA and FD-4 at the end of incubation (180 and 150 minutes for F-PHEA and FD-4, respectively) are shown in Fig. AV.2, compared to each of original MWD. These were unchanged following incubation, demonstrating the absence of significant metabolic cleavage of the polypeptides due to incubation.

F-PHEA molecules appeared to have a high resistance to enzymatic proteolysis due to the random distribution of α- and β- peptidic linkages and synthesis with a racemic mixture of D- and L- configured aspartic acid residues (Drobnik *et al.*, 1979a and 1979b; Rypacek *et al.*, 1980; Byron *et al.*, 1991). The fluorescence labels attached as shown in Fig. AIII.1 (Appendix III) were also shown to be chemically stable (Rypacek *et al.*, 1979; Rypacek *et al.*, 1980) and in fact, there was no evidence of detachment during incubation. These arguments were well-supported by Figs. AV.1 and AV.2 (a) and (b), which showed unchanged concentrations and MWDs during incubation. Similarly, FD-4 was shown to be stable with respect to both glucose unit structures and its fluorescent label (Riggs *et al.*, 1958; Arfors and Hint, 1971; Ringsdorf, 1975), as shown in Figs AV.1 and AV.2 (c). F-Na has been extensively studied both in vivo and in vitro in the IPRL and no chemical or metabolic degradation has been reported for this solute in the literature (Byron and Clark, 1985a; Byron *et al.*, 1986; Niven and Byron, 1988; Niven and Byron, 1990) or in this study (Fig. AV.1).

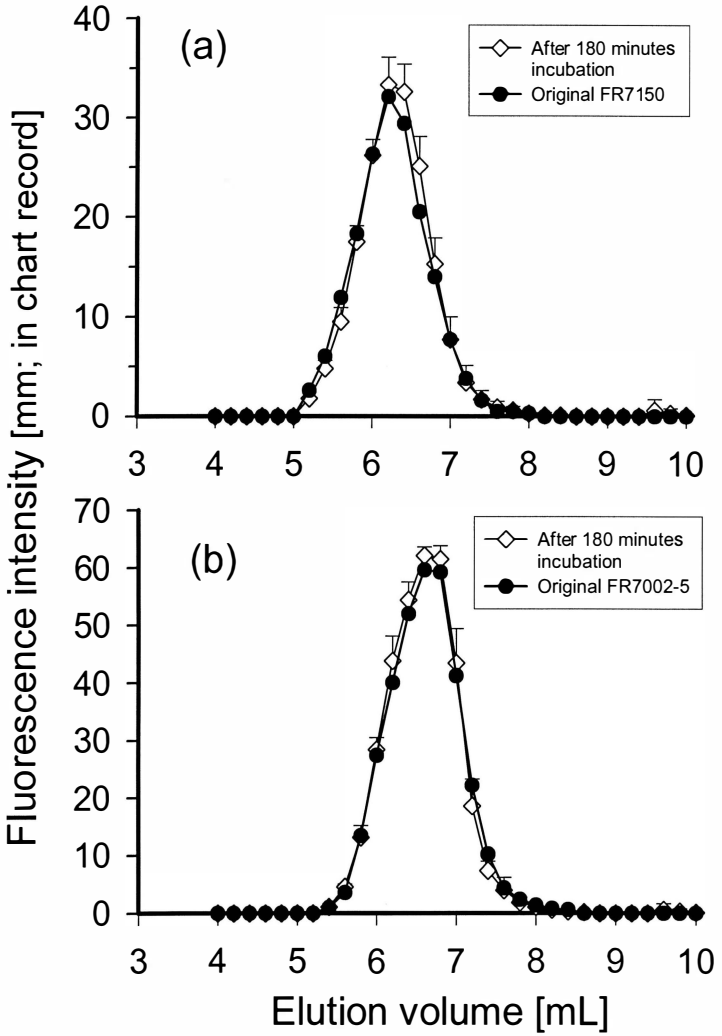

Figure AV.2. High performance gel permeation chromatograms for (a) 7.4 and (b) 4.3 kDa F-PHEA after 180 minutes incubation with lung homogenate at 37 °C, compared to each original chromatogram. The profiles were obtained following curve stripping, as described in Appendix IV. Data was mean±sample standard deviations (n=4).

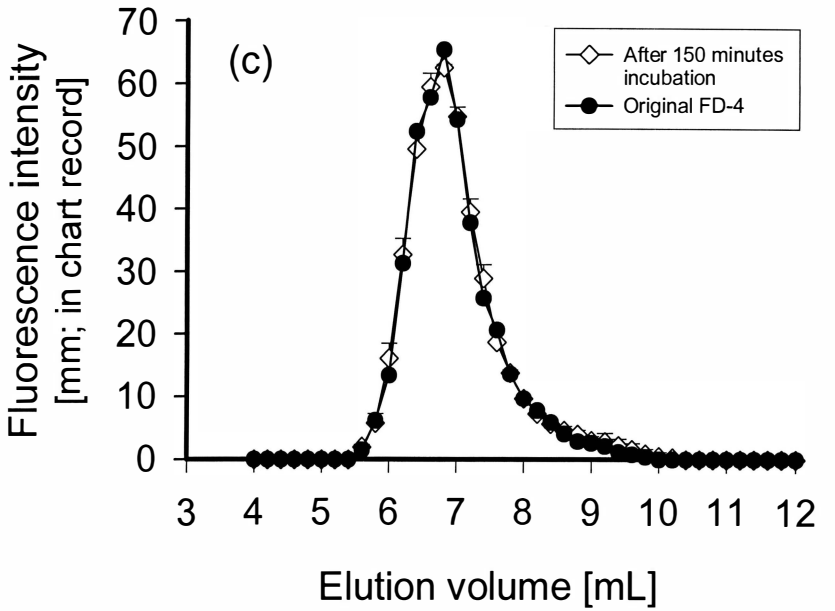

Figure AV.2. High performance gel permeation chromatogram for (c) FD-4 after 150 minutes incubation with lung homogenate at 37 °C, compared to the original chromatogram. The profiles were obtained following curve stripping, as described in Appendix IV. Data was mean±sample standard deviations (n=4).

The lung homogenate prepared with the BioHomogenizer (10,000 rpm for 2 minutes) contains proteolytic enzymes from both extracellular and cytosolic fractions alongside subcellular pellets (Liu *et al.*, 1992; Shen *et al.*, 1999). In fact, even in the absence of co-factors, it was demonstrated that a tri-peptide, thyrotropin-releasing hormone (TRH) was metabolized in these lung homogenate at 37 ^{o}C extensively and quite rapidly (≥ 80 % was metabolized within 20 minutes; Visich, 1996). Therefore, in this incubation study, model solutes were subjected to all possible lung enzymes and in such an "extreme" condition, no significant metabolism was observed for these solutes over the IPRL study period employed in this thesis.

AV.c TISSUE BINDING BY THE RAT LUNG: SOLUTE UPTAKE FROM THE PERFUSATE INTO LUNG TISSUE

The IPRL was prepared according to the operating procedure described in Appendix I and used unchanged except that solutes were administered into perfusate rather than the airways in concentrations representative of those seen in the remainder of the thesis. After perfusion commenced in the IPRL (Appendix AI.b.4), 50 μL of phosphate buffered saline solution (PBS; 0.05 M phosphate and 0.15 M NaCl; pH 7.4) containing either 7.4 or 4.3 kDa F-PHEA (0.05 mg) or FD-4 (0.05 mg) or F-Na (0.005 mg) was added to the perfusate reservoir (122.2 mL including flow line volumes; time = 0 [minute]). At different time intervals, the perfusate samples (0.5 mL) were taken from

the reservoir and analyzed by the methods described in Appendix IV. All studies were performed at 37 ^{o}C.

Solute amounts added into the perfusate were a half of each of the minimum doses for each solute studied in the IPRL and thus, the pefusate concentrations. Average solute concentrations (± SD; n = 4) in the perfusate for 7.4 and 4.3 kDa F-PHEA, FD-4 and F-Na *vs.* time are shown in Fig. AV.3. Each measured solute concentration was found to be time-independent and consistent with theory, assuming no uptake into lung tissue (0.41 μg/mL for F-PHEA and FD-4; 0.04 μg/mL for F-Na). The molecular weight distributions (MWD) of the perfusate samples for 7.4 and 4.3 kDa F-PHEA and FD-4 at the end of perfusion (180 and 150 minutes for F-PHEA and FD-4, respectively) were compared to each of the original MWDs, as shown in Fig. AV.4. There was no detectable difference in the MWD during perfusion (similar to the situation seen with lung homogenates earlier). It is unlikely therefore, that the model solutes used in this thesis underwent any significant tissue or protein binding-induced accumulation in the IPRL or in vivo.

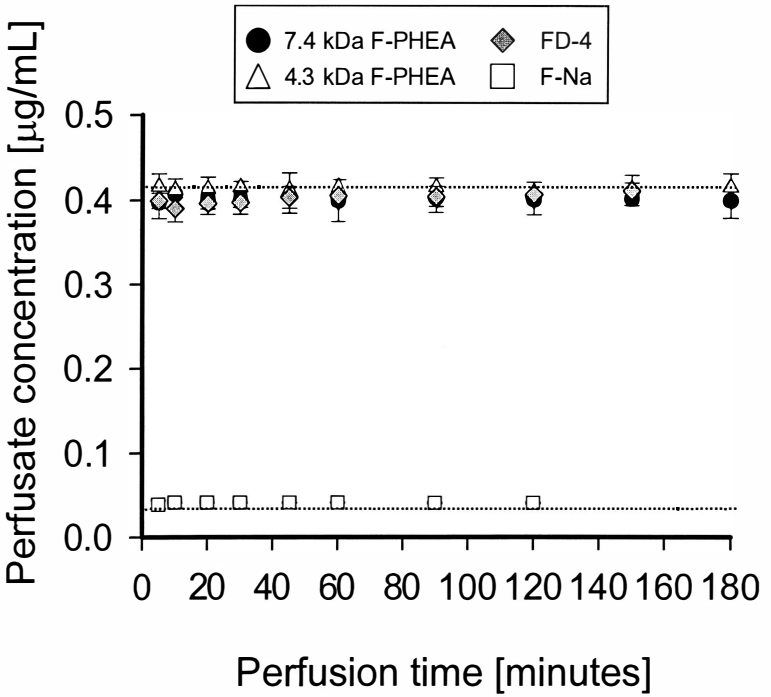

Figure AV.3. Average concentrations (± SD; n=4) of 7.4 and 4.3 kDa F-PHEA, FD-4 and F-Na in the perfusate in the IPRL *vs.* time. Each solute was added into the perfusate at 37 °C. Dashed lines were theoretical concentrations; 0.41 µg/mL for F-PHEA and FD-4 and 0.04 µg/mL for F-Na.

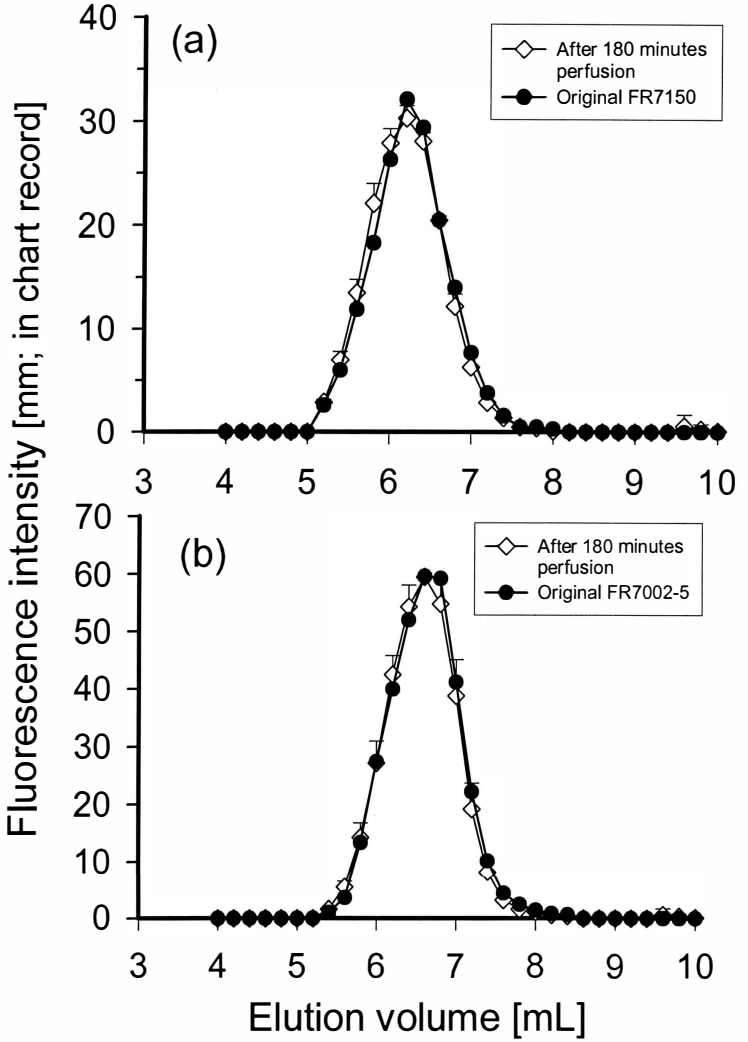

Figure AV.4. High performance gel permeation chromatograms for (a) 7.4 and (b) 4.3 kDa F-PHEA after 180 minutes perfusion in the IPRL at 37 °C, compared to each original chromatogram. The profiles were obtained following curve stripping, as described in Appendix IV. Data was mean±sample standard deviations (n=4).

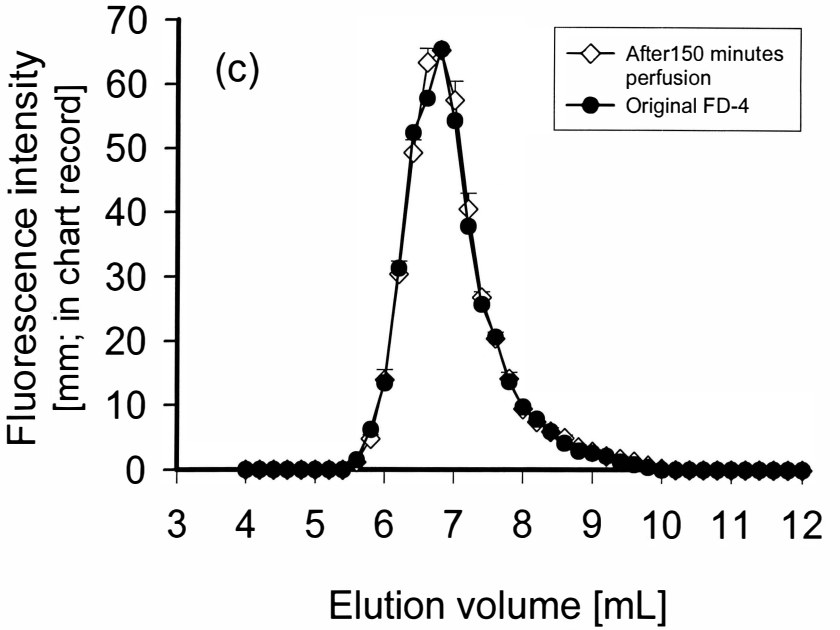

Figure AV.4. High performance gel permeation chromatogram for (c) FD-4 after 150 minutes perfusion in the IPRL at 37 °C, compared to the original chromatogram. The profiles were obtained following curve stripping, as described in Appendix IV. Data was mean±sample standard deviations (n=4).

APPENDIX VI

ACROSS-DOSE CURVE FITTING BY "SCIENTIST"

AVI.a INTRODUCTION

In this thesis, a nonlinear least-mean-square regression routine was employed to permit across-dose curve fitting of solute absorption *vs*. time data to a new kinetic model shown in Fig. AVI.1, in vitro (isolated perfused rat lung: IPRL) and in vivo, using a program, "Scientist" for Windows® (MicroMath Scientific Software, Salt Lake City, UT). The program required three types of electronic files for curve fitting. These were a Model File, a Data File and a Parameter File. The Model File defined independent- (time and/or dose) and dependent- (% transfer to perfusate (in vitro IPRL) or % remaining in lung (in vivo)) variables, the model's parameters (F, $k_{a,P}$, $k_{E,PT}$, $V_{max,P}$, $K_{m,P}$ and/or $k_{a,TB}$) and their mathematical interrelationships (differential equations and initial conditions). The Data File contained experimentally-observed values for all the independent- and dependent-variables defined in the Model File and these were obtained directly following either IPRL or in vivo studies. The Parameter File was comprised of a set of the model's parameters, defined in the Model File; these depended on the solute under investigation

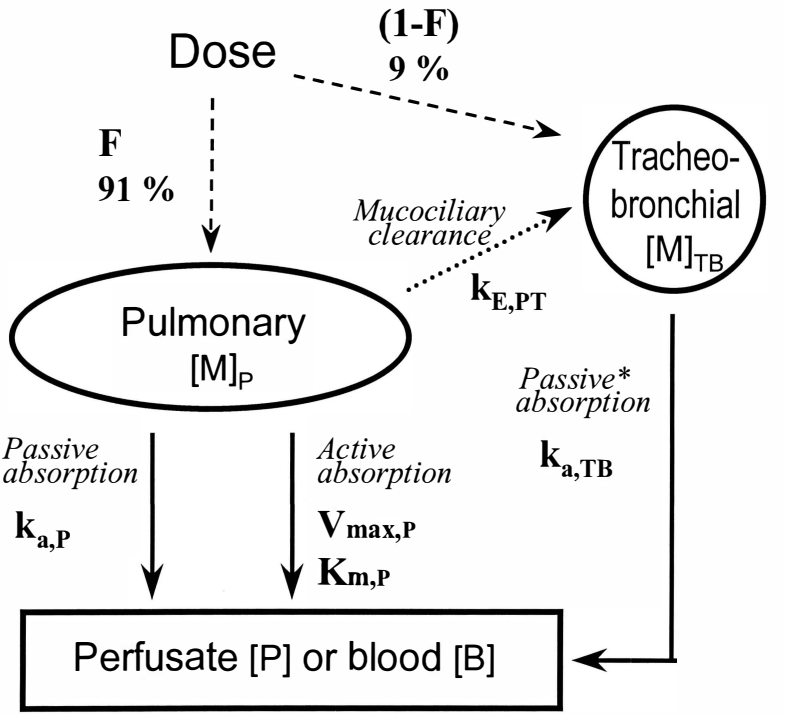

Figure AVI.1. A new kinetic model for solutes administered into the airways of the rat lung.

* Passive absorption from the tracheo-bronchial region is not present in the IPRL due to the severance of the bronchial circulation during surgery ($k_{a,TB} = 0$ in the IPRL).

Key: F - initial average penetration fraction following administration (0.91); $V_{max,P}$ and $K_{m,P}$ - the maximum rate and "affinity" of Michaelis-Menten-type active absorption, respectively; $k_{a,P}$ and $k_{a,TB}$ - first-order rate constants for passive absorption from the pulmonary and the tracheo-bronchial regions, respectively; $k_{E,PT}$ - first-order rate constant for mucociliary clearance.

and initially, initial estimates were assigned for each set of experimental data, as described in detail below. All three electronic files were necessary and subsequently, nonlinear regression was performed to obtain the best parameter estimates for the model, which provided a minimum sum of squared residuals (between experiment and theory) according to the program's minimization algorithms. The program, "Scientist" implemented Simplex and modified Gauss-Newton algorithms for this purpose. In this thesis, the Simplex technique was initially used to locate the region of the minimums and hence, to provide improved parameter estimates, compared to the initial estimates assigned by the operator. Subsequently, the best parameter estimates providing the minimum sum of squared residuals were obtained by the modified Gauss-Newton technique and the results were saved in the Parameter File. The best estimates and their "goodness-of-fit" were statistically assessed by several statistical parameters provided by the program's Statistical Output File. The "goodness-of-fit" was also visually inspected by generating the plots using the best estimates, as provided by the program's Plot File.

In this appendix, the procedure of across-dose curve fitting for 7.4 kDa F-PHEA and F-Na disposition in the IPRL at 37 ^{o}C are described, followed by that for F-Na disposition in vivo, as examples of in vivo curve fitting. The IPRL curve fittings for 4.3 kDa F-PHEA and FD-4 and those at 25 ^{o}C were performed similarly to either 7.4 kDa F-PHEA or F-Na and thus, are not documented here.

AVI.b EXAMPLES OF CURVE FITTING

(1) Across-dose curve fitting for 7.4 kDa F-PHEA disposition in the IPRL at 37 °C

The Model File, Parameter File (with initial estimates) and Data File are shown in Fig. AVI.2. The Model File defined time (T) and dose (DOSE) as independent-variables and % transfer to perfusate (FP) as a dependent-variable, followed by the model's parameters, the differential equations and the initial conditions. Based on the model shown in Fig. AVI.1, the differential equations were derived and are shown as follows:

$$(d[P]/dt)_{Active+Passive,IPRL} = V_{max,P}\cdot[M]_P/(K_{m,P} + [M]_P) + k_{a,P}\cdot[M]_P \qquad \text{(Eqn. AVI.1)}$$

$$(d[M]_P/dt)_{IPRL} = -(d[P]/dt) - k_{E,PT}\cdot[M]_P \qquad \text{(Eqn. AVI.2)}$$

$$(d[M]_{TB}/dt)_{IPRL} = k_{E,PT}\cdot[M]_P \qquad \text{(Eqn. AVI.3)}$$

where [P] is the cumulative solute amount absorbed from the pulmonary region into the recirculating perfusate of the IPRL, $[M]_P$ and $[M]_{TB}$ are the solute amounts remaining unabsorbed in the pulmonary and the tracheo-bronchial regions, respectively; $V_{max,P}$ is the maximum rate of active absorption, $K_{m,P}$ is the "affinity" or dose at which the active absorption rate = $0.5\cdot V_{max,P}$, $k_{a,P}$ is the first-order passive absorption rate constant from the pulmonary region and $k_{E,PT}$ is the first-order mucociliary clearance rate constant from the pulmonary to the tracheo-bronchial region. In the Model File (Fig. AVI.2), symbols, P, A and U represent [P], $[M]_P$ and $[M]_{TB}$, respectively and the parameters, F, KA, KE, VMAX and KM, respectively, were assigned to F, $k_{a,P}$, $k_{E,PT}$, $V_{max,P}$ and $K_{m,P}$, in the

(a)

```
//
// July 10, 1998
// Masahiro Sakagami, MCV/VCU
//
// F-PHEA Transfer Model in the IPRL study
// Final Version
//
// Passive & Active Transport involved
// Mucociliary Transport involved
//
// A : Alveoli
// U : Upper Airway
// P : Perfusate
//
IndVars: T, DOSE
DepVars: FP
Params: F, KA, KE, VMAX, KM
//
FP=P/DOSE*100
A'=-(KA+KE)*A-VMAX*A/(KM+A)
U'=KE*A
P'=KA*A+VMAX*A/(KM+A)
//
//
// Initial Conditions;
T=0
A=DOSE*F
U=DOSE*(1-F)
P=0
***
```

(b)

	Min	Parameter	Max
F	-Infinity	0.9100000	Infinity
KA	0.000000000	0.0020000	Infinity
KE	0.000000000	0.0350000	Infinity
VMAX	0.000000000	10.200000	Infinity
KM	0.000000000	202.40000	Infinity

Figure AVI.2. Model File (a) and Parameter File (b) of "Scientist"to be used for fitting 7.4 kDa F-PHEA absorption data obtained from the IPRL at 37 °C. Parameter values shown in (b) are initial estimates used for across-dose curve fitting. Data File is shown in Fig. AVI.2 (c).

(c)

T	DOSE	FP	T	DOSE	FP
0.00000000	100.000000	0.00000000	0.00000000	1000.00000	0.00000000
5.00000000	100.000000	15.8200000	5.00000000	1000.00000	3.89000000
10.0000000	100.000000	25.9100000	10.0000000	1000.00000	7.77000000
15.0000000	100.000000	30.8500000	15.0000000	1000.00000	10.4600000
20.0000000	100.000000	36.1500000	20.0000000	1000.00000	12.2800000
25.0000000	100.000000	44.8200000	25.0000000	1000.00000	13.6600000
30.0000000	100.000000	47.3100000	30.0000000	1000.00000	14.8500000
45.0000000	100.000000	53.0900000	45.0000000	1000.00000	17.7000000
60.0000000	100.000000	59.4800000	60.0000000	1000.00000	19.8400000
90.0000000	100.000000	57.7400000	90.0000000	1000.00000	23.5000000
120.000000	100.000000	60.1500000	120.000000	1000.00000	27.2400000
150.000000	100.000000	61.4500000	150.000000	1000.00000	31.9800000
180.000000	100.000000	63.8100000	180.000000	1000.00000	34.6600000
0.00000000	200.000000	0.00000000	0.00000000	5000.00000	0.00000000
5.00000000	200.000000	18.0300000	5.00000000	5000.00000	1.90000000
10.0000000	200.000000	25.6600000	10.0000000	5000.00000	3.11000000
15.0000000	200.000000	32.2400000	15.0000000	5000.00000	4.18000000
20.0000000	200.000000	34.5300000	20.0000000	5000.00000	4.84000000
25.0000000	200.000000	39.3500000	25.0000000	5000.00000	5.89000000
30.0000000	200.000000	44.3200000	30.0000000	5000.00000	6.22000000
45.0000000	200.000000	49.8000000	45.0000000	5000.00000	7.68000000
60.0000000	200.000000	56.2300000	60.0000000	5000.00000	8.44000000
90.0000000	200.000000	58.1900000	90.0000000	5000.00000	10.6000000
120.000000	200.000000	62.0600000	120.000000	5000.00000	10.9200000
150.000000	200.000000	61.1700000	150.000000	5000.00000	12.3700000
180.000000	200.000000	63.4300000	180.000000	5000.00000	13.6200000
0.00000000	500.000000	0.00000000			
5.00000000	500.000000	4.90000000			
10.0000000	500.000000	9.12000000			
15.0000000	500.000000	14.8000000			
20.0000000	500.000000	19.8100000			
25.0000000	500.000000	22.0400000			
30.0000000	500.000000	24.5800000			
45.0000000	500.000000	28.0600000			
60.0000000	500.000000	31.1800000			
90.0000000	500.000000	34.4100000			
120.000000	500.000000	36.9100000			
150.000000	500.000000	38.4200000			
180.000000	500.000000	39.9400000			

Figure AVI.2. Data File (c) of "Scientist" for 7.4 kDa F-PHEA absorption data obtained from the IPRL at 37 °C.

model; no tracheo-bronchial absorption could occur in the IPRL ($k_{a,TB}$ = 0), unlike the situation in vivo. In order to use % transfer values (FP) as a dependent-variable in the program with the solute amount-based differential equations, Eqns. AVI.1 to AVI.3 (also as Eqns. III.3-5 in Section III.b.7, Chapter 3), the following equation was incorporated in the program (Fig. AVI.2):

$$\% \text{ Transfer to perfusate (FP)} = \frac{\text{Amount in perfusate (P)}}{\text{Administered dose (DOSE)}} \times 100 \quad \text{(Eqn. AVI.4)}$$

Once all three files (Model, Data and Parameter Files) were compiled, the independent- and dependent- variables used in the Model File were automatically assigned in the Data File and hence, mean data for % transfer to perfusate was tabulated as a combination of dose and time (all data points in Fig. III.10), as shown in Fig. AVI.2. Similarly, each of the parameters (F, $k_{a,P}$, $k_{E,PT}$, $V_{max,P}$ and $K_{m,P}$) was assigned in the Parameter File. In order to perform curve fitting, initial estimates were assigned, based on the following assumptions and calculations:

Initial estimates:

- F (F):

The initial fraction of each administered dose delivered to the pulmonary compartment (Fig. AVI.1) was experimentally determined to be 0.91 (*0.910±0.003*; mean±SD; n=12). This was fixed throughout data fitting.

• $k_{a,P}$ (KA), $V_{max,P}$ (VMAX) and $K_{m,P}$ (KM):

The rate equation for F-PHEA absorption into perfusate (Eqn. AVI.1) was modified to obtain the initial estimates for curve fitting, assuming two extreme conditions for low and high dosing conditions:

When the amount of F-PHEA in the pulmonary compartment ($[M]_P$) was much larger than $K_{m,P}$ ($[M]_P >> K_{m,P}$), Eqn. AVI.1 was simplified to give:

$$(d[P]/dt)_{IPRL} = V_{max,P} + k_{a,P} \cdot [M]_P \qquad \text{(Eqn. AVI.5)}$$

Assuming that this was true at the higher 5.0 and 1.0 mg F-PHEA doses, the absorption rates at each dose, $(d[P]/dt)_{IPRL}$, were calculated from the experimental slopes of the absorption profiles over the first 30 minutes. Thus,

at 5.0 mg: $18.0\ [\mu g/min] = V_{max,P} + k_{a,P} \cdot [5000\ (\mu g)]_P$ (Eqn. AVI.6)

at 1.0 mg: $11.8\ [\mu g/min] = V_{max,P} + k_{a,P} \cdot [1000\ (\mu g)]_P$ (Eqn. AVI.7)

These equations yielded values for $V_{max,P} = 10.2\ [\mu g/min]$ and $k_{a,P} = 0.002\ [min^{-1}]$.

On the other hand, when the amount of F-PHEA in the pulmonary compartment ($[M]_P$) was much smaller than $K_{m,P}$ ($[M]_P << K_{m,P}$), Eqn. AVI.1 was simplified to give:

$$(d[P]/dt)_{IPRL} = V_{max,P} \cdot [M]_P / K_{m,P} + k_{a,P} \cdot [M]_P \qquad \text{(Eqn. AVI.8)}$$

$$= (V_{max,P}/(K_{m,P} + k_{a,P})) \cdot [M]_P \qquad \text{(Eqn. AVI.9)}$$

Assuming that this was true at the lowest 0.1 mg dose, logarithmic plots of remaining F-PHEA in lung *vs.* time provided a negative slope, $V_{max,P}/(K_{m,P} + k_{a,P}) = 0.052\ [min^{-1}]$, as

an apparent first-order rate constant for absorption. Using the values for $V_{max,P}$ = 10.2 [μg/min] and $k_{a,P}$ = 0.002 [min^{-1}] estimated above, the value for $K_{m,P}$ was estimated to be 202.4 [μg].

- $k_{E,PT}$ (KE):

If absorption was assumed to be apparent first-order (at the lowest 0.1 mg F-PHEA dose), then as time → ∞, the ratio of % loss to the tracheo-bronchial region to % transfer to perfusate (Fig. AVI.1) was determined by Eqn. AVI.10 (Notari, 1987):

$$\frac{\%\ \text{loss to the tracheo-bronchial region}}{\%\ \text{transfer to perfusate}} = \frac{k_{E,TB}}{k_{a,app}} \qquad \text{(Eqn. AVI.10)}$$

At the lowest, 0.1 mg F-PHEA dose, the final (asymptotic) % transfer to perfusate for F-PHEA was roughly 60 % (thus, the % loss to the tracheo-bronchial region = 40 %) and the apparent first-order rate constant ($k_{a,P}$ + $k_{E,PT}$) was found to be 0.052 [min^{-1}]. Therefore, the initial value for $k_{E,PT}$ was estimated:

$$k_{E,PT} = k_{a,app}\ (0.052\ [min^{-1}])\ x\ \frac{\%\ \text{loss to the tracheo-bronchial region (40 [\%])}}{\%\ \text{transfer to perfusate (60 [\%])}}$$

$$= 0.035\ [min^{-1}]$$

Curve fitting:

Following assignment of data, initial estimates and the definition of the model, as described above, "Scientist" was instructed to perform nonlinear least-mean-square regression analysis. In the example described above, this resulted in the Plot and Statistical Outputs shown as Figs. AVI.3 and AVI.4, respectively.

(2) Across-dose curve fitting for F-Na disposition in the IPRL at 37 ^{o}C

The Model File, Parameter File (with initial estimates) and Data File are shown in Fig. AVI.5. The dose-independence seen in the profiles for F-Na (Fig. III.6; Chapter 3) enabled to preclude the active absorption component from the kinetic model shown in Fig. AVI.1 ($V_{max,P} = K_{m,P} = 0$) and hence, the differential equations in the Model File are described as follows (the equations are also shown as Eqns. III.2, III.4 and III.5 in Section III.b.7, Chapter 3):

$$(d[P]/dt)_{Passive,IPRL} = k_{a,P} \cdot [M]_P \qquad \text{(Eqn. AVI.11)}$$

$$(d[M]_P/dt)_{IPRL} = - (d[P]/dt)_{Passive,IPRL} - k_{E,PT} \cdot [M]_P \qquad \text{(Eqn. AVI.12)}$$

$$(d[M]_{TB}/dt)_{IPRL} = k_{E,PT} \cdot [M]_P \qquad \text{(Eqn. AVI.13)}$$

The symbols in the Model File were assigned unchanged from those for F-PHEA. The Data File was prepared using mean data for % transfer to perfusate as a combination of dose and time following compilation (Fig. AVI.5). Each of the parameters (F, $k_{a,P}$ and

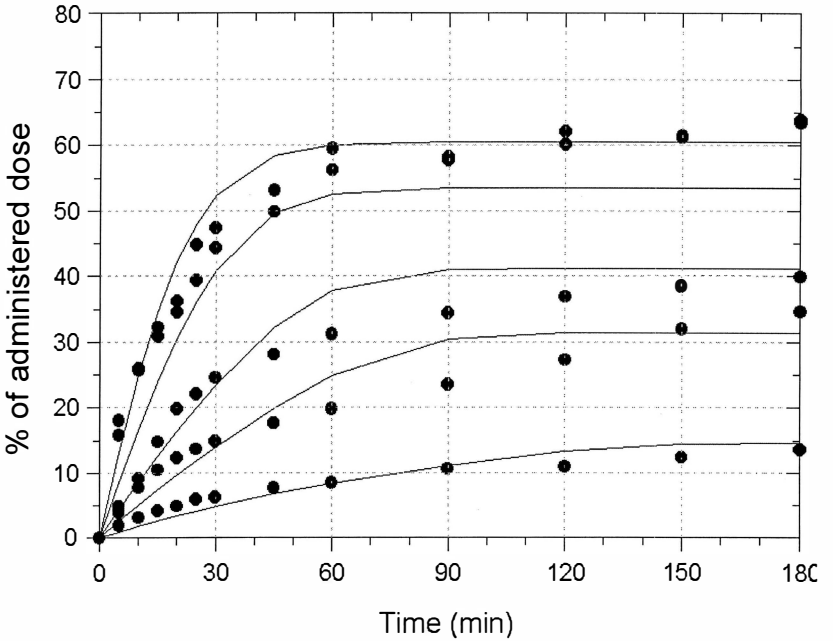

Figure AVI.3. Plot File obtained from across-dose fitting for 7.4 kDa F-PHEA absorption data in the IPRL at 37 °C. Data plots are experimental mean absorption data at different doses and curves are generated from the best parameter etimates obtained by the curve fitting; these are shown in Table III.2 (Chapter 3).

*** MicroMath Scientist Statistics Report ***

Model File Name : a:\f-phea.eqn
Data File Name : a:\data-37.mmd
Param File Name : a:\37-ini.par

Goodness-of-fit statistics for data set: a:\data-37.mmd

Data Column Name: FP

	Weighted	Unweighted
Sum of squared observations :	70937.6348	70937.6348
Sum of squared deviations :	1004.40593	1004.40593
Standard deviation of data :	4.05779139	4.05779139
R-squared :	0.985841001	0.985841001
Coefficient of determination :	0.961031051	0.961031051
Correlation :	0.980978323	0.980978323

Data Set Name: a:\data-37.mmd

	Weighted	Unweighted
Sum of squared observations :	70937.6348	70937.6348
Sum of squared deviations :	1004.40593	1004.40593
Standard deviation of data :	4.05779139	4.05779139
R-squared :	0.985841001	0.985841001
Coefficient of determination :	0.961031051	0.961031051
Correlation :	0.980978323	0.980978323
Model Selection Criterion :	3.12191322	3.12191322

Confidence Intervals:

Parameter Name :	KA		
Estimate Value =	0.00117717508		
Standard Deviation =	0.000693588225		
95% Range (Univar) =	-0.000209740293		0.00256409046
95% Range (S-Plane) =	-0.00102604148		0.00338039164
Parameter Name :	KE		
Estimate Value =	0.0233379971		
Standard Deviation =	0.00173152314		
95% Range (Univar) =	0.0198756026		0.0268003916
95% Range (S-Plane) =	0.0178377300		0.0288382641
Parameter Name :	VMAX		
Estimate Value =	4.36600215		
Standard Deviation =	0.565159738		
95% Range (Univar) =	3.23589541	5.49610889	
95% Range (S-Plane) =	2.57074489	6.16125941	
Parameter Name :	KM		
Estimate Value =	56.5958869		
Standard Deviation =	14.7080819		
95% Range (Univar) =	27.1852595	86.0065143	
95% Range (S-Plane) =	9.87495304	103.316821	

Variance-Covariance Matrix:

4.81064627E-7			
2.33468801E-7	2.99817239E-6		
-0.000302486774	5.87178927E-5	0.319405530	
-0.00702507801	-0.00586100968	7.57068919	216.327672

Correlation Matrix:

1.00000000			
0.194401155	1.00000000		
-0.771673280	0.0600027210	1.00000000	
-0.688641832	-0.230137876	0.910768839	1.00000000

Residual Analysis:

The following are normalized parameters with an expected value of 0.0. Values are in units of standard deviations from the expected value.
The serial correlation is 6.06 which indicates a systematic non-random trend in the residuals.
Skewness is -0.60 which is probably not significant.
Kurtosis is -0.00 which is probably not significant.
The weighting factor was 0.00 leading to a heteroscedacticity of 0.79 which suggests an optimal weight factor for this fit of about 0.79

Figure AVI.4. Statistical Output obtained from across-dose fitting for 7.4 kDa F-PHEA absorption data in the IPRL at 37 ºC.

(a)

```
//
// August 19, 1998
// Masahiro Sakagami, MCV/VCU
//
// F-Na Transfer Model in the IPRL study
// Final Version
//
// Passive Transport involved
// Mucociliary Transport involved
//
// A : Alveoli
// U : Upper Airway
// P : Perfusate
//
IndVars: T, DOSE
DepVars: FP
Params: F, KA, KE
//
FP=P/DOSE*100
A'=-(KA+KE)*A
U'=KE*A
P'=KA*A
//
//
// Initial Conditions;
T=0
A=DOSE*F
U=DOSE*(1-F)
P=0
***
```

(b)

	Min	Parameter	Max
F	-Infinity	0.910000000	Infinity
KA	0.000000000	0.072000000	Infinity
KE	0.000000000	0.048000000	Infinity

Figure AVI.5. Model File (a) and Parameter File (b) of "Scientist"to be used for fitting F-Na absorption data obtained from the IPRL at 37 °C. Parameter values shown in (b) are initial estimates used for across-dose curve fitting.
Data File is shown in Fig. AVI.5 (c).

(c)

T	DOSE	FP
0.00000000	10.0000000	0.00000000
1.00000000	10.0000000	1.45000000
3.00000000	10.0000000	8.22000000
5.00000000	10.0000000	17.3200000
10.0000000	10.0000000	34.0400000
15.0000000	10.0000000	45.1900000
20.0000000	10.0000000	51.2000000
30.0000000	10.0000000	56.5900000
40.0000000	10.0000000	59.0900000
50.0000000	10.0000000	60.5400000
60.0000000	10.0000000	61.2400000
75.0000000	10.0000000	61.5700000
90.0000000	10.0000000	62.0700000
120.000000	10.0000000	62.3900000
0.00000000	20.0000000	0.00000000
1.00000000	20.0000000	0.00000000
3.00000000	20.0000000	4.26000000
5.00000000	20.0000000	10.6600000
10.0000000	20.0000000	25.3500000
15.0000000	20.0000000	36.1700000
20.0000000	20.0000000	43.8800000
30.0000000	20.0000000	49.9800000
40.0000000	20.0000000	52.9500000
50.0000000	20.0000000	54.9800000
60.0000000	20.0000000	56.2300000
75.0000000	20.0000000	56.8200000
90.0000000	20.0000000	57.9900000
120.000000	20.0000000	57.9500000
0.00000000	40.0000000	0.00000000
1.00000000	40.0000000	0.41000000
3.00000000	40.0000000	4.17000000
5.00000000	40.0000000	16.4600000
10.0000000	40.0000000	35.7700000
15.0000000	40.0000000	47.0500000
20.0000000	40.0000000	54.4000000
30.0000000	40.0000000	59.8800000
40.0000000	40.0000000	63.8500000
50.0000000	40.0000000	64.2900000
60.0000000	40.0000000	64.9000000
75.0000000	40.0000000	65.4200000
90.0000000	40.0000000	66.4200000
120.000000	40.0000000	66.0500000

Figure AVI.5. Data File (c) of "Scientist"for F-Na absorption data obtained from the IPRL at 37 °C.

$k_{E,PT}$) was assigned in the Parameter File as initial estimates, based on the following assumptions and calculations:

Initial estimates:

• F (F):

The initial fraction of each administered dose delivered to the pulmonary compartment (Fig. AVI.1) was experimentally determined to be 0.91 (0.910±0.003; mean±SD; n=12). This was fixed throughout data fitting.

• $k_{a,P}$ (KA):

The rate equation for F-Na absorption into perfusate (Eqn. AVI.11) was assumed to be first-order. Thus, logarithmic plots of remaining F-Na in lung *vs.* time (Fig. III.11, Chapter 3) provided a negative slope, $k_{a,P}$ = 0.072 [min^{-1}] as an apparent first-order rate constant for absorption and this value was used as the initial estimate.

• $k_{E,PT}$ ($k_{E,T}$):

If absorption was assumed to be apparent first-order, then as time $\rightarrow \infty$, the ratio of % loss to the tracheo-bronchial region to % transfer to perfusate (Fig. AVI.1) was determined by Eqn. AVI.10. At all doses, The final (asymptotic) % transfer to perfusate for F-Na was roughly 60 % (thus, the % loss to the tracheo-bronchial region = 40 %) and the apparent first-order rate constant ($k_{a,P}$ + $k_{E,PT}$) was found to be 0.072 [min^{-1}] (Fig. III.11, Chapter 3). Therefore, the initial value for $k_{E,PT}$ was estimated:

$$k_{E,PT} = k_{a,app}\,(0.072\ [min^{-1}])\ x\ \frac{\%\ \text{loss to the tracheo-bronchial region (40 [\%])}}{\%\ \text{transfer to perfusate (60 [\%])}}$$

$$= 0.048\ [min^{-1}]$$

Curve fitting:

Following assignment of data, initial estimates and the definition of the model, as described above, "Scientist" was instructed to perform nonlinear least-mean-square regression analysis. In the example described above, this resulted in the Plot and Statistical Outputs shown as Figs. AVI.6 and AVI.7, respectively.

(3) Across-dose curve fitting for F-Na disposition in vivo

Single-dose curve fitting was employed to describe the in vivo disposition of F-Na. The Model File, Parameter File (with initial estimates) and Data File are shown in Fig. AVI.8. The Model File defined time (T) and % remaining unabsorbed from the lung (FL) as independent- and dependent-variables, respectively. This was followed by a definition of the model parameters, the differential equations and the initial conditions. Based on the model shown in Fig. AVI.1, the differential equations were derived for F-Na as follows (the equations are also shown as Eqns. III.2, III.7, III.8 and III.9 in Section III.b.7, Chapter 3):

$$(d[B]/dt)_{in\ vivo} = k_{a,P}\cdot[M]_P + k_{a,TB}\cdot[M]_{TB} \qquad \text{(Eqn. AVI.14)}$$

$$(d[M]_P/dt)_{in\ vivo} = -\,k_{a,P}\cdot[M]_P - k_{E,PT}\cdot[M]_P \qquad \text{(Eqn. AVI.15)}$$

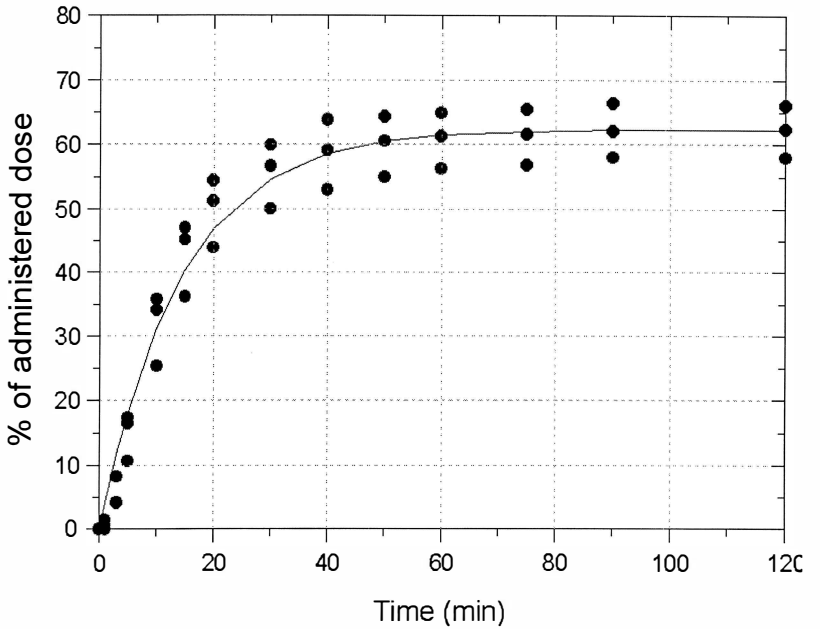

Figure AVI.6. Plot File obtained from across-dose fitting for F-Na absorption data in the IPRL at 37 °C. Data plots are experimental mean absorption data at different doses and curves are generated from the best parameter etimates obtained by the curve fitting; these are shown in Table III.2 (Chapter 3).

*** MicroMath Scientist Statistics Report ***

Model File Name : a:\f-na.eqn
Data File Name : a:\fna-37.mmd
Param File Name : Untitled1

Goodness-of-fit statistics for data set: a:\fna-37.mmd

Data Column Name: FP

	Weighted	Unweighted
Sum of squared observations :	93084.1888	93084.1888
Sum of squared deviations :	765.132504	765.132504
Standard deviation of data :	4.37359264	4.37359264
R-squared :	0.991780210	0.991780210
Coefficient of determination :	0.968771561	0.968771561
Correlation :	0.985809251	0.985809251

Data Set Name: a:\fna-37.mmd

	Weighted	Unweighted
Sum of squared observations :	93084.1888	93084.1888
Sum of squared deviations :	765.132504	765.132504
Standard deviation of data :	4.37359264	4.37359264
R-squared :	0.991780210	0.991780210
Coefficient of determination :	0.968771561	0.968771561
Correlation :	0.985809251	0.985809251
Model Selection Criterion :	3.37118801	3.37118801

Confidence Intervals:

Parameter Name :	KA	
Estimate Value =	0.0477436096	
Standard Deviation =	0.00281685229	
95% Range (Univar) =	0.0420505388	0.0534366805
95% Range (S-Plane) =	0.0405822348	0.0549049844

Parameter Name :	KE	
Estimate Value =	0.0218780006	
Standard Deviation =	0.00220141465	
95% Range (Univar) =	0.0174287756	0.0263272255
95% Range (S-Plane) =	0.0162812728	0.0274747283

Variance-Covariance Matrix:
7.93465682E-6
5.24027804E-6 4.84622645E-6

Correlation Matrix:
1.00000000
0.845061672 1.00000000

Residual Analysis:

The following are normalized parameters with an expected value of 0.0. Values are in units of standard deviations from the expected value.
The serial correlation is 5.44 which indicates a systematic non-random trend in the residuals.
Skewness is 0.43 which is probably not significant.
Kurtosis is -0.00 which is probably not significant.
The weighting factor was 0.00 leading to a heteroscedacticity of -0.16 which suggests an optimal weight factor for this fit of about -0.16

Figure AVI.7. Statistical Output obtained from across-dose fitting for F-Na absorption data in the IPRL at 37 °C.

(a)

```
//
// August 19, 1998
// Masahiro Sakagami, MCV/VCU
//
// F-Na Transfer Model in in vivo study
// Final Version
//
// Passive Transport involved
// Mucociliary Transport involved
//
// A : Alveoli
// U : Upper Airway
// L : Upper airway + Alveoli
// P : Blood
//
IndVars: T
DepVars: FL
Params: DOSE, F, KAA, KAU, KE
//
L=A+U
FL=L/DOSE*100
A'=-(KAA+KE)*A
U'=-KAU*U+KE*A
P'=KAA*A+KAU*U
//
//
// Initial Conditions;
T=0
A=DOSE*F
U=DOSE*(1-F)
P=0
***
```

(b)

	Min	Parameter	Max
DOSE	-Infinity	0.020000000	Infinity
F	0.000000000	0.910000000	Infinity
KAA	0.000000000	0.048000000	Infinity
KAU	0.000000000	0.048000000	Infinity
KE	0.000000000	0.022000000	Infinity

(c)

T	FL
0.00000000	100.000000
5.00000000	84.2400000
10.0000000	59.4900000
20.0000000	34.4500000
30.0000000	18.4900000
60.0000000	7.51000000
120.000000	0.53000000

Figure AVI.8. Model File (a), Parameter File (b) and Data File (c) of "Scientist" to be used for fitting in vivo F-Na absorption data. Parameter values shown in (b) are initial estimates used for across-dose curve fitting.

$$(d[M]_{TB}/dt)_{in\ vivo} = k_{E,PT}\cdot[M]_P - k_{a,TB}\cdot[M]_{TB} \qquad \text{(Eqn. AVI.16)}$$

where [B] is the cumulative F-Na amount absorbed from both the pulmonary and tracheo-bronchial regions into blood. $[M]_P$ and $[M]_{TB}$ are the F-Na amounts remaining unabsorbed in the pulmonary and the tracheo-bronchial regions, respectively; $k_{a,P}$ and $k_{a,TB}$ are the first-order passive absorption rate constants from the pulmonary and the tracheo-bronchial regions, respectively, and $k_{E,PT}$ is the first-order mucociliary clearance rate constant from the pulmonary to the tracheo-bronchial region. In the Model File (Fig. AVI.8), symbols, P, A, U and L were used to represent [B], $[M]_P$, $[M]_{TB}$ and $[M]_P+[M]_{TB}$, respectively, and DOSE, F, KAA, KAU and KE, respectively, were the dose, F, $k_{a,P}$, $k_{a,TB}$ and $k_{E,PT}$; active absorption was assumed absent for F-Na in vivo ($V_{max,P} = K_{m,P} = 0$). In order to use % remaining unabsorbed in lung (FL) as a dependent-variable in this program, with the solute amount-based differential equations (Eqns. AVI.14 to AVI.16), the following equations were incorporated in the program (Fig. AVI.4):

Amount in a whole lung (L)
= Sum of amounts in the pulmonary and the tracheo-bronchial regions (A + U)
(Eqn. AVI.17)

% Remaining to be absorbed in a whole lung (FL)

$$= \frac{\text{Amount remaining unabsorbed in lung (L)}}{\text{Administered dose (DOSE)}} \times 100 \qquad \text{(Eqn. AVI.18)}$$

Following compilation, mean data for % remaining unabsorbed in lung (F-Na nominal dose = 0.02 mg; Fig. III.6, Chapter 3) were tabulated in the Data File (Fig. AVI.8). Each parameter (F, $k_{a,P}$, $k_{a,TB}$ and $k_{E,TB}$) was initially obtained from the IPRL profiles (Fig. III.6, Chapter 3) and used as an initial estimate, based on the following assumptions and calculations:

• F (F):

The fraction of the administered dose delivered to the pulmonary compartment was experimentally determined to be 0.91 (0.910±0.004; mean±SD; n=4). This was fixed throughout data fitting.

• $k_{a,P}$ (KAA) and $k_{E,PT}$ (KE):

Absorption from the pulmonary region and the mucociliary clearance from the pulmonary to the tracheo-bronchial regions were assumed to be the same as those determined in vitro. Therefore, values for $k_{a,P}$ and $k_{E,PT}$, obtained from the IPRL data are the same as those in Table III.2 ($k_{a,P}$ = 0.048 [min^{-1}] and $k_{E,PT}$ = 0.022 [min^{-1}]; Chapter 3). These were fixed throughout data fitting.

• $k_{a,TB}$ (KAU):

It was not possible to estimate a value for $k_{a,TB}$ from the experimental data. Therefore, an identical value to that for $k_{a,P}$, 0.048 [min^{-1}], was used as an initial estimate to perform the data fitting.

In this case, all parameters, dose (0.02 mg), F, $k_{a,P}$ and $k_{E,PT}$ were fixed at their initial estimates and only $k_{a,TB}$ was floated during data fitting; $k_{a,TB}$ was constrained between 0 and infinity (Fig. AVI.8). The data fitting was initially performed by the Simplex algorithm, followed by the Gauss-Newton technique to provide the best estimate for $k_{a,TB}$ in the kinetic model (Table III.3, Chapter 3).

AVI.c "GOODNESS-OF-FIT" PARAMETERS

The model fits were assessed using "goodness-of-fit" parameters provided by the program's statistical output. In this thesis, Model Selection Criterion (MSC) and R-squared (R^2) were used. These are described below:

<Model Selection Criterion (MSC)>

Model Selection Criterion (MSC) was calculated as follows:

$$MSC = \ln\left[\frac{\Sigma\,[w_i\cdot(Y_{obs,i}-Y_{obs,mean})^2]}{\Sigma[w_i\cdot(Y_{obs,i}-Y_{cal,i})^2]}\right] - 2p/n \qquad \text{(Eqn. AI.19)}$$

where w_i is the weight applied to each data point, $Y_{obs,i}$ and $Y_{cal,i}$ are the observed and the calculated data values, respectively, $Y_{obs,mean}$ is the weighted mean of the observed data, p is the number of parameters and n is the number of data points. Values for MSC provided

the rankings between the models, independent of the scaling of the data points. Thus, the values allowed a selection of the most appropriate model as well as indicating how well the model described the data. Generally, greater MSC values indicate better fits.

<R-squared (R^2)>

R-squared (R^2) values were calculated as follows:

$$R^2 = \frac{\left| \Sigma \left[w_i \cdot Y_{obs,i}^2 \right] - \Sigma \left[w_i \cdot (Y_{obs,i} - Y_{cal,i})^2 \right] \right|}{\Sigma \left[w_i \cdot Y_{obs,i}^2 \right]} \qquad \text{(Eqn. AI.20)}$$

The R-squared (R^2) values were used to assess what proportion of the data could be described by the theoretical model with appropriate (best) parameter estimates.

APPENDIX VII

ORIGINAL DATA

This appendix summarizes the original and individual data obtained from each of the isolated perfused rat lung (IPRL) and in vivo whole rat studies. The appendix is followed by all statistical outputs of across-dose curve fitting by "Scientist". These are reported here for completeness and to allow a regeneration of the plots and/or further data derivation in future stages.

The appendix is comprised of:

- Tables AVII.1 to AVII.10: Initial solute regional distribution in lung in vitro and in vivo.
- Tables AVII.11 to AVII.13: Dose and remaining solute amount in each lung component at different sacrifice time in vivo.
- Tables AVII.14 to AVII.63: Dose, and amount and % absorbed from airways to perfusate in the IPRL.
- Figs. AVII.1 to AVII.8: Statistical output of across-dose curve fitting by "Scientist".

The following abbreviations are used throughout:

BW: Body weight of the rat.

Dose:

- D_L: Loading solute dose in the dosing cartridge.
- D_{ctg}: Solute amount remaining in the dosing cartridge after administration.
- D_{cnl}: Solute amount remaining in the tracheal cannula after administration.
- D_{ad}: Administered dose, calculated by $D_L - (D_{ctg} + D_{cnl})$.

Lung component (Fig. AI.6):

- TB: Tracheo and bronchi
- L: Left lung lobe
- PC: Right postcaval or median lobe
- RS: Right superior or apical lobe
- RC: Right middle lobe
- RI: Right inferior or diaphragmatic lobe

Table AVII.1 Initial regional distribution of 7.4 kDa F-PHEA in lung in vitro. The solute was administered into the airways of the IPRL at 37 °C (FR7150; nominal dose = 0.2 mg; used in Section III.b.7, Chapter 3).

Wet weight:

		Rat#				mean	SD
		I-5	I-6	I-7	I-8		
BW	[g]	354	349	360	338	350.25	9.32
TB	[g]	0.34	0.28	0.24	0.22	0.27	0.05
L	[g]	0.54	0.45	0.51	0.49	0.50	0.04
PC	[g]	0.18	0.14	0.19	0.17	0.17	0.02
RS	[g]	0.20	0.18	0.21	0.20	0.20	0.01
RC	[g]	0.22	0.19	0.20	0.19	0.20	0.01
RI	[g]	0.41	0.39	0.40	0.44	0.41	0.02
Total	[g]	1.89	1.63	1.75	1.71	1.75	0.11
%TB	[%]	17.99	17.18	13.71	12.87	15.44	2.52
%Lobe	[%]	82.01	82.82	86.29	87.13	84.56	2.52

Amount delivered:

		Rat#				mean	SD
		I-5	I-6	I-7	I-8		
D_L	[µg]	234.37	226.30	231.75	206.70	224.78	12.51
D_{ctg}	[µg]	25.72	12.68	6.58	7.41	13.10	8.84
D_{cnl}	[µg]	3.87	17.39	16.64	14.32	13.06	6.26
D_{ad}	[µg]	204.78	196.23	208.53	184.97	198.63	10.46
TB	[µg]	17.82	8.57	24.90	17.89	17.30	6.70
L	[µg]	47.27	33.21	105.05	57.52	60.76	31.16
PC	[µg]	12.72	15.88	7.57	2.51	9.67	5.87
RS	[µg]	34.70	46.05	16.09	17.96	28.70	14.28
RC	[µg]	24.95	10.02	12.45	6.69	13.53	7.97
RI	[µg]	52.04	75.78	29.42	70.64	56.97	21.01
Total (D_r)	[µg]	189.50	189.51	195.48	173.21	186.93	9.57

% delivered:

		Rat#				mean	SD
		I-1	I-2	I-3	I-4		
TB	[%]	9.40	4.52	12.74	10.33	9.25	3.45
L	[%]	24.94	17.52	53.74	33.21	32.35	15.63
PC	[%]	6.71	8.38	3.87	1.45	5.10	3.07
RS	[%]	18.31	24.30	8.23	10.37	15.30	7.40
RC	[%]	13.17	5.29	6.37	3.86	7.17	4.13
RI	[%]	27.46	39.99	15.05	40.78	30.82	12.16
Total	[%]	100.00	100.00	100.00	100.00	100.00	0.00
%TB	[%]	9.40	4.52	12.74	10.33	9.25	3.45
%Lobe	[%]	90.60	95.48	87.26	89.67	90.75	3.45

Table AVII.2 Initial regional distribution of 7.4 kDa F-PHEA in lung in vitro. The solute was administered into the airways of the IPRL at 37 °C (FR7150; nominal dose = 1.0 mg; used in Fig. III.5, Chapter 3).

Wet weight:

		Rat#				mean	SD
		I-1	I-2	I-3	I-4		
BW	[g]	360	354	349	348	352.75	5.50
TB	[g]	0.21	0.30	0.22	0.28	0.25	0.04
L	[g]	0.64	0.54	0.45	0.57	0.55	0.08
PC	[g]	0.13	0.18	0.17	0.17	0.16	0.02
RS	[g]	0.16	0.15	0.13	0.16	0.15	0.01
RC	[g]	0.18	0.20	0.19	0.20	0.19	0.01
RI	[g]	0.41	0.38	0.41	0.43	0.41	0.02
Total	[g]	1.73	1.75	1.57	1.81	1.72	0.10
%TB	[%]	12.14	17.14	14.01	15.47	14.69	2.13
%Lobe	[%]	87.86	82.86	85.99	84.53	85.31	2.13

Amount delivered:

		Rat#				mean	SD
		I-1	I-2	I-3	I-4		
D_L	[µg]	1030.92	1190.00	1095.00	1055.00	1092.73	70.03
D_{ctg}	[µg]	5.35	14.70	19.65	45.95	21.41	17.40
D_{cnl}	[µg]	40.95	19.55	19.10	22.85	25.61	10.36
D_{ad}	[µg]	984.62	1155.75	1056.25	986.20	1045.71	80.61
TB	[µg]	50.50	94.71	66.99	33.22	61.36	26.16
L	[µg]	386.59	410.82	367.65	276.54	360.40	58.63
PC	[µg]	4.95	4.29	7.59	111.54	32.09	52.98
RS	[µg]	37.62	44.55	102.96	197.78	95.73	74.08
RC	[µg]	30.69	15.51	39.27	100.76	46.56	37.45
RI	[µg]	400.14	279.10	318.42	91.74	272.35	130.54
Total (D_r)	[µg]	910.49	848.98	902.88	811.58	868.48	46.78

% delivered:

		Rat#				mean	SD
		I-1	I-2	I-3	I-4		
TB	[%]	5.55	11.16	7.42	4.09	7.05	3.05
L	[%]	42.46	48.39	40.72	34.07	41.41	5.89
PC	[%]	0.54	0.51	0.84	13.74	3.91	6.56
RS	[%]	4.13	5.25	11.40	24.37	11.29	9.29
RC	[%]	3.37	1.83	4.35	12.42	5.49	4.73
RI	[%]	43.95	32.87	35.27	11.30	30.85	13.87
Total	[%]	100.00	100.00	100.00	100.00	100.00	0.00
%TB	[%]	5.55	11.16	7.42	4.09	7.05	3.05
%Lobe	[%]	94.45	88.84	92.58	95.91	92.95	3.05

Table AVII.3 Initial regional distribution of 7.4 kDa F-PHEA in lung in vitro. The solute was administered into the airways of the IPRL at 25 °C (FR7150; nominal dose = 1.0 mg; used in Section IV.b.4, Chapter 4).

Wet weight:

		Rat#				mean	SD
		I-9	I-10	I-11	I-12		
BW	[g]	352	334	328	348	340.50	11.36
TB	[g]	0.27	0.29	0.22	0.30	0.27	0.04
L	[g]	0.54	0.48	0.55	0.50	0.52	0.03
PC	[g]	0.14	0.14	0.16	0.13	0.14	0.01
RS	[g]	0.30	0.35	0.28	0.34	0.32	0.03
RC	[g]	0.22	0.17	0.23	0.17	0.20	0.03
RI	[g]	0.45	0.46	0.43	0.38	0.43	0.04
Total	[g]	1.92	1.89	1.87	1.82	1.88	0.04
%TB	[%]	14.06	15.34	11.76	16.48	14.41	2.02
%Lobe	[%]	85.94	84.66	88.24	83.52	85.59	2.02

Amount delivered:

		Rat#				mean	SD
		I-9	I-10	I-11	I-12		
D_L	[µg]	1032.40	1026.30	1010.34	973.53	1010.64	26.43
D_{ctg}	[µg]	22.30	17.35	30.00	37.98	26.91	9.03
D_{cnl}	[µg]	40.53	24.27	34.25	25.50	31.14	7.68
D_{ad}	[µg]	969.57	984.68	946.09	910.05	952.60	32.51
TB	[µg]	92.41	105.34	103.67	38.41	84.96	31.56
L	[µg]	389.74	352.36	297.90	332.45	343.11	38.37
PC	[µg]	10.21	5.29	35.80	28.97	20.07	14.63
RS	[µg]	32.09	31.79	45.20	36.98	36.52	6.26
RC	[µg]	35.01	55.27	61.20	67.42	54.73	14.05
RI	[µg]	384.10	405.90	358.74	374.12	380.72	19.77
Total (D_r)	[µg]	943.56	955.95	902.51	878.35	920.09	36.00

% delivered:

		Rat#				mean	SD
		I-9	I-10	I-11	I-12		
TB	[%]	9.79	11.02	11.49	4.37	9.17	3.28
L	[%]	41.31	36.86	33.01	37.85	37.26	3.41
PC	[%]	1.08	0.55	3.97	3.30	2.23	1.66
RS	[%]	3.40	3.33	5.01	4.21	3.99	0.79
RC	[%]	3.71	5.78	6.78	7.68	5.99	1.70
RI	[%]	40.71	42.46	39.75	42.59	41.38	1.38
Total	[%]	100.00	100.00	100.00	100.00	100.00	0.00
%TB	[%]	9.79	11.02	11.49	4.37	9.17	3.28
%Lobe	[%]	90.21	88.98	88.51	95.63	90.83	3.28

Table AVII.4 Initial regional distribution of 4.3 kDa F-PHEA in lung in vitro. The solute was administered into the airways of the IPRL at 37 °C (FR7002-5; nominal dose = 0.1 mg; used in Section V.b.3, Chapter 5).

Wet weight:

		Rat#				mean	SD
		I-25	I-26	I-27	I-28		
BW	[g]	335	328	350	348	340.25	10.53
TB	[g]	0.26	0.24	0.29	0.25	0.26	0.02
L	[g]	0.58	0.57	0.55	0.53	0.56	0.02
PC	[g]	0.18	0.22	0.18	0.18	0.19	0.02
RS	[g]	0.20	0.17	0.17	0.23	0.19	0.03
RC	[g]	0.21	0.23	0.17	0.16	0.19	0.03
RI	[g]	0.42	0.50	0.41	0.42	0.44	0.04
Total	[g]	1.85	1.93	1.77	1.77	1.83	0.08
%TB	[%]	14.05	12.44	16.38	14.12	14.25	1.62
%Lobe	[%]	85.95	87.56	83.62	85.88	85.75	1.62

Amount delivered:

		Rat#				mean	SD
		I-25	I-26	I-27	I-28		
D_L	[µg]	172.71	172.71	96.87	96.87	134.79	43.79
D_{ctg}	[µg]	21.58	14.75	2.08	9.02	11.86	8.30
D_{cnl}	[µg]	30.03	32.67	21.17	17.43	25.32	7.20
D_{ad}	[µg]	121.10	125.30	73.62	70.42	97.61	29.63
TB	[µg]	9.24	13.53	5.17	3.52	7.87	4.48
L	[µg]	24.20	17.05	17.38	12.98	17.90	4.65
PC	[µg]	12.10	25.19	11.99	10.67	14.99	6.83
RS	[µg]	23.98	13.42	11.21	13.63	15.56	5.72
RC	[µg]	22.00	16.06	10.94	8.74	14.44	5.90
RI	[µg]	13.80	13.40	14.90	20.40	15.63	3.25
Total (D_r)	[µg]	105.32	98.65	71.59	69.94	86.38	18.24

% delivered:

		Rat#				mean	SD
		I-25	I-26	I-27	I-28		
TB	[%]	8.77	13.72	7.22	5.03	8.69	3.69
L	[%]	22.98	17.28	24.28	18.56	20.77	3.38
PC	[%]	11.49	25.53	16.75	15.26	17.26	5.95
RS	[%]	22.77	13.60	15.66	19.49	17.88	4.07
RC	[%]	20.89	16.28	15.28	12.50	16.24	3.49
RI	[%]	13.10	13.58	20.81	29.17	19.17	7.54
Total	[%]	100.00	100.00	100.00	100.00	100.00	0.00
%TB	[%]	8.77	13.72	7.22	5.03	8.69	3.69
%Lobe	[%]	91.23	86.28	92.78	94.97	91.31	3.69

Table AVII.5 Initial regional distribution of 4.4 kDa FD-4 in lung in vitro. The solute was administered into the airways of the IPRL at 37 °C (nominal dose = 0.2 mg; used in Section III.b.7, Chapter 3).

Wet weight:

		Rat#				mean	SD
		I-21	I-22	I-23	I-24		
BW	[g]	330	325	320	327	325.50	4.20
TB	[g]	0.21	0.22	0.20	0.18	0.20	0.02
L	[g]	0.52	0.51	0.47	0.48	0.50	0.02
PC	[g]	0.17	0.16	0.18	0.19	0.18	0.01
RS	[g]	0.20	0.20	0.17	0.17	0.19	0.02
RC	[g]	0.19	0.18	0.17	0.24	0.20	0.03
RI	[g]	0.39	0.39	0.44	0.40	0.41	0.02
Total	[g]	1.68	1.66	1.63	1.66	1.66	0.02
%TB	[%]	12.50	13.25	12.27	10.84	12.22	1.01
%Lobe	[%]	87.50	86.75	87.73	89.16	87.78	1.01

Amount delivered:

		Rat#				mean	SD
		I-21	I-22	I-23	I-24		
D_L	[µg]	291.46	205.19	256.06	248.47	250.30	35.43
D_{ctg}	[µg]	4.50	5.98	18.93	19.97	12.34	8.24
D_{cnl}	[µg]	41.72	11.63	29.74	29.56	28.16	12.40
D_{ad}	[µg]	245.24	187.58	207.40	198.95	209.79	24.99
TB	[µg]	20.05	11.25	13.20	24.65	17.29	6.19
L	[µg]	74.95	47.30	31.40	43.70	49.34	18.38
PC	[µg]	15.70	5.65	12.40	12.35	11.53	4.22
RS	[µg]	69.40	28.60	19.35	9.40	31.69	26.34
RC	[µg]	17.75	20.85	50.70	55.70	36.25	19.72
RI	[µg]	23.60	43.15	55.30	28.90	37.74	14.33
Total (D_r)	[µg]	221.45	156.80	182.35	174.70	183.83	27.27

% delivered:

		Rat#				mean	SD
		I-21	I-22	I-23	I-24		
TB	[%]	9.05	7.17	7.24	14.11	9.39	3.26
L	[%]	33.85	30.17	17.22	25.01	26.56	7.20
PC	[%]	7.09	3.60	6.80	7.07	6.14	1.70
RS	[%]	31.34	18.24	10.61	5.38	16.39	11.28
RC	[%]	8.02	13.30	27.80	31.88	20.25	11.41
RI	[%]	10.66	27.52	30.33	16.54	21.26	9.24
Total	[%]	100.00	100.00	100.00	100.00	100.00	0.00
%TB	[%]	9.05	7.17	7.24	14.11	9.39	3.26
%Lobe	[%]	90.95	92.83	92.76	85.89	90.61	3.26

Table AVII.6 Initial regional distribution of 376 Da F-Na in lung in vitro. The solute was administered into the airways of the IPRL at 37 °C (nominal dose = 0.02 mg; used in Fig. III.4 and Section III.b.7, Chapter 3).

Wet weight:

		Rat#				mean	SD
		I-13	I-14	I-15	I-16		
BW	[g]	340	368	380	390	369.50	21.63
TB	[g]	0.23	0.24	0.22	0.26	0.24	0.02
L	[g]	0.53	0.57	0.56	0.56	0.55	0.02
PC	[g]	0.18	0.16	0.17	0.19	0.18	0.01
RS	[g]	0.17	0.20	0.20	0.17	0.19	0.02
RC	[g]	0.19	0.17	0.24	0.16	0.19	0.04
RI	[g]	0.40	0.48	0.44	0.47	0.45	0.04
Total	[g]	1.70	1.82	1.83	1.81	1.79	0.06
%TB	[%]	13.53	13.19	12.05	14.36	13.28	0.96
%Lobe	[%]	86.47	86.81	87.95	85.64	86.72	0.96

Amount delivered:

		Rat#				mean	SD
		I-13	I-14	I-15	I-16		
D_L	[µg]	20.83	23.20	25.40	21.50	22.73	2.04
D_{ctg}	[µg]	1.00	0.58	1.65	2.86	1.52	0.99
D_{cnl}	[µg]	3.44	5.21	5.86	3.88	4.60	1.13
D_{ad}	[µg]	16.39	17.41	17.90	14.76	16.61	1.39
TB	[µg]	1.43	1.33	1.05	1.77	1.40	0.30
L	[µg]	7.20	3.36	3.11	4.20	4.46	1.88
PC	[µg]	0.04	0.08	1.76	1.72	0.90	0.97
RS	[µg]	0.74	4.05	2.78	1.25	2.21	1.50
RC	[µg]	0.98	2.31	2.92	1.52	1.93	0.86
RI	[µg]	2.88	3.80	3.25	3.97	3.47	0.50
Total (D_r)	[µg]	13.27	14.92	14.87	14.42	14.37	0.77

% delivered:

		Rat#				mean	SD
		I-13	I-14	I-15	I-16		
TB	[%]	10.78	8.91	7.04	12.30	9.76	2.28
L	[%]	54.25	22.48	20.89	29.10	31.68	15.46
PC	[%]	0.29	0.56	11.84	11.89	6.15	6.61
RS	[%]	5.61	27.13	18.72	8.67	15.03	9.82
RC	[%]	7.36	15.48	19.63	10.55	13.26	5.41
RI	[%]	21.70	25.45	21.87	27.49	24.13	2.83
Total	[%]	100.00	100.00	100.00	100.00	100.00	0.00
%TB	[%]	10.78	8.91	7.04	12.30	9.76	2.28
%Lobe	[%]	89.22	91.09	92.96	87.70	90.24	2.28

Table AVII.7 Initial regional distribution of 376 Da F-Na in lung in vitro. The solute was administered into the airways of the IPRL at 25 °C (nominal dose = 0.02 mg; used in Section IV.b.4, Chapter 4).

Wet weight:

		Rat#				mean	SD
		I-17	I-18	I-19	I-20		
BW	[g]	395	360	310	330	348.75	37.05
TB	[g]	0.21	0.19	0.15	0.18	0.18	0.03
L	[g]	0.49	0.52	0.50	0.49	0.50	0.01
PC	[g]	0.16	0.19	0.14	0.19	0.17	0.02
RS	[g]	0.19	0.22	0.20	0.21	0.21	0.01
RC	[g]	0.20	0.22	0.18	0.20	0.20	0.02
RI	[g]	0.43	0.48	0.34	0.44	0.42	0.06
Total	[g]	1.68	1.82	1.51	1.71	1.68	0.13
%TB	[%]	12.50	10.44	9.93	10.53	10.85	1.13
%Lobe	[%]	87.50	89.56	90.07	89.47	89.15	1.13

Amount delivered:

		Rat#				mean	SD
		I-17	I-18	I-19	I-20		
D_L	[µg]	23.28	21.68	20.46	22.41	21.96	1.19
D_{ctg}	[µg]	0.86	2.61	1.00	1.32	1.45	0.80
D_{cnl}	[µg]	2.98	3.49	2.22	1.89	2.64	0.72
D_{ad}	[µg]	19.44	15.58	17.25	19.20	17.87	1.81
TB	[µg]	1.61	1.38	1.37	0.98	1.33	0.26
L	[µg]	1.61	6.27	3.81	4.74	4.11	1.95
PC	[µg]	1.67	1.30	1.83	0.45	1.31	0.62
RS	[µg]	3.80	0.91	2.89	2.29	2.47	1.21
RC	[µg]	3.51	1.65	2.81	1.47	2.36	0.97
RI	[µg]	3.24	3.29	3.90	3.56	3.50	0.30
Total (D_r)	[µg]	15.44	14.79	16.61	13.49	15.08	1.30

% delivered:

		Rat#				mean	SD
		I-17	I-18	I-19	I-20		
TB	[%]	10.41	9.31	8.25	7.26	8.81	1.36
L	[%]	10.45	42.40	22.93	35.14	27.73	14.04
PC	[%]	10.80	8.76	11.01	3.34	8.48	3.57
RS	[%]	24.60	6.15	17.41	16.98	16.29	7.61
RC	[%]	22.72	11.14	16.94	10.90	15.42	5.61
RI	[%]	21.02	22.24	23.46	26.39	23.28	2.30
Total	[%]	100.00	100.00	100.00	100.00	100.00	0.00
%TB	[%]	10.41	9.31	8.25	7.26	8.81	1.36
%Lobe	[%]	89.59	90.69	91.75	92.74	91.19	1.36

Table AVII.8 Initial regional distribution of 7.4 kDa F-PHEA in lung in vivo. The solute was administered into the airways by "forced solution instillation" (nominal dose = 0.2 mg).

Wet weight:

		Rat#				mean	SD
		61	62	63	67		
BW	[g]	348	349	348	338	345.75	5.19
TB	[g]	0.25	0.21	0.21	0.21	0.22	0.02
L	[g]	0.48	0.50	0.49	0.53	0.50	0.02
PC	[g]	0.19	0.20	0.22	0.17	0.20	0.02
RS	[g]	0.20	0.20	0.19	0.23	0.21	0.02
RC	[g]	0.21	0.20	0.23	0.20	0.21	0.01
RI	[g]	0.43	0.40	0.46	0.44	0.43	0.02
Total	[g]	1.76	1.71	1.80	1.78	1.76	0.04
%TB	[%]	14.20	12.28	11.67	11.80	12.49	1.17
%Lobe	[%]	85.80	87.72	88.33	88.20	87.51	1.17

Amount delivered:

		Rat#				mean	SD
		61	62	63	67		
D_L	[µg]	228.46	245.23	244.71	214.06	233.11	14.90
D_{ctg}	[µg]	4.76	1.87	4.77	19.33	7.68	7.88
D_{cnl}	[µg]	29.52	27.09	18.27	44.20	29.77	10.77
D_{ad}	[µg]	194.18	216.27	221.67	150.53	195.66	32.35
TB	[µg]	13.61	18.38	17.17	10.19	14.84	3.70
L	[µg]	58.45	48.75	67.21	50.20	56.15	8.52
PC	[µg]	11.69	13.56	14.52	13.29	13.27	1.18
RS	[µg]	8.88	10.24	11.24	7.95	9.58	1.45
RC	[µg]	2.96	3.47	6.20	3.47	4.03	1.47
RI	[µg]	52.38	105.43	70.27	25.69	63.44	33.45
Total (D_r)	[µg]	147.97	199.83	186.61	110.79	161.30	40.22

% delivered:

		Rat#				mean	SD
		61	62	63	67		
TB	[%]	9.20	9.20	9.20	9.20	9.20	0.00
L	[%]	39.50	24.40	36.02	45.31	36.31	8.82
PC	[%]	7.90	6.79	7.78	12.00	8.62	2.31
RS	[%]	6.00	5.12	6.02	7.18	6.08	0.84
RC	[%]	2.00	1.74	3.32	3.13	2.55	0.80
RI	[%]	35.40	52.76	37.66	23.19	37.25	12.14
Total	[%]	100.00	100.00	100.00	100.00	100.00	0.00
%TB	[%]	9.20	9.20	9.20	9.20	9.20	0.00
%Lobe	[%]	90.80	90.80	90.80	90.80	90.80	0.00

Table AVII.9 Initial regional distribution of 7.4 kDa F-PHEA in lung in vivo. The solute was administered into the airways by "forced solution instillation" (nominal dose = 1.0 mg; used in Fig. III.5 and Section III.b.7, Chapter 3).

Wet weight:

		Rat#				mean	SD
		163	168	176	179		
BW	[g]	350	330	330	320	332.50	12.58
TB	[g]	0.27	0.21	0.21	0.21	0.23	0.03
L	[g]	0.63	0.50	0.43	0.48	0.51	0.09
PC	[g]	0.20	0.16	0.13	0.18	0.17	0.03
RS	[g]	0.21	0.17	0.12	0.15	0.16	0.04
RC	[g]	0.25	0.23	0.14	0.17	0.20	0.05
RI	[g]	0.49	0.41	0.35	0.35	0.40	0.07
Total	[g]	2.05	1.68	1.38	1.54	1.66	0.29
%TB	[%]	13.17	12.50	15.22	13.64	13.63	1.16
%Lobe	[%]	86.83	87.50	84.78	86.36	86.37	1.16

Amount delivered:

		Rat#				mean	SD
		163	168	176	179		
D_L	[µg]	928.04	1056.47	1089.94	1158.40	1058.21	96.60
D_{ctg}	[µg]	15.02	47.81	6.94	48.83	29.65	21.81
D_{cnl}	[µg]	134.16	72.70	83.60	367.11	164.39	137.77
D_{ad}	[µg]	778.86	935.96	999.40	742.46	864.17	123.20
TB	[µg]	71.40	51.95	52.55	47.05	55.74	10.73
L	[µg]	316.76	295.35	308.70	361.40	320.55	28.63
PC	[µg]	44.10	65.60	82.30	82.00	68.50	18.04
RS	[µg]	41.16	29.45	37.35	40.75	37.18	5.43
RC	[µg]	1.26	18.20	10.15	24.90	13.63	10.21
RI	[µg]	265.44	360.70	319.95	180.00	281.52	78.13
Total (D_r)	[µg]	740.12	821.25	811.00	736.10	777.12	45.27

% delivered:

		Rat#				mean	SD
		163	168	176	179		
TB	[%]	9.65	6.33	6.48	6.39	7.21	1.63
L	[%]	42.80	35.96	38.06	49.10	41.48	5.83
PC	[%]	5.96	7.99	10.15	11.14	8.81	2.31
RS	[%]	5.56	3.59	4.61	5.54	4.82	0.94
RC	[%]	0.17	2.22	1.25	3.38	1.76	1.37
RI	[%]	35.86	43.92	39.45	24.45	35.92	8.33
Total	[%]	100.00	100.00	100.00	100.00	100.00	0.00
%TB	[%]	9.65	6.33	6.48	6.39	7.21	1.63
%Lobe	[%]	90.35	93.67	93.52	93.61	92.79	1.63

Table AVII.10 Initial regional distribution of 376 Da F-Na in lung in vivo. The solute was administered into the airways by "forced solution instillation" (nominal dose = 0.02 mg; used in Fig. III.4 and Section III.b.7, Chapter 3).

Wet weight:

		Rat#				mean	SD
		121	124	128	132		
BW	[g]	330	338	335	330	333.25	3.95
TB	[g]	0.16	0.24	0.22	0.26	0.22	0.04
L	[g]	0.47	0.57	0.56	0.56	0.54	0.05
PC	[g]	0.12	0.16	0.17	0.19	0.16	0.03
RS	[g]	0.13	0.20	0.20	0.17	0.18	0.03
RC	[g]	0.14	0.17	0.24	0.16	0.18	0.04
RI	[g]	0.36	0.48	0.44	0.47	0.44	0.05
Total	[g]	1.38	1.82	1.83	1.81	1.71	0.22
%TB	[%]	11.59	13.19	12.05	14.36	12.80	1.24
%Lobe	[%]	88.41	86.81	87.95	85.64	87.20	1.24

Amount delivered:

		Rat#				mean	SD
		121	124	128	132		
D_L	[µg]	26.72	20.02	22.59	20.45	22.45	3.06
D_{ctg}	[µg]	0.77	0.48	2.13	0.20	0.89	0.86
D_{cnl}	[µg]	1.68	0.87	4.47	1.08	2.02	1.67
D_{ad}	[µg]	24.27	18.67	15.99	19.17	19.53	3.46
TB	[µg]	1.29	1.40	1.37	1.30	1.34	0.05
L	[µg]	5.17	4.66	4.90	5.05	4.95	0.22
PC	[µg]	2.46	1.41	1.32	1.42	1.65	0.54
RS	[µg]	2.04	1.17	2.11	3.04	2.09	0.76
RC	[µg]	1.09	0.70	1.38	1.28	1.11	0.30
RI	[µg]	5.13	4.83	4.78	5.40	5.04	0.29
Total (D_r)	[µg]	17.18	14.17	15.86	17.49	16.18	1.51

% delivered:

		Rat#				mean	SD
		121	124	128	132		
TB	[%]	7.51	9.88	8.64	7.43	8.36	1.15
L	[%]	30.09	32.89	30.90	28.87	30.69	1.69
PC	[%]	14.32	9.95	8.32	8.12	10.18	2.88
RS	[%]	11.87	8.26	13.30	17.38	12.70	3.77
RC	[%]	6.34	4.94	8.70	7.32	6.83	1.59
RI	[%]	29.86	34.09	30.14	30.87	31.24	1.95
Total	[%]	100.00	100.00	100.00	100.00	100.00	0.00
%TB	[%]	7.51	9.88	8.64	7.43	8.36	1.15
%Lobe	[%]	92.49	90.12	91.36	92.57	91.64	1.15

Table AVII.11. Dose and remaining 7.4 kDa F-PHEA in each dissected component of the lung at different sacrifice time in vivo, following solute administration into the airways by "forced solution instillation" (FR7150; nominal dose = 0.2 mg; used in Fig. III.8, Chapter 3).

Time	Rat#	BW	Dose [µg]				Remaining F-PHEA [µg]						Total	$\%D_{ad}$
[min]		[g]	D_L	D_{ctg}	D_{cnl}	D_{ad}	TB	L	PC	RS	RC	RI	[µg]	[%]
	61	348	228.46	4.76	29.52	194.18	13.61	58.45	11.69	8.88	2.96	52.38	147.97	76.20
	62	349	245.23	1.87	27.09	216.27	18.38	48.75	13.56	10.24	3.47	105.43	199.83	92.40
5	63	348	244.71	4.77	18.27	221.67	17.17	67.21	14.52	11.24	6.20	70.27	186.61	84.18
	67	338	214.06	19.33	44.20	150.53	10.19	50.20	13.29	7.95	3.47	25.69	110.79	73.60
	mean													81.60
	SD													8.49
	69	320	259.88	7.61	22.22	230.05	16.96	127.40	15.74	25.16	2.82	8.04	196.12	85.25
	72	325	216.02	3.19	8.34	204.49	10.78	117.76	2.80	12.78	0.00	16.44	160.56	78.52
10	79	340	220.82	3.77	22.46	194.59	14.64	40.86	26.12	4.82	9.50	40.58	136.52	70.16
	81	350	213.72	5.93	14.97	192.82	13.08	47.66	4.90	15.46	0.00	35.66	116.76	60.56
	mean													73.62
	SD													10.68
	74	325	240.18	5.87	10.06	224.25	2.80	45.82	6.10	14.48	5.20	50.00	124.40	55.47
	75	315	201.70	10.50	34.06	157.14	5.14	54.40	1.12	12.76	1.24	24.24	98.90	62.94
30	83	320	290.00	5.86	14.90	269.24	6.44	103.56	9.78	17.18	7.80	36.38	181.14	67.28
	84	338	258.93	3.84	17.61	237.48	8.20	87.44	35.54	13.44	12.76	5.24	162.62	68.48
	mean													63.54
	SD													5.88
	68	325	198.46	7.71	9.70	181.05	11.78	36.56	3.66	9.18	4.96	28.76	94.90	52.42
	71	315	236.69	11.97	12.37	212.35	4.24	49.18	0.00	29.10	0.00	24.94	107.46	50.60
60	78	320	256.89	25.69	10.57	220.63	5.12	32.78	7.42	31.94	4.56	20.22	102.04	46.25
	82	338	308.08	7.46	14.90	285.72	12.36	45.46	20.48	25.40	8.68	51.88	164.26	57.49
	mean													51.69
	SD													4.65

Table AVII.11. Dose and remaining 7.4 kDa F-PHEA in each dissected component of the lung at different sacrifice time in vivo, following solute administration into the airways by "forced solution instillation" (FR7150; nominal dose = 0.2 mg; used in Fig. III.8, Chapter 3).

Time	Rat#	BW	Dose [µg]				Remaining F-PHEA [µg]						Total	$\%D_{ad}$
[min]		[g]	D_L	D_{ctg}	D_{cnl}	D_{ad}	TB	L	PC	RS	RC	RI	[µg]	[%]
	73	320	210.78	5.52	13.24	192.02	3.82	46.00	9.24	14.66	3.42	15.02	92.16	48.00
	77	325	215.93	21.59	6.41	187.93	2.80	40.54	2.60	22.28	9.30	15.42	92.94	49.45
120	86	360	326.06	13.53	1.00	311.53	5.88	4.36	15.24	54.30	4.26	59.84	143.88	46.18
	87	340	323.67	35.72	27.26	260.69	2.52	84.92	3.44	8.62	1.70	18.92	120.12	46.08
	mean													47.43
	SD													1.61
	70	325	228.13	4.19	26.67	197.27	10.70	22.04	13.86	20.26	5.08	25.20	97.14	49.24
	76	325	223.56	22.36	9.10	192.10	0.54	39.58	4.60	8.88	0.00	30.16	83.76	43.60
180	80	340	241.09	1.29	23.54	216.26	4.02	20.56	0.00	12.68	1.08	27.46	65.80	30.43
	85	350	295.83	9.11	25.24	261.48	5.30	17.38	4.88	21.74	6.32	90.88	146.50	56.03
	mean													44.82
	SD													10.86

Table AVII.12. Dose and remaining 7.4 kDa F-PHEA in each dissected component of the lung at different sacrifice time in vivo, following solute administration into the airways by "forced solution instillation" (FR7150; nominal dose = 1.0 mg; used in Figs. III.8 and III.9, Chapter 3).

Time	Rat#	BW	Dose [μg]				Remaining F-PHEA [μg]						Total	$\%D_{ad}$
[min]		[g]	D_L	D_{ctg}	D_{cnl}	D_{ad}	TB	L	PC	RS	RC	RI	[μg]	[%]
	163	350	928.04	15.02	134.16	778.86	71.40	316.76	44.10	41.16	1.26	265.44	740.12	95.03
	168	330	1056.47	47.81	72.70	935.96	51.95	295.35	65.60	29.45	18.20	360.70	821.25	87.74
5	176	330	1089.94	6.94	83.60	999.40	52.55	308.70	82.30	37.35	10.15	319.95	811.00	81.15
	179	320	1158.40	48.83	367.11	742.46	47.05	361.40	82.00	40.75	24.90	180.00	736.10	99.14
	mean													90.77
	SD													7.96
	162	345	904.67	16.85	230.27	657.55	26.04	261.45	42.63	43.26	60.19	158.76	592.33	90.08
	167	321	1028.30	20.71	95.94	911.64	52.65	231.35	30.95	65.75	115.65	265.80	762.15	83.60
10	173	350	1117.33	10.53	55.37	1051.44	49.35	261.80	112.60	128.30	132.40	306.15	990.60	94.21
	181	380	1287.26	42.18	175.41	1069.66	63.45	274.35	29.00	156.00	38.80	326.25	887.85	83.00
	mean													87.72
	SD													5.38
	192	350	1120.39	44.36	91.20	984.84	13.80	344.80	21.00	111.15	200.00	145.60	836.35	84.92
	193	350	1031.82	4.23	42.37	985.22	12.65	303.10	11.55	142.45	113.80	249.40	832.95	84.54
20	194	330	1263.78	30.38	213.67	1019.72	46.85	328.95	59.60	103.30	207.00	115.70	861.40	84.47
	195	340	1310.16	10.13	116.74	1183.29	47.90	472.10	42.65	38.00	213.65	150.90	965.20	81.57
	mean													83.88
	SD													1.55
	161	338	816.45	57.11	160.99	598.35	6.30	135.24	7.77	28.35	0.00	335.16	512.82	85.71
	170	320	954.49	10.31	51.97	892.21	18.05	226.55	32.40	47.30	18.00	362.90	705.20	79.04
30	175	330	1153.86	14.73	15.61	1123.52	143.90	271.40	36.30	57.70	10.70	310.15	830.15	73.89
	182	380	1286.23	50.26	361.29	874.69	26.00	222.30	35.40	19.25	68.20	235.25	606.40	69.33
	mean													76.99
	SD													7.04

Table AVII.12. Dose and remaining 7.4 kDa F-PHEA in each dissected component of the lung at different sacrifice time in vivo, following solute administration into the airways by "forced solution instillation" (FR7150; nominal dose = 1.0 mg; used in Figs. III.8 and III.9, Chapter 3).

Time	Rat#	BW	Dose [µg]				Remaining F-PHEA [µg]						Total	$\%D_{ad}$
[min]		[g]	D_L	D_{ctg}	D_{cnl}	D_{ad}	TB	L	PC	RS	RC	RI	[µg]	[%]
	196	350	1302.05	25.13	37.04	1239.89	230.50	333.45	69.50	47.10	31.60	218.20	930.35	75.03
	197	330	1153.80	29.52	70.82	1053.46	119.90	387.10	52.70	40.90	21.55	113.55	735.70	69.84
45	198	330	1225.52	9.62	71.27	1144.63	179.55	413.50	23.30	30.05	7.95	179.45	833.80	72.84
	199	320	1176.36	34.64	151.94	989.79	178.05	314.75	50.80	22.20	22.60	179.90	768.30	77.62
	mean													73.83
	SD													3.30
	160	345	950.09	61.25	125.66	763.19	128.77	61.11	84.42	71.82	10.29	316.05	672.46	88.11
	166	320	1045.78	44.81	136.28	864.70	121.80	172.60	9.25	49.50	6.85	303.35	663.35	76.71
60	172	350	989.82	15.08	102.72	872.02	120.30	199.60	9.10	64.20	3.35	249.15	645.70	74.05
	183	310	1179.70	28.92	119.82	1030.96	145.15	79.85	25.65	16.95	90.60	287.00	645.20	62.58
	mean													75.36
	SD													10.48
	164	351	945.79	16.19	115.16	814.44	275.40	129.50	40.37	45.32	8.03	95.92	594.54	73.00
	169	320	976.07	12.80	67.31	895.96	215.95	113.05	66.05	53.20	10.50	110.70	569.45	63.56
120	174	330	1133.31	10.25	81.95	1041.12	218.25	141.65	15.60	59.65	24.55	165.95	625.65	60.09
	180	380	1382.36	46.16	199.30	1136.89	150.20	175.15	12.00	0.90	43.55	266.50	648.30	57.02
	mean													63.42
	SD													6.92
	165	358	947.20	12.77	108.05	826.38	295.30	118.54	39.38	43.22	12.04	94.78	603.26	73.00
	171	320	1033.17	14.30	37.04	981.84	285.65	172.35	13.45	35.75	15.65	61.00	583.85	59.47
180	177	320	1084.58	20.58	87.00	977.00	310.10	172.15	32.70	53.85	15.55	138.75	723.10	74.01
	178	320	1079.29	66.88	201.29	811.12	210.80	249.60	26.55	18.15	33.75	85.90	624.75	77.02
	mean													70.88
	SD													7.80

Table AVII.13. Dose and remaining 376 Da F-Na in each dissected component of the lung at different sacrifice time in vivo, following solute administration into the airways by "forced solution instillation" (nominal dose = 0.02 mg; used in Figs. III.6 and III.7, Chapter 3).

Time	Rat#	BW	Dose [µg]				Remaining F-Na [µg]						Total	$\%D_{ad}$
[min]		[g]	D_L	D_{ctg}	D_{cnl}	D_{ad}	TB	L	PC	RS	RC	RI	[µg]	[%]
	121	330	26.72	0.77	1.68	24.27	1.29	5.17	2.46	2.04	1.09	5.13	17.18	70.78
	124	338	20.02	0.48	0.87	18.67	1.40	4.66	1.41	1.17	0.70	4.83	14.17	75.90
5	128	335	22.59	2.13	4.47	15.99	1.37	4.90	1.32	2.11	1.38	4.78	15.86	99.20
	132	330	20.45	0.20	1.08	19.18	1.30	5.05	1.42	3.04	1.28	5.40	17.49	91.21
	mean													84.27
	SD													13.20
	90	315	26.85	2.58	4.33	19.95	0.63	1.73	2.06	1.31	0.00	3.29	9.02	45.22
	94	335	25.43	0.37	1.37	23.69	0.81	4.87	2.12	1.73	0.12	4.82	14.47	61.08
10	127	350	21.95	2.02	1.84	18.08	1.01	3.76	0.37	2.36	2.12	3.18	12.80	70.78
	131	350	20.78	0.27	2.22	18.29	0.85	2.79	0.15	1.97	0.95	4.45	11.16	61.00
	mean													59.52
	SD													10.58
	92	330	24.24	3.00	6.12	15.12	0.40	1.91	0.38	1.33	0.56	1.22	5.80	38.35
	93	325	25.81	0.44	2.36	23.02	0.71	1.42	0.67	1.58	0.49	1.88	6.75	29.32
20	119	320	24.27	0.43	2.46	21.38	0.66	1.90	1.15	1.40	0.36	1.22	6.69	31.29
	130	325	21.32	1.56	0.97	18.79	1.22	1.82	1.06	1.38	0.51	1.32	7.31	38.90
	mean													34.47
	SD													4.87
	88	320	27.68	1.08	2.67	23.93	0.19	1.39	0.74	0.56	0.13	0.72	3.73	15.59
	122	335	23.67	0.40	0.88	22.40	0.19	1.79	0.82	0.53	0.25	0.69	4.27	19.07
30	126	340	21.78	0.83	2.00	18.95	0.38	0.82	0.58	0.53	0.21	0.52	3.04	16.04
	134	350	20.96	0.23	2.21	18.53	0.44	1.66	0.35	0.55	0.51	0.82	4.33	23.37
	mean													18.52
	SD													3.59

Table AVII.13. Dose and remaining 376 Da F-Na in each dissected component of the lung at different sacrifice time in vivo, following solute administration into the airways by "forced solution instillation" (nominal dose = 0.02 mg; used in Figs. III.6 and III.7, Chapter 3).

Time	Rat#	BW	Dose [µg]				Remaining F-Na [µg]						Total	$\%D_{ad}$
[min]		[g]	D_L	D_{ctg}	D_{cnl}	D_{ad}	TB	L	PC	RS	RC	RI	[µg]	[%]
	89	310	26.24	0.85	1.90	23.49	3.82	46.00	9.24	14.66	3.42	15.02	92.16	392.34
	120	330	25.57	2.35	0.59	22.63	2.80	40.54	2.60	22.28	9.30	15.42	92.94	410.78
60	123	330	22.13	2.40	1.42	18.30	5.88	4.36	15.24	54.30	4.26	59.84	143.88	786.19
	133	330	19.78	0.23	0.69	18.85	2.52	84.92	3.44	8.62	1.70	18.92	120.12	637.17
	mean													556.62
	SD													189.25
	91	325	25.87	3.81	1.83	20.23	0.08	0.00	0.00	0.00	0.00	0.08	0.16	0.79
	118	345	21.02	3.27	1.09	16.67	0.08	0.03	0.00	0.04	0.00	0.00	0.15	0.90
120	125	325	21.40	0.84	1.03	19.53	0.04	0.04	0.01	0.00	0.00	0.00	0.09	0.46
	129	340	24.65	0.63	0.78	23.24	0.06	0.03	0.00	0.00	0.00	0.00	0.09	0.39
	mean													0.63
	SD													0.25

Table AVII.14. Dose, and amount and % of administered dose of 7.4 kDa F-PHEA absorbed from airways to perfusate in the IPRL at 37 °C. (FR7150; nominal dose = 0.1 mg; used in Fig. III.10, Chapter 3 and Fig. V.4, Chapter 5).

Amount delivered:

		Rat#					
		97	98	99	100		
BW	[g]	300	340	320	340		
D_L	[µg]	127.53	121.03	91.19	91.73		
D_{ctg}	[µg]	3.46	7.70	3.38	3.77		
D_{cnl}	[µg]	23.59	19.39	1.44	22.23	mean	SD
D_{ad}	[µg]	100.48	93.94	86.37	65.73	86.63	15.08

Transferred amount: [µg]

		Rat#			
		97	98	99	100
0	[min]	0.000	0.000	0.000	0.000
5		32.712	4.810	13.104	6.954
10		49.169	6.369	22.315	14.662
15		43.496	24.574	23.752	17.550
20		44.044	21.420	30.968	27.882
25		43.037	32.052	34.646	41.112
30		44.173	30.732	37.086	45.998
45		51.462	49.473	33.938	45.687
60		55.974	59.009	41.153	47.420
90		57.328	49.551	45.159	45.552
120		55.271	49.138	51.039	49.097
150		58.034	59.070	46.670	47.041
180		59.705	64.734	54.000	42.678

% transferred: [%]						mean	SD
0	[min]	0.00	0.00	0.00	0.00	**0.00**	**0.00**
5		32.56	5.12	15.17	10.58	**15.86**	**11.87**
10		48.93	6.78	25.84	22.31	**25.96**	**17.41**
15		43.29	26.16	27.50	26.70	**30.91**	**8.27**
20		43.83	22.80	35.86	42.42	**36.23**	**9.60**
25		42.83	34.12	40.11	62.55	**44.90**	**12.31**
30		43.96	32.71	42.94	69.98	**47.40**	**15.89**
45		51.22	52.66	39.29	69.51	**53.17**	**12.43**
60		55.71	62.82	47.65	72.14	**59.58**	**10.42**
90		57.05	52.75	52.29	69.30	**57.85**	**7.93**
120		55.01	52.31	59.09	74.69	**60.28**	**10.01**
150		57.76	62.88	54.03	71.57	**61.56**	**7.59**
180		59.42	68.91	62.52	64.93	**63.95**	**4.01**

Table AVII.15. Dose, and amount and % of administered dose of 7.4 kDa F-PHEA absorbed from airways to perfusate in the IPRL at 37 °C. (FR7150; nominal dose = 0.2 mg; used in Fig. III.10, Chapter 3 and Fig. IV.4, Chapter 4).

Amount delivered:

		Rat#					
		28	29	32	33		
BW	[g]	316	320	320	340		
D_L	[µg]	244.81	222.05	204.45	210.28		
D_{ctg}	[µg]	4.55	1.00	1.27	3.83		
D_{cnl}	[µg]	9.31	41.21	5.32	44.14	mean	SD
D_{ad}	[µg]	230.95	179.84	197.86	162.31	192.74	29.32

Transferred amount: [µg]

	Rat#			
	28	29	32	33
0 [min]	0.000	0.000	0.000	0.000
5	56.305	30.331	33.839	22.367
10	76.241	46.874	54.380	26.071
15	85.250	67.120	66.884	33.979
20	92.448	72.954	66.533	38.806
25	107.621	91.048	69.982	40.236
30	95.405	99.755	100.574	48.144
45	111.823	104.814	110.574	59.297
60	127.315	119.839	118.417	70.300
90	123.973	121.747	123.325	79.622
120	132.877	121.701	133.231	90.373
150	122.375	119.726	133.631	93.464
180	138.691	120.635	135.091	94.619

% transferred: [%]					mean	SD
0 [min]	0.00	0.00	0.00	0.00	**0.00**	**0.00**
5	24.38	16.87	17.10	13.78	**18.03**	**4.49**
10	33.01	26.06	27.48	16.06	**25.66**	**7.06**
15	36.91	37.32	33.80	20.93	**32.24**	**7.70**
20	40.03	40.57	33.63	23.91	**34.53**	**7.75**
25	46.60	50.63	35.37	24.79	**39.35**	**11.66**
30	41.31	55.47	50.83	29.66	**44.32**	**11.41**
45	48.42	58.28	55.88	36.53	**49.78**	**9.78**
60	55.13	66.64	59.85	43.31	**56.23**	**9.82**
90	53.68	67.70	62.33	49.06	**58.19**	**8.39**
120	57.53	67.67	67.34	55.68	**62.06**	**6.34**
150	52.99	66.57	67.54	57.58	**61.17**	**7.06**
180	60.05	67.08	68.28	58.30	**63.43**	**4.99**

Table AVII.16. Dose, and amount and % of administered dose of 7.4 kDa F-PHEA absorbed from airways to perfusate in the IPRL at 37 °C. (FR7150; nominal dose = 0.5 mg; used in Fig. III.10, Chapter 3).

Amount delivered:

		Rat#					
		101	102	103	104		
BW	[g]	360	345	330	330		
D_L	[µg]	585.04	566.28	554.78	535.42		
D_{ctg}	[µg]	23.86	16.33	11.33	53.16		
D_{cnl}	[µg]	154.46	173.75	204.90	142.05	mean	SD
D_{ad}	[µg]	406.72	376.20	338.55	340.21	365.42	32.55

Transferred amount: [µg]

		Rat#			
		101	102	103	104
0	[min]	0.000	0.000	0.000	0.000
5		0.000	33.594	13.763	22.441
10		7.124	59.805	26.219	37.707
15		54.018	75.215	31.380	56.604
20		59.057	97.137	54.873	77.189
25		74.727	96.412	50.465	99.465
30		93.362	109.277	51.095	106.296
45		108.048	114.903	61.787	125.410
60		135.872	132.072	62.913	128.038
90		155.865	141.266	76.028	133.717
120		165.382	138.725	86.855	151.252
150		165.140	159.437	89.380	150.710
180		169.537	168.024	91.992	157.254

% transferred: [%]						mean	SD
0	[min]	0.00	0.00	0.00	0.00	**0.00**	**0.00**
5		0.00	8.93	4.07	6.60	**4.90**	**3.82**
10		1.75	15.90	7.74	11.08	**9.12**	**5.94**
15		13.28	19.99	9.27	16.64	**14.80**	**4.59**
20		14.52	25.82	16.21	22.69	**19.81**	**5.33**
25		18.37	25.63	14.91	29.24	**22.04**	**6.56**
30		22.95	29.05	15.09	31.24	**24.58**	**7.23**
45		26.57	30.54	18.25	36.86	**28.06**	**7.79**
60		33.41	35.11	18.58	37.63	**31.18**	**8.58**
90		38.32	37.55	22.46	39.30	**34.41**	**8.00**
120		40.66	36.88	25.65	44.46	**36.91**	**8.12**
150		40.60	42.38	26.40	44.30	**38.42**	**8.15**
180		41.68	44.66	27.17	46.22	**39.94**	**8.71**

Table AVII.17. Dose, and amount and % of administered dose of 7.4 kDa F-PHEA absorbed from airways to perfusate in the IPRL at 37 °C. (FR7150; nominal dose = 1.0 mg; used in Fig. III.10, Chapter 3 and Fig. V.5, Chapter 5).

Amount delivered:

		Rat#					
		Pre#1	1	2	3		
BW	[g]	360	335	338	320		
D_L	[µg]	1056.00	1129.55	997.50	1013.42		
D_{ctg}	[µg]	19.61	80.35	13.85	78.60		
D_{cnl}	[µg]	0.00	21.15	48.60	94.89	mean	SD
D_{ad}	[µg]	1036.39	1028.05	935.05	839.93	959.86	92.21

Transferred amount: [µg]

		Rat#			
		Pre#1	1	2	3
0	[min]	0.000	0.000	0.000	0.000
5		44.483	75.571	24.226	11.292
10		73.584	136.624	62.912	33.443
15		118.736	159.297	82.621	50.870
20		136.952	159.607	118.496	64.783
25		158.397	185.524	118.549	72.622
30		161.993	205.923	131.979	80.887
45		187.130	240.553	155.633	106.510
60		214.321	261.511	177.879	119.493
90		207.616	284.691	272.887	143.433
120		280.357	341.718	275.482	161.425
150		320.230	459.997	294.658	174.395
180		372.001	472.772	330.966	179.582

% transferred: [%]						mean	SD
0	[min]	0.00	0.00	0.00	0.00	**0.00**	**0.00**
5		4.29	7.35	2.59	1.34	**3.89**	**2.60**
10		7.10	13.29	6.73	3.98	**7.77**	**3.93**
15		11.46	15.50	8.84	6.06	**10.46**	**4.02**
20		13.21	15.53	12.67	7.71	**12.28**	**3.29**
25		15.28	18.05	12.68	8.65	**13.66**	**4.00**
30		15.63	20.03	14.11	9.63	**14.85**	**4.29**
45		18.06	23.40	16.64	12.68	**17.70**	**4.43**
60		20.68	25.44	19.02	14.23	**19.84**	**4.63**
90		20.03	27.69	29.18	17.08	**23.50**	**5.86**
120		27.05	33.24	29.46	19.22	**27.24**	**5.92**
150		30.90	44.74	31.51	20.76	**31.98**	**9.83**
180		35.89	45.99	35.40	21.38	**34.66**	**10.11**

Table AVII.18. Dose, and amount and % of administered dose of 7.4 kDa F-PHEA absorbed from airways to perfusate in the IPRL at 37 °C. (FR7150; nominal dose = 5.0 mg; used in Fig. III.10, Chapter 3 and Fig. IV.5, Chapter 4).

Amount delivered:

		Rat#					
		34	63	65	66		
BW	[g]	340	310	320	310		
D_L	[µg]	5430.41	4915.70	5775.32	6066.67		
D_{ctg}	[µg]	546.78	518.32	396.99	242.53		
D_{cnl}	[µg]	56.67	884.62	887.10	93.87	mean	SD
D_{ad}	[µg]	4826.96	3512.76	4491.23	5730.27	4640.31	915.87

Transferred amount: [µg]

		Rat#			
		34	63	65	66
0	[min]	0.000	0.000	0.000	0.000
5		68.803	202.030	17.305	1.953
10		156.824	283.563	46.248	6.232
15		225.552	362.523	68.741	11.668
20		293.515	389.294	89.800	12.056
25		393.420	442.989	108.222	23.122
30		384.408	484.131	116.577	30.969
45		468.267	555.121	184.931	63.419
60		520.815	618.480	164.760	98.076
90		674.130	767.234	194.098	129.216
120		689.220	757.194	229.110	156.256
150		755.954	871.323	252.819	193.961
180		769.876	994.786	303.068	198.277

% transferred: [%]						mean	SD
0	[min]	0.00	0.00	0.00	0.00	**0.00**	**0.00**
5		1.43	5.75	0.39	0.03	**1.90**	**2.64**
10		3.25	8.07	1.03	0.11	**3.11**	**3.56**
15		4.67	10.32	1.53	0.20	**4.18**	**4.50**
20		6.08	11.08	2.00	0.21	**4.84**	**4.83**
25		8.15	12.61	2.41	0.40	**5.89**	**5.55**
30		7.96	13.78	2.60	0.54	**6.22**	**5.93**
45		9.70	15.80	4.12	1.11	**7.68**	**6.48**
60		10.79	17.61	3.67	1.71	**8.44**	**7.25**
90		13.97	21.84	4.32	2.25	**10.60**	**9.07**
120		14.28	21.56	5.10	2.73	**10.92**	**8.67**
150		15.66	24.80	5.63	3.38	**12.37**	**9.86**
180		15.95	28.32	6.75	3.46	**13.62**	**11.13**

Table AVII.19. Dose, and amount and % of administered dose of 7.4 kDa F-PHEA absorbed from airways to perfusate in the IPRL at 30 °C. (FR7150; nominal dose = 0.2 mg; used in Fig. IV.4, Chapter 4).

Amount delivered:

		Rat#					
		4	9	50	52		
BW	[g]	348	330	340	320		
D_L	[µg]	213.44	215.72	204.46	234.16		
D_{ctg}	[µg]	2.48	12.20	14.63	8.69		
D_{cnl}	[µg]	16.58	18.96	10.20	21.10	mean	SD
D_{ad}	[µg]	194.38	184.56	179.63	204.37	190.74	10.96

Transferred amount: [µg]

		Rat#			
		4	9	50	52
0	[min]	0.000	0.000	0.000	0.000
5		16.464	18.235	12.179	15.164
10		24.978	28.736	19.759	28.612
15		34.502	35.749	27.376	33.414
20		36.446	39.385	34.794	41.794
25		45.524	46.232	42.536	59.962
30		54.154	56.402	43.506	66.768
45		60.724	69.505	46.111	68.893
60		68.266	73.104	53.296	69.486
90		75.556	79.619	55.416	67.646
120		76.216	79.416	59.727	71.734
150		77.111	79.435	63.068	79.950
180		77.752	77.238	63.625	78.723

% transferred: [%]						mean	SD
0	[min]	0.00	0.00	0.00	0.00	**0.00**	**0.00**
5		8.47	9.88	6.78	7.42	**8.14**	**1.35**
10		12.85	15.57	11.00	14.00	**13.36**	**1.93**
15		17.75	19.37	15.24	16.35	**17.18**	**1.79**
20		18.75	21.34	19.37	20.45	**19.98**	**1.15**
25		23.42	25.05	23.68	29.34	**25.37**	**2.74**
30		27.86	30.56	24.22	32.67	**28.83**	**3.65**
45		31.24	37.66	25.67	33.71	**32.07**	**5.02**
60		35.12	39.61	29.67	34.00	**34.60**	**4.08**
90		38.87	43.14	30.85	33.10	**36.49**	**5.57**
120		39.21	43.03	33.25	35.10	**37.65**	**4.37**
150		39.67	43.04	35.11	39.12	**39.24**	**3.25**
180		40.00	41.85	35.42	38.52	**38.95**	**2.72**

Table AVII.20. Dose, and amount and % of administered dose of 7.4 kDa F-PHEA absorbed from airways to perfusate in the IPRL at 25 °C. (FR7150; nominal dose = 0.2 mg; used in Figs. IV.4 and IV.6, Chapter 4).

Amount delivered:

		Rat#					
		24	35	36	37		
BW	[g]	370	325	358	348		
D_L	[µg]	293.43	238.61	197.71	185.08		
D_{ctg}	[µg]	4.37	1.65	8.92	15.38		
D_{cnl}	[µg]	40.34	15.72	39.55	7.76	mean	SD
D_{ad}	[µg]	248.72	221.24	149.24	161.94	195.29	47.47

Transferred amount: [µg]

	Rat#			
	24	35	36	37
0 [min]	0.000	0.000	0.000	0.000
5	10.426	8.745	2.717	3.065
10	26.329	17.435	4.554	1.821
15	29.580	30.200	7.981	6.416
20	31.122	33.635	14.949	7.021
25	39.222	39.750	15.020	14.948
30	43.062	43.758	17.932	15.700
45	49.802	62.423	24.941	22.839
60	61.375	68.499	25.102	30.103
90	68.479	78.649	30.771	38.297
120	70.840	95.968	32.866	41.009
150	70.924	103.339	33.574	40.626
180	76.842	109.910	34.773	47.524

% transferred: [%]						mean	SD
0 [min]	0.00	0.00	0.00	0.00	**0.00**	**0.00**
5	4.19	3.95	1.82	1.89	**2.96**	**1.28**
10	10.59	7.88	3.05	1.12	**5.66**	**4.34**
15	11.89	13.65	5.35	3.96	**8.71**	**4.77**
20	12.51	15.20	10.02	4.34	**10.52**	**4.63**
25	15.77	17.97	10.06	9.23	**13.26**	**4.28**
30	17.31	19.78	12.02	9.69	**14.70**	**4.65**
45	20.02	28.22	16.71	14.10	**19.76**	**6.13**
60	24.68	30.96	16.82	18.59	**22.76**	**6.42**
90	27.53	35.55	20.62	23.65	**26.84**	**6.46**
120	28.48	43.38	22.02	25.32	**29.80**	**9.43**
150	28.52	46.71	22.50	25.09	**30.70**	**10.95**
180	30.89	49.68	23.30	29.35	**33.31**	**11.40**

Table AVII.21. Dose, and amount and % of administered dose of 7.4 kDa F-PHEA absorbed from airways to perfusate in the IPRL at 25 °C. (FR7150; nominal dose = 0.5 mg; used in Figs. IV.6, Chapter 4).

Amount delivered:

		Rat#					
		135	136	137	138		
BW	[g]	380	320	350	360		
D_L	[µg]	581.75	558.07	546.82	502.47		
D_{ctg}	[µg]	25.47	25.69	43.47	27.70		
D_{cnl}	[µg]	85.26	84.76	13.32	102.66	mean	SD
D_{ad}	[µg]	471.02	447.62	490.03	372.11	445.20	51.72

Transferred amount: [µg]

		Rat#			
		135	136	137	138
0	[min]	0.000	0.000	0.000	0.000
5		5.076	5.889	0.000	0.825
10		10.558	7.061	8.118	9.803
15		11.284	9.736	9.103	18.946
20		19.191	14.634	21.397	25.612
25		46.064	18.400	33.071	37.561
30		54.976	19.428	35.186	45.141
45		63.171	32.314	59.479	55.767
60		75.351	32.415	71.060	72.739
90		93.653	52.266	93.774	87.030
120		113.870	56.326	101.555	98.467
150		127.337	59.010	109.874	106.971
180		137.952	75.359	136.360	119.380

% transferred: [%]						mean	SD
0	[min]	0.00	0.00	0.00	0.00	**0.00**	**0.00**
5		1.08	1.32	0.00	0.22	**0.65**	**0.64**
10		2.24	1.58	1.66	2.63	**2.03**	**0.50**
15		2.40	2.18	1.86	5.09	**2.88**	**1.49**
20		4.07	3.27	4.37	6.88	**4.65**	**1.56**
25		9.78	4.11	6.75	10.09	**7.68**	**2.82**
30		11.67	4.34	7.18	12.13	**8.83**	**3.74**
45		13.41	7.22	12.14	14.99	**11.94**	**3.36**
60		16.00	7.24	14.50	19.55	**14.32**	**5.17**
90		19.88	11.68	19.14	23.39	**18.52**	**4.93**
120		24.18	12.58	20.72	26.46	**20.99**	**6.08**
150		27.03	13.18	22.42	28.75	**22.85**	**6.97**
180		29.29	16.84	27.83	32.08	**26.51**	**6.69**

Table AVII.22. Dose, and amount and % of administered dose of 7.4 kDa F-PHEA absorbed from airways to perfusate in the IPRL at 25 °C. (FR7150; nominal dose = 1.0 mg; used in Fig. IV.6, Chapter 4).

Amount delivered:

		Rat#					
		5	6	7	17		
BW	[g]	370	360	364	380		
D_L	[µg]	1052.81	1065.00	1136.98	1135.08		
D_{ctg}	[µg]	44.51	37.26	34.40	53.02		
D_{cnl}	[µg]	12.99	41.30	27.77	18.45	mean	SD
D_{ad}	[µg]	995.31	986.44	1074.81	1063.61	1030.04	45.60

Transferred amount: [µg]

	Rat#			
	5	6	7	17
0 [min]	0.000	0.000	0.000	0.000
5	3.500	0.407	10.856	0.179
10	11.646	15.202	7.967	8.834
15	23.566	18.937	21.059	19.728
20	25.586	25.786	42.140	28.366
25	35.308	41.683	59.845	36.074
30	53.607	47.007	73.509	50.618
45	64.412	67.309	108.023	73.830
60	88.716	87.096	128.680	99.040
90	110.109	110.843	176.726	123.029
120	133.964	132.068	192.729	158.494
150	163.675	149.434	218.081	171.724
180	171.871	152.132	250.350	196.174

% transferred: [%]					mean	SD
0 [min]	0.00	0.00	0.00	0.00	**0.00**	**0.00**
5	0.35	0.04	1.01	0.02	**0.35**	**0.46**
10	1.17	1.54	0.74	0.83	**1.07**	**0.36**
15	2.37	1.92	1.96	1.85	**2.03**	**0.23**
20	2.57	2.61	3.92	2.67	**2.94**	**0.65**
25	3.55	4.23	5.57	3.39	**4.18**	**0.99**
30	5.39	4.77	6.84	4.76	**5.44**	**0.98**
45	6.47	6.82	10.05	6.94	**7.57**	**1.66**
60	8.91	8.83	11.97	9.31	**9.76**	**1.49**
90	11.06	11.24	16.44	11.57	**12.58**	**2.59**
120	13.46	13.39	17.93	14.90	**14.92**	**2.13**
150	16.44	15.15	20.29	16.15	**17.01**	**2.26**
180	17.27	15.42	23.29	18.44	**18.61**	**3.36**

Table AVII.23. Dose, and amount and % of administered dose of 7.4 kDa F-PHEA absorbed from airways to perfusate in the IPRL at 25 °C. (FR7150; nominal dose = 5.0 mg; used in Figs. IV.5 and IV.6, Chapter 4).

Amount delivered:

		Rat#					
		44	46	47	49		
BW	[g]	385	387	385	335		
D_L	[µg]	4883.15	5485.39	5064.19	5272.13		
D_{ctg}	[µg]	92.36	256.29	38.91	14.48		
D_{cnl}	[µg]	862.98	508.44	747.56	248.99	mean	SD
D_{ad}	[µg]	3927.81	4720.66	4277.72	5008.66	4483.71	477.21

Transferred amount: [µg]

	Rat#			
	44	46	47	49
0 [min]	0.000	0.000	0.000	0.000
5	8.612	5.739	48.966	21.866
10	45.218	18.997	182.002	79.023
15	87.678	35.185	252.336	117.036
20	138.756	44.919	317.349	164.087
25	185.317	64.548	353.957	198.745
30	226.032	82.626	430.032	240.988
45	295.449	126.949	533.042	294.134
60	382.533	168.234	586.335	467.801
90	557.657	214.567	679.641	561.391
120	603.952	255.981	831.123	681.972
150	649.603	301.536	841.936	734.562
180	708.367	370.583	984.380	818.216

% transferred: [%]					mean	SD
0 [min]	0.00	0.00	0.00	0.00	**0.00**	**0.00**
5	0.22	0.12	1.14	0.44	**0.48**	**0.46**
10	1.15	0.40	4.25	1.58	**1.85**	**1.68**
15	2.23	0.75	5.90	2.34	**2.80**	**2.19**
20	3.53	0.95	7.42	3.28	**3.79**	**2.68**
25	4.72	1.37	8.27	3.97	**4.58**	**2.85**
30	5.75	1.75	10.05	4.81	**5.59**	**3.43**
45	7.52	2.69	12.46	5.87	**7.14**	**4.08**
60	9.74	3.56	13.71	9.34	**9.09**	**4.18**
90	14.20	4.55	15.89	11.21	**11.46**	**5.00**
120	15.38	5.42	19.43	13.62	**13.46**	**5.89**
150	16.54	6.39	19.68	14.67	**14.32**	**5.68**
180	18.03	7.85	23.01	16.34	**16.31**	**6.31**

Table AVII.24. Dose, and amount and % of administered dose of 7.4 kDa F-PHEA absorbed from airways to perfusate in the IPRL in the absence of DNP/OUA at 37 °C (FR7150; nominal dose = 0.2 mg; used in Figs. IV.9, IV.10 and IV.16, Chapter 4).

Amount delivered:

		Rat#					
		214	215	219	221		
BW	[g]	350	325	335	335		
D_L	[µg]	248.99	255.33	274.77	263.26		
D_{ctg}	[µg]	43.40	5.43	2.14	2.93		
D_{cnl}	[µg]	12.05	62.54	42.19	61.21	mean	SD
D_{ad}	[µg]	193.54	187.36	230.44	199.12	202.62	19.16

Transferred amount: [µg]

	Rat#			
	214	215	219	221
0 [min]	0.000	0.000	0.000	0.000
5	13.175	7.419	9.417	11.973
10	34.839	18.901	17.780	19.174
15	47.415	26.756	32.514	27.035
20	62.799	33.873	41.363	45.931
25	77.011	46.046	53.237	70.079
30	86.923	47.883	69.028	72.127
45	107.647	58.115	89.277	99.352
60	129.952	62.149	120.997	105.487

% transferred: [%]					mean	SD
0 [min]	0.00	0.00	0.00	0.00	**0.00**	**0.00**
5	6.81	3.96	4.09	6.01	**5.22**	**1.42**
10	18.00	10.09	7.72	9.63	**11.36**	**4.55**
15	24.50	14.28	14.11	13.58	**16.62**	**5.26**
20	32.45	18.08	17.95	23.07	**22.89**	**6.81**
25	39.79	24.58	23.10	35.19	**30.67**	**8.13**
30	44.91	25.56	29.95	36.22	**34.16**	**8.40**
45	55.62	31.02	38.74	49.90	**43.82**	**11.04**
60	67.14	33.17	52.51	52.98	**51.45**	**13.95**

Table AVII.25. Dose, and amount and % of administered dose of 7.4 kDa F-PHEA absorbed from airways to perfusate in the IPRL in the presence of 0.05 mM DNP at 37 °C (FR7150; nominal dose = 0.2 mg; used in Figs. IV.9 and IV.10, Chapter 4).

Amount delivered:

		Rat#					
		244	245	246	247		
BW	[g]	325	320	320	320		
D_L	[µg]	225.24	230.78	228.84	217.86		
D_{ctg}	[µg]	3.34	3.73	2.86	2.02		
D_{cnl}	[µg]	23.47	70.95	42.32	44.99	mean	SD
D_{ad}	[µg]	198.43	156.10	183.66	170.85	177.26	18.06

Transferred amount: [µg]

	Rat#			
	244	245	246	247
0 [min]	0.000	0.000	0.000	0.000
5	19.231	10.447	8.795	15.470
10	40.742	21.100	22.112	29.367
15	50.558	29.208	35.290	39.806
20	59.450	39.394	43.487	42.126
25	66.959	50.039	52.625	48.151
30	76.278	56.577	53.526	52.500
45	95.792	62.650	62.584	64.190
60	100.940	69.504	71.778	75.132

% transferred: [%]					mean	SD
0 [min]	0.00	0.00	0.00	0.00	**0.00**	**0.00**
5	9.69	6.69	4.79	9.05	**7.56**	**2.25**
10	20.53	13.52	12.04	17.19	**15.82**	**3.82**
15	25.48	18.71	19.21	23.30	**21.68**	**3.26**
20	29.96	25.24	23.68	24.66	**25.88**	**2.79**
25	33.74	32.06	28.65	28.18	**30.66**	**2.68**
30	38.44	36.24	29.14	30.73	**33.64**	**4.42**
45	48.27	40.13	34.08	37.57	**40.01**	**6.04**
60	50.87	44.53	39.08	43.98	**44.61**	**4.84**

Table AVII.26. Dose, and amount and % of administered dose of 7.4 kDa F-PHEA absorbed from airways to perfusate in the IPRL in the presence of 0.1 mM DNP at 37 °C (FR7150; nominal dose = 0.2 mg; used in Figs. IV.9 and IV.10, Chapter 4).

Amount delivered:

		Rat#					
		250	251	252	253		
BW	[g]	320	350	350	350		
D_L	[µg]	237.99	224.53	244.90	247.66		
D_{ctg}	[µg]	2.40	3.57	2.53	0.85		
D_{cnl}	[µg]	36.51	64.03	59.97	54.39	mean	SD
D_{ad}	[µg]	199.08	156.93	182.40	192.42	182.71	18.50

Transferred amount: [µg]

		Rat#			
		250	251	252	253
0	[min]	0.000	0.000	0.000	0.000
5		18.040	9.306	13.909	21.189
10		25.751	20.019	26.228	35.371
15		41.000	31.301	39.315	40.833
20		35.411	37.557	41.982	45.603
25		45.313	44.091	48.721	60.408
30		48.717	46.530	51.923	63.254
45		57.871	54.824	60.774	70.588
60		63.738	64.538	71.498	84.332

% transferred: [%]						mean	SD
0	[min]	0.00	0.00	0.00	0.00	**0.00**	**0.00**
5		9.06	5.93	7.63	11.01	**8.41**	**2.16**
10		12.94	12.76	14.38	18.38	**14.61**	**2.62**
15		20.59	19.95	21.55	21.22	**20.83**	**0.71**
20		17.79	23.93	23.02	23.70	**22.11**	**2.91**
25		22.76	28.10	26.71	31.39	**27.24**	**3.57**
30		24.47	29.65	28.47	32.87	**28.87**	**3.47**
45		29.07	34.94	33.32	36.68	**33.50**	**3.26**
60		32.02	41.13	39.20	43.83	**39.04**	**5.05**

Table AVII.27. Dose, and amount and % of administered dose of 7.4 kDa F-PHEA absorbed from airways to perfusate in the IPRL in the presence of 0.2 mM DNP at 37 °C (FR7150; nominal dose = 0.2 mg; used in Figs. IV.9 and IV.10, Chapter 4).

Amount delivered:

		Rat#					
		213	216	248	249		
BW	[g]	345	320	320	340		
D_L	[µg]	192.34	250.72	219.40	213.67		
D_{ctg}	[µg]	9.36	2.26	8.73	1.57		
D_{cnl}	[µg]	66.63	52.89	51.05	45.85	mean	SD
D_{ad}	[µg]	116.35	195.57	159.62	166.25	159.45	32.70

Transferred amount: [µg]

		Rat#			
		213	216	248	249
0	[min]	0.000	0.000	0.000	0.000
5		3.236	9.756	9.179	11.287
10		8.716	17.950	16.255	19.356
15		14.979	27.265	18.840	28.354
20		22.318	33.831	27.264	36.653
25		30.475	35.028	28.770	38.819
30		32.816	39.250	32.418	43.081
45		39.658	44.687	40.029	51.315
60		37.240	57.724	49.041	55.885

% transferred: [%]						mean	SD
0	[min]	0.00	0.00	0.00	0.00	**0.00**	**0.00**
5		2.78	4.99	5.75	6.79	**5.08**	**1.70**
10		7.49	9.18	10.18	11.64	**9.62**	**1.75**
15		12.87	13.94	11.80	17.06	**13.92**	**2.27**
20		19.18	17.30	17.08	22.05	**18.90**	**2.30**
25		26.19	17.91	18.02	23.35	**21.37**	**4.10**
30		28.20	20.07	20.31	25.91	**23.62**	**4.08**
45		34.09	22.85	25.06	30.87	**28.22**	**5.17**
60		32.01	29.52	30.72	33.62	**31.47**	**1.76**

Table AVII.28. Dose, and amount and % of administered dose of 7.4 kDa F-PHEA absorbed from airways to perfusate in the IPRL in the presence of 0.5 mM DNP at 37 °C (FR7150; nominal dose = 0.2 mg; used in Figs. IV.9 and IV.10, Chapter 4).

Amount delivered:

		Rat#					
		211	212	220	222		
BW	[g]	355	325	325	330		
D_L	[µg]	219.30	243.73	247.31	258.56		
D_{ctg}	[µg]	2.25	2.60	3.59	1.51		
D_{cnl}	[µg]	53.70	48.24	62.08	46.62	mean	SD
D_{ad}	[µg]	163.35	192.89	181.64	210.43	187.08	19.76

Transferred amount: [µg]

	Rat#			
	211	212	220	222
0 [min]	0.000	0.000	0.000	0.000
5	4.249	7.817	8.140	16.588
10	7.703	13.875	17.090	19.170
15	12.087	19.268	23.035	31.925
20	13.935	29.712	29.258	40.044
25	11.564	30.489	24.991	42.983
30	19.122	36.823	41.078	44.007
45	23.410	37.256	41.105	63.128
60	25.903	36.490	42.614	71.871

% transferred: [%]					mean	SD
0 [min]	0.00	0.00	0.00	0.00	**0.00**	**0.00**
5	2.60	4.05	4.48	7.88	**4.75**	**2.24**
10	4.72	7.19	9.41	9.11	**7.61**	**2.16**
15	7.40	9.99	12.68	15.17	**11.31**	**3.36**
20	8.53	15.40	16.11	19.03	**14.77**	**4.44**
25	7.08	15.81	13.76	20.43	**14.27**	**5.54**
30	11.71	19.09	22.62	20.91	**18.58**	**4.80**
45	14.33	19.31	22.63	30.00	**21.57**	**6.57**
60	15.86	18.92	23.46	34.15	**23.10**	**8.01**

Table AVII.29. Dose, and amount and % of administered dose of 7.4 kDa F-PHEA absorbed from airways to perfusate in the IPRL in the presence of 1.0 mM DNP at 37 °C (FR7150; nominal dose = 0.2 mg; used in Figs. IV.9, IV.10 and IV.17, Chapter 4).

Amount delivered:

		Rat#					
		209	210	217	218		
BW	[g]	330	360	355	345		
D_L	[µg]	213.87	212.81	245.48	244.89		
D_{ctg}	[µg]	3.88	9.59	3.66	2.68		
D_{cnl}	[µg]	52.95	38.57	46.21	34.79	mean	SD
D_{ad}	[µg]	157.04	164.65	195.61	207.42	181.18	24.17

Transferred amount: [µg]

	Rat#			
	209	210	217	218
0 [min]	0.000	0.000	0.000	0.000
5	10.748	5.266	6.148	6.980
10	18.417	8.555	14.487	12.212
15	21.687	8.061	18.581	18.704
20	22.030	11.240	22.156	23.584
25	28.957	14.203	27.486	28.946
30	33.803	14.924	35.268	33.795
45	42.358	21.145	39.419	41.146
60	43.198	22.877	44.093	44.076

% transferred: [%]					mean	SD
0 [min]	0.00	0.00	0.00	0.00	**0.00**	**0.00**
5	6.84	3.20	3.14	3.37	**4.14**	**1.81**
10	11.73	5.20	7.41	5.89	**7.55**	**2.93**
15	13.81	4.90	9.50	9.02	**9.31**	**3.64**
20	14.03	6.83	11.33	11.37	**10.89**	**2.99**
25	18.44	8.63	14.05	13.96	**13.77**	**4.02**
30	21.53	9.06	18.03	16.29	**16.23**	**5.25**
45	26.97	12.84	20.15	19.84	**19.95**	**5.77**
60	27.51	13.89	22.54	21.25	**21.30**	**5.63**

Table AVII.30. Dose, and amount and % of administered dose of 7.4 kDa F-PHEA absorbed from airways to perfusate in the IPRL in the presence of 5 μM OUA at 37 °C (FR7150; nominal dose = 0.2 mg; used in Figs. IV.11 and IV.12, Chapter 4).

Amount delivered:

		Rat#					
		223	226	230	231		
BW	[g]	325	305	330	345		
D_L	[μg]	255.39	243.76	251.84	257.12		
D_{ctg}	[μg]	1.29	4.79	30.30	3.87		
D_{cnl}	[μg]	29.90	43.47	74.88	37.75	mean	SD
D_{ad}	[μg]	224.20	195.50	146.66	215.50	195.47	34.68

Transferred amount: [μg]

	Rat#			
	223	226	230	231
0 [min]	0.000	0.000	0.000	0.000
5	11.998	15.909	14.194	21.401
10	48.500	25.178	24.363	27.006
15	58.189	45.950	40.997	46.999
20	87.321	63.483	46.365	55.021
25	95.697	69.790	56.445	55.584
30	100.768	69.741	67.081	61.240
45	111.978	84.805	68.779	63.978
60	122.581	88.324	69.574	62.918

% transferred: [%]					mean	SD
0 [min]	0.00	0.00	0.00	0.00	**0.00**	**0.00**
5	5.35	8.14	9.68	9.93	**8.27**	**2.10**
10	21.63	12.88	16.61	12.53	**15.91**	**4.24**
15	25.95	23.50	27.95	21.81	**24.81**	**2.70**
20	38.95	32.47	31.61	25.53	**32.14**	**5.49**
25	42.68	35.70	38.49	25.79	**35.67**	**7.18**
30	44.95	35.67	45.74	28.42	**38.69**	**8.23**
45	49.95	43.38	46.90	29.69	**42.48**	**8.94**
60	54.67	45.18	47.44	29.20	**44.12**	**10.74**

Table AVII.31. Dose, and amount and % of administered dose of 7.4 kDa F-PHEA absorbed from airways to perfusate in the IPRL in the presence of 50 μM OUA at 37 °C (FR7150; nominal dose = 0.2 mg; used in Figs. IV.11 and IV.12, Chapter 4).

Amount delivered:

		Rat#					
		205	206	207	208		
BW	[g]	370	350	350	350		
D_L	[μg]	192.52	223.77	227.65	207.84		
D_{ctg}	[μg]	1.24	1.68	3.43	6.53		
D_{cnl}	[μg]	30.68	38.70	32.22	55.86	mean	SD
D_{ad}	[μg]	160.60	183.39	192.00	145.45	170.36	21.24

Transferred amount: [μg]

	Rat#			
	205	206	207	208
0 [min]	0.000	0.000	0.000	0.000
5	5.471	6.791	6.651	0.000
10	7.870	13.171	11.901	4.341
15	13.396	19.245	19.211	6.473
20	18.639	20.612	22.714	8.405
25	22.278	27.731	26.931	8.845
30	22.910	28.705	31.796	10.128
45	28.850	45.718	38.339	10.739
60	31.586	45.179	41.440	15.531

% transferred: [%]					mean	SD
0 [min]	0.00	0.00	0.00	0.00	**0.00**	**0.00**
5	3.41	3.70	3.46	0.00	**2.64**	**1.77**
10	4.90	7.18	6.20	2.98	**5.32**	**1.81**
15	8.34	10.49	10.01	4.45	**8.32**	**2.74**
20	11.61	11.24	11.83	5.78	**10.11**	**2.90**
25	13.87	15.12	14.03	6.08	**12.28**	**4.17**
30	14.27	15.65	16.56	6.96	**13.36**	**4.37**
45	17.96	24.93	19.97	7.38	**17.56**	**7.39**
60	19.67	24.64	21.58	10.68	**19.14**	**6.00**

Table AVII.32. Dose, and amount and % of administered dose of 7.4 kDa F-PHEA absorbed from airways to perfusate in the IPRL in the presence of 100 μM OUA at 37 °C (FR7150; nominal dose = 0.2 mg; used in Figs. IV.11, IV.12 and IV.17, Chapter 4).

Amount delivered:

		Rat#					
		201	202	203	204		
BW	[g]	345	330	325	335		
D_L	[μg]	263.08	264.61	271.60	230.07		
D_{ctg}	[μg]	4.93	36.33	1.12	6.68		
D_{cnl}	[μg]	44.10	33.74	23.07	59.95	mean	SD
D_{ad}	[μg]	214.05	194.54	247.41	163.44	204.86	35.20

Transferred amount: [μg]

	Rat#			
	201	202	203	204
0 [min]	0.000	0.000	0.000	0.000
5	5.116	4.632	7.255	9.145
10	5.557	7.917	7.710	12.178
15	9.018	13.521	17.676	14.247
20	6.300	12.070	21.919	19.363
25	11.493	13.536	21.239	16.895
30	10.507	14.881	24.270	21.223
45	13.474	18.136	37.471	25.544
60	10.711	22.500	39.126	26.787

% transferred: [%]					mean	SD
0 [min]	0.00	0.00	0.00	0.00	**0.00**	**0.00**
5	2.39	2.38	2.93	5.60	**3.32**	**1.54**
10	2.60	4.07	3.12	7.45	**4.31**	**2.18**
15	4.21	6.95	7.14	8.72	**6.76**	**1.87**
20	2.94	6.20	8.86	11.85	**7.46**	**3.79**
25	5.37	6.96	8.58	10.34	**7.81**	**2.13**
30	4.91	7.65	9.81	12.98	**8.84**	**3.42**
45	6.29	9.32	15.15	15.63	**11.60**	**4.55**
60	5.00	11.57	15.81	16.39	**12.19**	**5.25**

Table AVII.33. Dose, and amount and % of administered dose of 7.4 kDa F-PHEA absorbed from airways to perfusate in the IPRL in the absence of MON at 37 °C (FR7150; nominal dose = 0.2 mg; used in Figs. IV.13, IV.15 and IV.16, Chapter 4).

Amount delivered:

		Rat#					
		254	255	260	263		
BW	[g]	310	310	360	330		
D_L	[µg]	242.72	243.74	251.21	255.84		
D_{ctg}	[µg]	0.51	2.76	12.52	6.47		
D_{cnl}	[µg]	65.79	51.16	63.12	100.63	mean	SD
D_{ad}	[µg]	176.42	189.82	175.57	148.74	172.64	17.22

Transferred amount: [µg]

	Rat#			
	254	255	260	263
0 [min]	0.000	0.000	0.000	0.000
5	14.855	18.881	9.685	7.187
10	25.111	32.573	22.910	14.529
15	38.146	47.342	32.025	27.973
20	50.381	55.087	37.335	42.417
25	58.041	61.226	49.805	50.135
30	66.351	74.619	53.993	56.080
45	73.843	86.977	68.178	66.921
60	77.088	98.550	75.689	75.782
90	90.198	103.949	84.482	79.725
120	94.563	110.377	92.854	87.109

% transferred: [%]					mean	SD
0 [min]	0.00	0.00	0.00	0.00	**0.00**	**0.00**
5	8.42	9.95	5.52	4.83	**7.18**	**2.41**
10	14.23	17.16	13.05	9.77	**13.55**	**3.06**
15	21.62	24.94	18.24	18.81	**20.90**	**3.07**
20	28.56	29.02	21.27	28.52	**26.84**	**3.72**
25	32.90	32.25	28.37	33.71	**31.81**	**2.37**
30	37.61	39.31	30.75	37.70	**36.34**	**3.81**
45	41.86	45.82	38.83	44.99	**42.88**	**3.19**
60	43.70	51.92	43.11	50.95	**47.42**	**4.66**
90	51.13	54.76	48.12	53.60	**51.90**	**2.94**
120	53.60	58.15	52.89	58.56	**55.80**	**2.97**

Table AVII.34. Dose, and amount and % of administered dose of 7.4 kDa F-PHEA absorbed from airways to perfusate in the IPRL in the presence of 5 μM MON at 37 °C (FR7150; nominal dose = 0.2 mg; used in Figs. IV.13 and IV.15, Chapter 4).

Amount delivered:

		Rat#					
		261	265	266	267		
BW	[g]	340	340	340	340		
D_L	[μg]	230.85	237.24	233.27	233.47		
D_{ctg}	[μg]	25.79	9.46	2.69	24.94		
D_{cnl}	[μg]	42.23	86.66	33.15	60.34	mean	SD
D_{ad}	[μg]	162.83	141.12	197.43	148.19	162.39	25.05

Transferred amount: [μg]

	Rat#			
	261	265	266	267
0 [min]	0.000	0.000	0.000	0.000
5	11.583	4.991	21.524	9.188
10	21.797	14.952	45.268	9.850
15	35.039	18.756	64.288	26.892
20	41.965	25.067	71.104	32.194
25	49.412	28.736	80.201	36.466
30	52.966	32.388	87.954	36.666
45	67.929	41.450	95.522	39.504
60	73.007	40.508	104.146	42.428
90	80.490	45.736	113.320	51.997
120	83.314	54.279	123.728	54.844

% transferred: [%]					mean	SD
0 [min]	0.00	0.00	0.00	0.00	**0.00**	**0.00**
5	7.11	3.54	10.90	6.20	**6.94**	**3.05**
10	13.39	10.60	22.93	6.65	**13.39**	**6.93**
15	21.52	13.29	32.56	18.15	**21.38**	**8.18**
20	25.77	17.76	36.01	21.72	**25.32**	**7.84**
25	30.35	20.36	40.62	24.61	**28.98**	**8.77**
30	32.53	22.95	44.55	24.74	**31.19**	**9.83**
45	41.72	29.37	48.38	26.66	**36.53**	**10.26**
60	44.84	28.70	52.75	28.63	**38.73**	**12.06**
90	49.43	32.41	57.40	35.09	**43.58**	**11.86**
120	51.17	38.46	62.67	37.01	**47.33**	**12.04**

Table AVII.35. Dose, and amount and % of administered dose of 7.4 kDa F-PHEA absorbed from airways to perfusate in the IPRL in the presence of 10 μM MON at 37 °C (FR7150; nominal dose = 0.2 mg; used in Figs. IV.13 and IV.15, Chapter 4).

Amount delivered:

		Rat#					
		268	269	270	276		
BW	[g]	340	340	340	380		
D_L	[μg]	263.84	265.92	259.62	295.22		
D_{ctg}	[μg]	4.23	26.57	5.47	0.48		
D_{cnl}	[μg]	103.04	75.87	90.59	47.57	mean	SD
D_{ad}	[μg]	156.57	163.48	163.56	247.17	182.70	43.11

Transferred amount: [μg]

	Rat#			
	268	269	270	276
0 [min]	0.000	0.000	0.000	0.000
5	4.910	2.389	5.829	0.000
10	11.339	13.576	8.599	1.206
15	16.803	17.686	13.490	23.878
20	22.811	32.137	14.785	33.282
25	27.348	33.168	22.313	58.327
30	30.427	40.096	31.652	71.371
45	39.519	51.896	32.317	106.762
60	56.856	66.538	42.281	142.935
90	69.204	71.801	55.033	158.677
120	83.003	82.629	60.876	172.319

% transferred: [%]					mean	SD
0 [min]	0.00	0.00	0.00	0.00	**0.00**	**0.00**
5	3.14	1.46	3.56	0.00	**2.04**	**1.63**
10	7.24	8.30	5.26	0.49	**5.32**	**3.46**
15	10.73	10.82	8.25	9.66	**9.86**	**1.20**
20	14.57	19.66	9.04	13.47	**14.18**	**4.36**
25	17.47	20.29	13.64	23.60	**18.75**	**4.23**
30	19.43	24.53	19.35	28.88	**23.05**	**4.58**
45	25.24	31.74	19.76	43.19	**29.98**	**10.08**
60	36.31	40.70	25.85	57.83	**40.17**	**13.32**
90	44.20	43.92	33.65	64.20	**46.49**	**12.78**
120	53.01	50.54	37.22	69.72	**52.62**	**13.34**

Table AVII.36. Dose, and amount and % of administered dose of 7.4 kDa F-PHEA absorbed from airways to perfusate in the IPRL in the presence of 30 μM MON at 37 °C (FR7150; nominal dose = 0.2 mg; used in Figs. IV.13, IV.15 and IV.17, Chapter 4).

Amount delivered:

		Rat#					
		240	241	242	243		
BW	[g]	310	310	330	325		
D_L	[μg]	240.99	214.37	265.98	239.96		
D_{ctg}	[μg]	2.02	1.93	17.04	8.18		
D_{cnl}	[μg]	69.16	64.25	82.99	80.31	mean	SD
D_{ad}	[μg]	169.81	148.19	165.95	151.47	158.86	10.62

Transferred amount: [μg]

	Rat#			
	240	241	242	243
0 [min]	0.000	0.000	0.000	0.000
5	4.762	7.794	5.139	2.599
10	11.484	12.530	8.804	4.460
15	25.350	25.806	14.397	7.469
20	25.629	29.542	14.707	9.496
25	30.274	29.349	19.173	11.896
30	30.356	36.503	21.414	11.592
45	41.389	43.704	26.544	15.542
60	42.870	45.671	27.659	17.799
90	48.476	51.277	33.723	21.195
120	53.768	57.283	36.447	23.465

% transferred: [%]					mean	SD
0 [min]	0.00	0.00	0.00	0.00	**0.00**	**0.00**
5	2.80	5.26	3.10	1.72	**3.22**	**1.48**
10	6.76	8.46	5.31	2.94	**5.87**	**2.34**
15	14.93	17.41	8.68	4.93	**11.49**	**5.71**
20	15.09	19.94	8.86	6.27	**12.54**	**6.17**
25	17.83	19.80	11.55	7.85	**14.26**	**5.53**
30	17.88	24.63	12.90	7.65	**15.77**	**7.24**
45	24.37	29.49	16.00	10.26	**20.03**	**8.57**
60	25.25	30.82	16.67	11.75	**21.12**	**8.54**
90	28.55	34.60	20.32	13.99	**24.37**	**9.06**
120	31.66	38.66	21.96	15.49	**26.94**	**10.25**

Table AVII.37. Dose, and amount and % of administered dose of 7.4 kDa F-PHEA absorbed from airways to perfusate in the IPRL in the presence of 100 μM MON at 37 °C (FR7150; nominal dose = 0.2 mg; used in Figs. IV.13 and IV.15, Chapter 4).

Amount delivered:

		Rat#					
		257	258	259	262		
BW	[g]	365	365	365	340		
D_L	[μg]	223.35	213.62	230.11	225.72		
D_{ctg}	[μg]	0.66	18.12	8.48	3.76		
D_{cnl}	[μg]	74.95	62.55	77.41	77.14	mean	SD
D_{ad}	[μg]	147.74	132.95	144.22	144.82	142.43	6.51

Transferred amount: [μg]

	Rat#			
	257	258	259	262
0 [min]	0.000	0.000	0.000	0.000
5	1.608	1.608	5.250	4.850
10	6.771	9.621	6.858	12.093
15	7.611	8.866	12.175	15.067
20	11.023	11.363	13.312	22.550
25	11.986	13.591	15.623	33.527
30	14.113	15.145	18.159	26.035
45	16.384	19.795	18.672	32.079
60	17.268	23.574	20.600	35.545
90	21.306	25.088	25.462	45.052
120	22.016	32.958	26.489	48.853

% transferred: [%]					mean	SD
0 [min]	0.00	0.00	0.00	0.00	**0.00**	**0.00**
5	1.09	1.21	3.64	3.35	**2.32**	**1.36**
10	4.58	7.24	4.76	8.35	**6.23**	**1.86**
15	5.15	6.67	8.44	10.40	**7.67**	**2.27**
20	7.46	8.55	9.23	15.57	**10.20**	**3.65**
25	8.11	10.22	10.83	23.15	**13.08**	**6.81**
30	9.55	11.39	12.59	17.98	**12.88**	**3.62**
45	11.09	14.89	12.95	22.15	**15.27**	**4.84**
60	11.69	17.73	14.28	24.54	**17.06**	**5.57**
90	14.42	18.87	17.65	31.11	**20.51**	**7.31**
120	14.90	24.79	18.37	33.73	**22.95**	**8.28**

Table AVII.38. Dose, and amount and % of administered dose of 7.4 kDa F-PHEA absorbed from airways to perfusate in the IPRL in the absence of NOC at 37 °C (FR7150; nominal dose = 0.2 mg; used in Figs. IV.14, IV.15 and IV.16, Chapter 4).

Amount delivered:

		Rat#					
		294	295	296	297		
BW	[g]	380	380	375	375		
D_L	[µg]	190.21	195.58	315.12	319.41		
D_{ctg}	[µg]	3.35	2.51	6.82	3.28		
D_{cnl}	[µg]	65.87	68.33	69.92	62.99	mean	SD
D_{ad}	[µg]	120.99	124.74	238.38	253.14	184.31	71.23

Transferred amount: [µg]

	Rat#			
	294	295	296	297
0 [min]	0.000	0.000	0.000	0.000
5	18.980	19.619	27.484	34.086
10	28.319	27.525	61.209	72.267
15	36.386	41.155	71.450	85.501
20	37.420	51.771	87.359	90.091
25	47.264	55.106	99.951	101.752
30	48.894	61.705	113.411	107.315
45	61.507	73.398	124.436	133.724
60	72.806	76.550	137.134	152.696
90	73.755	78.082	141.484	149.479
120	74.495	79.771	147.768	138.822

% transferred: [%]

					mean	SD
0 [min]	0.00	0.00	0.00	0.00	**0.00**	**0.00**
5	15.69	15.73	11.53	13.47	**14.10**	**2.01**
10	23.41	22.07	25.68	28.55	**24.92**	**2.84**
15	30.07	32.99	29.97	33.78	**31.70**	**1.97**
20	30.93	41.50	36.65	35.59	**36.17**	**4.34**
25	39.06	44.18	41.93	40.20	**41.34**	**2.23**
30	40.41	49.47	47.58	42.39	**44.96**	**4.26**
45	50.84	58.84	52.20	52.83	**53.68**	**3.54**
60	60.18	61.37	57.53	60.32	**59.85**	**1.64**
90	60.96	62.60	59.35	59.05	**60.49**	**1.64**
120	61.57	63.95	61.99	54.84	**60.59**	**3.97**

Table AVII.39. Dose, and amount and % of administered dose of 7.4 kDa F-PHEA absorbed from airways to perfusate in the IPRL in the presence of 0.5 μM NOC at 37 °C (FR7150; nominal dose = 0.2 mg; used in Figs. IV.14 and IV.15, Chapter 4).

Amount delivered:

		Rat#					
		318	319	320	321		
BW	[g]	390	375	360	370		
D_L	[μg]	229.40	248.43	255.08	262.73		
D_{ctg}	[μg]	2.30	0.00	1.63	5.11		
D_{cnl}	[μg]	78.93	47.47	79.05	61.92	mean	SD
D_{ad}	[μg]	148.17	200.96	174.40	195.71	179.81	24.02

Transferred amount: [μg]

	Rat#			
	318	319	320	321
0 [min]	0.000	0.000	0.000	0.000
5	14.538	14.147	13.534	13.570
10	29.438	35.895	24.422	24.233
15	50.449	42.588	36.755	37.651
20	59.820	71.341	47.425	46.624
25	63.495	79.356	61.137	53.672
30	67.335	81.522	66.959	62.699
45	70.790	86.220	69.147	68.242
60	78.255	88.996	76.828	78.536
90	82.103	98.622	77.824	83.511
120	86.716	100.812	83.630	86.872

% transferred: [%]						mean	SD
0 [min]	0.00	0.00	0.00	0.00	**0.00**	**0.00**
5	9.81	7.04	7.76	6.93	**7.89**	**1.34**
10	19.87	17.86	14.00	12.38	**16.03**	**3.44**
15	34.05	21.19	21.08	19.24	**23.89**	**6.83**
20	40.37	35.50	27.19	23.82	**31.72**	**7.57**
25	42.85	39.49	35.06	27.42	**36.21**	**6.67**
30	45.44	40.57	38.39	32.04	**39.11**	**5.56**
45	47.78	42.90	39.65	34.87	**41.30**	**5.43**
60	52.81	44.29	44.05	40.13	**45.32**	**5.35**
90	55.41	49.08	44.62	42.67	**47.95**	**5.65**
120	58.53	50.17	47.95	44.39	**50.26**	**6.00**

Table AVII.40. Dose, and amount and % of administered dose of 7.4 kDa F-PHEA absorbed from airways to perfusate in the IPRL in the presence of 1.0 μM NOC at 37 °C (FR7150; nominal dose = 0.2 mg; used in Figs. IV.14 and IV.15, Chapter 4).

Amount delivered:

		Rat#					
		314	315	316	317		
BW	[g]	360	380	370	385		
D_L	[μg]	289.09	288.92	260.85	255.55		
D_{ctg}	[μg]	1.48	5.21	0.00	1.09		
D_{cnl}	[μg]	73.16	55.50	38.92	69.27	mean	SD
D_{ad}	[μg]	214.45	228.21	221.93	185.19	212.45	19.02

Transferred amount: [μg]

		Rat#			
		314	315	316	317
0	[min]	0.000	0.000	0.000	0.000
5		6.828	5.511	8.267	11.497
10		12.651	12.342	12.354	22.715
15		23.711	23.233	25.028	26.099
20		35.660	35.546	35.868	31.036
25		48.774	47.915	47.636	43.439
30		51.872	52.274	53.302	47.069
45		60.712	59.296	60.381	51.744
60		66.688	64.908	65.562	51.916
90		78.269	79.071	81.836	63.979
120		77.350	79.898	83.533	67.677

% transferred: [%]						mean	SD
0	[min]	0.00	0.00	0.00	0.00	**0.00**	**0.00**
5		3.18	2.41	3.73	6.21	**3.88**	**1.64**
10		5.90	5.41	5.57	12.27	**7.28**	**3.33**
15		11.06	10.18	11.28	14.09	**11.65**	**1.69**
20		16.63	15.58	16.16	16.76	**16.28**	**0.54**
25		22.74	21.00	21.46	23.46	**22.17**	**1.13**
30		24.19	22.91	24.02	25.42	**24.13**	**1.03**
45		28.31	25.98	27.21	27.94	**27.36**	**1.03**
60		31.10	28.44	29.54	28.03	**29.28**	**1.37**
90		36.50	34.65	36.87	34.55	**35.64**	**1.22**
120		36.07	35.01	37.64	36.54	**36.32**	**1.09**

Table AVII.41. Dose, and amount and % of administered dose of 7.4 kDa F-PHEA absorbed from airways to perfusate in the IPRL in the presence of 10 μM NOC at 37 °C (FR7150; nominal dose = 0.2 mg; used in Figs. IV.14 and IV.15, Chapter 4).

Amount delivered:

		Rat#					
		310	311	312	313		
BW	[g]	360	380	380	370		
D_L	[μg]	204.71	196.95	278.59	341.73		
D_{ctg}	[μg]	2.57	3.06	5.34	4.67		
D_{cnl}	[μg]	58.15	70.57	97.62	133.04	mean	SD
D_{ad}	[μg]	143.99	123.32	175.63	204.02	161.74	35.46

Transferred amount: [μg]

	Rat#			
	310	311	312	313
0 [min]	0.000	0.000	0.000	0.000
5	0.000	0.000	6.744	2.966
10	6.669	2.572	6.703	6.379
15	11.598	6.622	9.059	13.191
20	15.790	8.372	16.472	13.276
25	21.843	15.188	13.436	20.183
30	20.381	14.920	20.186	23.936
45	30.920	18.617	28.899	25.812
60	31.312	18.917	29.240	24.384
90	39.533	27.667	41.286	35.814
120	49.081	26.746	42.805	41.981

% transferred: [%]					mean	SD
0 [min]	0.00	0.00	0.00	0.00	**0.00**	**0.00**
5	0.00	0.00	3.84	1.45	**1.32**	**1.81**
10	4.63	2.09	3.82	3.13	**3.42**	**1.08**
15	8.05	5.37	5.16	6.47	**6.26**	**1.33**
20	10.97	6.79	9.38	6.51	**8.41**	**2.14**
25	15.17	12.32	7.65	9.89	**11.26**	**3.23**
30	14.15	12.10	11.49	11.73	**12.37**	**1.22**
45	21.47	15.10	16.45	12.65	**16.42**	**3.72**
60	21.75	15.34	16.65	11.95	**16.42**	**4.06**
90	27.46	22.44	23.51	17.55	**22.74**	**4.07**
120	34.09	21.69	24.37	20.58	**25.18**	**6.15**

Table AVII.42. Dose, and amount and % of administered dose of 7.4 kDa F-PHEA absorbed from airways to perfusate in the IPRL in the presence of 30 μM NOC at 37 °C (FR7150; nominal dose = 0.2 mg; used in Figs. IV.14, IV.15 and IV.17, Chapter 4).

Amount delivered:

		Rat#					
		290	291	292	293		
BW	[g]	330	335	335	330		
D_L	[μg]	268.03	275.86	226.06	225.82		
D_{ctg}	[μg]	1.93	1.82	5.77	12.05		
D_{cnl}	[μg]	70.03	68.50	85.84	57.52	mean	SD
D_{ad}	[μg]	196.07	205.54	134.45	156.25	173.08	33.46

Transferred amount: [μg]

	Rat#			
	290	291	292	293
0 [min]	0.000	0.000	0.000	0.000
5	1.946	4.706	3.802	1.078
10	8.000	5.911	6.777	4.158
15	8.120	10.660	10.562	7.527
20	12.657	14.692	13.425	9.946
25	17.251	19.437	12.693	13.426
30	17.920	25.435	20.063	14.138
45	20.770	34.491	20.374	16.441
60	21.223	44.619	24.985	25.024
90	27.939	49.327	28.975	25.889
120	29.145	52.987	37.005	27.035

% transferred: [%]					mean	SD
0 [min]	0.00	0.00	0.00	0.00	**0.00**	**0.00**
5	0.99	2.29	2.83	0.69	**1.70**	**1.02**
10	4.08	2.88	5.04	2.66	**3.66**	**1.11**
15	4.14	5.19	7.86	4.82	**5.50**	**1.63**
20	6.46	7.15	9.99	6.37	**7.49**	**1.70**
25	8.80	9.46	9.44	8.59	**9.07**	**0.44**
30	9.14	12.37	14.92	9.05	**11.37**	**2.83**
45	10.59	16.78	15.15	10.52	**13.26**	**3.19**
60	10.82	21.71	18.58	16.02	**16.78**	**4.60**
90	14.25	24.00	21.55	16.57	**19.09**	**4.47**
120	14.86	25.78	27.52	17.30	**21.37**	**6.22**

Table AVII.43. Dose, and amount and % of administered dose of 7.4 kDa F-PHEA absorbed from airways to perfusate in the IPRL in the presence of 100 μM NOC at 37 °C (FR7150; nominal dose = 0.2 mg; used in Figs. IV.14 and IV.15, Chapter 4).

Amount delivered:

		Rat#					
		302	303	304	305		
BW	[g]	340	370	370	330		
D_L	[μg]	295.34	305.93	311.43	280.24		
D_{ctg}	[μg]	3.01	9.08	3.53	1.02		
D_{cnl}	[μg]	44.49	72.32	76.87	94.13	mean	SD
D_{ad}	[μg]	247.84	224.53	231.03	185.09	222.12	26.57

Transferred amount: [μg]

	Rat#			
	302	303	304	305
0 [min]	0.000	0.000	0.000	0.000
5	6.622	1.304	1.116	0.986
10	17.606	8.607	3.576	4.275
15	22.076	13.639	4.257	9.887
20	29.472	18.687	10.391	12.567
25	34.331	21.917	13.475	15.975
30	41.398	23.561	16.389	17.149
45	54.296	31.626	21.365	19.988
60	60.249	31.342	25.673	26.094
90	69.548	38.928	30.534	30.082
120	74.394	40.543	28.278	35.831

% transferred: [%]					mean	SD
0 [min]	0.00	0.00	0.00	0.00	**0.00**	**0.00**
5	2.67	0.58	0.48	0.53	**1.07**	**1.07**
10	7.10	3.83	1.55	2.31	**3.70**	**2.46**
15	8.91	6.07	1.84	5.34	**5.54**	**2.91**
20	11.89	8.32	4.50	6.79	**7.88**	**3.10**
25	13.85	9.76	5.83	8.63	**9.52**	**3.33**
30	16.70	10.49	7.09	9.27	**10.89**	**4.12**
45	21.91	14.09	9.25	10.80	**14.01**	**5.64**
60	24.31	13.96	11.11	14.10	**15.87**	**5.79**
90	28.06	17.34	13.22	16.25	**18.72**	**6.47**
120	30.02	18.06	12.24	19.36	**19.92**	**7.41**

Table AVII.44. Dose, and amount and % of administered dose of 4.3 kDa F-PHEA absorbed from airways to perfusate in the IPRL at 37 °C (FR7002-5; nominal dose = 0.1 mg; used in Figs. V.2 and V.4, Chapter 4).

Amount delivered:

		Rat#					
		97	98	99	100		
BW	[g]	282	283	284	287		
D_L	[µg]	128.02	130.25	124.94	165.57		
D_{ctg}	[µg]	1.53	0.34	1.75	1.25		
D_{cnl}	[µg]	24.20	43.45	32.86	41.08	mean	SD
D_{ad}	[µg]	102.29	86.46	90.33	123.24	100.58	16.54

Transferred amount: [µg]

		Rat#			
		97	98	99	100
0	[min]	0.000	0.000	0.000	0.000
5		18.509	3.727	14.379	17.104
10		32.301	9.898	29.193	37.029
15		47.829	19.006	38.800	48.900
20		56.582	26.390	48.470	55.686
25		60.689	31.748	49.866	66.796
30		64.153	37.932	50.226	68.773
45		65.761	43.071	48.618	75.282
60		68.230	49.862	55.554	78.524
90		72.156	50.345	58.521	84.868
120		73.461	53.005	60.481	86.331
150		73.444	57.626	62.250	83.968
180		73.324	56.006	63.404	85.250

% transferred: [%]						mean	SD
0	[min]	0.00	0.00	0.00	0.00	**0.00**	**0.00**
5		18.09	4.31	15.92	13.88	**13.05**	**6.08**
10		31.58	11.45	32.32	30.05	**26.35**	**9.98**
15		46.76	21.98	42.95	39.68	**37.84**	**10.96**
20		55.32	30.52	53.66	45.19	**46.17**	**11.34**
25		59.33	36.72	55.20	54.20	**51.36**	**10.01**
30		62.72	43.87	55.60	55.80	**54.50**	**7.82**
45		64.29	49.82	53.82	61.09	**57.25**	**6.61**
60		66.70	57.67	61.50	63.72	**62.40**	**3.80**
90		70.54	58.23	64.79	68.86	**65.60**	**5.48**
120		71.82	61.31	66.96	70.05	**67.53**	**4.61**
150		71.80	66.65	68.91	68.13	**68.87**	**2.16**
180		71.68	64.78	70.19	69.17	**68.96**	**2.97**

Table AVII.45. Dose, and amount and % of administered dose of 4.3 kDa F-PHEA absorbed from airways to perfusate in the IPRL at 37 °C (FR7002-5; nominal dose = 0.2 mg; used in Fig. V.2, Chapter 4).

Amount delivered:

		Rat#					
		256	264	271	277		
BW	[g]	325	340	350	360		
D_L	[µg]	224.54	283.54	270.57	256.43		
D_{ctg}	[µg]	3.35	5.91	1.02	5.61		
D_{cnl}	[µg]	3.22	75.98	71.66	61.72	mean	SD
D_{ad}	[µg]	217.97	201.65	197.89	189.10	201.65	12.08

Transferred amount: [µg]

	Rat#			
	256	264	271	277
0 [min]	0.000	0.000	0.000	0.000
5	36.161	29.554	22.582	35.226
10	56.013	46.153	44.911	48.635
15	69.321	60.476	54.763	56.090
20	95.192	76.007	66.485	66.699
25	112.665	83.939	73.710	77.488
30	117.772	94.938	78.193	91.056
45	130.124	112.765	88.882	101.518
60	145.375	119.862	89.736	106.325
90	148.051	124.215	110.794	113.400
120	156.719	131.172	120.777	118.781
150	156.887	139.413	125.974	124.495
180	157.583	140.664	144.435	133.301

% transferred: [%]					mean	SD
0 [min]	0.00	0.00	0.00	0.00	**0.00**	**0.00**
5	16.59	14.66	11.41	18.63	**15.32**	**3.07**
10	25.70	22.89	22.69	25.72	**24.25**	**1.69**
15	31.80	29.99	27.67	29.66	**29.78**	**1.69**
20	43.67	37.69	33.60	35.27	**37.56**	**4.41**
25	51.69	41.63	37.25	40.98	**42.88**	**6.18**
30	54.03	47.08	39.51	48.15	**47.19**	**5.96**
45	59.70	55.92	44.91	53.68	**53.55**	**6.27**
60	66.69	59.44	45.35	56.23	**56.93**	**8.88**
90	67.92	61.60	55.99	59.97	**61.37**	**4.96**
120	71.90	65.05	61.03	62.81	**65.20**	**4.76**
150	71.98	69.14	63.66	65.84	**67.65**	**3.66**
180	72.30	69.76	72.99	70.49	**71.38**	**1.51**

Table AVII.46. Dose, and amount and % of administered dose of 4.3 kDa F-PHEA absorbed from airways to perfusate in the IPRL at 37 °C (FR7002-5; nominal dose = 1.0 mg; used in Figs. V.2 and V.4, Chapter 4).

Amount delivered:

		Rat#					
		188	189	190	191		
BW	[g]	350	365	345	345		
D_L	[µg]	1083.94	1133.14	1093.49	1139.29		
D_{ctg}	[µg]	0.80	36.38	41.17	21.76		
D_{cnl}	[µg]	251.28	467.51	50.07	42.33	mean	SD
D_{ad}	[µg]	831.86	629.25	1002.25	1075.20	884.64	198.46

Transferred amount: [µg]

	Rat#			
	188	189	190	191
0 [min]	0.000	0.000	0.000	0.000
5	78.888	29.964	130.369	52.779
10	155.121	70.537	270.782	138.935
15	211.261	108.190	326.644	193.632
20	250.761	123.052	347.553	255.627
25	277.972	137.654	423.464	283.645
30	311.987	161.425	410.313	320.606
45	331.744	189.480	472.267	357.346
60	371.982	202.460	501.964	415.140
90	428.084	231.712	544.230	467.286
120	443.115	257.172	557.534	533.298
150	458.076	249.526	565.926	583.208
180	442.730	251.382	627.268	691.795

% transferred: [%]					mean	SD
0 [min]	0.00	0.00	0.00	0.00	**0.00**	**0.00**
5	9.48	4.76	13.01	4.91	**8.04**	**3.97**
10	18.65	11.21	27.02	12.92	**17.45**	**7.13**
15	25.40	17.19	32.59	18.01	**23.30**	**7.21**
20	30.14	19.56	34.68	23.77	**27.04**	**6.70**
25	33.42	21.88	42.25	26.38	**30.98**	**8.89**
30	37.50	25.65	40.94	29.82	**33.48**	**6.99**
45	39.88	30.11	47.12	33.24	**37.59**	**7.55**
60	44.72	32.17	50.08	38.61	**41.40**	**7.73**
90	51.46	36.82	54.30	43.46	**46.51**	**7.92**
120	53.27	40.87	55.63	49.60	**49.84**	**6.48**
150	55.07	39.65	56.47	54.24	**51.36**	**7.86**
180	53.22	39.95	62.59	64.34	**55.02**	**11.17**

Table AVII.47. Dose, and amount and % of administered dose of 4.3 kDa F-PHEA absorbed from airways to perfusate in the IPRL at 25 °C (FR7002-5; nominal dose = 0.1 mg; used in Fig. V.3, Chapter 4).

Amount delivered:

		Rat#					
		285	286	288	289		
BW	[g]	320	320	330	330		
D_L	[µg]	130.44	133.09	152.52	153.95		
D_{ctg}	[µg]	1.23	0.58	3.99	1.60		
D_{cnl}	[µg]	23.83	31.49	34.37	48.13	mean	SD
D_{ad}	[µg]	105.38	101.02	114.16	104.22	106.20	5.62

Transferred amount: [µg]

	Rat#			
	285	286	288	289
0 [min]	0.000	0.000	0.000	0.000
5	1.825	0.901	3.257	3.073
10	6.081	4.494	8.136	7.982
15	9.146	9.965	18.988	18.528
20	13.488	14.402	22.117	22.232
25	16.922	16.719	27.074	28.050
30	21.788	20.227	31.023	31.477
45	19.596	28.271	40.919	37.016
60	28.694	33.996	45.550	42.659
90	38.537	40.050	48.576	48.911
120	39.840	43.998	49.280	50.697
150	42.781	48.684	52.562	51.702
180	38.505	49.092	55.007	51.812

% transferred: [%]					mean	SD
0 [min]	0.00	0.00	0.00	0.00	**0.00**	**0.00**
5	1.73	0.89	2.85	2.95	**2.11**	**0.98**
10	5.77	4.45	7.13	7.66	**6.25**	**1.44**
15	8.68	9.86	16.63	17.78	**13.24**	**4.63**
20	12.80	14.26	19.37	21.33	**16.94**	**4.06**
25	16.06	16.55	23.72	26.91	**20.81**	**5.37**
30	20.68	20.02	27.18	30.20	**24.52**	**4.98**
45	18.60	27.99	35.84	35.52	**29.49**	**8.12**
60	27.23	33.65	39.90	40.93	**35.43**	**6.34**
90	36.57	39.65	42.55	46.93	**41.42**	**4.41**
120	37.81	43.55	43.17	48.64	**43.29**	**4.43**
150	40.60	48.19	46.04	49.61	**46.11**	**3.96**
180	36.54	48.60	48.18	49.71	**45.76**	**6.18**

Table AVII.48. Dose, and amount and % of administered dose of 4.3 kDa F-PHEA absorbed from airways to perfusate in the IPRL at 25 °C (FR7002-5; nominal dose = 0.2 mg; used in Fig. V.3, Chapter 4).

Amount delivered:

		Rat#					
		278	279	280	281		
BW	[g]	360	320	320	320		
D_L	[µg]	263.99	264.50	270.62	243.28		
D_{ctg}	[µg]	0.39	0.95	1.30	2.94		
D_{cnl}	[µg]	45.54	48.06	66.08	3.30	mean	SD
D_{ad}	[µg]	218.06	215.49	203.24	237.04	218.46	13.97

Transferred amount: [µg]

	Rat#			
	278	279	280	281
0 [min]	0.000	0.000	0.000	0.000
5	3.357	5.808	7.693	6.289
10	8.562	15.201	18.304	15.016
15	18.183	22.675	34.468	21.978
20	24.355	33.919	39.811	29.826
25	28.649	40.264	46.616	34.923
30	32.069	44.580	52.090	45.598
45	48.584	58.718	63.431	55.834
60	51.968	71.476	72.682	59.289
90	64.121	83.631	89.064	73.755
120	70.630	95.656	88.684	73.978
150	81.007	97.002	89.132	79.521
180	86.009	99.885	91.120	86.199

% transferred: [%]					mean	SD
0 [min]	0.00	0.00	0.00	0.00	**0.00**	**0.00**
5	1.54	2.70	3.79	2.65	**2.67**	**0.92**
10	3.93	7.05	9.01	6.33	**6.58**	**2.10**
15	8.34	10.52	16.96	9.27	**11.27**	**3.89**
20	11.17	15.74	19.59	12.58	**14.77**	**3.74**
25	13.14	18.68	22.94	14.73	**17.37**	**4.38**
30	14.71	20.69	25.63	19.24	**20.07**	**4.50**
45	22.28	27.25	31.21	23.55	**26.07**	**4.02**
60	23.83	33.17	35.76	25.01	**29.44**	**5.91**
90	29.41	38.81	43.82	31.12	**35.79**	**6.74**
120	32.39	44.39	43.64	31.21	**37.91**	**7.07**
150	37.15	45.01	43.86	33.55	**39.89**	**5.47**
180	39.44	46.35	44.83	36.36	**41.75**	**4.66**

Table AVII.49. Dose, and amount and % of administered dose of 4.3 kDa F-PHEA absorbed from airways to perfusate in the IPRL at 25 °C (FR7002-5; nominal dose = 1.0 mg; used in Fig. V.3, Chapter 4).

Amount delivered:

		Rat#					
		184	185	186	187		
BW	[g]	330	330	310	365		
D_L	[µg]	1056.99	1118.89	1135.40	1084.10		
D_{ctg}	[µg]	8.56	14.85	12.85	93.47		
D_{cnl}	[µg]	199.71	246.39	264.86	75.36	mean	SD
D_{ad}	[µg]	848.72	857.65	857.69	915.27	869.83	30.58

Transferred amount: [µg]

	Rat#			
	184	185	186	187
0 [min]	0.000	0.000	0.000	0.000
5	7.484	13.394	9.486	7.658
10	26.263	36.409	30.554	29.840
15	58.119	58.693	56.509	48.387
20	88.833	81.750	63.398	71.176
25	112.813	98.715	76.587	90.993
30	137.505	115.425	84.818	111.543
45	199.207	165.153	122.678	149.532
60	248.901	181.707	156.115	192.091
90	322.247	238.437	198.307	234.359
120	327.140	241.943	230.448	245.866
150	384.336	271.826	249.104	265.883
180	408.294	366.262	256.938	260.513

% transferred: [%]					mean	SD
0 [min]	0.00	0.00	0.00	0.00	**0.00**	**0.00**
5	0.88	1.56	1.11	0.84	**1.10**	**0.33**
10	3.09	4.25	3.56	3.26	**3.54**	**0.51**
15	6.85	6.84	6.59	5.29	**6.39**	**0.75**
20	10.47	9.53	7.39	7.78	**8.79**	**1.45**
25	13.29	11.51	8.93	9.94	**10.92**	**1.91**
30	16.20	13.46	9.89	12.19	**12.93**	**2.63**
45	23.47	19.26	14.30	16.34	**18.34**	**3.98**
60	29.33	21.19	18.20	20.99	**22.43**	**4.80**
90	37.97	27.80	23.12	25.61	**28.62**	**6.52**
120	38.55	28.21	26.87	26.86	**30.12**	**5.65**
150	45.28	31.69	29.04	29.05	**33.77**	**7.78**
180	48.11	42.71	29.96	28.46	**37.31**	**9.63**

Table AVII.50. Dose, and amount and % of administered dose of 4.4 kDa FD-4 absorbed from airways to perfusate in the IPRL at 37 °C (nominal dose = 0.1 mg; used in Figs. III.6 and III.11, Chapter 3 and Fig. V.4, Chapter 5).

Amount delivered:

		Rat#					
		FD4-1	FD4-2	FD4-3	FD4-4		
BW	[g]	340	310	329	325		
D_L	[µg]	100.67	105.03	102.21	109.37		
D_{ctg}	[µg]	1.77	4.15	2.88	1.70		
D_{cnl}	[µg]	31.36	3.75	15.41	14.26	mean	SD
D_{ad}	[µg]	67.54	97.14	83.92	93.41	85.50	13.21

Transferred amount: [µg]

	Rat#			
	FD4-1	FD4-2	FD4-3	FD4-4
0 [min]	0.000	0.000	0.000	0.000
5	1.763	11.439	6.697	5.110
10	4.074	21.212	14.334	9.892
15	7.335	24.660	23.682	9.360
20	8.942	30.580	24.930	12.461
25	11.485	32.412	29.401	16.384
30	15.992	31.280	26.612	20.401
45	15.776	34.495	30.877	15.366
60	15.437	38.378	33.498	18.645
90	20.250	38.504	36.296	22.596
120	20.665	37.494	37.038	21.718
150	19.535	38.124	37.283	25.015

% transferred: [%]					mean	SD
0 [min]	0.00	0.00	0.00	0.00	**0.00**	**0.00**
5	2.61	11.78	7.98	5.47	**6.96**	**3.89**
10	6.03	21.84	17.08	10.59	**13.88**	**6.98**
15	10.86	25.39	28.22	10.02	**18.62**	**9.52**
20	13.24	31.48	29.71	13.34	**21.94**	**10.02**
25	17.00	33.37	35.03	17.54	**25.74**	**9.80**
30	23.68	32.20	31.71	21.84	**27.36**	**5.37**
45	23.36	35.51	36.79	16.45	**28.03**	**9.81**
60	22.86	39.51	39.92	19.96	**30.56**	**10.63**
90	29.98	39.64	43.25	24.19	**34.26**	**8.74**
120	30.60	38.60	44.13	23.25	**34.14**	**9.14**
150	28.92	39.25	44.43	26.78	**34.84**	**8.39**

Table AVII.51. Dose, and amount and % of administered dose of 4.4 kDa FD-4 absorbed from airways to perfusate in the IPRL at 37 °C (nominal dose = 0.2 mg; used in Figs. III.6 and III.11, Chapter 3 and Fig. V.4, Chapter 5).

Amount delivered:

		Rat#					
		FD4-5	FD4-6	FD4-7	FD4-8		
BW	[g]	342	320	325	320		
D_L	[µg]	255.07	223.42	232.12	218.63		
D_{ctg}	[µg]	9.05	8.39	5.54	8.75		
D_{cnl}	[µg]	2.44	38.66	31.57	9.91	mean	SD
D_{ad}	[µg]	243.58	176.37	195.02	199.98	203.74	28.44

Transferred amount: [µg]

	Rat#			
	FD4-5	FD4-6	FD4-7	FD4-8
0 [min]	0.000	0.000	0.000	0.000
5	5.575	5.519	20.178	9.985
10	12.279	6.498	32.437	24.788
15	21.208	13.596	47.133	31.404
20	30.940	16.062	58.821	34.894
25	36.931	18.977	63.638	40.801
30	38.686	20.830	66.473	44.056
45	45.955	24.832	74.583	51.270
60	51.914	28.702	76.262	55.144
90	58.803	30.266	85.581	61.057
120	59.278	36.561	91.135	64.273
150	60.695	40.945	90.258	63.845

% transferred: [%]					mean	SD
0 [min]	0.00	0.00	0.00	0.00	**0.00**	**0.00**
5	2.29	3.13	10.35	4.99	**5.19**	**3.62**
10	5.04	3.68	16.63	12.40	**9.44**	**6.14**
15	8.71	7.71	24.17	15.70	**14.07**	**7.61**
20	12.70	9.11	30.16	17.45	**17.36**	**9.20**
25	15.16	10.76	32.63	20.40	**19.74**	**9.46**
30	15.88	11.81	34.09	22.03	**20.95**	**9.71**
45	18.87	14.08	38.24	25.64	**24.21**	**10.49**
60	21.31	16.27	39.11	27.58	**26.07**	**9.85**
90	24.14	17.16	43.88	30.53	**28.93**	**11.37**
120	24.34	20.73	46.73	32.14	**30.98**	**11.53**
150	24.92	23.22	46.28	31.93	**31.59**	**10.50**

Table AVII.52. Dose, and amount and % of administered dose of 4.4 kDa FD-4 absorbed from airways to perfusate in the IPRL at 25 °C (nominal dose = 0.1 mg; used in Fig. IV.7, Chapter 4).

Amount delivered:

		Rat#					
		FD4-9	FD4-10	FD4-11	FD4-12		
BW	[g]	320	315	310	340		
D_L	[µg]	128.86	119.22	117.91	110.90		
D_{ctg}	[µg]	4.12	9.98	2.97	2.36		
D_{cnl}	[µg]	16.85	4.32	9.30	12.75	mean	SD
D_{ad}	[µg]	107.89	104.93	105.65	95.79	103.56	5.33

Transferred amount: [µg]

	Rat#			
	FD4-9	FD4-10	FD4-11	FD4-12
0 [min]	0.000	0.000	0.000	0.000
5	1.035	3.322	2.960	0.723
10	6.818	5.690	11.086	1.724
15	5.564	15.233	11.881	2.503
20	10.015	13.861	18.745	4.065
25	11.961	19.571	21.275	5.296
30	14.379	26.761	20.892	5.926
45	18.056	28.965	26.626	9.678
60	22.527	32.446	36.276	10.113
90	28.891	41.958	34.341	12.926
120	28.394	38.376	43.702	13.174
150	31.035	41.779	43.833	14.445

% transferred: [%]					mean	SD
0 [min]	0.00	0.00	0.00	0.00	**0.00**	**0.00**
5	0.96	3.17	2.80	0.75	**1.92**	**1.24**
10	6.32	5.42	10.49	1.80	**6.01**	**3.57**
15	5.16	14.52	11.25	2.61	**8.38**	**5.46**
20	9.28	13.21	17.74	4.24	**11.12**	**5.74**
25	11.09	18.65	20.14	5.53	**13.85**	**6.82**
30	13.33	25.50	19.78	6.19	**16.20**	**8.32**
45	16.74	27.60	25.20	10.10	**19.91**	**8.03**
60	20.88	30.92	34.34	10.56	**24.17**	**10.73**
90	26.78	39.99	32.51	13.49	**28.19**	**11.19**
120	26.32	36.57	41.37	13.75	**29.50**	**12.23**
150	28.77	39.82	41.49	15.08	**31.29**	**12.19**

Table AVII.53. Dose, and amount and % of administered dose of 4.4 kDa FD-4 absorbed from airways to perfusate in the IPRL at 25 °C (nominal dose = 0.2 mg; used in Fig. IV.7, Chapter 4).

Amount delivered:

		Rat#					
		FD4-13	FD4-14	FD4-15	FD4-16		
BW	[g]	360	350	340	370		
D_L	[µg]	201.54	243.33	227.33	181.63		
D_{ctg}	[µg]	2.23	2.67	8.41	18.47		
D_{cnl}	[µg]	19.89	29.61	15.36	47.79	mean	SD
D_{ad}	[µg]	179.42	211.06	203.56	115.36	177.35	43.48

Transferred amount: [µg]

	Rat#			
	FD4-13	FD4-14	FD4-15	FD4-16
0 [min]	0.000	0.000	0.000	0.000
5	5.772	13.560	10.535	2.361
10	13.131	23.152	8.268	2.556
15	23.132	33.580	11.673	7.128
20	30.352	42.753	17.280	10.936
25	40.000	51.601	23.242	12.603
30	45.581	56.194	28.878	13.694
45	58.248	62.407	43.154	18.965
60	66.398	80.675	49.145	22.601
90	76.148	85.894	64.589	27.244
120	88.195	95.320	69.756	30.896
150	89.472	101.139	77.494	35.257

% transferred: [%]					mean	SD
0 [min]	0.00	0.00	0.00	0.00	**0.00**	**0.00**
5	3.22	6.42	5.18	2.05	**4.22**	**1.96**
10	7.32	10.97	4.06	2.22	**6.14**	**3.85**
15	12.89	15.91	5.73	6.18	**10.18**	**5.03**
20	16.92	20.26	8.49	9.48	**13.79**	**5.72**
25	22.29	24.45	11.42	10.92	**17.27**	**7.10**
30	25.40	26.62	14.19	11.87	**19.52**	**7.57**
45	32.46	29.57	21.20	16.44	**24.92**	**7.40**
60	37.01	38.22	24.14	19.59	**29.74**	**9.29**
90	42.44	40.70	31.73	23.62	**34.62**	**8.71**
120	49.16	45.16	34.27	26.78	**38.84**	**10.21**
150	49.87	47.92	38.07	30.56	**41.60**	**8.99**

Table AVII.54. Dose, and amount and % of administered dose of 376 Da F-Na absorbed from airways to perfusate in the IPRL at 37 °C (nominal dose = 0.01 mg; used in Figs. III.6 and III.11, Chapter 3).

Amount delivered:

		Rat#					
		11	12	13	19		
BW	[g]	360	375	368	335		
D_L	[μg]	10.87	10.66	10.46	9.76		
D_{ctg}	[μg]	1.63	1.25	1.25	1.89		
D_{cnl}	[μg]	1.03	0.68	0.76	0.16	mean	SD
D_{ad}	[μg]	8.21	8.73	8.46	7.70	8.28	0.44

Transferred amount: [μg]

	Rat#			
	11	12	13	19
0 [min]	0.000	0.000	0.000	0.000
1	0.121	0.000	0.254	0.101
3	0.660	0.309	1.170	0.576
5	1.517	0.972	1.926	1.304
10	3.344	22.391	3.138	2.386
15	4.264	3.433	3.981	3.271
20	4.627	4.043	4.562	3.716
30	5.062	4.467	5.078	4.124
40	5.152	4.895	5.279	4.250
50	5.222	5.069	5.453	4.317
60	5.325	5.132	5.459	4.377
75	5.252	5.231	5.539	4.387
90	5.396	5.235	5.529	4.411
120	5.334	5.401	5.571	4.383

% transferred: [%]					mean	SD
0 [min]	0.00	0.00	0.00	0.00	**0.00**	**0.00**
1	1.47	0.00	3.00	1.31	**1.45**	**1.23**
3	8.04	3.54	13.83	7.48	**8.22**	**4.24**
5	18.47	11.14	22.76	16.93	**17.32**	**4.81**
10	40.71	256.51	37.09	30.98	**91.32**	**110.20**
15	51.91	39.33	47.05	42.47	**45.19**	**5.49**
20	56.33	46.32	53.92	48.25	**51.20**	**4.70**
30	61.63	51.17	60.02	53.54	**56.59**	**5.02**
40	62.72	56.08	62.39	55.18	**59.09**	**4.02**
50	63.57	58.07	64.45	56.05	**60.54**	**4.11**
60	64.83	58.79	64.52	56.83	**61.24**	**4.04**
75	63.94	59.93	65.47	56.96	**61.57**	**3.86**
90	65.69	59.97	65.35	57.27	**62.07**	**4.13**
120	64.94	61.87	65.84	56.91	**62.39**	**4.03**

Table AVII.55. Dose, and amount and % of administered dose of 376 Da F-Na absorbed from airways to perfusate in the IPRL at 37 °C (nominal dose = 0.02 mg; used in Figs. III.6 and III.11, Chapter 3).

Amount delivered:

		Rat#					
		39	42	44	96		
BW	[g]	350	354	348	320		
D_L	[µg]	22.82	20.57	19.90	20.88		
D_{ctg}	[µg]	1.54	0.58	1.17	1.18		
D_{cnl}	[µg]	5.13	2.47	0.71	0.88	mean	SD
D_{ad}	[µg]	16.16	17.53	18.03	18.81	17.63	1.12

Transferred amount: [µg]

	Rat#			
	39	42	44	96
0 [min]	0.000	0.000	0.000	0.000
1	0.000	0.186	0.212	0.000
3	0.576	0.678	1.573	0.165
5	1.890	1.730	2.937	0.898
10	4.564	4.417	5.872	2.894
15	6.920	6.268	7.765	4.333
20	8.447	7.556	8.752	5.943
30	9.655	7.816	9.783	7.778
40	10.188	8.281	10.404	8.239
50	10.499	8.510	10.816	8.733
60	10.632	8.626	11.116	9.080
75	10.722	8.897	11.024	9.221
90	10.844	9.066	11.175	9.623
120	10.869	9.234	11.071	9.495

% transferred: [%]					mean	SD
0 [min]	0.00	0.00	0.00	0.00	**0.00**	**0.00**
1	0.00	1.06	1.18	0.00	**0.56**	**0.65**
3	3.57	3.87	8.72	0.88	**4.26**	**3.27**
5	11.70	9.87	16.29	4.77	**10.66**	**4.76**
10	28.25	25.20	32.56	15.38	**25.35**	**7.30**
15	42.83	35.76	43.06	23.03	**36.17**	**9.39**
20	52.28	43.11	48.53	31.59	**43.88**	**9.02**
30	59.76	44.59	54.25	41.34	**49.98**	**8.52**
40	63.06	47.24	57.69	43.79	**52.95**	**8.97**
50	64.99	48.55	59.98	46.42	**54.98**	**8.94**
60	65.81	49.21	61.64	48.26	**56.23**	**8.83**
75	66.37	50.76	61.13	49.01	**56.82**	**8.32**
90	67.12	51.72	61.97	51.15	**57.99**	**7.86**
120	67.28	52.68	61.39	50.47	**57.95**	**7.80**

Table AVII.56. Dose, and amount and % of administered dose of 376 Da F-Na absorbed from airways to perfusate in the IPRL at 37 °C (nominal dose = 0.04 mg; used in Figs. III.6 and III.11, Chapter 3).

Amount delivered:

		Rat#					
		106	107	108	109		
BW	[g]	380	365	380	340		
D_L	[µg]	41.48	43.61	41.53	50.53		
D_{ctg}	[µg]	1.00	1.12	2.48	2.11		
D_{cnl}	[µg]	8.69	8.23	3.91	8.40	mean	SD
D_{ad}	[µg]	31.80	34.26	35.14	40.02	35.30	3.45

Transferred amount: [µg]

	Rat#			
	106	107	108	109
0 [min]	0.000	0.000	0.000	0.000
1	0.082	0.179	0.168	0.158
3	1.830	3.541	2.516	2.173
5	5.308	7.579	4.813	5.334
10	12.512	13.020	12.056	12.582
15	16.151	16.960	15.956	17.009
20	18.914	19.170	18.657	19.646
30	20.907	21.183	20.030	21.993
40	22.802	21.773	21.933	23.108
50	22.362	21.920	22.568	23.470
60	22.865	22.179	22.777	23.271
75	23.494	22.492	22.183	23.622
90	24.013	22.776	22.667	23.679
120	23.970	22.559	22.796	23.255

% transferred: [%]					mean	SD
0 [min]	0.00	0.00	0.00	0.00	**0.00**	**0.00**
1	0.26	0.52	0.48	0.39	**0.41**	**0.12**
3	5.75	10.34	7.16	5.43	**7.17**	**2.24**
5	16.69	22.12	13.70	13.33	**16.46**	**4.06**
10	39.34	38.01	34.31	31.44	**35.77**	**3.59**
15	50.79	49.51	45.41	42.50	**47.05**	**3.80**
20	59.47	55.96	53.10	49.09	**54.40**	**4.40**
30	65.74	61.83	57.00	54.96	**59.88**	**4.85**
40	71.70	63.56	62.42	57.74	**63.85**	**5.80**
50	70.32	63.99	64.23	58.65	**64.29**	**4.77**
60	71.90	64.74	64.82	58.15	**64.90**	**5.62**
75	73.88	65.65	63.13	59.03	**65.42**	**6.26**
90	75.51	66.48	64.51	59.17	**66.42**	**6.80**
120	75.37	65.85	64.88	58.11	**66.05**	**7.10**

Table AVII.57. Dose, and amount and % of administered dose of 376 Da F-Na absorbed from airways to perfusate in the IPRL at 25 °C (nominal dose = 0.01 mg; used in Fig. IV.7, Chapter 4).

Amount delivered:

		Rat#					
		14	15	16	18		
BW	[g]	318	320	340	378		
D_L	[µg]	10.87	10.18	12.18	11.46		
D_{ctg}	[µg]	0.90	0.10	0.56	0.95		
D_{cnl}	[µg]	0.23	0.35	0.29	0.79	mean	SD
D_{ad}	[µg]	9.74	9.73	11.34	9.72	10.13	0.80

Transferred amount: [µg]

	Rat#			
	14	15	16	18
0 [min]	0.000	0.000	0.000	0.000
1	0.000	0.101	0.067	0.041
3	0.230	0.637	0.990	0.185
5	0.736	1.175	1.999	0.449
10	2.062	2.298	3.275	1.154
15	3.118	3.036	4.094	1.778
20	3.749	3.418	4.783	2.355
30	4.765	4.148	5.552	3.252
40	5.442	4.546	6.175	4.023
50	5.850	4.925	6.578	4.551
60	6.107	5.282	6.855	5.057
75	6.301	5.657	7.247	5.536
90	6.226	5.832	7.416	5.863
120	6.225	5.813	7.603	5.963

% transferred: [%]					mean	SD
0 [min]	0.00	0.00	0.00	0.00	**0.00**	**0.00**
1	0.00	1.04	0.59	0.42	**0.51**	**0.43**
3	2.36	6.55	8.73	1.90	**4.89**	**3.31**
5	7.56	12.08	17.63	4.62	**10.47**	**5.67**
10	21.17	23.62	28.89	11.87	**21.39**	**7.11**
15	32.02	31.21	36.11	18.29	**29.41**	**7.71**
20	38.50	35.13	42.19	24.23	**35.01**	**7.74**
30	48.93	42.64	48.97	33.46	**43.50**	**7.33**
40	55.88	46.73	54.47	41.39	**49.62**	**6.80**
50	60.07	50.62	58.02	46.83	**53.89**	**6.22**
60	62.71	54.29	60.47	52.03	**57.38**	**5.04**
75	64.71	58.15	63.92	56.96	**60.93**	**3.95**
90	63.94	59.94	65.41	60.33	**62.40**	**2.69**
120	63.92	59.75	67.06	61.35	**63.02**	**3.20**

Table AVII.58. Dose, and amount and % of administered dose of 376 Da F-Na absorbed from airways to perfusate in the IPRL at 25 °C (nominal dose = 0.02 mg; used in Fig. IV.7, Chapter 4).

Amount delivered:

		Rat#					
		40	41	43	95		
BW	[g]	366	358	358	300		
D_L	[µg]	22.78	20.92	21.33	21.50		
D_{ctg}	[µg]	1.20	0.34	0.77	0.87		
D_{cnl}	[µg]	2.12	3.09	4.45	0.61	mean	SD
D_{ad}	[µg]	19.46	17.50	16.12	20.02	18.28	1.80

Transferred amount: [µg]

	Rat#			
	40	41	43	95
0 [min]	0.000	0.000	0.000	0.000
1	0.028	0.050	0.000	0.118
3	0.266	0.334	0.117	1.144
5	0.694	0.614	0.371	1.974
10	1.778	1.487	1.148	4.143
15	2.846	2.277	2.027	5.232
20	3.758	3.136	2.943	7.251
30	5.332	4.564	4.690	8.411
40	6.761	6.404	5.861	9.060
50	7.632	6.561	6.865	10.431
60	8.483	7.514	7.350	11.732
75	8.950	8.529	8.219	12.080
90	9.323	8.942	8.543	12.426
120	10.100	9.175	9.050	12.356

% transferred: [%]					mean	SD
0 [min]	0.00	0.00	0.00	0.00	**0.00**	**0.00**
1	0.14	0.29	0.00	0.59	**0.25**	**0.25**
3	1.37	1.91	0.73	5.71	**2.43**	**2.24**
5	3.57	3.51	2.30	9.86	**4.81**	**3.42**
10	9.14	8.50	7.12	20.69	**11.36**	**6.28**
15	14.62	13.01	12.58	26.13	**16.59**	**6.42**
20	19.31	17.92	18.26	36.21	**22.93**	**8.88**
30	27.40	26.08	29.10	42.01	**31.15**	**7.34**
40	34.74	36.60	36.36	45.25	**38.24**	**4.75**
50	39.21	37.50	42.59	52.10	**42.85**	**6.52**
60	43.59	42.94	45.60	58.59	**47.68**	**7.36**
75	45.99	48.75	50.99	60.33	**51.51**	**6.22**
90	47.90	51.11	53.00	62.06	**53.52**	**6.07**
120	51.90	52.44	56.15	61.71	**55.55**	**4.52**

Table AVII.59. Dose, and amount and % of administered dose of 376 Da F-Na absorbed from airways to perfusate in the IPRL at 25 °C (nominal dose = 0.04 mg; used in Fig. IV.7, Chapter 4).

Amount delivered:

		Rat#					
		114	115	116	117		
BW	[g]	320	310	330	340		
D_L	[µg]	46.51	54.11	49.61	42.29		
D_{ctg}	[µg]	1.12	1.99	4.34	2.68		
D_{cnl}	[µg]	4.87	12.18	4.39	1.17	mean	SD
D_{ad}	[µg]	40.53	39.94	40.89	38.44	39.95	1.08

Transferred amount: [µg]

		Rat#			
		114	115	116	117
0	[min]	0.000	0.000	0.000	0.000
1		0.099	0.315	0.086	0.107
3		1.869	1.630	1.283	1.318
5		4.403	3.882	3.467	3.331
10		8.774	8.524	7.442	7.704
15		12.508	10.214	11.221	11.088
20		15.060	12.233	14.076	13.861
30		18.405	17.467	19.026	17.386
40		21.253	21.330	21.967	19.866
50		22.900	22.287	24.136	21.543
60		23.837	22.743	25.506	22.359
75		24.613	23.433	26.683	23.271
90		25.219	23.608	27.226	23.574
120		25.617	23.801	27.800	24.086

% transferred: [%]						mean	SD
0	[min]	0.00	0.00	0.00	0.00	**0.00**	**0.00**
1		0.24	0.79	0.21	0.28	**0.38**	**0.27**
3		4.61	4.08	3.14	3.43	**3.81**	**0.66**
5		10.86	9.72	8.48	8.67	**9.43**	**1.10**
10		21.65	21.34	18.20	20.04	**20.31**	**1.57**
15		30.86	25.57	27.44	28.84	**28.18**	**2.23**
20		37.16	30.63	34.43	36.06	**34.57**	**2.86**
30		45.41	43.73	46.53	45.23	**45.22**	**1.15**
40		52.44	53.40	53.73	51.68	**52.81**	**0.93**
50		56.50	55.80	59.03	56.04	**56.84**	**1.49**
60		58.81	56.94	62.38	58.17	**59.07**	**2.34**
75		60.72	58.66	65.26	60.54	**61.30**	**2.80**
90		62.22	59.10	66.59	61.33	**62.31**	**3.14**
120		63.20	59.59	67.99	62.66	**63.36**	**3.47**

Table AVII.60. Dose, and amount and % of administered dose of 376 Da F-Na absorbed from airways to perfusate in the IPRL in the presence of 1 mM DNP at 37 °C (nominal dose = 0.02 mg; used in Fig. IV.8, Chapter 4).

Amount delivered:

		Rat#					
		234	235	236	237		
BW	[g]	315	315	340	345		
D_L	[µg]	20.54	21.18	24.27	25.48		
D_{ctg}	[µg]	0.29	0.32	0.10	0.74		
D_{cnl}	[µg]	5.06	5.32	2.89	5.09	mean	SD
D_{ad}	[µg]	15.19	15.54	21.28	19.65	17.92	3.02

Transferred amount: [µg]

	Rat#			
	234	235	236	237
0 [min]	0.000	0.000	0.000	0.000
1	0.101	0.387	0.680	0.082
3	1.249	2.754	4.040	1.733
5	2.555	4.637	7.337	3.863
10	4.270	7.266	10.761	7.327
15	5.162	9.336	12.926	8.756
20	5.435	10.024	13.312	9.683
30	5.730	10.434	14.323	10.587
40	5.754	10.592	15.029	10.874
50	6.165	10.761	14.914	10.873
60	6.157	10.701	14.840	11.103

% transferred: [%]					mean	SD
0 [min]	0.00	0.00	0.00	0.00	**0.00**	**0.00**
1	0.66	2.49	3.20	0.42	**1.69**	**1.36**
3	8.22	17.72	18.98	8.82	**13.44**	**5.71**
5	16.82	29.84	34.48	19.66	**25.20**	**8.34**
10	28.11	46.76	50.57	37.29	**40.68**	**10.07**
15	33.98	60.08	60.74	44.56	**49.84**	**12.95**
20	35.78	64.50	62.56	49.28	**53.03**	**13.34**
30	37.72	67.14	67.31	53.88	**56.51**	**14.02**
40	37.88	68.16	70.63	55.34	**58.00**	**14.99**
50	40.59	69.25	70.08	55.33	**58.81**	**13.91**
60	40.53	68.86	69.74	56.50	**58.91**	**13.66**

Table AVII.61. Dose, and amount and % of administered dose of 376 Da F-Na absorbed from airways to perfusate in the IPRL in the presence of 100 μM OUA at 37 °C (nominal dose = 0.02 mg; used in Fig. IV.8, Chapter 4).

Amount delivered:

		Rat#					
		224	225	227	229		
BW	[g]	330	330	330	325		
D_L	[μg]	20.89	21.44	21.08	21.23		
D_{ctg}	[μg]	0.22	1.02	0.12	0.29		
D_{cnl}	[μg]	4.24	3.26	4.62	4.06	mean	SD
D_{ad}	[μg]	16.43	17.16	16.34	16.88	16.70	0.39

Transferred amount: [μg]

		Rat#			
		224	225	227	229
0	[min]	0.000	0.000	0.000	0.000
1		0.035	0.258	0.171	0.060
3		3.130	2.761	2.463	3.511
5		4.807	4.558	4.350	5.188
10		8.369	7.669	7.787	6.321
15		9.882	9.320	9.161	6.547
20		10.718	10.089	10.156	8.597
30		11.512	10.531	10.679	9.571
40		11.180	10.990	10.605	9.962
50		11.788	11.015	11.095	9.949
60		11.682	11.176	11.221	9.923

% transferred: [%]

						mean	SD
0	[min]	0.00	0.00	0.00	0.00	**0.00**	**0.00**
1		0.21	1.50	1.05	0.36	**0.78**	**0.60**
3		19.05	16.09	15.07	20.80	**17.75**	**2.64**
5		29.26	26.56	26.62	30.73	**28.29**	**2.06**
10		50.94	44.69	47.66	37.45	**45.18**	**5.75**
15		60.15	54.31	56.06	38.79	**52.33**	**9.35**
20		65.23	58.79	62.15	50.93	**59.28**	**6.16**
30		70.07	61.37	65.35	56.70	**63.37**	**5.69**
40		68.05	64.04	64.90	59.02	**64.00**	**3.74**
50		71.75	64.19	67.90	58.94	**65.69**	**5.46**
60		71.10	65.13	68.67	58.79	**65.92**	**5.35**

Table AVII.62. Dose, and amount and % of administered dose of 376 Da F-Na absorbed from airways to perfusate in the IPRL in the presence of 100 μM MON at 37 °C (nominal dose = 0.02 mg; used in Fig. IV.8, Chapter 4).

Amount delivered:

		Rat#					
		272	273	274	275		
BW	[g]	380	380	350	330		
D_L	[μg]	20.21	21.56	19.94	19.22		
D_{ctg}	[μg]	0.79	1.89	2.01	0.20		
D_{cnl}	[μg]	5.20	6.18	5.77	7.02	mean	SD
D_{ad}	[μg]	14.22	13.49	12.16	12.00	12.97	1.07

Transferred amount: [μg]

	Rat#			
	272	273	274	275
0 [min]	0.000	0.000	0.000	0.000
1	0.022	0.000	0.204	0.129
3	0.785	0.343	0.570	1.531
5	1.888	1.043	1.441	2.649
10	5.099	3.142	3.199	4.336
15	6.897	4.586	4.656	5.270
20	8.014	5.609	5.414	5.783
30	8.650	6.322	6.320	6.149
40	8.330	6.713	6.535	6.404
50	9.447	6.790	6.860	6.523
60	9.576	6.889	6.933	6.629
90	9.274	7.017	7.395	6.738
120	9.210	7.220	7.143	6.686

% transferred: [%]					mean	SD
0 [min]	0.00	0.00	0.00	0.00	**0.00**	**0.00**
1	0.15	0.00	1.68	1.08	**0.73**	**0.79**
3	5.52	2.54	4.69	12.76	**6.38**	**4.44**
5	13.28	7.73	11.85	22.08	**13.73**	**6.04**
10	35.86	23.29	26.31	36.13	**30.40**	**6.58**
15	48.50	34.00	38.29	43.92	**41.18**	**6.35**
20	56.36	41.58	44.52	48.19	**47.66**	**6.40**
30	60.83	46.86	51.97	51.24	**52.73**	**5.85**
40	58.58	49.76	53.74	53.37	**53.86**	**3.62**
50	66.43	50.33	56.41	54.36	**56.89**	**6.85**
60	67.34	51.07	57.01	55.24	**57.67**	**6.92**
90	65.22	52.02	60.81	56.15	**58.55**	**5.72**
120	64.77	53.52	58.74	55.72	**58.19**	**4.88**

Table AVII.63. Dose, and amount and % of administered dose of 376 Da F-Na absorbed from airways to perfusate in the IPRL in the presence of 100 μM NOC at 37 °C (nominal dose = 0.02 mg; used in Fig. IV.8, Chapter 4).

Amount delivered:

		Rat#					
		298	299	300	301		
BW	[g]	360	370	380	380		
D_L	[μg]	20.56	21.51	22.21	22.63		
D_{ctg}	[μg]	0.63	0.46	0.31	0.95		
D_{cnl}	[μg]	1.62	1.69	1.92	1.99	mean	SD
D_{ad}	[μg]	18.32	19.36	19.98	19.69	19.34	0.73

Transferred amount: [μg]

	Rat#			
	298	299	300	301
0 [min]	0.000	0.000	0.000	0.000
1	0.009	0.073	0.103	0.155
3	0.339	1.112	1.115	1.259
5	0.949	2.805	2.803	2.713
10	3.176	6.201	6.075	7.086
15	5.186	8.709	8.375	9.681
20	6.866	9.983	9.713	10.286
30	8.462	11.602	10.774	11.806
40	9.694	11.846	11.635	12.632
50	10.111	12.437	11.762	12.584
60	10.434	12.713	11.752	12.410
90	11.163	12.683	12.512	12.772
120	11.579	12.399	12.653	13.159

% transferred: [%]					mean	SD
0 [min]	0.00	0.00	0.00	0.00	**0.00**	**0.00**
1	0.05	0.38	0.52	0.79	**0.43**	**0.31**
3	1.85	5.74	5.58	6.39	**4.89**	**2.06**
5	5.18	14.49	14.03	13.78	**11.87**	**4.47**
10	17.34	32.03	30.40	35.98	**28.94**	**8.08**
15	28.32	44.98	41.91	49.16	**41.09**	**9.02**
20	37.49	51.56	48.60	52.23	**47.47**	**6.84**
30	46.20	59.92	53.91	59.95	**55.00**	**6.51**
40	52.93	61.18	58.22	64.14	**59.12**	**4.78**
50	55.21	64.24	58.86	63.90	**60.55**	**4.33**
60	56.97	65.66	58.81	63.02	**61.11**	**3.95**
90	60.95	65.51	62.61	64.86	**63.48**	**2.09**
120	63.22	64.04	63.32	66.82	**64.35**	**1.69**

*** MicroMath Scientist Statistics Report ***

Model File Name : a:\f-phea.eqn
Data File Name : a:\data-37.mmd
Param File Name : a:\37-ini.par

Goodness-of-fit statistics for data set: a:\data-37.mmd

Data Column Name: FP

	Weighted	Unweighted
Sum of squared observations :	70937.6348	70937.6348
Sum of squared deviations :	1004.40593	1004.40593
Standard deviation of data :	4.05779139	4.05779139
R-squared :	0.985841001	0.985841001
Coefficient of determination :	0.961031051	0.961031051
Correlation :	0.980978323	0.980978323

Data Set Name: a:\data-37.mmd

	Weighted	Unweighted
Sum of squared observations :	70937.6348	70937.6348
Sum of squared deviations :	1004.40593	1004.40593
Standard deviation of data :	4.05779139	4.05779139
R-squared :	0.985841001	0.985841001
Coefficient of determination :	0.961031051	0.961031051
Correlation :	0.980978323	0.980978323
Model Selection Criterion :	3.12191322	3.12191322

Confidence Intervals:

Parameter Name :	KA		
Estimate Value =	0.00117717506		
Standard Deviation =	0.000693588225		
95% Range (Univar) =	-0.000209740293		0.00256409046
95% Range (S-Plane) =	-0.00102604148		0.00338039164
Parameter Name :	KE		
Estimate Value =	0.0233379971		
Standard Deviation =	0.00173152314		
95% Range (Univar) =	0.0198756026		0.0268003916
95% Range (S-Plane) =	0.0178377300		0.0288382641
Parameter Name :	VMAX		
Estimate Value =	4.36600215		
Standard Deviation =	0.565159738		
95% Range (Univar) =	3.23589541	5.49610889	
95% Range (S-Plane) =	2.57074489	6.16125941	
Parameter Name :	KM		
Estimate Value =	56.5958869		
Standard Deviation =	14.7080819		
95% Range (Univar) =	27.1852595	66.0065143	
95% Range (S-Plane) =	9.87495304	103.316821	

Variance-Covariance Matrix:

4.81064627E-7			
2.33468801E-7	2.99817239E-6		
-0.000302486774	5.87178927E-5	0.319405530	
-0.00702507801	-0.00586100968	7.57068919	216.327672

Correlation Matrix:

1.00000000			
0.194401155	1.00000000		
-0.771673280	0.0600027210	1.00000000	
-0.688641832	-0.230137876	0.910768839	1.00000000

Residual Analysis:

The following are normalized parameters with an expected value of 0.0. Values are in units of standard deviations from the expected value.
The serial correlation is 6.06 which indicates a systematic non-random trend in the residuals.
Skewness is -0.60 which is probably not significant.
Kurtosis is -0.00 which is probably not significant.
The weighting factor was 0.00 leading to a heteroscedasticity of 0.79 which suggests an optimal weight factor for this fit of about 0.79

Figure AVII.1. Statistical Output obtained from across-dose fitting for 7.4 kDa F-PHEA absorption data in the IPRL at 37 °C.

*** MicroMath Scientist Statistics Report ***

Model File Name : a:\f-phea.eqn
Data File Name : a:\data-25.mmd
Param File Name : Untitled16

Goodness-of-fit statistics for data set: a:\data-25.mmd

Data Column Name: FP

	Weighted	Unweighted
Sum of squared observations :	9942.32950	9942.32950
Sum of squared deviations :	85.0274254	85.0274254
Standard deviation of data :	1.33094128	1.33094128
R-squared :	0.991447937	0.991447937
Coefficient of determination :	0.979576657	0.979576657
Correlation :	0.989877125	0.989877125

Data Set Name: a:\data-25.mmd

	Weighted	Unweighted
Sum of squared observations :	9942.32950	9942.32950
Sum of squared deviations :	85.0274254	85.0274254
Standard deviation of data :	1.33094128	1.33094128
R-squared :	0.991447937	0.991447937
Coefficient of determination :	0.979576657	0.979576657
Correlation :	0.989877125	0.989877125
Model Selection Criterion :	3.73723063	3.73723063

Confidence Intervals:

Parameter Name :	KA	
Estimate Value =	0.00231607203	
Standard Deviation =	0.000224894983	
95% Range (Univar) =	0.00186389036	0.00276825370
95% Range (S-Plane) =	0.00159567186	0.00303647220
Parameter Name :	KE	
Estimate Value =	0.0160359853	
Standard Deviation =	0.00141635407	
95% Range (Univar) =	0.0131882146	0.0188837560
95% Range (S-Plane) =	0.0114990156	0.0205729550
Parameter Name :	VMAX	
Estimate Value =	0.666531969	
Standard Deviation =	0.103191970	
95% Range (Univar) =	0.459050606	0.874013330
95% Range (S-Plane) =	0.335979852	0.997084085
Parameter Name :	KM	
Estimate Value =	30.3172395	
Standard Deviation =	16.3668178	
95% Range (Univar) =	-2.59045317	63.2249321
95% Range (S-Plane) =	-22.1101565	82.7446354

Variance-Covariance Matrix

5.05777533E-8			
2.31486683E-7	2.00605885E-6		
-1.87752988E-5	-6.42090731E-5	0.0106485826	
-0.00302305785	-0.0159178916	1.55774477	267.872723

Correlation Matrix

1.00000000			
0.726732211	1.00000000		
-0.809023596	-0.439317662	1.00000000	
-0.821301176	-0.686672194	0.922329617	1.00000000

Residual Analysis:

The following are normalized parameters with an expected value of 0.0. Values are in units of standard deviations from the expected value.
The serial correlation is 5.20 which indicates a systematic non-random trend in the residuals.
Skewness is -0.22 which is probably not significant.
Kurtosis is -0.00 which is probably not significant.
The weighting factor was 0.00 leading to a heteroscedacticity of 0.27 which suggests an optimal weight factor for this fit of about 0.27

Figure AVII.2. Statistical Output obtained from across-dose fitting for 7.4 kDa F-PHEA absorption data in the IPRL at 25 °C.

*** MicroMath Scientist Statistics Report ***

Model File Name : a:\f-phea.eqn
Data File Name : a:\7002-5\fit-37.mmd
Param File Name : Untitled2

Goodness-of-fit statistics for data set: a:\7002-5\fit-37.mmd

Data Column Name: FP

	Weighted	Unweighted
Sum of squared observations :	83716.4199	83716.4199
Sum of squared deviations :	340.155224	340.155224
Standard deviation of data :	3.11748627	3.11748627
R-squared :	0.995936816	0.995936816
Coefficient of determination :	0.979804353	0.979804353
Correlation :	0.990176849	0.990176849

Data Set Name: a:\7002-5\fit-37.mmd

	Weighted	Unweighted
Sum of squared observations :	83716.4199	83716.4199
Sum of squared deviations :	340.155224	340.155224
Standard deviation of data :	3.11748627	3.11748627
R-squared :	0.995936816	0.995936816
Coefficient of determination :	0.979804353	0.979804353
Correlation :	0.990176849	0.990176849
Model Selection Criterion :	3.69715997	3.69715997

Confidence Intervals:

Parameter Name :	KA	
Estimate Value =	0.0135128562	
Standard Deviation =	0.00260703011	
95% Range (Univar) =	0.00822030368	0.0188054087
95% Range (S-Plane) =	0.00503866049	0.0219870519
Parameter Name :	KE	
Estimate Value =	0.0163476500	
Standard Deviation =	0.00112350182	
95% Range (Univar) =	0.0140668201	0.0186284800
95% Range (S-Plane) =	0.0126956883	0.0199996118
Parameter Name :	VMAX	
Estimate Value =	3.59568887	
Standard Deviation =	1.52981124	
95% Range (Univar) =	0.490006948	6.70137080
95% Range (S-Plane) =	-1.37698856	8.56836630
Parameter Name :	KM	
Estimate Value =	76.7830413	
Standard Deviation =	46.4369781	
95% Range (Univar) =	-17.4890362	171.055119
95% Range (S-Plane) =	-74.1611454	227.727228

Variance-Covariance Matrix

6.79660601E-6			
1.27201917E-6	1.26225635E-6		
-0.00371022316	-0.000500372154	2.34032243	
-0.108007668	-0.0189567550	69.8596318	2156.39294

Correlation Matrix

1.00000000			
0.434283996	1.00000000		
-0.930285255	-0.291126342	1.00000000	
-0.892163790	-0.363350921	0.983387072	1.00000000

Residual Analysis:

The following are normalized parameters with an expected value of 0.0. Values are in units of standard deviations from the expected value.
The serial correlation is 3.74 which indicates a systematic non-random trend in the residuals.
Skewness is 0.19 which is probably not significant.
Kurtosis is 0.00 which is probably not significant.
The weighting factor was 0.00 leading to a heteroscedasticity of 0.96 which suggests an optimal weight factor for this fit of about 0.96

Figure AVII.3. Statistical Output obtained from across-dose fitting for 4.3 kDa F-PHEA absorption data in the IPRL at 37 °C.

*** MicroMath Scientist Statistics Report ***

Model File Name : a:\f-phea.eqn
Data File Name : a:\7002-5\fit-25.mmd
Param File Name : Untitled2

Goodness-of-fit statistics for data set: a:\7002-5\fit-25.mmd

Data Column Name: FP	Weighted	Unweighted
Sum of squared observations :	25690.0931	25690.0931
Sum of squared deviations :	62.5947746	62.5947746
Standard deviation of data :	1.33731901	1.33731901
R-squared :	0.997563466	0.997563466
Coefficient of determination :	0.992470996	0.992470996
Correlation :	0.996496326	0.996496326

Data Set Name: a:\7002-5\fit-25.mmd	Weighted	Unweighted
Sum of squared observations :	25690.0931	25690.0931
Sum of squared deviations :	62.5947746	62.5947746
Standard deviation of data :	1.33731901	1.33731901
R-squared :	0.997563466	0.997563466
Coefficient of determination :	0.992470996	0.992470996
Correlation :	0.996496326	0.996496326
Model Selection Criterion :	4.68386430	4.68386430

Confidence Intervals:

Parameter Name :	KA	
Estimate Value =	0.0054259451	
Standard Deviation =	0.000580804780	
95% Range (Univar) =	0.00423349812	0.0065169090
95% Range (S-Plane) =	0.00352467870	0.00730061032

Parameter Name :	KE	
Estimate Value =	0.0123984804	
Standard Deviation =	0.000638862782	
95% Range (Univar) =	0.0111015199	0.0136954408
95% Range (S-Plane) =	0.0103218460	0.0144751147

Parameter Name :	VMAX	
Estimate Value =	0.915892575	
Standard Deviation =	0.314507792	
95% Range (Univar) =	0.277407812	1.55437734
95% Range (S-Plane) =	-0.106420350	1.93820550

Parameter Name :	KM	
Estimate Value =	84.7188645	
Standard Deviation =	39.3070241	
95% Range (Univar) =	4.92136317	164.516366
95% Range (S-Plane) =	-43.0492855	212.487015

Variance-Covariance Matrix

3.37334192E-7			
2.03889954E-7	4.08145667E-7		
-0.000170776495	-8.15465658E-5	0.0989151514	
-0.0206642082 -0.0124625538	12.1562164	1545.04215	

Correlation Matrix

1.00000000			
0.549487796	1.00000000		
-0.934902893	-0.405851046	1.00000000	
-0.905145551	-0.496282871	0.983324471	1.00000000

Residual Analysis:

The following are normalized parameters with an expected value of 0.0. Values are in units of standard deviations from the expected value.
The serial correlation is 3.01 which indicates a systematic non-random trend in the residuals.
Skewness is -0.11 which is probably not significant.
Kurtosis is 0.00 which is probably not significant.
The weighting factor was 0.00 leading to a heteroscedasticity of 0.02 which suggests an optimal weight factor for this fit of about 0.02

Figure AVII.4. Statistical Output obtained from across-dose fitting for 4.3 kDa F-PHEA absorption data in the IPRL at 25 °C.

*** MicroMath Scientist Statistics Report ***

Model File Name : a:\fd-4.eqn
Data File Name : a:\fd4-37.mmd
Param File Name : Untitled9

Goodness-of-fit statistics for data set: a:\fd4-37.mmd

Data Column Name: FP

	Weighted	Unweighted
Sum of squared observations :	13257.6229	13257.6229
Sum of squared deviations :	131.677935	131.677935
Standard deviation of data :	2.44649968	2.44649968
R-squared :	0.990067757	0.990067757
Coefficient of determination:	0.950066223	0.950066223
Correlation :	0.974717342	0.974717342

DataSet Name: a:\fd4-37.mmd

	Weighted	Unweighted
Sum of squared observations :	13257.6229	13257.6229
Sum of squared deviations :	131.677935	131.677935
Standard deviation of data :	2.44649968	2.44649968
R-squared :	0.990067757	0.990067757
Coefficient of determination :	0.950066223	0.950066223
Correlation :	0.974717342	0.974717342
Model Selection Criterion :	2.83039094	2.83039094

Confidence Intervals:

Parameter Name :	KA	
Estimate Value =	0.0159854945	
Standard Deviation =	0.00113833447	
95% Range (Univar) =	0.0136247333	0.0183462557
95% Range(S-Plane) =	0.0129982147	0.0189727743
Parameter Name :	KE	
Estimate Value =	0.0293346819	
Standard Deviation =	0.00299367339	
95% Range (Univar) =	0.0231261833	0.0355431805
95% Range(S-Plane) =	0.0214785200	0.0371908439

Variance-Covariance Matrix
1.29580536E-6
3.11320360E-6 8.96208036E-6

Correlation Matrix
1.00000000
0.913551891 1.00000000

Residual Analysis:

The following are normalized parameters with an expected value of 0.0. Values are in units of standard deviations from the expected value.
The serial correlation is 4.08 which indicates a systematic non-random trend in the residuals.
Skewness is -0.38 which is probably not significant.
Kurtosis is 0.12 which is probably not significant.
The weighting factor was 0.00 leading to a heteroscedacticity of 0.66 which suggests an optimal weight factor for this fit of about 0.66

Figure AVII.5. Statistical Output obtained from across-dose fitting for 4.4 kDa FD-4 absorption data in the IPRL at 37 °C.

*** MicroMath Scientist Statistics Report ***

Model File Name : a:\fd-4.eqn
Data File Name : a:\fd4-25.mmd
Param File Name : Untitled9

Goodness-of-fit statistics for data set: a:\fd4-25.mmd

Data Column Name: FP

	Weighted	Unweighted
Sum of squared observations :	11274.9864	11274.9884
Sum of squared deviations :	169.148729	169.148729
Standard deviation of data :	2.77282862	2.77282862
R-squared :	0.984997877	0.984997877
Coefficient of determination :	0.952052084	0.952052084
Correlation :	0.975816638	0.975816638

Data Set Name: a:\fd4-25.mmd

	Weighted	Unweighted
Sum of squared observations :	11274.9864	11274.9864
Sum of squared deviations :	169.148729	169.148729
Standard deviation of data :	2.77282862	2.77282862
R-squared :	0.984997877	0.984997877
Coefficient of determination :	0.952052084	0.952052084
Correlation :	0.975816638	0.975816638
Model Selection Criterion :	2.87097327	2.87097327

Confidence Intorvals:

Parameter Name :	KA	
Estimate Value =	0.00837423934	
Standard Deviation =	0.000647325213	
95% Range (Univar) =	0.00703176901	0.00971670966
95% Range (S-Plane) =	0.00667549300	0.0100729857

Parameter Name :	KE	
Estimate Value =	0.0117131325	
Standard Deviation =	0.00180269537	
95% Range (Univar) =	0.00797457108	0.0154516938
95% Range (S-Plane) =	0.00698240038	0.0164438645

Variance-Covariance Matrix:
4.19029931E-7
1.04026552E-6 3.24971058E-6

Correlation Matrix:
1.00000000
0.891454826 1.00000000

Residual Analysis:

The following are normalized parameters with an expected value of 0.0. Values are in units of standard deviations from the expected value.
The serial correlation is 3.76 which indicates a systematic non-random trend in the residuals.
Skewness is -0.13 which is probably not significant.
Kurtosis is 0.04 which is probably not significant.
The weighting factor was 0.00 leading to a heteroscedacticity of 1.55 which suggests an optimal weight factor for this fit of about 1.55

Figure AVII.6. Statistical Output obtained from across-dose fitting for 4.4 kDa FD-4 absorption data in the IPRL at 25 °C.

*** MicroMath Scientist Statistics Report ***

Model File Name : a:\f-na.eqn
Data File Name : a:\fna-37.mmd
Param File Name : Untitled1

Goodness-of-fit statistics for data set: a:\fna-37.mmd

Data Column Name: FP

	Weighted	Unweighted
Sum of squared observations :	93084.1888	93084.1888
Sum of squared deviations :	765.132504	765.132504
Standard deviation of data :	4.37359264	4.37359264
R-squared :	0.991780210	0.991780210
Coefficient of determination :	0.968771561	0.968771561
Correlation :	0.985809251	0.985809251

Data Set Name: a:\fna-37.mmd

	Weighted	Unweighted
Sum of squared observations :	93084.1888	93084.1888
Sum of squared deviations :	765.132504	765.132504
Standard deviation of data :	4.37359264	4.37359264
R-squared :	0.991780210	0.991780210
Coefficient of determination :	0.968771561	0.968771561
Correlation :	0.985809251	0.985809251
Model Selection Criterion :	3.37118801	3.37118801

Confidence Intervals:

Parameter Name :	KA	
Estimate Value =	0.0477436096	
Standard Deviation =	0.00281685229	
95% Range (Univar) =	0.0420505388	0.0534366805
95% Range (S-Plane) =	0.0405822348	0.0549049844

Parameter Name :	KE	
Estimate Value =	0.0218780006	
Standard Deviation =	0.00220141465	
95% Range (Univar) =	0.0174287756	0.0263272255
95% Range (S-Plane) =	0.0162812728	0.0274747283

Variance-Covariance Matrix:
7.93465682E-6
5.24027804E-6 4.84622645E-6

Correlation Matrix:
1.00000000
0.845061672 1.00000000

Residual Analysis:

The following are normalized parameters with an expected value of 0.0. Values are in units of standard deviations from the expected value.
The serial correlation is 5.44 which indicates a systematic non-random trend in the residuals.
Skewness is 0.43 which is probably not significant.
Kurtosis is -0.00 which is probably not significant.
The weighting factor was 0.00 leading to a heteroscedacticity of -0.16 which suggests an optimal weight factor for this fit of about -0.16

Figure AVII.7. Statistical Output obtained from across-dose fitting for F-Na absorption data in the IPRL at 37 °C.

*** MicroMath Scientist Statistics Report ***

Model File Name : a:\f-na.eqn
Data File Name : a:\fna-25.mmd
Param File Name : Untitled1

Goodness-of-fit statistics for data set: a:\fna-25.mmd

Data Column Name: FP

	Weighted	Unweighted
Sum of squared observations :	66641.7283	66641.7283
Sum of squared deviations :	881.526093	881.526093
Standard deviation of data :	4.69448105	4.69448105
R-squared :	0.986772160	0.986772160
Coefficient of determination :	0.959963745	0.959963745
Correlation :	0.980124204	0.980124204

Data Set Name: a:\fna-25.mmd

	Weighted	Unweighted
Sum of squared observations :	66641.7283	66641.7283
Sum of squared deviations :	881.526093	881.526093
Standard deviation of data :	4.69448105	4.69448105
R-squared :	0.986772160	0.986772160
Coefficient of determination :	0.959963745	0.959963745
Correlation :	0.980124204	0.980124204
Model Selection Criterion :	3.12273176	3.12273176

Confidence Intervals:

Parameter Name :	KA	
Estimate Value =	0.0233656026	
Standard Deviation =	0.00149113153	
95% Range (Univar) =	0.0203519134	0.0263792919
95% Range (S-Plane) =	0.0195746506	0.0271565546

Parameter Name :	KE	
Estimate Value =	0.0102098294	
Standard Deviation =	0.00162482798	
95% Range (Univar) =	0.00692592954	0.0134937292
95% Range (S-Plane) =	0.00607897658	0.0143406822

Variance-Covariance Matrix
2.22347324E-6
2.05607212E-6 2.64006597E-6

Correlation Matrix
1.00000000
0.848623396 1.00000000

Residual Analysis:

The following are normalized parameters with an expected value of 0.0. Values are in units of standard deviations from the expected value.
The serial correlation is 6.04 which indicates a systematic non-random trend in the residuals.
Skewness is 0.80 which is probably not significant.
Kurtosis is -0.00 which is probably not significant.
The weighting factor was 0.00 leading to a heteroscedacticity of 0.31 which suggests an optimal weight factor for this fit of about 0.31

Figure AVII.8. Statistical Output obtained from across-dose fitting for F-Na absorption data in the IPRL at 25 °C.

REFERENCES

REFERENCES

A. Adjei and J. Garren. **Pulmonary delivery of peptide drugs: effect of particle size on bioavailability of leuprolide acetate in healthy male volunteers.** *Pharm. Res.*, **7**:565-569 (1990).

A. Adjei and P. Gupta. **Pulmonary delivery of therapeutic peptides and proteins.** *J. Contol. Rel.*, **29**:361-373 (1994).

A. Adjei and P. Gupta. *Inhalation Delivery of Therapeutic Peptides and Proteins.* Marcel Dekker, Inc., New York, 1997.

B. M Alberts and P. Bedinger. **The 3'-5' proofreading exonuclease of bacteriophage T4DNA polymerase is stimulated by other T4DNA replication proteins.** *J. Biol. Chem.*, **258**:9649-9656 (1983).

B. Alberts, D. Bray, J. Lewis, M. Raff, K. Roberts and J. D. Watson. *Molecular Biology of The Cell.* Garland Publishing, Inc., New York, 1994.

R. G. Andersen, B. A. Kamen, K. G. Rothberg, S. W. Lacey. **Potocytosis: sequestration and transport of small molecules by caveolae.** *Science*, **255**:410-411 (1992).

T. E. Andreoli, J. F. Hoffman, D. D. Fanestil and S. G. Sshultz. *Membrane Transport Processes in Organized Systems,* Plenum Medical Book Company, New York, 1986.

G. Antoni and P. Neri. **Hydrodynamic properties of a new plasma expander: polyhydroxyethylaspartamide.** *Biopolymers*, **13**:1721-1729 (1974).

K. E. Arfors and H. Hint. **Studies of the microcirculation using fluorescent dextran.** *Microvasc. Res.*, **3**:440 (1971).

J. H. Ashton, B. R. Pitt and C. N. Gillis. **Apparent kinetics of angiotensin converting enzyme: hydrolysis of [^{3}H]benzoyl-phenylalanyl-alanyl-proline in the isolated perfused lung.** *J. Pharmacol. Exp. Ther.*, **232**:602-607 (1985).

K. L. Audus, R. L. Bartel, I. J. Hidalgo and R. T. Borchardt. **The use of culture epithelial and endothelial cells for drug transport and metabolism studies.** *Pharm. Res.*, **7**:435-451 (1990).

D. G. Baker, B. R. Toth, M. E. P. Goad, S. A. Barker and J. C. Means. **Establishment and validation of an isolated rat lung model for pulmonary metabolism studies.** *J. Appl. Toxicol.*, **19**:83-91 (1999).

M. D. Barrowcliffe and J. G. Jones. **Solute permeability of the alveolar capillary barrier.** *Thorax*, **42**:1-10 (1987).

M. L. Barnard, W. G. Olivera, D. M. Rutschman, A. M. Bertorello, A. I. Katz and J. J. Sznajder. **Dopamine stimulates sodium transport and liquid clearance in rat lung epithelium.** *Am. J. Respir. Crit. Care Med.*, **156**:709-714 (1997).

D. J. P. Basset and A. B. Fisher. **Stimulation of rat lung metabolism with 2,4-dinitrophenol and phenazine methosulfate.** *Am. J. Physiol.*, **231**:898-902 (1976).

D. J. P. Basset, E. Bowen-Kelly and S. S. Richenbaugh. **Rat lung glucose metabolism after 24 h of exposure to 100 % oxygen.** *J. Appl. Physiol.*, **66**:989-996 (1989).

G. Basset, C. Crone and G. Saumon. **Significance of active ion transport in transalveolar water absorption: a study on isolated rat lung.** *J. Physiol.*, **384**:311-324 (1987a).

G. Basset, C. Crone and G. Saumon. **Fluid absorption by rat lung in situ: pathways for sodium entry in the luminal membrane of alveolar epithelium.** *J. Physiol. Lond.*, **384**:325-345 (1987b).

G. Basset, G. Saumon and C. Crone. **Fluid and electrolyte transport in the isolated lung.** *In*: Effros RM and Chang HK (Eds.), *Fluid and Solute Transport in the Airspaces of the Lungs*, Marcel Dekker, Inc., New York, 1994, pp. 71-99.

J. Bastacky, C. Y. Lee, H. Koushafar, D. Yager, L. Kenaga, T.P. Speed, Y. Chen and J. A. Clements. **Alveolar lining layer is thin and continuous: low-temperature scanning electron microscopy of rat lung.** *J. Appl. Physiol.*, **79**:1615-1628 (1995).

R. R. Ben-Harari and Y. S. Bakhle. **Uptake of β-pheynylamine in rat isolated lung.** *Biochem. Pharmacol.*, **29**:489-494 (1980).

T. Berg, R. Blomhoff, L. Naess, H. Tolleshaug and C. A. Drevon. **Monensin inhibits receptor-mediated endocytosis of asialoglycoproteins in rat hepatocytes.** *Exp. Cell Res.*, **148**:319-330 (1983).

M. Bhat, D. Toledo-Velasquez, L. Wang, C. J. Malanga, J. K. Ma and Y. Rojanasakul. **Regulation of tight junction permeability by calcium mediators and cell cytoskeleton in rabbit tracheal epithelium.** *Pharm. Res.*, **10**:991-997 (1993).

R. T. Borchardt, P. L. Smith and G. Wilson. *Models for Assessing Drug Absorption and Metabolism.* Plenum Press, New York, 1996.

J. D. Brain, D. E. Knudson, S. P. Sorokin and M. A. Davis. **Pulmonary distribution of particles given by intratracheal instillation or by aerosol inhalation.** *Environ. Res.*, **11**:13-33 (1976).

J. D. Brain and J. D. Blanchard. **Mechanisms of particle deposition and clearance.** *In*: Moren F, Dolovich MB, Newhouse MT and Newman SP (Eds.), *Aerosols in Medicine, Principle, Diagnosis and Therapy*, Elsevier Science Publishers, The Netherlands, 1993, pp. 117-156.

A. W. Brandli, R. G. Parton and K. Simons. **Transcytosis in MDCK cells: identification of glycoproteins transported bidirectionally between membrane domain.** *J. Cell Biol.*, **111**:2909-2921 (1990).

P. P. Breitfeld, W. C. McKinnon and K. E. Mostor. **Effect of nocodazole on vesicular traffic to the apical and basolateral surfaces of polarized MDCK cells.** *J. Cell Biol.*, **111**:2365-2373 (1990).

R. A. Brown and L. S. Schanker. **Absorption of aerosolized drugs from the rat lung.** *Drug Metab. Dispos.*, **11**:355-360 (1983).

P. H. Burri. **Cellular components of the alveolar unit.** *In*: Favez G, Junod A and Leuenberger P (Eds.), *The Cells of The Alveolar Unit*, Hans Huber Publishers, Bern, 1983, pp. 11-22.

J. A. Burton, T. H. Gardiner and L. S. Schanker. **Absorption of herbicides from the rat lung.** *Arch. Environ. Health*, **29**:31-33 (1974).

J. A. Burton and L. S. Schanker. **Absorption of antibiotics from the rat lung.** *Proc. Soc. Exp. Biol. Med.*, **145**:752-756 (1974).

J. H. Byrne and S. G. Schultz. *An Introduction to Membrane Transport and Bioelectricity*, Raven Press, New York, 1991.

P. R. Byron and A. R. Clark. **Drug absorption from inhalation aerosols administered by positive-pressure ventilation I: administration of a characterized, solid disodium fluorescein aerosol under a controlled respiratory regime to the beagle dog.** *J. Pharm. Sci.*, **74**:934-938 (1985).

P. R. Byron. **Prediction of drug residence times in regions of the human respiratory tract following aerosol inhalation.** *J. Pharm. Sci.*, **75**:433-438 (1986).

P. R. Byron, N. S. R. Roberts and A. R. Clark. **An isolated perfused rat lung preparation for the study of aerosolized drug deposition and absorption.** *J. Pharm. Sci.*, **75**:168-171 (1986).

P. R. Byron and R. W. Niven. **A novel dosing method for drug administration to the airways of the isolated perfused rat lung.** *J. Pham. Sci.*, **77**:693-695 (1988).

P. R. Byron and E. M. Phillips. **Absorption, clearance and dissolution in the lung.** *In*: Byron, PR (Ed.), *Respiratory Drug Delivery*, CRC Press, Inc., Florida, 1990, pp. 107-142.

P. R. Byron, H. Katayama, Z. Sun, and F. Rypacek. **Opportunities for protein delivery by aerosol.** *Pol. Prep.*, **31**:167-168 (1990).

P. R. Byron, H. Katayama, Z. Sun, and F. Rypacek. **Airway retention and pulmonary absorption of poly-α,β-[N(2-hydroxyethyl-DL-aspartamide].** *J. Bioactive and Compatible Polymers*, **6**:25-35 (1991).

P. R. Byron, Z. Sun, H. Katayama and F. Rypacek. **Solute absorption from the airways of the isolated rat lung. IV. Mechanisms of absorption of fluorophore-labeled poly-a,b-[N(2-hydroxyethyl)-DL-aspartamide].** *Pharm. Res.*, **11**:221-225 (1994).

P. R. Byron and J. S. Patton. **Drug delivery via the respiratory tract.** *J. Aerosol Med.*, **7**:49-75 (1994).

P. R. Byron, M. Sakgami and F. Rypacek. **New pulmonary biopharmaceutics: rate-determining absorption and macromolecular transporters.** *In*: Dalby RN, Byron PR, Farr SJ and Peart J (Eds.), *Respiratory Drug Delivery VII*, Serentec Press, Inc., North Carolina, 2000, pp. 41-48.

P. Camner and B. Mossberg. **Airway mucus clearance and mucociliary transport.** *In*: Moren F, Dolovich MB, Newhouse MT and Newman SP (Eds.), *Aerosols in Medicine, Principle, Diagnosis and Therapy*, Elsevier Science Publishers, The Netherlands, 1993, pp. 247-260.

L. Campbell, A. Al-Eid, G. R. Newman, B. Jansai, P. J. Nicholls and M. Gumbleton. **Caveolin association with plasmalemmal vesicles in the in-vitvo and the cultured lung alveolar epithelial cell: functional implications for the pulmonary transport of macromolecules.** In: Byron PR, Dalby RN and Farr SJ (Eds)., *Respiratory Drug Delivery VI*, Interpharm Press, Illinois, 1988, pp. 279-282.

T. Chandra, I. M. Miller and D. B. Yeates, **A pore transport model for pulmonary alveolar epithelium.** *Am. Biomed. Eng.*, **20**:481-494 (1992).

F. P. Chinard and W. O. Cua. **Endothelial extraction of tracer water is independent of temperature in dog lungs.** *Am J. Physiol.*, **250**:H1017-H1021 (1986).

A. R. Clark and P. R. Byron. **Drug absorption from inhalation aerosols administered by positive-pressure ventilation II: Effect of disodium fluorescein aerosol particle size on fluorescein absorption kinetics in the beagle dog respiratory tract.** *J. Pharm.Sci.*, **74**:939-942 (1985).

P. Claude. **Morphologic factors influencing transepithelial permeability: a model for the resistance of the zennula occludens.** *J. Membr. Biol.*, **39**:219-232 (1978).

J. M. Cheek, M. J. Evans and E. D. Crandall. **Type I cell-like morphology in tight alveolar epithelial monolayers.** *Exp. Cell Res.*, **184**:375-387 (1989).

P. Colthorpe, S. J. Farr, G. Taylor, I. J. Smith and D. Wyatt. **The pharmacokinetics of pulmonary delivered insulin: a comparison of i.t. and aerosol administration to the rabbit.** *Pharm. Res.*, **9**:746-768 (1992).

P. Colthorpe, S. J. Farr, I. J. Smith, D. Wyatt and G. Taylor. **The influence of regional deposition on the pharmacokinetics of pulmonary delivered human growth hormone in rabbits.** *Pharm. Res.*, **12**:356-359 (1995).

B. Corrin. **The structure of the normal lungs.** *In*: Corrin B (Ed.), *The Lungs*, Edinburgh, UK, 1987, pp. 1-28.

G. R. Cott. **Active transport of Na^+ across epithelial monolayers.** *In*: Effros RM and Chang HK (Eds.), *Fluid and Solute Transport in the Airspaces of the Lungs*, Marcel Dekker, Inc., New York, 1994, pp. 101-122.

J. D. Crapo, B. E. Barry, P. Geher, M. Bachofen and E. R. Weibel. **Cell number and cell characteristics of the normal human lung.** *Am. Rev. Respir. Dis.*, **125**:332-337 (1982).

W. O. Cua, G. Basset, F. Bouchonnet, R. A. Garrick, G. Saumon and F. P. Chinard. **Endothelial and epithelial permeabilities to antipyrine in rat and dog lungs.** *Am. J. Physiol.*, **258**:H1321-H1333 (1990).

A. N. DeBelder and K. A. Gratath. **Preparation and properties of fluorescein-labeled dextran.** *Carbohydrate Res.*, **30**:375-378 (1973).

M. F. Deffebach, C. J. Bryan and C. M. Hoy. **Protein movement across cultured guinea pig trachea: specificity and effect of transcytosis inhibitors.** *Am. J. Physiol.*, **271**:L744-L752 (1996).

A. Dinter and E. G. Berger. **Golgi-disturbing agents.** *Histchem. Cell Biol.*, **109**:571-590 (1998).

L. G. Dobbs. **Isolation and culture of alveolar type II cells.** *Lung Cell Mol. Physiol.*, **2**:L134-L147 (1990).

A. N. Dodoo, S. Bansal, D. J. Barlow, F. C. Bennet, R. C. Hider, A. B. Lansley, M. J. Lawrence and C. Marriott. **Systematic investigations of the influence of molecular structure on the transport of peptides across cultured alveolar cell monolayers.** *Pharm. Res.*, **17**:7-14 (2000).

C. T. Dollery and A. F. Junod. **Concentration of (±)-propranolol in isolated, perfused lungs of rat.** *Br. J. Pharmacol.*, **57**:67-71 (1976).

J. Drobnik, V. Saudek, J. Vlasak and J. Kalal. **Polyaspartamide – a potential drug carrier.** *J. Polym. Sci. Polym. Sympo.*, **66**:65-74 (1979a).

J. Drobnik, J. Kalal, I. Dabrowska, R. Praw, M. Vachova and J. Elis. **The effect of polyaspartamides on drug-metabolizing enzymes.** *J. Polym. Sci. Polym. Sympo.*, **66**:75-81 (1979b).

R. M. Effros and G. R. Maon. **Measurements of pulmonary epithelial permeability in vivo.** *Am. Rev. Respir. Dis.*, **127**:S59-S66 (1983).

R. M. Effros, G. R. Mason, E. Reid, L. Graham and P. Silverman. **Diffusion of labeled water and lipophilic solutes in the lung.** *Microvas. Res.*, **29**:45-55 (1985).

R. M. Effros, G. R. Maon, P. Silverman, E. Reid and J. Hukkanen. **Movement of ions and small solutes across endothelium and epithelium of perfused rabbit lungs.** *J. Appl. Physiol.*, **60**:100-107 (1986).

R. M. Effros, G. R. Mason, K. Sietsema, J. Hukkanen, P. Silverman. **Pulmonary epithelial sieving of small solutes in rat lungs.** *J. Appl. Physiol.*, **65**:640-648 (1988).

R. M. Effros, G. R. Mason, J. Hukkanen and P. Silverman. **New evidence for active sodium transport from fluid-filled rat lungs.** *J. Appl. Physiol.*, **66**:906-919 (1989).

R. M. Effros. **Role of the pulmonary epithelium in governing fluid and solute transport in the lung.** *In*: Effros RM and Chang HK (Eds.), *Fluid and Solute Transport in the Airspaces of the Lungs*, Marcel Dekker, Inc., New York, 1994, pp. 55-70.

U. Eilers, J. Klunperman and H-P. Hauri. **Nocodazole, a microtubule-active drug, interferes with apical protein delivery in cultured intestinal epithelial cells (Caco-2).** *J. Cell Biol.*, **198**:13-22 (1989).

S. J. Enna and L. S. Schanker. **Absorption of drugs from the rat lung.** *Am. J. Physiol.*, **223**:1227-1231 (1972).

S. J. Enna and L. S. Schanker. **Phenol red absorption from the rat lung: evidence for carrier transport.** *Life Sci.*, **12**:231-239 (1973).

G. S. Filippatos, W. F. Hughes, R. Qiao, J. I. Sznajder and B. D. Uhal. **Mechanisms of liquid flux across pulmonary alveolar epithelial cell monolayers.** *In Vitro Cell Dev. Biol.*, **33**:195-200 (1997).

A. B. Fisher, C. Dodia and J. Linask. **Perfusate composition and edema formation in isolated rat lungs.** *Exp. Lung Res.*, **1**:13-21 (1980).

H. G. Folkesson, B. R. Westrom, M. Dahlback, S. Lundin and B. W. Karlsson. **Passage of aerosolized BSA and the nonapeptide dDAVP via the respiratory tract in young and adult rats.** *Exp. Lung Res.*, **18**:5595-614 (1992).

H. Folkesson, M. A. Matthay, B. R. Westron, K.J. Kim, B. W. Karlsson and R. H. Hastings. **Alveolar epithelial clearance of protein.** *J. Appl. Physiol.*, **80**: 1431-1445 (1996).

H. Foth. **Role of the lung in accumulation and metabolism of xenobiotic compounds - implications for chemically induced toxicity.** *Crit. Rev. Toxicol.*, **25**:165-205 (1995).

H. J. Fuchs, D. S. Borowitz, D. H. Christiansen, E. M. Morris, M. L. Nash, B. W. Ramsey, B. J. Rosenstein, A. L. Smith and M. E. Wohl. **Effect of aerosolized recombinant human Dnase on exacerbations of respiratory symptoms and on pulmonary function in patients with cystic fibrosis.** *New E. J. Med.*,**331**:637-642 (1994).

L. S. Gan, M. A. Moseley, B. Khosla, P. F. Augustijns, T. P. Bradshaw, R. W. Hendren and D. R. Thakker. **CYP3A-like cytochrome P450-mediated metabolism and polarized efflux of cyclosporin A in Caco-2 cells.** *Drug Metab. Dispos.*, **24**:344-349 (1996).

T. H. Gardiner and L. S. Schanker. **Absorption of disodium cromoglycate from the rat lung: evidence for carrier transport.** *Xenobiotica*, **4**:725-731 (1974).

T. H. Gardiner and F. R. Goodman. **Comparison of uptake and binding of disodium cromoglycate and phenol red in rat lung.** *J. Pharmacol. Exp. Ther.*, **198**:395-402 (1976).

G. Giammona, G. Cavellaro, G. Pitarresi, C. Ventura and S. Palazzo. **Synthesis and therapeutic potential of a macromolecular prodrug of diflunisal.** *Int. J. Pharm.*, **105**:57-63 (1994).

I. Gonda. **Deoxyribonuclease inhalation.** *In*: Adjei AL and Gupta PK (Eds.), *Inhalation Delivery of Therapeutic Peptides and Proteins*, Marcel Dekker, Inc., New York, 1997, pp. 355-365.

B. E. Goodman, R. S. Fleischer and E. D. Crandall. **Evidence for active Na^+ transport by cultured monolayers of pulmonary alveolar epithelial cells.** *Am. J. Physiol.*, **245**:C78-C83 (1983).

B. E. Goodman, K. J. Kim and E. D. Crandall. **Evidence for active sodium transport across alveolar epithelium of isolated rat lung.** *J. Appl. Physiol.*, **62**:2460-2466 (1987).

J. Gore and C. Hoinard. **Linolenic acid transport in hamster intestinal cells is carrier-mediated.** *J. Nutr.*, **123**:66-73 (1993).

A. B. Gorin and P. A. Stewart. **Differential permeability of endothelial and epithelial barriers to albumin flux.** *J. Apply. Physiol.*, **47**:1315-1324 (1979).

G. M. Green. **Alveolobronchiolar transport mechanisms.** *Arch. Intern. Med.*, **131**:109-115 (1981).

M. Halme, P. Maasilta, K. Mattson and K. Cantell. **Pharmacokinetics and toxicity of inhaled human natural interferon-beta in patients with lung cancer.** *Repiration*, **61**:105-107 (1994).

W. G. Hanstein. **Uncoupling of oxidative phosphorylation.** *TIBS*, March, 65-67 (1976).

R. H. Hastings, M. Crady, T. Sakuma and M. A. Matthay. **Clearance of different-sized proteins from the alveolar space in humans and rabbits.** *J. Appl Physiol.*, **73**:1310-1316 (1992).

R. H. Hastings, J. R. Wright, K. H. Albertine, R. Ciriales and M. A. Matthay. **Effect of endocytosis inhibitors on alveolar clearance of albumin, immunoglobulin G, and SP-A in rabbits.** *Am. J. Physiol.*, **266**:L544-L552 (1994).

R. H. Hastings, H. G. Folkesson, V. Petersen, R. Ciriales and M. A. Matthay. **Cellular uptake of albumin from lungs of anesthetized rabbits.** *Am. J. Physiol.*, **269**:*L453-L462* (1995).

U. Hedin and J. Thyberg. **Receptor-mediated endocytosis of immunoglobulin-coated colloidal particles in cultured mouse peritoneal macrophages. Chloroquine and monenin inhibit transfer of the ligand from endocytic vesicles to lysosomes.** *Eur. J. Cell Biol.*, **39**:130-135 (1985).

P. A. Helliwell, D. Meredith, C. A. Boyd, J. R. Bronk, N. Lister and P. D. Bailey. **Tripeptide transport in rat lung.** *Biochim. Biophys. Acta.*, **1190**:430-434 (1994).

M. R. Hill, L. M. Vaughan. **Effect of delivery mode on pharmacokinetics of inhaled drugs: experience with beclomethasone.** *In*: Dalby RN, Byron PR and Farr SJ (Eds.), *Respiratory Drug Delivery VI*, Interpharm Press, Illinois, 1998, pp. 53-60.

R. Hori, N. Okamura, T. Aiba and Y. Tanigawara. **Role of P-glycoprotein in renal tubular secretion of digoxin in the isolated perfused rat kidney.** *J. Pharmacol. Exp. Ther.*, **266**:1620-1625 (1993).

M. W. Hostetter, C. A. Dawson and D. L. Moore. **Influence of temperature on the absorption of inhaled bovine serum albumin through isolated rabbit lungs.** *Proc. Soc. Exp. Biol. Med.*, **167**:412-418 (1981).

R. C. Hubbard, N. G. McEvarey, S. E. Sellers, J. T. Healy, D. B. Czerski and R. G. Crystal. **Recombinant DNA-produced α_1-antitrypsin administered by aerosol augments lower respiratory tract antineutrophil elastase defenses individuals with α_1-antitrypsin deficiency.** *J. Clin. Invest.*, **84**:1349-1354 (1989).

E. Huland, H. Hulan and H. Heinzer. **Interleukin-2 by inhalation: local therapy for metastatic renal cell carcinoma.** *J. Urology*, **147**:344-348 (1992).

A. L. Iacono, R. J. Keenan, S. R. Duncan, G. C. Smaldone, J. H. Dauber, I. L. Paradis, N. PP. Ohori, Y. F. Grgurich, G. J. Burckart, A. Zeevi, E. Delgado, T. G. O'riordan, M. M. Zendarsky, S. A. Yousem and B. P. Griffith. **Aerosolized cyclosporine in lung recipients with refractory chronic rejection.** *Am. J. Repir. Crit. Care Med.*, **153**:1451-*1455 (1996).*

ICHQ2B, **"Validation of Analytical Procedures: Methodology"**, *International Conference on Harmonization of Technical Requirements for Registration of Pharmaceuticals for Human Use*, Geneva, Switzerland, November, 1996.

K. Iwamoto, J. Watanabe and H. Yonekawa. **Effects of metabolic inhibitors and incubation temperature on the saturable uptake of propranolol by isolated rat lung tissue.** *J. Pharm. Pharmacol.*, **41**:572-574 (1989).

H. A. Jaffe, R. Buhl, A. Mastrangeli, K. J. Holroyd, C. Saltine, D. Czerski, H. S. Jaffe, S. Kramer, S. Sherwin and R. G. Crystal. **Organ specific cytokine therapy: local activation of mononuclear phagocytes by delivery of an aerosol of recombinant interferon-g to the human lung.** *J. Clin. Invest.*, **88**:297-302 (1991).

O. G. Johnson, M. A. Lugg and T. E. Nicholas. **Uptake of [^{14}C]choline and incorporation into lung phospholipid by the isolated perfused rat lung.** *Lipids*, **14**:555-558 (1979).

A. F. Junod. **Accumulation of ^{14}C-imipramine in isolated perfused rat lungs.** *J. Pharmacol. Exp. Ther.*, **183**:182-187 (1972).

K. J. Kim and E. D. Crandall. **Sodium-dependent lysine flux across bullfrog alveolar epithelium.** *J. Appl. Physiol.*, **65**:1655-1661 (1988).

K. J. Kim and E. D. Crandall. **Specialized alveolar epithelial transport processes.** *In*: Effros RM and Chang HK (Eds.), *Fluid and Solute Transport in the Airspaces of the Lungs*, Marcel Dekker, Inc., New York, 1994, pp. 219-248.

K. J. Kim, V. Ratten, P. Oh, J. E. Schnitzer, V. K. Kalra and E. D. Crandall. **Specific albumin-binding protein in alveolar epithelial cell monolayers.** *Am. J. Respir. Crit. Care Med.*, **151**:A190 (1995).

K. J. Kim and E. D. Crandall. **Models for investigation of peptide and protein transport across cultured mammalian respiratory epithelial barriers.** *In*: Borchardt RT, Smith PL and Wilson G (Eds.), *Models for Assessing Drug Absorption and Metabolism*, Plenum Press, New York, 1996, pp. 325-346.

V. Kinnula, K. Mattson and K. Cantell. **Pharmacokinetics and toxicity of inhaled human interferon-α in patients with lung cancer.** *J. Interferon Res.*, **9**:419-423 (1989).

K. G. Knickelbein, T. Seres, G. Lam, R. B. Johnston and J. B. Warshaw. **Characterization of multiple cysteine and cysteine transporters in rat alveolar type II cell.** *Am. J. Physiol.*, **273**:L1147-L1155 (1997).

T. Komai, E. Shigehara, T. Tokui, T. Koga, M. Ishigami, C. Kuroiwa and S. Horiuchi. **Carrier-mediated uptake of pravastatin by rat hepatocytes in primary culture.** *Biopham. Pharmac.*, **43**:667-670 (1992).

J. Komura, I. Tamai, M. Senmaru, T. Terasaki, Y. Sai and A. Tsuji. **Sodium and chloride ion-dependent transport of β-alanine across the blood-brain barrier.** *J. Neurochem.*, **67**:330-336 (1996).

R. A. Kovelesky. **A novel isolated perfused guinea pig lung model for assessment of anti-leukototriene effects in vitro.** Ph.D. Dissertation, Virginia Commonwealth University, 1998.

H. A. Krebs and K. Henseleit. **Untersuchungen uber die Harnstoffbildung im Tierkorper.** *Hoppe-Seyler's Zeitschrift fur Physiologische Chemie*, 33-66 (1932).

A. Kydonieus. *Treatise on Controlled Drug Delivery*, Marcel Dekker, Inc., New York, 1991.

P. N. Lanken, J. H. Hansen-Flaschen, P. M. Sampson, G. G. Pietra, F. R. Haselton and A. D. Fishman. **Passage of uncharged dextrans from blood to lung lymph in awake sheep.** *J. Appl. Physiol.*, **59**:588-591 (1985).

R. C. Lanman, R. M. Gillilan and L. S. Schanker. **Absorption of cardiac glycosides from the rat respiratory tract.** *J. Pharmacol. Exp. Ther.*, **187**:105-111 (1973).

A. B. Lansley. **Mucociliary clearance and drug delivery via the respiratory tract.** *Adv. Drug Deliv. Rev.*, **11**:299-327 (1993).

B. L. Laube, A. Georrgopoulos and G. K. Adams. **Preliminary study of the efficacy of insulin aerosol delivered by oral inhalation in diabetic patients.** *JAMA*, **269**:2106-2109 (1993).

V. H. L. Lee. **Changing needs in drug delivery in the era of peptides and protein drugs.** In: Lee VHL (Ed.), *Peptide and Protein Drug Delivery*, Marcel Dekker, Inc., New York, 1990, pp. 1-56.

B. K. Leong, J. K. Coombs, C. P. Sabaitis, D. A. Rop and C. S. Aaron. **Quantitative morphologic analysis of pulmonary deposition of aerosol particles inhaled via intratracheal nebulization, intratracheal instillation or nose-only inhalation in rats.** *J. Appl. Toxicol.*, **18**:149-160 (1998).

P. Lepage and P. Gros. **Structural and functional aspects of P-glycoprotein and related transport proteins.** *Current Opinion in Nephrology and Hypertension*, **2**:735-743 (1993).

S. Levey and R. Gast. **Isolated perfused rat lung preparation.** *J. Appl. Physiol.*, **21**:313-316 (1966).

M. A. Libermand and R. G. Sleight. **Energy production and metabolism.** *In*: Sperelakis N (Ed.), *Cell Physiology Source Book*, Academic Press, London, 1995, pp.96-116.

W. Linder and J. W. Wainer. **Validated assays in the Journal of Chromatography B: an initial editorial position.** *J. Chromatogr.*, **683**:133-134 (1996).

F. Liu, D. O. Kildsig and A. K. Mitra. **Pulmonary biotransformation of insulin in rat and rabbit.** *Life Sci.*, **51**:1683-1689 (1992).

F. Liu, Z. Shao, D. Kildsig and A. K. Mitra. **Pulmonary delivery of free and liposomal insulin.** *Pharm. Res.*, **10**:228-232 (1993).

P. Macheras, C. Reppas and J. B. Dressman. *Biopharmaceutics of orally administered drugs*, Ellis Horwood Ltd., Hertfordshire, UK, 1995.

A. B. Maksymowych and L. L. Simpson. **Binding and transcytosis of botulinum newrotoxin by polarized human colon carcinoma cells.** *J. Biol. Chem.*, **273**:21950-21957 (1998).

D. Meredith and C. A. R. Boyd. **Dipeptide transport characteristics of the apical membrane of rat lung type II pneumocytes.** *Am. J. Physiol.*, **269**:L137-143 (1995).

M. Marsh, J. Wellsteed, H. Kern, E. Harms and A. Helenius. **Monensin inhibits Semliki Forest virus penetration into culture cells.** *Proc. Natl. Acad. Sci. USA*, **79**:5297-5301 (1982).

A. Martin, P. Bustamante and A. H. C. Chun. *Physical Pharmacy (Fourth Edition)*, Lea & Febiger, Philadelphia, 1993.

N. R. Mathias, K. J. Kim and V. H. L. Lee. **Targeted drug delivery to the respiratory tract: solute permeability of air-interface cultured rabbit tracheal epithelial cell monolayers.** *J. Drug Targeting*, **4**:79-86 (1996).

Y. Matsukawa, H. Yamahara, V. H. L. Lee, E. D. Crandall and K.J. Kim. **Horseradish peroxidase transport across rat alveolar epithelial cell monolayers.** *Pharm. Res.*, **13**:1331-1335 (1996).

Y. Matsukawa, V. H. L. Lee, E. D. Crandall and K, J. Kim. **Size-dependent dextran transport across rat alveolar epithelial cell monolayers.** *J. Pharm Sci.*, **86**:305-309 (1997).

K. Matter , K. Bucher and H. P. Hauri. **Microtubule perturbation retards both the direct and the indirect apical pathway but not affect sorting of plasma membrane proteins in intestinal epithelial cells (Caco-2).** *The EMBO J.*, **9**:3163-3170 (1990).

M. A. Matthay. **Function of the alveolar epithelial barrier under pathologic conditions.** *Chest*, **105**:675-745 (1994).

B. Mayrick and L. Reid. **The alveolar brush cell in rat lung - a third pneumocyte.** *J. Ultrastruct. Res.*, **23**:71-80 (1968).

N. G. McElvaney, R. C. Hubbard, P. Birrer, M. S. Cherhick, D. B. Caplan, M. M. Frank and R. G. Crystal. **Aerosol α_1-antitrypsin treatment for cystic fibrosis.** *Lancet*, **337**:392-394 (1991).

G. E. McLaughlin, K. Kim, M. M. Berg, P. Agoris, R. L. Lubman and E. D. Crandall. **Measurement of solute fluxes in isolated rat lungs.** Rep. Physiol., **91**:321-334 (1993).

H. M. Mehandale, L. S. Angevine and Y Ohmiya. **The isolated perfused lung: a critical evalution.** *Toxicology*, **21**:1-36 (1981).

R. R. Mercer, M. L. Russell, V. L. Roggli and J. D. Crapo. **Cell number and distributions in human and rat airways.** *Am. J. Respir. Cell Mol. Biol.*, **10**:613-624 (1994).

R. M. Mercer. **Structure of the Na, K-ATPase.** *Int. Rev. Cytol.*, **137C**:139-168 (1993).

P. Michaut, C. Planes, B. Escoubet, A. Clement, C. Amiel and C. Clerici. **Rat lung alveolar type II cell line maintains sodium transport characteristics of primary culture.** *J. Cell Physiol.*, **169**:78-86 (1996).

R. W. Miller. **Allosteric inhibitors.** *In*: Mochster RM, Kates M and Quastel JH (Eds.), *Metablic Inhibitors*, Vol. IV, Academic Press, New York, 1973, pp. 1-44.

W. E. M. Mol, G. N. Follema, B. Weert and D. K. F. Meijer. **Mechanisms for the hepatic uptake of organic cations. Studies with the muscle relaxant vecuronium in isolated rat hepatocytes.** *J. Pharmacol. Exp. Ther.*, **244**:268-275 (1988).

H. H. Mollenhauler, D. J. Morre and L. D. Rowe. **Alternation of intracellular traffic by monensin: mechanism, specificity and relationship to toxicity.** *Biochim. Biophys. Acta*, **1031**:225-246 (1990).

K. Morimoto, H. Yamahara, V. H. L. Lee and K. Kim. **Dipeptide transport across rat alveolar epithelial cell monolayers.** *Pharm. Res.*, **10**:1668-1674 (1993).

K. Morimoto, H. Yamahara, V. H. L. Lee and K. Kim. **Transport of thyrotropin-releasing hormone across rat alveolar epithelial monolayers.** *Life Sci.*, **54**:2083-2092 (1994).

N. Muranushi, K. Horie, K. Masuda and K. Hirano. **Characteristics of ceftibuten uptake into Caco-2 cells.** *Pharm. Res.*, **11**:1761-1765 (1994).

P. Murchie, P. W. Johnston, J. A. Rose and D. J. Godden. **Effects of hyperoxia on bronchial wall dimensions and lung mechanics in rats.** *Acta Physiol. Scand.*, **148**:363-370 (1993).

P. Neri, G. Antoni, F. Benvenuti, F. Cocola and G. Gazzei. **Synthesis of poly-α,β-[N(2-hydroxyethyl)-D,L-aspartamide], a new plasma expander.** *J. Med. Chem.*, **16**:893-897 (1973).

G. Nicolaysen. **Perfusate qualities and spontaneous edema formation in an isolated perfused lung preparation.** *Acta Physiol. Scand.*, **83**:563-570 (1971).

R. W. Niemeir and E. Bingham. **An isolated perfused rat lung preparation for metabolic studies.** *Life Sci.*, **11**:807-820 (1972).

R. W. Niven. **Application of the isolated perfused rat lung to evaluate pharmaceuticals presented to the airways.** Ph.D. Dissertation. University of Kentucky, 1988.

R. W. Niven and P. R. Byron. **Solute absorption from the airways of the isolated rat lung. I. - The use of absorption data to quantify drug dissolution or release in the respiratory tract.** *Pharm. Res.*, **5**:574-579 (1988).

R. W. Niven, F. Rypacek and P. R. Byron. **Solute absorption from the airways of the isolated rat lung. III. – Absorption of several peptidase-resistant, synthetic polypeptides: poly-(2-hydroxy-ethyl)-aspartamides.** *Pharm. Res.*, **7**:990-994 (1990).

R. E. Notari. *Biopharmaceutics and Chemical Pharmaceutics: An Introduction.* Marcel Dekker, Inc., New York, 1987.

T. Ogihara, I. Tamai and A. Tsuji. **Structural characterization of substrates for the anion exchange transporter in Caco-2 cells.** *J. Pharm. Sci.*, **88**:1217-1221 (1999).

S. Ohkuma, J. Tamura and K. Kuriyama. **Characteristics of cholic acid uptake in primary cultured hepatocytes.** *Steroids*, **42**:205-215 (1983).

T. Ohtani, M. Murakami, A. Yamamoto, K. Takada and S. Munanishi. **Effect of absorption enhancers on pulmonary absorption of fluorescein isothiocyanate dextrans with various molecular weights.** *Int. J. Pharm.*, **77**:141-150 (1991).

K. Okumura, H. Yoshida, R. Hori. **Tissue distributions and metabolism of drug III. Accumulation of drugs by the isolated perfused rat lung.** *J. Pharmacobi-Dyn.*, **1**:230-237 (1978).

K. Okumura, S. Iwakawa, T. Yoshida, T. Seki and F. Komada. **Intratracheal delivery of insulin and absorption from solution and aerosol by rat lung.** *Int. J. Pharm.*, **88**:63-77 (1992).

T. C. Paino and A. D. Moore. **Determination of the LOD and LOQ of an HPLC method using four different techniques.** *Pharm. Technol.*, October, 86-90 (1999).

J. S. Patton and R. M. Platz. **Pulmonary delivery of peptides and proteins for systemic action.** *Adv. Drug Deliv. Rev.*, **8**:179-196 (1992).

J. S. Patton. **Mechanisms of macromolecule absorption by the lungs.** *Adv. Drug Deliv. Rev.*, **19**:3-36 (1996).

J. S. Patton. **Deep-lung delivery of therapeutic proteins.** *CHEMTECH*, **27**:34-38 (1997).

J. S. Patton, S. Nagarajan and A. Clark. **Pulmonary absorption and metabolism of peptides and proteins.** *In*: Dalby RN, Byron PR and Farr SJ (Eds.), *Respiratory Drug Delivery VI*, Interpharm Press, Illinois, 1998, pp. 17-24.

J. N. Pritchard, A. Holmes, J. C. Evans, N. Evans, R. J. Evans and A. Morgan. **The distribution of dust in the rat lung following administration by inhalation and by single intratracheal instillation.** *Environ. Res.*, **36**:268-297 (1985).

B. R. Pitt, R. Moalli, S. F. P. Man and C. N. Gillis. **Alveolar transfer of prostaglandin E_2 in isolated perfused guinea pig lungs.** *J. Appl. Physiol.*, **59**:691-697 (1985).

N. Potau, A. C. Bailey, E. Roach, J. A. Williams and I. D. Goldfine. **Methylamine and monensin do not block insulin internalization, but do influence the intracellular distribution and action of insulin in pancreatic acini from diabetic mice.** *Endocrinology*, **115**:205-213 (1984).

L. Reuss. **Tight junction permeability.** *In*: Cereijido M (Ed.), *Tight junctions*, CRC Press, Florida, 1991, pp. 49-66.

J. L. Riggs, R. J. Seiwald, J. H. Burckhalter, C. M. Downs and T. G. Metacalf. **Isothiocyanate compounds as fluorescent labeling agents for immune serum.** *Am. J. Pathol.*, **34**:1081-1097 (1958).

N. S. R. Roberts. **Aerosol deposition and airway-to-perfusate transfer in the isolated perfused rat lung.** Ph.D. Dissertation. University of Aston, 1984.

R. Rognstad and J. Katz. **The mechanism of the non-oxidative segment of the pentose cycle in the liver.** *Biochem. Biophys. Res Commun.*, **61**:774-780 (1974).

A. M. Rose and R. Valdes. **Understanding the sodium pump and its relevance to disease.** *Clin. Chem.*, **40**:1674-1685 (1994).

S. Rounds and I. F. McMurtry. **Inhibition of oxidative ATP production cause transient vasoconstriction and block subsequent pressor responses in rat lungs.** *Circ. Res.*, **48**:393-400 (1981).

D. H. Rutschman, W. Olivera and J. I. Sznajder. **Active transport and passive liquid movement in isolated perfused rat lung.** *J. Appl. Physiol.*, **75**:574-580 (1993).

J. T. Ruzinski, S. J. Skerrett, E. Y. Chi and T. R. Martin. **Deposition of particles in the lungs of infant and adult rats after direct intratracheal administration.** *Lab. Animal Sci.*, **45**:205-210 (1995).

F. Rypacek, J. Drobnik, J. Krejcoves and J. Kalal. **Fluorescent labeling of soluble polymers.** *J. Polym. Sci. Polym. Sympo.*, **66**:53-58 (1979).

F. Rypacek, J. Drobnik and J. Kalal. **Fluorescence labeling method for estimation of soluble polymers in the living material.** *Anal. Biochem.*, **104**:141-149 (1980).

K. Saito. **Effect of cations and some compounds on paraquat accumulation into cultured pnemocytes.** *Tohoku J. Exp. Med.*, **148**:41-47 (1986).

M. Sakagami, W. Kinoshita, K. Sakon, Y. Makino and T. Fujii. **Prolonged pulmonary absorption using inhalable powder microspheres.** *Pharm. Res.*, **13**:Suppl. 5, 167 (1996).

M. Sakagami, P. R. Byron and F. Rypacek. **Effect of temperature on pulmonary absorption from the airways of the isolated perfused rat lung.** *Pharm. Res.*, **14**:Suppl. S135 (1997).

F. J. Saldias, K. Lecuona, E. Friedman, M. L. Barnard, K. M. Ridge and J. I. Sznajder. **Modulation of lung liquid clearance by isoproterenol in rat lungs.** *Am. J. Physiol.*, **274**:L694-L701 (1998a).

F. J. Saldias, A. Comellas, C. Guerrero, K. M. Ridge, D.M. Rutschman and J. I. Sznajder. **Time course of active and passive liquid and solute movement in the isolated perfused rat lung model.** *J. Apply. Physiol.*, **85**:1572-1577 (1988b).

G. Sauman and G. Martlet. **Effect of metabolic inhibitors on Na^+ transport in isolated perfused rat lungs.** *Am. J. Respir. Cell Mol. Biol.*, **9**:157-165 (1993).

J. D. Schaeffer, K. J. Kim and E. D. Crandall. **Effects of cell swelling on fluid flow across alveolar epithelium.** *J. Appl. Physiol.*, **56**:72-77 (1984).

L. S. Schanker and J. A. Burton. **Absorption of heparin and cyanocobalamin from the rat lung.** *Proc. Soc. Exp. Biol. Med.*, **152**:377-380 (1976).

L. S. Schanker and J. A. Hemberger. **Relation between molecular weight and pulmonary absorption rate of lipid-insoluble compounds in neonatal and adult rats.** *Biochem. Pharmacol.*, **32**:2599-2601 (1983).

L. S. Schanker, E. W. Mitchell and R. A. Brown. **Species comparison of drug absorption from the lung after aerosol inhalation or intratracheal injection.** *Drug Met. Dispos.*, **14**:79-88 (1986).

E. E. Schneeberger and M. J. Kornovsky. **The ultrastructural basis of alveolar-capillary membrane permeability to peroxidase used as a tracer.** *J. Cell Biol.*, **37**:781-793 (1968).

E. E. Schneeberger and R. D. Lynch. **Tight junctions in the lung.** *In*: Cereijido M (Ed.), *Tight Junctions*, CRC Press, Florida, 1991, pp. 337-351.

E. E. Schneeberger and R. D. Lynch. **Structure, function and regulation of cellular tight junctions.** *Am. J. Physiol.*, **262**:L647-661 (1992).

A. Seelig. **How does P-glycoprotein recognize its substrates?** *Int. J. Clin. Pharmacol. Ther.*, **36**:50-54 (1998a).

A. Seelig. **A general pattern for substrate recognition by P-glycoprotein.** *Eur. J. Biochem.*, **215**:252-261 (1998b).

V. B. Serikov, M. Grady and M. A. Matthay. **Effect of temperature on alveolar liquid and protein clearance in an in situ perfused goat lung.** *J. Appl. Physiol.*, **75**:940-947 (1993).

J. Shen, K. J. Elbert, F. Yamashita, C. M. Lehr, K. J. Kim and V. H. L. Lee. **Organic cation transport in rabbit alveolar cell monolayers.** *Pharm. Res.*, **16**:1280-1287 (1999).

E. C. Slater. **Uncouplers and inhibitors of oxidative phosphorylation.** *In*: Mochster RM and Quastel (Eds.), *Metabolic Inhibitors*, Vol. II, Academic Press, New York, 1963, pp. 503-516.

D. O. Slosman, A. B. Bill, B. S. Polla and P. O. Alderson. **Evaluation of [iodine-125]*N,N,N'*-trimethyl-*N'*-[2-hydroxy-3-methyl-5-iodobenzyl]-1,3-propanediamine lung uptake using an isolated-perfused lung model.** *J. Nucl. Med.*, **28**:203-208 (1987).

D. O. Slosman, D. Davidson, A. B. Brill and P.O. Alderson. **^{131}I-metaiodo benzyl guanidine uptake in the isolated rat lung: a potential marker of endothelial cell function.** *Eur. J. Nucl. Med.*, **13**:543-547 (1988).

M. B. Snipes, B. B. Boecker and R. O. McClellan. **Retention of monodisperse or polydisperse aluminosilicate particles inhaled by dogs, rats and mice.** *Toxicol. Appl. Pharmacol.*, **69**:345-352 (1983).

A. Soldner, L. Z. Benet, E. Mutschler and U. Christians. **Active transport of the angiotensin-II antagonist losartan and its main metabolite EXP3174 across MDCK-MDR1 and caco-2 cell monolayers.** *Br. J. Pharmacol.*, **129**:1235-1243 (2000).

N. Sperelakis. *Cell Physiology Source Book*, Academic Press, London, UK, 1995.
H. Steen, J. G. Maring and D. K. F. Meijer. **Differential effects of metabolic inhibitors on cellular and mitochondrial uptake of organic cations in rat liver.** *Biochem. Pharmacol.*, **45**:809-818 (1993).

K. Stenseth and J. Thyberg. **Monensin and chloroquine inhibit transfer to lysosomes of endocytosed macromolecules in cultured mouse peritoneal macrophages.** *Eur. J. Cell. Biol.*, **49**:326-333 (1989).

K. C. Stone, R. R. Mercer, B. A. Freeman, L. Chang and J. D. Crapo. **Distribution of lung cell numbers and volumes between alveolar and nonalveolar tissue.** *Am. Rev. Respir. Dis.*, **125**:332-337 (1992).

J. Z. Sun. **Pulmonary absorption of fluorophore-labeled polyaspartamides from the airways of the isolated perfused rat lung.** Ph.D. Dissertation, Virginia Commonwealth University, 1995.

J. Z. Sun, P R. Byron and F. Rypacek. **Solute absorption from the airways of the isolated rat lung. V. - Charge effects on the absorption of copolymers of N(2-hyrdoxyethly)-DL-aspartamide with DL-aspartic acid or dimethylaminopropyl-DL-aspratamide.** *Pharm. Res.*, **16**:1104-1108 (1999).

K. Takada, M. Yamamoto and S. Asada. **Evidence for the pulmonary absorption of fluorescent-labeled macromolecular compounds.** *J. Pharm. Dyn.*, **1**:281-287 (1978).

A. M. Taratakoff and P. Vasalli. **Plasma cell immunoglobulin secretion: arrest is accompanied by alterations of the Golgi complex.** *J. Exp. Med.*, **146**:1332-1345 (1977).

A. E. Taylor, A. C. Guyton and V. S. Bishop. **Permeability of the alveolar membrane to solutes.** *Circ. Res.*, **16**:353-362 (1965).

A. E. Taylor and K. A. Gaar. **Estimation of equivalent pore radii of pulmonary capillary and alveolar membranes.** *Am. J. Physiol.*, **218**:1133-1140 (1970).

G. Taylor, P. Colthorpe and S. J. Farr. **Pulmonary absorption of proteins: influence of deposition site and competitive elimination processes.** *In*: Dalby RN, Byron PR and Farr SJ (Eds.), *Respiratory Drug Delivery IV*, Interpharm Press, Illinois, 1994, pp. 25-30.

J. R. Turner and A. M. Tartakoff. **The response of the Golgi complex to microtubule alteration: the roles of metabolic energy and membrane traffic in Golgi complex organization.** *J. Cell Biol.*, **109**:2081-2088 (1989).

S. U. Uhlig and L. Wollin. **An improved setup for the isolated perfused rat lung.** *J. Pharmacol. Toxicol. Method*, **31**:85-94 (1994).

F. J. Veith, J. W. C. Hgstrom, S. L. Nehlsen, R. C. Karl and M. Deysine. **Functional hemodynamic, and anatomic changes in isolated perfused dog lungs: the importance of perfusate characteristics.** *Annals Surgery*, **165**:267-278 (1967).

F. J. Veith, S. B. Sinha, J. S. Graves, S. J. Boley and J. C. Dougheerty. **Ischemic tolerance of the lung: the effect of ventilation and inflation.** *J. Thorac. Caridovasc. Sur.*, **61**:804-810 (1971).

R. E. Vestal, D. M. Kornhauser and D. G. Shand. **Active uptake of propranolol by isolated rabbit alveolar macrophages and its inhibition by other amines.** *J. Pharmacol. Exp. Ther.*, **214**:106-111 (1980).

S. Villaschi, L. Johns, M. Cirigliano and G. G. Pietra. **Binding and uptake of native and glycosylated albumin-gold complexes in perfusate rat lungs.** *Microvasc. Res.*, **32**:190-199 (1986).

J. Visich. **Pulmonary disposition of thyrotropin-releasing hormone administered to the isolated perfused rat lung.** Ph.D. Dissertation, Virginia Commonwealth University, 1996.

J. Vlasak, F. Rypacek, J. Drobnik and V. Saudek. **Properties and reactivity of polysuccinimide.** *J. Polym. Sci. Polm. Sympo.*, **66**:59-64 (1979).

L. Wang, D. Toledo-Velasquez, D. Schwegler-Berry, J. K. H. Ma and Y. Rojanasakul. **Transport and hydrolysis of enkephalins in cultured alveolar epithelial monolayers.** *Pharm. Res.*, **10**:1662-1667 (1993).

D. Wangensteen and M. Bartlett. **D- and L-glucose transport across the pulmonary epithelium.** *J. Appl. Physiol.*, **57**:1722-1730 (1984).

D. Wangensteen. **Microstructural aspects of macromolecule transport across pulmonary epithelium.** *In*: Dalby RN and Evans R (Eds.), *Respiratory Drug Delivery II*, Univcrsity of Kentucky, 1990, pp. 117-140.

D. Wangensteen, M. M. Burtlett, J. K. James, Z. F. Yang and P. S. Low. **Riboflavin-enhanced transport of serum albumin across the distal pulmonary epithelium.** *Pharm. Res.*, **13**:1861-1864 (1996).

A. Wanner, R. J. Phipps and C. S. Kim. **Mucus clearance: cilia and cough.** *In*: Chernick V and Mellins RB (Eds.), *Basic Mechanisms of Pediatric Respiratory Disease*, Sect. V, Chapter 26, B. C. Dekker, Inc., Pennsylvania, 1991, pp. 361-382.

L. C. Ward and P. J. Buttery. **The patho-physiological basis for tests of viability in isolated perfused organs.** *Biomedicine*, **30**:181-186 (1979).

D. B. Warheit. **Interspecies comparisons of lung responses to inhaled particles and gases.** *Toxicology*, **20**:1-29 (1989).

E. R. Weibel. **Lung cell biology.** *In*: Am. Physiol. Soc. (Eds.), *Handbook of Physiology. The Repsiratory System, Circulation and Non-respiratory Functions*, Bethesda, Maryland, 1985, Sect 3, Vol. I, Chapter 2, pp. 47-91.

J. Whittaker, V. A. Hammond, R. Taylor and K. G. M. M. Alberti. **Effects of monensin on insulin interactions with isolated hepatocytes.** *Biochem. J.*, **234**:463-468 (1986).

D. K. Wilcox, R. P. Kitson and C. C. Widnell. **Inhibition of pinocytosis in rat embryo fibroblasts treated with monensin.** *J Cell Biol.*, **92**:859-864 (1982).

D. K. Wilcox, R. P. Kitson and C. C. Widnell. **Inhibition of pinocytosis in rat embro fibroblasts treated with monensin.** *J. Cell Biol.*, **92**:859-864 (1989).

T. Wileman, R. L. Boshans, P. Schlesinger and P. Stahl. **Monensin inhibits recycling of macrophage mannose-glycoprotein receptors and ligand delivery to lysosomes.** *Biochem. J.*, **220**:665-675 (1984).

D. A. Wiersma and R. A. Roth. **Clearance of 5-hydroxytryptamine by rat lung and liver: the importance of relative perfusion and intrinsic clearance.** *J. Pharmacol. Exp. Ther.*, **212**:97-102 (1980).

S. K. Williams, M. A. Matthews and R. C. Wagner. **Metabolic studies of the micropinocytic process in the endothelial cells.** *Microvas. Res.*, **18**:175-184 (1979).

M. C. Williams. **The alveolar epithelium.** *In*: Schraufnagel DE (Ed.), *Electron Microscopy of The Lung*, Marcel Dekker, Inc., New York, 1990, pp. 121-147.

M. C. Williams. **Endocytosis and trancytosis by alveolar epithelial cells in the adult ray lung.** *J. Biopharm. Sci.*, **3**:209-214 (1992).

M. C. Willighams and I. Paston. **Experimental protocols for the study of endocytosis.** *In*: Paston I and Willingham MC (Eds.), *Endocytosis*, Plenum Press, New York, 1985, pp. 316-317.

F. Yamashita, K. J. Kim and V. H. L. Lee. **Gly-L-Phe Transport and metabolism across primary cultured rabbit tracheal epithelial cell monolayers.** *Pharm. Res.*, **14**:238-240 (1997).

F. Yamashita, K. J. Kim and V. H. L. Lee. **Dipeptide uptake and transport characteristics in rabbit tracheal epithelial cell layers cultured at an air interface.** *Pharm. Res.*, **15**:979-983 (1998).

W. W. Yau, J. J. Kirkland and D. D. Bly. *Modern Size-Exclusion Liquid Chromatography: Practice of Gel Permeation and Gel Filtration Chromatography.* John Wiley and Sons, New York, 1979.

S. L. Young. **An isolated perfused rat lung preparation.** *Environ. Health Pers.*, **16**:61-66 (1976).

VITA